Etude et optimisation d'une batterie à circulation tout vanadium

Ranine El Hage

THÈSE

En vue de l'obtention du

DOCTORAT DE L'UNIVERSITÉ DE TOULOUSE

Délivré par l'Université Toulouse 3 - Paul Sabatier

Présentée et soutenue par

Ranine EL HAGE

Le 2 novembre 2020

Etude et optimisation d'une batterie à circulation tout vanadium

---

Ecole doctorale : **MEGEP - Mécanique, Energétique, Génie civil, Procédés**

Spécialité : **Génie des Procédés et de l'Environnement**

Unité de recherche :
LGC - Laboratoire de Génie Chimique

Thèse dirigée par
Théo TZEDAKIS et Fabien CHAUVET

Jury

M. Carlos PONCE DE LEóN ALBARRáN, Rapporteur
M. Vincent VIVIER, Rapporteur
Mme Béatrice BISCANS, Examinatrice
M. Mathieu ETIENNE, Examinateur
M. Théo TZEDAKIS, Directeur de thèse
M. Fabien CHAUVET, Co-directeur de thèse

Acknowledgments

I am not the best person at expressing my feelings but I could not start this manuscript without thanking all the people who contributed directly or indirectly to this work, especially during the past three years spent at the Laboratoire de Génie Chimique, which I consider to be one of the greatest adventures in my life...

First of all, I would like to express my endless thanks to my supervisor Prof. Theo Tzedakis, who granted me the opportunity to explore the universe of electrochemistry and encouraged me to do better on a daily basis. His inspiration, motivation, insight and stimulation have helped me to achieve this work and I believe that in the past three and a half years most of his support was beyond his supervisory responsibility.
Also, I would like to thank my co-supervisor, Dr. Fabien Chauvet, with whom I had the pleasure to discuss experimental issues and interpret the different results. His continuous support, especially during the last months, was of great help.
In addition, countless thanks are dedicated to Dr. Fadia Najjar who provided me the opportunity to come to Toulouse for an internship and my adventure only grew from there.

I would like to acknowledge all the members of the jury who accepted to evaluate the present work: Dr. Carlos Ponce De Leon and Dr. Vincent Vivier for reading and commenting the manuscript and Dr. Mathieu Etienne and Prof. Béatrice Biscans for the examination and participation to the defense. Even though I would have preferred to meet all of you on the day of the defense, which was not possible due to the COVID-19 pandemic, it was still an honor to discuss with you over ZOOM.

Special thanks go to Prof. Biscans and Dr. Laurent Cassayre for their great input to the project and the numerous occasions on which we were able to exchange ideas and point of views for a better comprehension of the encountered problems. I would like to thank also Delphine and Waldemir, both post-doctorate candidates, who were a part of the team as well and contributed to the scientific and experimental progress of the project.

My deepest gratitude goes to the technical staff in the lab, Brigitte, Laure, Sandrine, Christelle and Vincent, for always being available for the smallest issues, as well as Pierre for the NMR analysis and Stéphane for preparing all the glassware I needed for my experiments.

As for all the researchers, the PhD and master students that I met throughout the years, I just want you to know that you made my life in the lab much more fun; thank you for all the good times, the laughs and the many activities we shared together. Charaf, Nabiil, Dihia, Chloé and Christophe, I will miss you all and good luck for your PhDs...enjoy it while it lasts. As for the girls closer to my heart, Chams, Fatma and Melissa, our “pauses café” and debatable “questions

existentielles" are among my favorite moments! Thank you for being always the source of good mood no matter the situation.

Now outside the LGC, I would not even know where to start to thank each and every person who was there during the past three years, from the Lebanese community in Toulouse to "منتدى الصدفة" (Fatuta, Ranime, Sousou...), all of you made me feel at home away from home especially the "Chorale Maronite de Toulouse" (Charbel Y., Rouaida, Pierre, Mouin, Marie-Lou) to whom I owe most of my gratitude.

Special thanks go to my closer friends, Yolla, Georges, Ali, Mohammad/Marcel (aka. Houhou), Mcheik, Chams and Farah for all the memorable nights we spent together laughing and eating (the most sacred part of our gatherings!) and for being the most supportive people anyone could ever wish for in their life (yes you Yoyo, thank you brother). I could not forget to thank also my lifetime friends, Joelle, Eddy S., Elsi and Charbel Z. who have been there since longer than I can remember, you guys are the best...

I would like to thank from the bottom of my heart, the person who is the closest to this heart: Ali, thank you for believing in me when I did not believe in myself, thank you for the continuous support and thank you for tolerating and understanding me through the hard times.

Finally, I dedicate this thesis to my parents Gaby and Maha, without whom I would have never reached this far. I can never express how grateful I am towards them and my siblings Elie, Caline and Edy for their endless love and continuous motivation from the beginning.

Table of contents

General introduction

The continuous development of industries and the global population growth are increasing the energy consumption worldwide, thus increasing the demand for fossil fuels, which constitutes the main energy source for its high energy density and ease of handling. However, the instability of the fuel prices on one hand and the greenhouse gas emissions and the substantial environmental impact of fuel consumption on the other hand, led to look for alternatives and invest in the renewable energy sources such as solar, wind, water…

Exploiting renewable energy sources requires developing corresponding storage devices, because of their intermittent nature; thus it is essential to conceive energy storage systems suitable for the grid needs and able to balance between supply and demand of energy.
The types of energy storage systems (ESS) are numerous and expand on a wide range of capacity, power density and capital costs. Some of them are dependent on the geographic localization (hydropower, compressed air, wind) and others are very costly (flywheels, 1500 and 6000 $/kWh) or still dependant on raw material from fossil fuels (hydrogen fuel cells). The electrochemical storage in redox flow batteries (RFBs) came as a solution of choice because it resolved the problems of geo-localization and fossil fuels dependency and the cost was significantly reduced to 180 - 250 $/kWh (depending on the redox couples and material used). In addition, they introduced the advantages of independent sizing of the power and energy and the possibility of operating at room temperature. However, compared to the previously cited ESS, their power rating is still low: between 0.5 and 100 MW compared to the size of the pumped hydro energy storage, for example, in the range of 1000 – 3000 MW. The RFBs types can be divided mainly into two categories, the organic and the aqueous systems. The first ones allow achieving cell voltages greater than 3 V but they are compromised by the difficulty to achieve high energy densities due to the low solubility of the electroactive species in non aqueous media. In return, the aqueous RFBs involve generally soluble metal ions but the cell voltage is less than 2 V in general.

One of the major drawbacks of the RFBs, constituted by two “very different” electroactives species (two separate redox couples), is the cross-contamination problems between the two compartments which i) decreases the energy efficiency of the battery and ii) largely increases the recycling costs of the system.

The redox battery of interest in this work is the all-vanadium redox flow battery (VRFB) which was the only system that could reduce the cost of the cross-contamination, since the only element used for the electrolyte solutions is the vanadium in its four oxidation states. In this case, the cross-contamination is simply a fraction of electricity loss, and a periodic need to re-equilibrate the volume of the electrolytes. Nevertheless, because of the relatively high weight of the vanadium, the VRFB suffers from a low energy density (~ 40 $Wh.kg^{-1}$ compared to ~ 150 $Wh.kg^{-}$

[1] for Li-ion stationary batteries) in addition to the relatively low solubility (< 2 $mol.L^{-1}$) of the vanadium salts in sulfuric acid and in a limited temperature range (10 to 40 °C).

An objective of this thesis is to define the formulation of the electrolytes in order to increase the stored energy density by using vanadium suspensions as electrolytes, i.e. excess solid particles in a saturated solution. The study consists first in preparing, analyzing and characterizing the electrolytes (posolyte $V^{(IV)}/V^{(V)}$ and negolyte $V^{(II)}/V^{(III)}$), thus expecting to find their optimal composition. Therefore, it is essential to understand the physico-chemical phenomena occurring during the charge-discharge cycling and thus determining the unexpected problems and establishing laws governing these processes to overcome any eventual limitation.

The presence of vanadium solid particles will be studied in order to examine how to manage the mixed suspensions (presence of both the dissolved and liquid forms) and their effect on the stored energy density. On the other hand, being inspired by their use in Li batteries as electric conductor, carbon nanoparticles are also involved; their interactions with both the current collector (electronic percolation) and the vanadium particles are analyzed as well as the corresponding effects on power and capacity of the battery.

Therefore, it was essential to carry out several preliminary studies to get the required knowledge of the system and the laws controlling it, before conceiving and elaborating a VRFB (at the laboratory scale). The idea is to reduce as much as possible the stored volume and simultaneously to increase the energy density stored. Note that the optimization of the power density of the reactor is also an objective of the thesis which implies the design of an efficient electrochemical reactor with continuous flow.
Mass and charge balances are performed for charge/discharge cycles, expecting i) to establish correlations that link the response of the system (current, voltage, energy and reversibility) to the (influencing) operating parameters, and ii) to compare the various yields (voltage, energy, faradic) between the cycles of the battery.

In order to achieve these objectives, this manuscript is structured in five parts. In the first chapter, an overview of the existing energy storage systems is presented with a focus on redox flow batteries. The working principle of the RFBs along with the different types and their limitations are presented leading to the introduction of the all-vanadium redox flow battery. The components of the VRFB are introduced (electrodes, membrane, additives…) while the existing studies of the electrolyte characteristics (solubility, density, viscosity) are developed in order to have a complete vision of the factors inducing the low energy density of this system.

The second section is devoted to the methods used for the characterization and analysis of the vanadium electrolytes, which can be divided into three categories. First, the tools used for the electrochemical preparation of the vanadium salts/solutions and the setup for the electrochemical

analysis in a half-cell configuration (three electrodes cell) are presented. Then, in order to be able to have a quantitative follow-up of the four oxidation states, analytical techniques are examined and we have defined the appropriated methods for the corresponding species of the vanadium: UV-Vis spectrometry and potentiometric titration. Finally, for the analysis of the physico-chemical properties of vanadium solutions and suspensions, experimental setups are conceived, elaborated and calibrated to measure the density and apparent viscosity of the studied electrolytes.

The electrochemical analysis in the three electrodes cell of the vanadium electrolytes is undertaken in chapter III, expecting to understand the effect of several parameters on the resulting limiting current, aiming to extrapolate the results on the reactor/VRFB. The studied parameters include the electrode material (graphite felt and solid graphite), the vanadium oxidation states ($V^{(III)}$, $V^{(IV)}$ and $V^{(V)}$), the concentration of the active species and the presence of solid particles (vanadium salts and/or Ketjen Black).

In chapter IV the dissolution kinetics of two vanadium species (vanadyl sulfate $VOSO_4$ and vanadium pentoxide V_2O_5) are addressed. The aim is to get a better understanding of their dissolution mechanisms. The general purpose will then be to establish, through simple models, the corresponding kinetic laws; these laws will be used to calculate the dissolution rate and to describe the temporal evolution of the vanadium concentrations.

The last chapter of this thesis is dedicated to the conception, design and study of a VRFB based on a filter press reactor connected to two external storage tanks. The system operates with vanadium suspensions as electrolytes and the aim is to evaluate the enhancement of the energy density of the battery compared to the ‘all liquid’ VRFB. Recharge-discharge cycles are undertaken and the cell voltage, the electrodes overpotentials and the vanadium concentrations are monitored. Moreover mass balances for the various species at the macroscopic scale established and solved, and the corresponding results are compared with the experiments.

The study presented in this manuscript is closed with a general conclusion along with the required points remaining to consider finalizing the project (indicated as perspectives).

Chapter I – Vanadium redox flow battery: Positioning and State of the art

Table of contents:

Introduction

The production of energy has received considerable development in the recent years due to massive industrialization and technology developments. Fossil fuels and petroleum products were and still are very popular because of their high energy density, their ease of handling and their relatively easy storage and transport. However, when burned, carbon dioxide (CO_2) is formed in majority, and as function of the system various other gases *(carbon monoxide (CO), nitrogen oxides (NO_x), sulfur oxides (SO_x), volatile organic compounds (VOCs))* most often having a certain toxicity are produced. Moreover, particulate matter are emitted, having noticeable impact on health and environment and leading to global warming. Thus, a global campaign to search for effective and clean alternative fuels and energy storage systems started; it expects to expand the energy from different "natural" processes, mainly wind, hydropower and solar sources which became the focus of many governments, and encouraged research teams to take that path. Most of the sources of energy were widely studied, and optimized systems are currently operational; however, a need to find suitable storage systems that are cost effective and reliable at the grid scale is essential. The intermittency of the renewable energy sources adds a challenge to their storage in particular for non-stationary applications, where autonomy is needed (electric vehicles, computers, cell phones…).

Various methods were proposed for the energy storage for stationary systems: mechanical systems, water reservoirs (hydropower-dams), air compression systems, flywheels, chemical and thermal systems, hydrogen storage systems and electrochemistry (batteries, fuel cells). Until now, except the water reservoirs no other system can be considered as cost effective for large storage applications.

In this chapter, the different modes of stationary energy storage systems (ESS) will be developed briefly with their specifications and drawbacks. The main focus will be on the electrochemical storage through all-vanadium redox flow batteries (VRFB) which are the aim of this project. The different components of the VRFB will be developed with a focus on the characteristics of the electrolyte solutions and the problems encountered, facing the commercialization of the battery.

I.1. Energetic context and energy storage systems

Nowadays around the world, the energy is stored mainly by pumped hydro energy storage (PHES) that accounts for 140 GW of the centralized energy, followed by 400 MW stored through compressed air and wind turbines, 300 MW in sodium–sulfur batteries, 270 MW in lithium–ion batteries and 100 MW in lead batteries [1]; this energy stored accounts for only 1/130 of the worldwide energy consumption which was 18 TW in 2019 [2]. The electrochemical storage of energy with different kinds of batteries has increased in interest in the last decade,

mainly because they are easier to handle and more susceptible to be used for non-stationary applications, and large scale energy grids can be achieved through redox flow batteries.

The selection of an appropriate energy storage system (ESS) for energies from renewable sources depends on a number of factors such as storage investment costs and electrical power, cycling life, energy efficiency, temperature, humidity and salinity conditions and most importantly security and environment [3]. Numerous techniques have been introduced in the past few decades and are based mainly on hydropower, air compression and electrochemical conversion.

Hydropower or pumped hydro energy storage (PHES) had a peak evolution in the 1970s, after the oil crisis and most of the plants were build between the 1960s and the late 1980s [4-5]. The fundamental principle of PHES is hydraulic potential energy: at times of low demand, the electricity serves to pump water from a lower reservoir to a higher reservoir. Recovering the electricity during periods of high demand is done by powering a turbine through the descent of water by gravity from the higher to the lower reservoir. The efficiency of this storage system can reach between 70 and 80 % with a typical rating between 1000 and 3000 MW [6]. The limitations of this ESS are the water availability, a favorable geographical location and topography (high surfaces), satisfactory geotechnical conditions and access to electricity transmission networks. The power capital cost of the PHES is estimated to be between 2000 and 4300 $/kWh and the energy capital cost between 5 and 100 $/kWh [4].

Another storage system is compressed air energy storage (CAES), introduced in the 1940s but was not truly developed until the 1970s. The basic concept of the CAES system is that the electricity powers a compressor that converts the electric energy into potential energy of pressurized air, stored typically in underground caverns. The release of this air by expansion through an air turbine regenerates the electricity stored, according to demand [7-8]. However, the limited success of CAES comes from several economical and technical aspects such as lower cycle efficiencies than PHES or batteries, geological restrictions and efficiency losses due to dissipation of thermal energy during compression and expansion. Hybrid techniques between CAES and PHES have been considered using a micro-pump turbine (MPT) [5] including two tanks, one open to the air and the other subjected to compressed air. The MPT uses the exceeding power from the grid to pump the water, which compresses the air, to be stored. In the recovery process, the energy in the air is released to drive water through the MPT to generate power. PHES and CAES are considered to have large power and storage capacities compared to other storage systems, but as mentioned before, they are limited by the geology and the availability of water and empty underground caverns and this contributes in the increase of the power capital costs to a range between 400 and 800 $/kW [6].

Energy can also be stored in the form of kinetic energy using flywheels (FW) [9], which is considered to be one of the oldest mechanical ESS; for example, they were used on trains and steam engine boats and as energy accumulators in factories during the 18th century. It is only in recent years that the improvements in materials, magnetic bearings, power electronics, and the introduction of high speed electric machines that allowed the introduction of the FW as a valid option for energy storage applications [10]. The energy in flywheels is stored in the form of rotational kinetic energy of a spinning mass, where a rotational disk connected to an electric machine speeds up for storing the energy and slows down for its regeneration as required [9-10]. The advantages of the FW such as low maintenance, fast response time, high energy efficiency and eco-friendly features are confronted with costly cryogenic cooling devices which increases the total cost of the FW and reduces the overall energy efficiency, in addition to containment problems, high friction and gyroscopic effects from the Earth's rotation. The installation costs of FW are also high, between 1500 and 6000 $/kWh [11], with power costs of 250-350 $/kW [6].

The fourth most important energy storage system is the thermal storage, first investigated in the 1970's after the energy shortage crisis [12], and it is divided to three main categories: sensible heat, phase change and chemical reaction. By using sensible heat technique, thermal energy is stored by raising the temperature of a liquid or a solid, and depends on the specific heat of the material, the temperature increase and the amount of available material. Aquifer systems, rock beds and ground and soil systems are among the most used structures for the sensible heat energy storage. For the phase change (or latent heat), as the name suggests, it is based on the phase change of a material with temperature, thus absorbing or releasing heat in the form of latent heat in isothermal conditions. Organic, inorganic or eutectic substances (phase change materials or PCM) are used for their thermal, physical, chemical, kinetic and economic properties and are chosen as a function of the application of the latent heat technology [13]. Lastly, thermal storage by chemical reaction relies upon a reversible reaction between two substances A and B (A + B ⇆ C + heat), with an exothermic synthesis and an endothermic decomposition process. The reaction can also occur by sorption processes (adsorption or absorption) depending on the material used. Chemical storage has some advantages, such as low heat losses, capability to conserve energy at ambient temperature as long as desired because the reagents A and B can be stored, after separation, for a long period, and finally, as function of the reaction, a high energy density can be stored. However, the studies on the chemical storage are still in their early stages and are not yet as developed as the phase change or the sensible heat techniques. The capital cost, calculated on a power density base, for thermal energy storage is 200 to 300 $/kW and 3 to 60 $/kWh for energy based calculations [14].

The numerous advantages provided by the thermal storage systems, such as reliability (sensible heat), providing thermal energy at constant temperature (phase change) and negligible heat loss (thermochemical), are confronted with the high cost of these techniques, the low energy density of the sensible heat, the corrosion that results from the latent heat processes and the uncertain

stability of the chemical reaction technique and many other setbacks that limit the applicability of these ESS.

The superconducting magnetic energy storage (SMES) is another ESS based on the creation of a magnetic field in an induction-coil, using electricity [15]; a superconductor with no resistive losses operates at a cryogenic temperature and produces a magnetic field. The energy produced remains constant and is stored until required usage. However, the energy density of the SMES is limited by mechanical considerations to a rather low value of around 10 $kJ.kg^{-1}$ [16]; the coil and the magnet must be strong enough to withstand the large magnetic forces when energized, but its power density can be extremely high with a cost of 150 to 250 $/kW [17]. Therefore, SMES are interesting for high-power and short-time applications but not applicable for large grid storage systems.

All the previously mentioned EES have their specific features, with their respective pros and cons, making each one suitable for their aimed applications: PHES, CAES and thermal energy storage correspond to long-time scale (hours) storage while flywheels and SMES have a fast response time (s-min time scale) but are considered as expensive systems.

Lastly, the storage techniques that are mostly spread are the ones using electrochemistry and they are classified according to their operating mode:

- quasi-reversible conversion of electrical to chemical/physical energy and the corresponding reverse process (batteries and super-capacitors);
- conversion of the electrical energy to chemical energy (electrolysers for the production of electroactive materials);
- conversion of the chemical energy to electricity (fuel cells).

Electrochemical energy storage strongly expanded in the last few decades, and important efforts were spent to optimize the techniques mentioned above. All of these techniques are presented in the simplified Ragone diagrams (Fig.I.1), which show comparatively the power and the energy of each system. In fact, power and energy are the two universal parameters that allow comparing all ESS. Capacitors, for example, have a specific power similar and even higher than combustion engines (based on fossil fuels) but their power is at least 10^4 times lower. The application range of capacitors is limited to backup circuits of microcomputers, smoothing circuits of power supplies and timer circuits that make use of the periods to charge or discharge electricity [18] because of the law quantity of energy that they can store despite their high specific power.

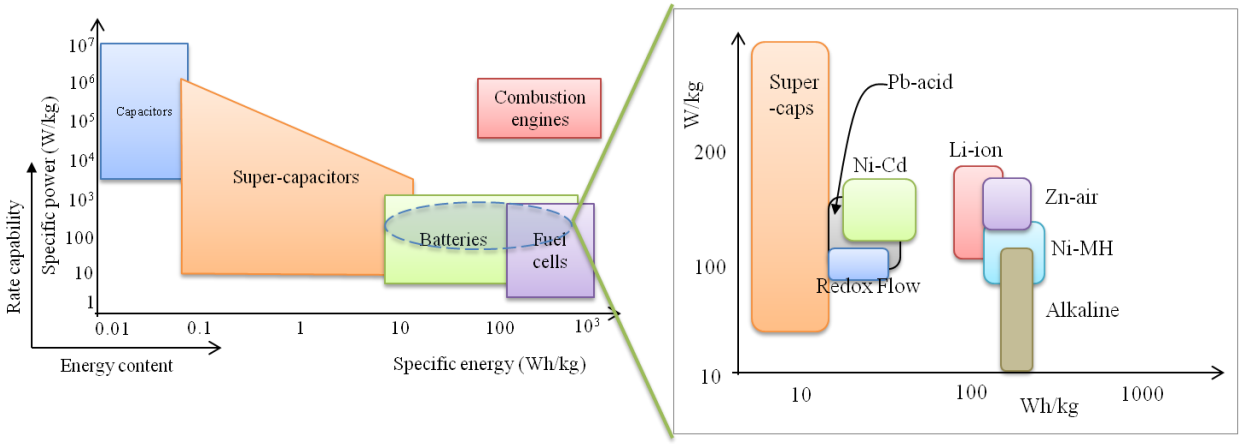

Fig.I.1: **Left**: Simplified Ragone diagram of the energy storage domain for electrochemical energy conversion systems compared to an internal combustion engine [adapted from 19]; **Right**: focus on the different battery types.

The electrolytic capacitors or super-capacitors or electric double-layer capacitor are considered as second generation capacitors; the electric energy is stored in an electrochemical double layer formed at a solid-electrolyte interface [20]. The capacitance can be increased by increasing the effective internal surface of the electrodes by using porous electrodes while various electrolyte – electrode couples were studied for improving the performances. Super-capacitors are considered to be safe devices, do not require cooling systems, are environmentally friendly and have high cycle-life. However, they are restricted to low energy applications, otherwise, it would require several cells. Also, they must become cost competitive in comparison with batteries since they cost 100 to 300 $/kW (or 300 to 2000 $/kWh) [14].

Before addressing batteries, one ESS remains: fuel cells, with the mostly known system, the hydrogen storage. The fuel cells are systems that produce electricity and heat as long as fuel is supplied. Different types of fuel cells exist nowadays such as polymer electrolyte membrane (PEM) fuel cells, direct-methanol fuel cell (DMFC), alkaline fuel cells and solid oxide fuel cells and they differ by the type of electrolyte employed. In fact, the fuel cells are formed by two electrodes separated by an electrolyte. Their operating mode can be described by the following: the hydrogen, stored in liquid, solid or gaseous forms, enters the fuel cell at the anode where it is split into protons, then the protons are transported to the cathode where they react with oxygen to form water and release heat [21]; thus, the principle of a fuel cell is not based on combustion but on an electrochemical reaction. Therefore, the direct production of electricity from hydrogen without the generation of undesirable waste products puts the fuel cells as a suitable candidate for stationary and non-stationary applications. Nonetheless, these systems are confronted with many disadvantages such as the production and source of hydrogen: 95 % of H_2 production is from fossil fuels reforming [22]; this not only generates CO_2 but also can be the source of impurities (CO residues, NO_x, H_2S…) in the fuel cells. These contaminants affect the performances of the cell by poisoning the electrode catalysts, reducing the conductivity and the mass transfer [23]. It is worth mentioning as well the high costs relative to a fuel cell system

from the membrane and the electrode materials usually noble metals. The average capital cost of a hydrogen fuel cell can go from 500 to 10 000 $/kW [14] depending on the material used.

Last but not least, the most commonly used form of energy storage, especially for mobile applications, are the batteries. A wide diversity of batteries (secondary batteries, i.e. rechargeable batteries) exists and some of them are presented in Fig.I.1; they are differentiated mainly by the nature of their electrolytes (aqueous or organic) and their operating temperature. The batteries are based on electrochemical reactions occurring for the charge and discharge: during the charge, the electricity provides the required energy to the system to perform the non-spontaneous reactions and during the discharge the opposite spontaneous reactions take place to regenerate the stored energy. The batteries could also be classified as function of the method employed for storing the electroactive elements [24]:

- inside the battery for stationary used systems (Pb-acid batteries, alkaline, Li,…);
- outside the battery with flowing electrolytic solutions containing redox active species through the battery (redox flow).

The first rechargeable batteries, introduced in 1859, were the lead-acid batteries. The positive electrode is composed by the system $PbO_2/PbSO_4$ while the system $PbSO_4/Pb$ constitutes the negative one; the electrodes are separated by a simple felt and sulfuric acid is the used electrolyte. They are among the systems that are still used nowadays because of their low cost for large power applications (< 300 $/kWh [14]), but due to the corrosive nature of their electrolytes and the toxicity of the lead, global tendency goes towards replacing them with more eco-friendly systems. Nickel – Cadmium (Ni-Cd) batteries were introduced after that with a higher capacity than the lead, but their success was hindered due to: i) the memory effect during charge – discharge cycles, problematic for the battery's life, and ii) because the toxicity of the cadmium. In table I.1, the different characteristics of the batteries are gathered together for comparison [3].

Lithium-ion (Li-ion) batteries have witnessed an important success thanks to their relatively high cell voltage (~ 3.7 V in the existing batteries). It can discharge to up to 95 % of its capacity and reach until more than 1000 cycles (if the cycling capacity is monitored between 40 and 75 %), compared to 1500 for the Pb-acid batteries. The positive electrode in Li-ion batteries is a lithium metal oxide ($LiCoO_2$) while the negative electrode is made of graphite. The electrolyte is an organic solvent in which is dissolved a lithium salt or polymer [6]. Their high energy density makes them a very good candidate for electric vehicles but their applicability is still hindered by their high costs (the power cost can reach up to 4000 $/Wh [6]) and safety concerns.

Table I.1: Main characteristics of the batteries used as energy storage systems with their respective advantages and disadvantages [3]

Technology	Pb-acid	Ni-Cd	Ni-MH	Li-ion
Cost (€/kWh)	25 – 200	80 – 1000	275 – 1500	459 – 560
Specific power (W/kg)	1 – 300	10 – 1000	10 – 1500	4 – 4500
Specific energy (Wh/kg)	30 – 50	40 – 60	50 – 80	75 – 250
Number of cycles	300 – 1500	1000 – 2000	500 – 800	1000 – 10000
Temperature (°C)	20 – 40	-40 – 50	0 – 45	-20 – 60
Energetic efficiency (%)	70 – 92	60 – 70	60 – 66	95 – 99
Auto-discharge (%/day)	0.1 – 0.3	0.2 – 0.6	1	0.1 – 0.3
Memory effect	No	Yes	Yes	Low
Advantages	Abundant raw material, low cost	Average energy density and energetic efficiency	Average energy density	High energy density, resistance, low auto-discharge, long lifespan
Disadvantages	Low energy density, limited lifespan, toxicity	Limited lifespan, toxicity	Low energetic efficiency	Security, high costs sometimes, limited raw material

The Nickel-Cadmium (Ni-Cd) batteries use metallic cadmium and nickel oxide as electrodes and an aqueous alkali solution as the electrolyte. Their weakness comes from the toxicity of the used material (Ni and Cd) and the decrease of the maximum capacity if repeatedly recharged after partial discharges [25]. The Nickel-Metal Hybride (Ni-MH) batteries are similar to the previous ones except that the cadmium electrode is replaced by a hydrogen absorbing alloy which makes them more environmentally friendly. However, their performances decrease as well after a few hundreds of cycles (table I.1).

Compared to all other types of batteries and capacitors, the redox flow batteries are systems having the advantage of decoupling the power and energy efficiencies which is a property that makes them interesting for many applications. The power depends both on the redox system involved as well as on the performances of the electrode/electrochemical reactor, while the amount of energy stored is a function of the quantity of the electrolytic solutions.

The next section of this chapter will be devoted to the development and description of the different types of existing redox flow batteries to better understand their operating mode and their different characteristics.

I.2. Redox flow batteries

The redox flow batteries (RFB) were first introduced by L.H. Thaller in the 1970s as a part of a National Aeronautics and Space Administration (NASA) project after the mid-70's energy crisis [26]. The objective was to find an energy storage system with a non destructive electrolyte during phases of charge and discharge, without the need to function at high temperatures and with a high overall energy efficiency and lifespan.

I.2.1. Definition and operating mode

A redox flow battery is a device conceived to convert the electric energy and store it into a chemical form. The reverse process aims to the regeneration of the electricity, according to demand. The basic design of RFBs is a divided electrochemical reactor connected to two storage tanks containing the (electro)active species at the chosen quantity. The electrolytes flow through the reactor via a pumping system (Fig.I.2). The electrolyte solution connected to the negative electrode (on which occurs the reduction during the charge and oxidation during the discharge) will be referred to in the manuscript as **negolyte**, and the electrolyte of the opposite compartment will be the **posolyte**.

The negolyte and the posolyte are fluid electrolytes containing each a redox couple dissolved in an adequate supporting electrolyte. The migration of ions, mainly protons in aqueous acidic systems, through the membrane ensures the ionic connection between both compartments [27-28].

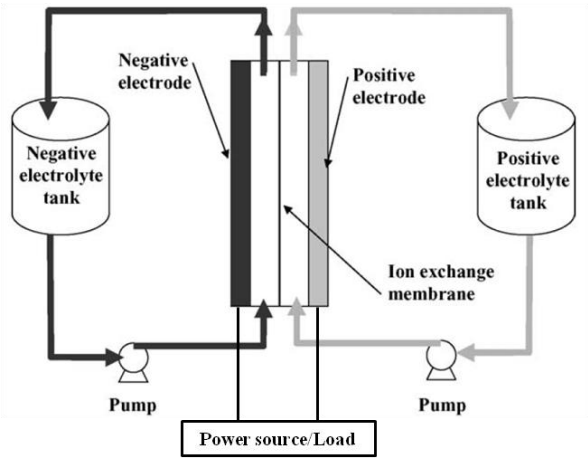

Fig.I.2: Schematic presentation of a single unit of a redox flow battery [adapted from 24]

The scale-up of the RFB can be achieved by: i) increasing the electrodes size, ii) connecting several single unit cells in parallel configuration and iii) increasing the electrolyte volumes. Theoretically, an unlimited capacity can be obtained by increasing the size of storage tanks, while practically the energy of the present designs reaches 10^2 to 10^7 Wh [29].

The performance of the redox flow battery depends strongly on: the reactive species properties and their affinity to the electrode, the electrodes material, the membrane selectivity and the efficiency of the mass-transfer in the reactor. The majority of RFBs electrolytes are based on metal ions and halogen ions because of the high solubility of these species in aqueous media [29]. Hence, the oxidized and reduced forms of each redox couple are soluble in the supporting electrolyte so that they can be circulated in and out of the corresponding electrode compartments and remain in the same liquid phase. During charge and discharge of the battery, theoretically no chemical consumption of the active species occur; only a change in the valence of the metal ions involved takes place, keeping a total amount of active species constant at all times, in addition to an unmodified electrode in ideal systems. These properties give the RFB its long lifespan (in the absence of crossover problems). Also, since the two electrolytes are stored in separate storage tanks, no self-discharge of the battery can occur (except for the solution contained into the electrolytic compartment, which is negligible compared to the volume of the storage tank) and it can be left completely discharged for long periods of time with no negative effects on the properties of the electrolyte solutions.

Another important component of the RFBs is the separation membrane; in acidic solutions, the cationic membrane used enables a selective passage of protons (to ensure the ionic conductivity and electroneutrality of the system) and, theoretically limits the transport of the electroactive species between compartments, thus expecting to prevent their transport and to limit as much as possible the crossover.
The choice of the materials of the working electrodes has a major impact on the total cost of the RBFs and also on its performance. Thus, a broad choice of electrode materials can be used; for the vanadium redox flow battery (the battery of interest) some of them are porous or massive/solid carbon, single or polymer-based graphite, modified or treated, and they will be discussed below.

Thus, the advantages of RFBs are their good scalability, flexible operation and moderate maintenance cost. They can be refueled easily by exchanging the discharged electrolyte solutions by a new fully charged one when needed [27]. The only moving parts of these batteries are the pumps circulating the electrolytes. In addition, the possibility of increasing the amount of stored energy by increasing the volume and/or concentration of electrolytes makes them suitable for large-grid energy storage applications. However, these technologies are still confronted with several setbacks:

- Low energy and power density compared to other ESS;

- The temperature of the electrolyte solutions should be controlled (to stay between 15 and 40 °C) to prevent the precipitation of the active species which are used at high concentrations, thus the possibility of precipitation;
- The crossover observed in many systems leads to electrolytes poisoning, which reduces the performance of the battery and causes its overall cost to increase (raw material and maintenance);
- Compared to other batteries, the RFBs have a significant global size conferred by the electrolyte storage tanks which can be voluminous making these systems unsuitable yet for mobile applications but more attractive for stationary uses. In fact, major installations of RFBs (all-vanadium, zin-bromine, and bromine-polysulphide) for load-leveling applications with multi-MW systems (from 100 kW to 120 MW) have been installed worldwide (Japan, Scotland, Australia, USA) [30].
- The toxicity of some of the active species employed does not concur with the general tendency of environmental-friendly and safe ESS. However the possibility to recycle the electrolyte for an infinite number of times minimizes this drawback;
- The use of aqueous electrolytes in highly acidic media poses the problem of corrosion as well, especially for the pumping system that could generate major issues [31].

I.2.2. Types of redox flow batteries and recent advances

The choice of the adequate redox couples for the battery must take into account their chemical stability and the necessity to prepare high concentrations, i.e. they must be highly soluble in the chosen supporting electrolyte. In addition, the redox potentials of the couples should be as far apart as possible in order to have an efficient battery (Power = cell voltage × current).

The first developed redox flow battery is the *iron/chromium redox systems*. The posolyte is constituted of the ferric–ferrous redox couple and the negolyte of the chromous–chromic couple both dissolved in concentrated hydrochloric acid HCl (2 $mol.L^{-1}$) [32], resulting in an open circuit voltage (OCP) of the battery of 1.18 V/SHE. This system, being one of the oldest ones existing, has been extensively studied, in order to improve its coulombic efficiency by:

- changing the electrode material;
- treating the electrode surface mainly to enhance the reversibility of the Cr^{2+}/Cr^{3+} system;
- the minimization of the crossover across the membrane (by changing the membrane type or by using pre-mixed electrolytes[1]).

However, several additional drawbacks such as the low density energy and the slow rate of the reaction of the Cr ions, compared to the rapid kinetics of the Fe^{2+}/Fe^{3+} system, led to halting further studies on the system.

[1] both the positive and negative electrolytes contain iron and chromium species as soluble salts in aqueous solutions of hydrochloric acid [27]

The *bromine/polysulfide flow battery* also called Regenesys cell, introduced in 1983, was found to be an interesting system owing to the low cost and abundance of the raw material in addition to their high solubility in aqueous media. The posolyte contains the bromine/bromide redox couple (Br^-/Br_3^-) while the negolyte is composed from the sulfide/polysulfide redox couple (S_2^{2-}/S_4^{2-}, as the simplified forms of the species), prepared initially from the dissolution of sodium bromide and sodium polysulfide. The open circuit voltage of a fully charged battery is 1.5 V [33] and could vary depending on the species concentrations, with cycling efficiencies of 60-65 %. A cation-exchange membrane is used in this system since all the active species are anions; thus the charge is carried through the membrane via the sodium ions without mixing of the species in the two compartments. However, one of the challenges encountered during the development of this system is the cross-contamination of the electrolytes, over a period of time, in addition to the possible loss of sulfur due to its deposition on the electrode or the membrane and also the formation of toxic gases such as Br_2 and H_2S [30,32].

Even if the bromine/polysulfide system did not reach a wide commercialization, the bromine/bromide redox couple was used as an electrolyte solution for other types of RFBs such as the *vanadium/bromine redox flow cell* which showed an energy density of up to 50 $Wh.kg^{-1}$ for 3-4 $mol.L^{-1}$ vanadium-bromide electrolyte solutions [34]. The system uses the $V^{(II)}/V^{(III)}$ couple in the negolyte and the Br^-/Br_3^- couple in the posolyte. However, this technology showed rapid losses of capacity due to the crossover across the membrane caused by the difference of ionic strength between the half-cells. Considerable efforts were put by several research teams to improve the properties of the membrane and add complexing agents to the bromine electrolyte [35] but these solutions appeared to be expensive for commercialization. Another bromine based battery is the *zinc/bromine redox flow cell* (ZBB) but this one is classified as a hybrid RFB, identically to all zinc-based batteries, because of the operating mode of the zinc inside the battery which involves its reversible deposition during the charge. The theoretical cell voltage of ZBB is between 1.5 and 1.6 V with a capacity ranging between 50 and 400 kWh, and a practical energy density around 65–75 $Wh.kg^{-1}$ [36]. The capital cost of the Zn-Br system is between 700 and 2500 $/kW (or 150-1000 $/kWh) [37]. Despite the favorable properties of this system, its drawbacks are numerous: dendrite formation during the zinc deposition, high cost electrode material, high self-discharge rate and most importantly, the difference between the kinetics of the Zn/Zn^{2+} and Br^-/Br_3^- electrode reactions. In fact, the zinc couple reacts faster which causes polarization and in the long run, battery failure. Even if modifications of the electrode were undertaken to improve the reactivity of the bromine/bromide redox couple on the positive electrode compartment, the problem never disappeared completely.

Various other zinc based hybrid redox batteries have been studied such as Zn-O_2, Zn-Ni and Zn-Ce and they all showed promising results in terms of energy efficiency; however, they also all show problems during the deposition of solid zinc and the appearance of dendrites and the subsequent short circuits [24, 30, 32, 36].

Another type of batteries is the *non-aqueous RFBs* which allow mainly expanding the operating electrochemical window, limited to 1.23 V in the case of water-based electrolytes. The redox couples employed include transition-metal bipyridyl complexes, acetylacetonate complexes and aromatic derivatives with lithium as the anode [38]. The main limitation of these systems is the difficulty to achieve high energy density due to the low solubility of the redox species in organic solvents (< 1 mol/L) [38] and the necessity to find adequate membrane material to reduce the cross-contamination and improve the ionic conductivity [39].

A novel approach for redox flow batteries is the semi-solid flow cell (SSFC); the new concept was introduced by Chiang and co-workers [40-41] in 2007 and it is based on the circulation of suspensions containing i) high concentration of the lithium active material, and ii) conductive nanoparticles expecting to create a percolating network. The aim of these batteries is to increase both the power and the energy densities. The lithium active species are in the form of micrometer-scale particles such as $LiCoO_2$, $LiFePO_4$, $LiNi_{0.5}Mn_{1.5}O_4$ (for the posolyte) and graphite/$Li_4Ti_5O_{12}$ (for example for the negolyte). The conductive nanoparticles are carbon particles: carbon blacks (ketjen black), vapor-grown carbon fibers or multiwall carbon nanotubes. The SSFC can be operated under two pumping modes:

i) under continuous flow in which the suspensions are only partially charged/discharged during the residence time in the electrolyser;

ii) an intermittent mode where a fraction of the suspension, introduced within the cell is completely charged or discharged, and then replaced by a new fraction of fresh suspension.

Other SSFC were introduced over the years such as Ni-MH flow cells [42].

The main drawback that could face the SSFC is the high viscosity of the suspensions, especially when increasing the solid load, which would introduce energy losses.

All the discussed RFBs have been tried over the years by important energy companies for scaling-up and large-grid usage. The capital cost of flow batteries is estimated to be between 180 and 250 $/kW [32] but this cost can vary depending on the specific technology, the electrode treatments and the membrane developments. Also, significant maintenance is required because of the cross-contamination problems inducing capacity losses in addition to poisoning of the electrolytes.

The introduction of the all-vanadium redox flow battery (VRFB) in the 1980's by M. Skyllas-Kazacos et al. [43] could help overcome one of these cited problems: the cross-contamination, since the active species in the electrolytes are formed by only one chemical element: vanadium.

The VRFB will be discussed in detail in the remaining part of the chapter with all its different components (electrolytes, electrodes, membrane) in addition to the drawbacks facing its commercialization and giving purpose to the present work. However, before that, some

characteristic parameters, used for the evaluation and comparison of batteries will be briefly developed in the next section.

I.2.3. Characteristic parameters for battery performance evaluation

The comparison between the performances of different types of batteries requires the evaluation of several parameters given the diversity of the systems and the material used (whether in terms of actives species, electrodes or membranes).

First of all, the energy density ($\mathbb{E}$) or stored capacity of the battery expressed in Wh/kg or in Wh /L, is calculated by the following relation [44]:

$$\mathbb{E} = \frac{\int_0^\infty \Delta V I dt}{3600 \xi MW} \qquad \text{Eq.I.1}$$

Where: ΔV: cell voltage of the battery (V);

I: flowing current (A);

dt: time for a total charge or discharge (s);

ξ: the lowest moles number of the posolyte or the negolyte, contained in the battery;

MW: molecular weight of the active species (kg/mol).

Secondly, the power density, expressed in W/kg or in W/L, is the rate at which energy can be extracted from the system per unit of its mass (or volume).

The operating cell voltage of the battery is partially fixed from the standard potentials $E°_{ox/red}$ of the redox couples constituting the system; this parameter is a function of the temperature and pressure of the systems.

The electrode potential of a redox couple is defined by the Nernst equation (Eq.I.2).

$$E = E°_{ox/red} + \frac{RT}{nF} log \frac{a_{ox}^{\alpha}}{a_{red}^{\beta}} \qquad \text{Eq.I.2}$$

Where:

a_{ox} and a_{red}: the activities of the activities of the active species in solution;

α and β: the stoechiometric coefficients of the oxidant and the reductant;

R: ideal gas constant, R = 8.314 $J.mol^{-1}.K^{-1}$ =1.98 $cal.mol^{-1}.K^{-1}$ = 0.082 $L.atm.K^{-1}.mol^{-1}$.

F: Faraday constant 96500 $C.mol^{-1}$.

n: the number of the electrons exchanged during the reaction

The efficiency of a system is defined as the ratio between the energy supplied during the discharge to the energy needed to recharge the battery to its full state of charge (SOC). The charge is expressed in Coulomb (C) but can be also given in Amperes – hours (Ah); 0 % SOC

corresponds to a completely discharged battery and a 100 % SOC corresponds to a fully charged battery. The opposite of the state of charge is the depth of discharge (DOD) sometimes used as well. The SOC can be defined by Eq.1.3:

$$SOC = 1 - \frac{\int_0^t I_{(t)}dt}{Q_n} = 1 - \frac{Q_{(t)}}{Q_n} = 1 - \frac{n_{mol\,(t)}}{n_{mol\,t=0}} \qquad \text{Eq.I.3}$$

Where:

Q_n: the maximum amount of charge that can be stored (usually defined by the manufacturer);

$\int_0^t I_{(t)}dt$: the amount of charge ($Q_{(t)}$) supplied by the battery after an electrolysis duration of t;

$n_{mol\,(t)}$: moles consumed after an electrolysis duration of t (determined by an external analysis);

$n_{mol\,t=0}$: moles initially present in the battery.

The SOC can be calculated also from the converted amount of species if their analysis or titration is possible; for example, the SOC of the vanadium redox flow battery can be calculated as:

$$SOC = \frac{[V^{(II)}]}{[V^{(II)}]+[V^{(III)}]} = \frac{[V^{(V)}]}{[V^{(V)}]+[V^{(IV)}]} \qquad \text{Eq.I.4}$$

Another important parameter presented in table I.1 is the number of cycles; this parameter is directly linked to the lifetime of the battery. A cycle is the process during which the battery undergoes a full charge followed by a complete discharge. The advantage of the all vanadium redox flow battery is its capacity to endure cycling without affecting much the lifespan of the battery. Deep discharges, i.e. to discharge the battery to its full capacity, are not recommended for solid batteries (such as for example the Pb-acid for which a solid-solid reaction occurs and it is advised not to discharge above 50 %) but could take place in the case of the redox flow batteries, because there is no destruction of the system.

The cost of a battery system is also a defining parameter for the choice of the storage system and its implementation. This cost embodies the installation and the maintenance costs; some technologies have a low capital cost (abundant raw material, classic and relatively low cost electrodes…) but they require important maintenance during their lifetime. The price of a system is often related to the power of the battery and expressed as $/kWh.

I.3. All-vanadium redox flow batteries

Vanadium has been the subject of many studies in different research domains. Its versatility as a metal made it useful in a variety of applications which led to its classification in 2017 as a critical raw material for the economy of the European Union [45]; Canada and the United States have also addressed this importance since the supply of these kinds of materials is not globally independent. The application of vanadium extends from the steel industry, where it is used in small quantities with other metals to improve the alloy properties and performances [46], to the medical and biological fields where it plays a role for the treatment of diabetes [47]. Table I.2 summarizes the main applications of the vanadium in the chemical and metallic industries [48].

Despite all that, the vanadium can be toxic and poisonous to the environment and to the human beings, depending on its form and its quantity [49-50]. Thus, due to this and to its several applications, numerous speciation and analysis techniques have been put in place for vanadium characterization but only the ones relative to the present work will be developed in chapter II.

Table I.2: Main applications of vanadium, as classified by the European commission in 2011 [48]

Application		Share
Chemical applications (catalyst for sulfuric acid and maleic anhydride production)		5 %
Steel industry	With carbon	12 %
	With tools/stainless	18 %
	Full alloy	25 %
	High strength low alloy	36 %
	Non-ferrous alloys	4 %

The vanadium sources are numerous and include ore feedstock from the earth's crust, seawater but also petroleum residues, and metallurgical slugs; it could be also recycled from steel scrap and spent catalysts [47-48]. However, vanadium is mostly imported to the EU and the amount recycled in Europe is only 44 % of the total vanadium used, according to the European Commission in 2017, and 40 % in the USA.

Until 2008 vanadium mining was concentrated in three countries: China, Russia and South Africa, to extend after that to the USA (0.4 %) and Brazil (10 %). Nonetheless, according to Petranikova et al. [48], the economy will not run out of vanadium in the near future and its criticality is not based on scarcity but on the concentration of mining in very few countries.

The introduction of the vanadium redox flow battery came as an additional source for vanadium consumption but its long lifetime and the possibility of vanadium regeneration and recycling during the functioning of the battery made its impact on the economy less heavy. The present part of the chapter will be dedicated to the detailed description of all the VRFB components, their drawbacks along with the recent advances.

I.3.1. Definition and characteristics of an all-vanadium battery

The vanadium redox flow battery was pioneered and developed by M. Skyllas-Kazacos and her co-workers, in the 1980's [43] at the University of New South Wales in Australia, and it came as a response to the problem of cross-contamination observed in all the other RFBs. In fact, the VRFB operates on the same principle as classic flow batteries: a divided continuously supplied

reactor in which the two compartments are separated by a membrane (Fig.I.3). Its difference (which is also its main advantage) is that the electrolytes are formed by the same chemical element, the vanadium at different oxidation states. Indeed, the vanadium exists in four main oxidation states: (II), (III), (IV) and (V), which also constitutes two redox couples. The posolyte is constituted by the VO_2^+/VO^{2+} couple (E° = 1.00 V/SHE) and the negolyte by the V^{3+}/V^{2+} couple (E° = -0.26 V/SHE), conferring to the VRFB a cell voltage of 1.26 V for a concentration of 1 mol.L^{-1} of each electrolyte and at 25 °C [24]. The capital cost of a VRFB is between 600 and 1500 $/kW (or 150 – 1000 $/kWh) [37].

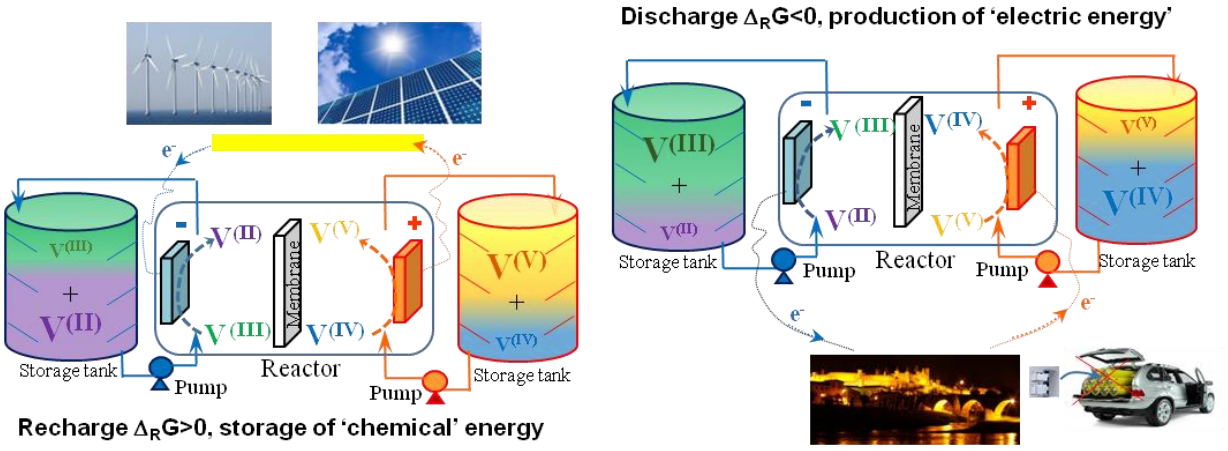

Fig.I.3: Schematic presentation of the all-vanadium redox flow battery during charge and discharge

As presented in the figure, each one of the four oxidation states of vanadium has a characteristic color when dissolved in concentrated sulfuric acid, used as supporting electrolyte: $V^{(II)}$ is violet, $V^{(III)}$ is green, $V^{(IV)}$ is blue and $V^{(V)}$ is yellow. This can be useful for a visual/qualitative interpretation of the state of charge of the battery. During the charge VO^{2+} is oxidized to VO_2^+ in the posolyte and V^{3+} reduced to V^{2+} in the negolyte; the opposite reactions take place during the discharge. All the reactions occurring in the battery's compartments are indicated in table I.3:

Table I.3: Reactions taking place in the battery's compartments

Simplified Half electronic reactions			Complete Half electronic reactions	
$VO^{2+} + H_2O \leftrightarrows VO_2^+ + 2\,H^+ + e^-$	Rx.I.1		$2\,VOSO_4 + 2\,H_2O \leftrightarrows (VO_2)_2SO_4 + H_2SO_4 + 2\,H^+ + 2\,e^-$	Rx.I.1'
$V^{3+} + e^- \leftrightarrows V^{2+}$	Rx.I.2		$V_2(SO_4)_3 + 2e^- + 2\,H^+ \leftrightarrows 2\,VSO_4 + H_2SO_4$	Rx.I.2'
Simplified global reaction			Complete global reaction	
$VO^{2+} + V^{3+} + H_2O \leftrightarrows VO_2^+ + V^{2+} + 2\,H^+$	Rx.I.3		$V_2(SO_4)_3 + 2\,H_2O + 2VOSO_4 \leftrightarrows (VO_2)_2SO_4 + 2\,H_2SO_4 + 2VSO_4$	Rx.I.3'

By writing the complete reactions (Rx.I.1' to Rx.I.3'), it appears that:

Phenomena occurring in the Posolyte		Phenomena occurring in the negolyte
recharge of the battery		
- consumption of 2 H_2O / 2 atoms of vanadium - production of 1 H_2SO_4/ 2 atoms of vanadium - production of 2 H^+/ 2 atoms of vanadium which must leave the posolyte and move to the negolyte towards the membrane.		- production of 1 H_2SO_4/ 2 atoms of vanadium - consumption of 2 H^+/ 2 atoms of vanadium which must arrive from the posolyte towards the membrane.
discharge of the battery		
- formation of 2 H_2O / 2 atoms of vanadium - consumption of 1 H_2SO_4 / 2 atoms of vanadium - consumption of 2 H^+/ 2 atoms of vanadium which must arrive from the negolyte towards the membrane.		- consumption of 1 H_2SO_4/ 2 atoms of vanadium - production of 2 H^+/ 2 atoms of vanadium which must leave the negolyte and go to the posolyte towards the membrane.

The first evident advantage brought by the VRFB is overcoming the poisoning of the electrolytes due to the cross-contamination occurring between the reactor compartments. In fact, if the vanadium crosses the membrane (depending on its selectivity), it will be converted to a species that already exists in solution. Even if there is a loss in the amount of charge, a complete recycling and treatment of the electrolytes is not necessary. The transfer of the vanadium between compartments can however lead to an imbalance of the concentrations but several solutions were found for that such as remixing the solutions and dividing them back into their respective compartments [51].

This advantage is added to all the pre-acquired characteristics of classic RFBs: short response time, low self discharge, long lifespan and decoupling of the power and energy densities for separate optimization as needed. The VRFB was found to have a lifetime between 5 and 10 years with more than 16 000 cycles [52] and a round-trip efficiency of 85 %. It is suitable for storage durations between a couple of hours and several months with autonomy ranging from seconds to 10 h and a power rating between 0.3 and 3 MW [52]. This battery is referred to as Generation 1 (G1) VRFB, whereas G2 corresponds to the vanadium–bromine system presented earlier.

Between 1996 and 2010, twelve major VRFB plants were installed around the world (Japan, South Africa, Italy, USA and Austria) with a specific power between 100 kWh and 5 MWh [27]. The implanted systems demonstrated very good performances in smoothing and leveling the fluctuating power generated by wind generators so worldwide development programs are working on improving and optimizing the vanadium redox flow battery to reach higher energy densities and become usable for wider applications.

I.3.2. Battery components: advances and specifications

The main parts constituting the battery and influencing its overall power and energy densities are: the electrodes, the electrolyte solutions and the membrane. Hence, each one of these components will be addressed separately in the following to present the different types and

configurations. In addition, the improvement of the stability and performances through additives (such as precipitation inhibitors) and electrode treatments will be briefly described as well.

I.3.2.1. Electrode types and activation techniques

The electrode is the key component of the core of the battery: it provides active site for the electrochemical reactions of the vanadium redox couples and thus plays a key role on the resulting power density as well as the life cycle of the battery. First of all, the kinetics of the electrodes reaction should be defined; they can be described by the Butler-Volmer law which takes into account the intrinsic heterogeneous electronic transfer kinetic constant (or rate constant) k°, the electrodes potential E, the concentration of the active species on the electrode-solution interface $C^{electrode}$ and the surface of the electrode S, i.e. in contact with the solution [53]. The most basic form of the BV law is expressed in Eq.I.5 for a reduction reaction on the cathode for example (ox. + ne^- → red.).

$$I = nFS(k°_c e^{\frac{-\beta nFE}{RT}} C_{ox.}^{electrode} - k°_a e^{\frac{-\alpha nFE}{RT}} C_{red.}^{electrode}) \qquad \text{Eq.I.5}$$

The constants $k°_c$ and $k°_b$ are respectively the intrinsic heterogeneous electronic transfer kinetic constants of the cathodic and anodic reactions while α and β correspond to the anodic and cathodic electronic transfer coefficients. However, this law is complex and in addition, the interfacial concentrations cannot be determined easily with the experimental conditions, so it is generally simplified according to the studied system; the idea is to be able to determine the characteristic rate constants which give an insight on the affinity between the electrode and the studied species.

Numerous electrode materials were studied as positive and negative electrodes for the VRFB using classic voltammetry curves (cyclic and linear voltammetry), charge-discharge cycles in addition to morphology studies of the electrode to be able to track the modification occurring on the surface and in depth of the studied material [54-55]. Voltammetry curves are used to measure the resulting current on a working electrode during potential scans; it gives information about the reversibility of the system and the electrochemical behavior of each species and its affinity to the electrode material. Note that fast charge transfer reactions, aiming to reduce the activation over-potentials of the active species, are of course preferred.

The chosen material must exhibit high electrical conductivity and should have high active surface area, low cost, good stability against acids, and electrochemical stability in the operation potential window of the VRFB. Carbon-based materials, such as graphite plates, glassy carbon, graphite felt, carbon paper, graphene oxide, carbon nanowires/nanotubes…, can be considered as interesting candidates for the battery as they are resistant to acid corrosion; in fact, it was found that they can be safely used for the negative compartment ($V^{(II)}/V^{(III)}$) but that they deteriorate

and mechanically disintegrate during the charge at the positive electrode due to oxygen evolution [56]. Metallic electrodes were addressed as well but often they are too expensive for subsequent large-scale storage. Thus, carbon-based electrodes were the ideal choice and the problem of degradation under high anodic potentials can be eliminated with voltage control during cycling.
On the other hand, it is important to understand the mechanisms taking place on the surface of the electrode. As proposed by Skyllas-Kazacos et al. [57-58] the interactions between the vanadium ions and a thermally treated carbon felt electrode were enhanced in the presence of oxygenated groups on its surface and the reactions occur in a three steps mechanism as schematically presented in Fig.I.4. In fact, the increase of the oxygen functional groups (especially hydroxyl groups) on the surface of the electrode provides active sites to catalyze the four active species [59]. It was suggested that the oxygen transfer on the positive electrode could be the limiting reaction of the overall mechanism, thus, an increase of the oxygen functional groups could help enhance the transfer process.

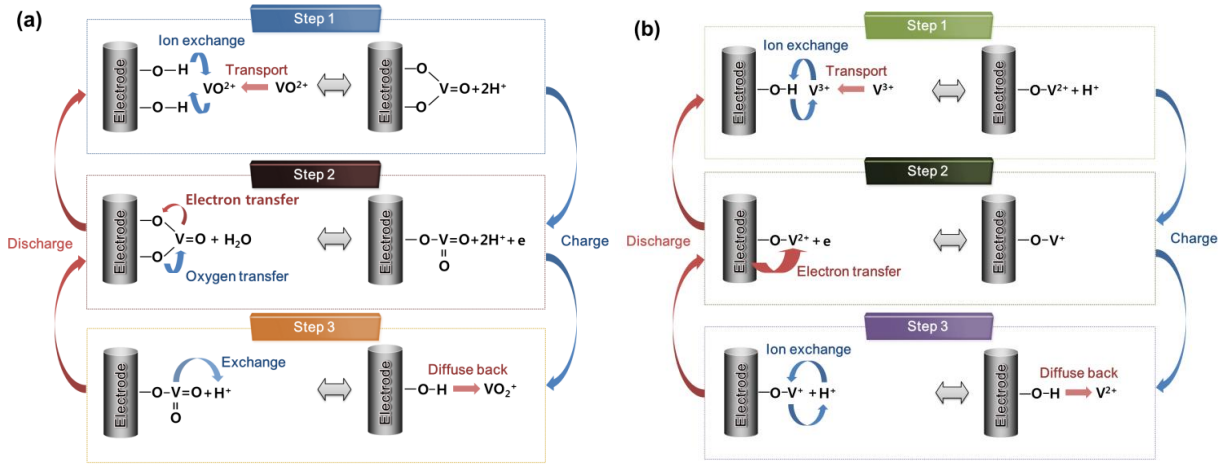

Fig.I.4: Schematic illustration of the redox reaction mechanisms for (a) the VO^{2+}/VO_2^{+} redox couple in the posolyte and (b) the V^{2+}/V^{3+} redox couple in the negolyte on the surface of a carbon felt electrode in a VRFB, proposed by Skyllas-Kazacos et al. [57-58]

Another study by Yue et al. [60] on carbon paper treated electrodes shows that hydroxyl functional groups on the electrode surface exhibits better electrochemical activity, especially for the negolyte, while Zhang et al. [61] emphasized the importance of C-OH and COOH groups to catalyze the oxidation of VO_2^{+} to VO^{2+}.

Thus, it is clear that on carbon based electrodes a treatment is necessary to produce oxygenated surface groups which are capable of enhancing the electrode reactions especially for the posolyte which appears to have more complicated kinetics due to the oxygen transfer between $V^{(IV)}$ and $V^{(V)}$. The electrode treatment techniques are various and include: structural modification, thermal treatment, acid treatment, metal doping….
In this work the untreated graphite was chosen and before any operation, it is submitted to an electrochemical treatment. The results will be presented in chapter III.

I.3.2.2. Electrolytic solutions

The composition (concentration of dissolved species) and the properties (density, viscosity and conductivity) of the active species affect the performances of the cell as well as the overall cost of the battery. In the case of the VRFB and as mentioned above, the electrolyte solutions are composed of vanadium ions dissolved in sulfuric acid acting as supporting electrolyte. The choice of this supporting electrolyte is of great importance, as it conditions the resulting vanadium dissolved concentrations, the conductivity and the aspect of the solutions.

In fact, the choice of an acidic instead of an alkaline supporting electrolyte was directly linked to a higher solubility of the vanadium salts in acidic media, in addition to a better conductivity insured by the presence of protons H^+ instead of hydroxide ions OH^-. On the other hand, M. Cheng studied the impact, on the vanadium reactions, of phosphoric and nitric acid as supporting electrolytes [62]. For solutions prepared in H_3PO_4, cyclic voltammetry curves of a $V^{(IV)}$ solution show the presence of several small peaks during the oxidation of $V^{(IV)}$ to $V^{(V)}$ instead of one large peak, which indicates the presence of more than one species in solution. In addition, the reduction peak of $V^{(V)}$ to $V^{(IV)}$ is not observed and this was attributed to the (insoluble) complex formed between $V^{(V)}$ and H_3PO_4 on the electrode surface.
As for the nitric acid HNO_3, the strong oxidizing properties of this solution were not suitable for the negolyte as it appeared to oxidize the $V^{(II)}$ formed on the electrode during the cyclic voltammetry scans and therefore will not be suitable for battery applications.

The other two acids studied are sulfuric and hydrochloric acid: the choice of H_2SO_4 was based on the gas production in case of overcharge. Indeed, HCl would produce the toxic chlorine Cl_2 gas whereas in presence of H_2SO_4 water oxidizes to oxygen, which is a much safer and environmentally acceptable gas [63]. Other researches were based on the use of a mixed supporting electrolyte H_2SO_4 – HCl and they will be discussed later.

The solubility and the behavior of the four vanadium salts strongly and specifically depend on the H_2SO_4 concentration and the temperature. It is thus necessary to find the adequate conditions which insure the maximum solubility and stability for these four species and correspond to the optimal energy density for the battery. Moreover the reaction produces/consumes protons, and it is important to operate with electrolytes having high conductivity and low viscosity.
The current VRFB operates with a dissolved vanadium concentration of 1.5–2 $mol.L^{-1}$ in 3–4 $mol.L^{-1}$ of H_2SO_4 with a maximum energy density of 40 $Wh.kg^{-1}$ and in a temperature range between 10 and 40 °C. It was found that a decrease in the total sulfate concentration or an increase in the temperature would lead to a decrease in the solubility of VO_2^+ and conversely an increase in the solubilities of the three other salts (V^{2+},V^{3+} and VO^{2+}) [63-65]; these characteristics will be developed in detail for each electrolyte further below.

The preparation of the electrolytes can be performed via numerous techniques but the most popular is the direct dissolution of vanadyl sulfate hydrate $VOSO_4.xH_2O$ because of its high solubility and its rapid dissolution in aqueous media (described below) giving VO^{2+} ions in solution. All the other oxidation states can be obtained by electro-oxidation or electro-reduction of the VO^{2+} in the battery, and this method was also adapted for the present work.
However, due to the high cost of this powder, researches aimed to replace it by lower cost raw materials such as vanadium pentoxide V_2O_5. This included the search for more complicated experimental setups for the solutions preparations by electrolytic or chemical dissolution methods for the production of the required vanadium concentrations [63]. A widely used technique is the reaction between vanadium pentoxide and vanadium trioxide in boiled sulfuric acid to form high concentrations of $V^{(IV)}$, instead of dissolution of the expensive sulfate, which can be later used for the electrolytic preparation of solutions of the other oxidation states.

The dissolved structures of the four oxidation states in aqueous media have been investigated by several techniques and it appears that both V^{2+} and V^{3+} ions are hydrated with 6 water molecules in an octahedral structure as $[V(H_2O)_6]^{2+}$ and $[V(H_2O)_6]^{3+}$ respectively [64]. As for the vanadium (IV), it has also an octahedral structure but it is composed of 5 water molecules and a vanadyl oxygen which results in a distorted structure for $[VO(H_2O)_5]^{2+}$. For the VO_2^+ ions, two hydration structures were suggested: the octahedral $[VO_2(H_2O)_4]^+$ and the bipyramidal $[VO_2(H_2O)_3]^+$ structures but by the intermediate of geometry optimization and thermodynamic calculations, the latter was found to be more stable and dominant.
Therefore, it is important to know the amount of water molecules immobilized in the structure of each vanadium molecule, because for concentrated electrolyte solutions this will be essential to be able to manage the water quantity in the battery.

I.3.2.2.1. Solubility and stability studies for the negolyte

The negolyte is a solution that contains the dissolved ions $V^{(II)}$ and $V^{(III)}$. The $V^{(II)}$ is known to be a strong reducing agent and was employed for a long time for visual potentiometric and amperometric titrations of various oxidizing agents [66]. Moreover, the V^{2+} ions are very sensitive to the presence of oxygen [67-68] and this induces instability of the negolyte and the necessity to maintain the storage tanks under continuous inert atmosphere.

Studies show that the $V^{(II)}$ and $V^{(III)}$ have the same behavior regarding the H_2SO_4 concentration and the temperature: their solubility increases with both temperature and pH. In fact, the decrease of the solubility with H_2SO_4 concentration is primarily due to the common sulfate ions effect, since both species precipitate in their sulfate forms, which shifts the equilibriums of Rx.I.4 and Rx.I.5 to the left. The solubilities of $V^{(II)}$ and $V^{(III)}$ in their sulfate forms, are presented in Fig.I.5 (according to Skyllas-Kazacos [63]).

$$VSO_{4\,(s)} \leftrightarrows V^{2+} + SO_4^{2-} \qquad \text{Rx.I.4}$$

$$V_2(SO_4)_{3\,(s)} \leftrightarrows 2\,V^{3+} + 3\,SO_4^{2-} \qquad \text{Rx.I.5}$$

It appears that the solubility of vanadium (II) is generally higher than that of vanadium (III) except for the lowest sulfuric acid concentration, where solubilities appear to be very close. The conclusion that we could draw from this figure is that for H_2SO_4 concentrations greater than 3 M and a temperature lower than 30 °C, the solubility of V^{3+} can be considered as limiting for the negolyte ($s_{V(III),\,10\,°C,\,3M\,H2SO4}$ = 1 M).

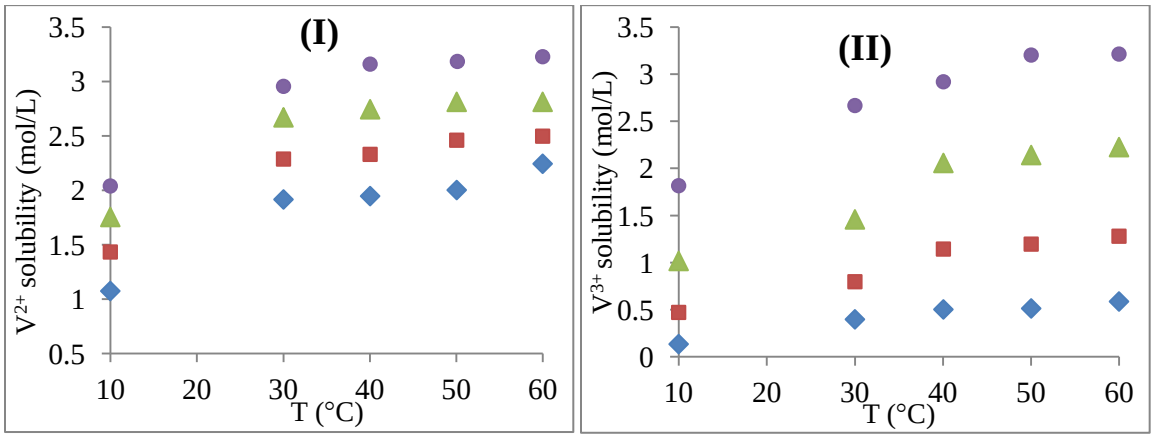

Fig.I.5: Variation of the V^{2+} **(I)** and V^{3+} **(II)** solubilities as a function of temperature (10, 30, 40, 50 and 60 °C) for H_2SO_4 concentrations of **2 (●), 3 (▲), 4 (■)** and **5 (◆)** $mol.L^{-1}$ [Adapted from 63]

The vanadium (III) solutions can be prepared by the direct dissolution of vanadium (III) chloride VCl_3 or vanadium trioxide V_2O_3 but both of them were not found suitable for the battery application. For the VCl_3, apart from releasing chloride ions in solution which may not be suitable for the functioning of the battery under H_2SO_4 conditions, it should also be handled carefully because it fumes in air if left exposed, and produces solid VCl_2 and gaseous VCl_4 and Cl_2 [69]. The dissolution of V_2O_3 allows obtaining a vanadium concentration of 2 M in 5 M sulfuric acid at 20 °C after 45 days under stirring, but the V_2O_3 of this solution transforms to $VOSO_4$ [70], impairing the stability of the solutions. Thus, the vanadium (III) solutions for most of the studies were usually prepared electrochemically by reduction of vanadium (IV) solutions.

A. Mousa studied the stability of vanadium (II) and (III) solutions in sulfuric acid [71]; it was found that the density and viscosity of $V^{(III)}$ solutions are proportional to the concentration of dissolved active species while the conductivity is inversely proportional to the vanadium (III) and sulfuric acid concentrations but directly proportional to the temperature. These interrelated parameters are important for the functioning of the battery as they have a direct impact on the current through the diffusion coefficient and could impact the kinetic rate constants as well. The viscosity of $V^{(III)}$ revealed a sharp increase in the high concentration range (1.3–1.5 M of $V_2(SO_4)_3$), from 1.7 cP for $[V_2(SO_4)_3]$ = 0.3 M to 6.2 cP for 1.3 M and 9.6 cP for 1.5 M of

$V_2(SO_4)_3$, in 2 M H_2SO_4 at 25 °C. This tendency was observed for all concentrations studied and was attributed to significant structure changes of the solution as the solute concentration increased above a critical value. The amount of free water molecules in solution becomes insufficient to hydrate the solute ions and this leads to more viscous fluids, closer to the flow properties of molten salts. Those studies were not performed on the vanadium (II) due to its instability to air which makes it difficult to handle.

An empirical model was put in place for the variation of the density d (g/cm^3) as a function of the vanadium (III) concentration ([V], mol/L), the temperature T (°C) and the sulfate concentration ($[SO_4^{2-}]$, mol/L) [71]; the model is presented in Eq.I.6, where A, B, C, D, E and F are empirical regression coefficients which exact values are not given in [71].

$$d = A + B[V] + C[V]^2 + D[SO_4^{2-}] + E[SO_4^{2-}]^2 + FT \qquad \text{Eq.I.6}$$

As for the variation of the viscosity of $V^{(III)}$ solutions, fitting a model to the experimental data was more complicated than for the density because of the high degree of saturation of the studied solutions and the lack of enough information to apply the known theoretical models [71] except for the modified form of the Jones-Doles equation, which led to the following model for the viscosity of $V^{(III)}$:

$$\eta = A + B[V]^{3.13} + C[SO_4^{2-}]^{0.61} + DT^{0.73} + E[V]^{0.74}[SO_4^{2-}]^{2.05} + F[V]^{2.02}T^{1.99} + G[SO_4^{2-}]^{0.75}T^{0.89} \qquad \text{Eq.I.7}$$

Where η is the measured viscosity in the solution in cP (centi-Poises) and [V], $[SO_4^{2-}]$ and T are as defined above. The values of the empirical regression coefficients (A to G) are not given.

On the other hand, the study of the precipitation kinetics of supersaturated $V^{(II)}$ and $V^{(III)}$ solutions [71-72] showed a different behavior for the two oxidation states. The degree of supersaturation is defined as the difference between the saturation concentration and the excess dissolved amount, i.e. the deviation from equilibrium.
The precipitation reaction order is confirmed by fitting the experimental results to the corresponding rate equations. A first-order mechanism (Eq.I.8) translates a diffusion-controlled precipitation, i.e. the diffusion of the precipitating species to the surface of the crystallization nuclei is the rate-determining step, while a second-order mechanism (Eq.I.9) describes a reaction controlled precipitation, i.e. the integration of the dissolved species into the structure of the crystal constitutes the rate-determining step.

1^{st} order: $$\ln(C_t - C_e) = \ln(C_0 - C_e) - kt \qquad \text{Eq.I.8}$$

2^{nd} order: $$\frac{1}{(C_t - C_e)} = \frac{1}{(C_0 - C_e)} - kt \qquad \text{Eq.I.9}$$

Where: C_t: vanadium concentration at time t (mol/L);

C_e: equilibrium vanadium concentration (mol/L);
C_0: initial vanadium concentration (mol/L);
k: rate constant.

$C_0 - C_e$: supersaturation

For $V^{(II)}$ sulfate solutions, the precipitation follows a first-order kinetic low, which means that it is a diffusion controlled mechanism and this was obtained whether the solution is stirred or stagnant and independently of the degree of supersaturation and with a low activation energy calculated for the precipitation studies at 1, 10,15 and 20 °C (10.7 and 14.5 kJ.mol^{-1} for stagnant and stirred respectively). However, in the case of vanadium (III) sulfate solutions, the observed behavior for the precipitation was different depending on the stirring and the degree of supersaturation; the results are grouped in table I.4.

Two cases from table I.4 are worth mentioning: high supersaturated stagnant and stirred solutions. For the stagnant solutions it appears that the mechanism changes during the precipitation and goes from a surface reaction controlled process to a diffusion control. This is attributed to the decrease of the diffusion rate with the decrease of the vanadium concentration gradient at the surface of the crystal as the supersaturation degree decreases [72]. Concerning the stirred solutions, it appears that the stirring supplies sufficiently the surface of the growing crystals with dissolved ions; this causes the decrease of the diffusion layer thickness and the increase of the diffusion flux. Consequently the limitation does not come from the mass transfer; it is assumed that the process of integrating the new particles into the structure of the crystal becomes the rate-determining step.

Table I.4: Kinetic law orders for the precipitation of vanadium (III) sulfate solutions as a function of the stirring and the degree of saturation

	Supersaturation	Kinetic order	Activation energy (kJ.mol^{-1})
Stagnant	Low	1 → diffusion control	14.6
	High	First 30 % → order 2	27.0
		Last 70 % → order 1	14.3
Stirred	Low	2 → surface reaction control	37.3
	High	1 but with surface reaction control	42.6

A comparison between the rate constant values of $V^{(II)}$ and $V^{(III)}$ sulfate precipitations, reported in [71] and determined as a function of the mechanism found for each case, shows that the values for $V^{(II)}$ are about 20 times higher than those of $V^{(III)}$. This is logical because the formation of $V^{(II)}$ crystals requires the integration of two atoms (1 V^{2+} and 1 SO_4^{2-}), without taking into

account their hydration degree, while the crystallization of $V^{(III)}$ requires the integration of five atoms (2 V^{3+} and 3 SO_4^{2-}) which would of course take more time.

In addition, kinetic studies of the co-precipitation of vanadium (II) sulfate and vanadium (III) sulfate in sulfuric acid media showed that each vanadium salt precipitates independently from the other with kinetic parameters similar to those established by its individual precipitation reported above.

The effect of temperature on the precipitation of 1.5 M solutions of V^{2+} and V^{3+} in 3.9 M total sulfate was studied by Xiao et al. [73] in order to try to extend the operating temperature range of the VRFB. It was found that the precipitation process is reversible and that after decreasing the temperatures of the solutions to – 35 °C, warming them for 30 minutes at 25 °C led to their complete re-dissolution. The electrochemical studies of these solutions across a temperature range between – 10 and 50 °C showed a decrease of the current density and increase of the irreversibility of the system when the temperature decreases. The diffusion coefficients, calculated for both ions, increase with the temperature which means that it intensifies the processes of mass transfer and charge transfer.

On the other hand, Fetyan et al. [74] studied the impact of the temperature on the evolution of hydrogen at the negative electrode during the charge of the battery, using a graphite felt electrode. It appears that increasing the temperature from 5 to 45 °C, causes the amount of hydrogen formed at the electrode to increase; besides the H^+ reduction starts at more positive potentials, which means that the faradaic yield of the vanadium reduction decreases thus implying losses in the energy efficiency. The study of the graphite felt used, by scanning electron microscopy and X-Ray photoelectron spectroscopy, showed a degradation of its surface, loss in conductive carbon and higher degree of oxidation on the surface of the fibers. This problem might be overcome if other electrode materials are used; however, even if the increase of the temperature stabilizes the electrolyte, the hydrogen evolution rate is never canceled.

It appears that the negolyte, apart from the instability of $V^{(II)}$ to air, does not introduce other limitations. Indeed, concentrations of around 3 $mol.L^{-1}$ can be reached for both V^{2+} and V^{3+} in 2 $mol.L^{-1}$ sulfuric acid at 30 °C. However, increasing the H_2SO_4 concentration only to 3 $mol.L^{-1}$ directly impacts the solubility of vanadium (III) which decreases approximately by half.

I.3.2.2.2. Solubility and stability studies for the posolyte

The posolyte has been widely addressed in the bibliography mainly because of the stability of its constituents. The vanadyl ion VO^{2+} is stable in aqueous acidic solutions for many months, but oxidation (by air) occurs easily in alkaline solutions [63]. It appears that VO^{2+} forms $VOSO_4$ ion

pairs with sulfate ions with an equilibrium constant of $3x10^2$ ($VO^{2+} + SO_4^{2+} \leftrightarrows VOSO_{4\ (ion\ pair)}$) but Vijayakumar el al. [75] found that the hydrated vanadyl ion $[VO(H_2O)_5]^{2+}$ is rather stable up to a concentration of 3 M within 240 – 340 K, with no strong interactions with sulfate anions which would occupy only its second coordination sphere. Therefore, dissolution of $VOSO_4$ powder in sulfuric acid should not encounter complexation problems. However, the concentration of sulfuric acid used influences the maximum concentration that can be dissolved, as does the operating temperature. The solubility values of vanadyl sulfate are reported in Fig.I.6, as given by F. Rahman [76]. The values presented in [63] for variable temperatures and H_2SO_4 concentrations are mostly identical to those presented below.

The study of the solubility of $V^{(IV)}$ as a function of H_2SO_4 concentration and temperature shows that the decrease of the solubility is more important when sulfuric acid is added to the solution: $s_{VO2+,\ 30°C}$ drops from 3.64 M to 2.15 M when $[H_2SO_4]_{initial}$ increases from 0 to 3 M then to 1.26 M for 5 M H_2SO_4. In fact, when the sulfate ions concentration is higher [76] the dissolution equilibrium of $VOSO_4$ powder, Rx.I.6, is shifted towards the left, leading to precipitation.

$$VOSO_4.xH_2O \leftrightarrow VO^{2+} + SO_4^{2-} + xH_2O \qquad \text{Rx.I.6}$$

The solubility variation of vanadium (IV) with the sulfuric acid concentration and the temperature was correlated by F. Rahman [70] by Eq.I.10. The average deviation obtained was about 4.5% and the maximum deviation was 12.0%, observed at the data point corresponding to 9M H_2SO_4 concentration and at 10 °C.

$$logS = C1 + \frac{C2}{T} + C3 \times T + \frac{C4\sqrt{m_s}}{1+C5\sqrt{m_s}} + C6m_s^{1/3} + \frac{C7 \times T}{m_s} \qquad \text{Eq.I.10}$$

Where: S: solubility of vanadyl sulfate (mol/L);

m_s: total sulfur concentration (SO_4^{2-} and HSO_4^-) (mol/L);

T: temperature (°C);

C1 to C7: regression constants (see table I.5)

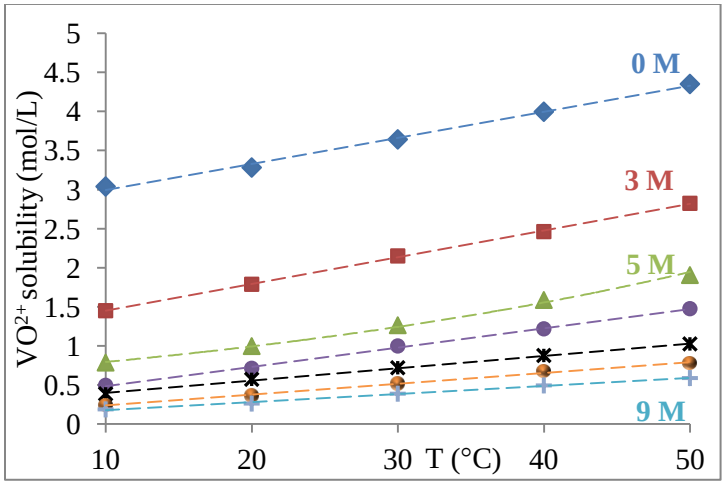

Fig.I.6: Effect of the temperature (10, 20, 30, 40 and 50 °C) on the solubility of vanadyl sulfate $VOSO_4$ in various initial sulfuric acid concentrations (from 0 to 9 M) [Adapted from 76]

Therefore, as observed in the case of $V^{(II)}$ and $V^{(III)}$ the solubility of vanadium (IV) ions is mostly limited by the common ion effect: the sulfate.
The second effect observed in Fig.I.6 is the temperature: the solubility increases with T from 1.5 to 2.8 mol.L^{-1} in 3 mol.L^{-1} initial acid when T increases from 10 to 50 °C.

The vanadium (V) was studied in aqueous solutions, by numerous authors who inferred the existence of many species as a function of the pH of the solution, presented in a predominance diagram in Fig.I.7.

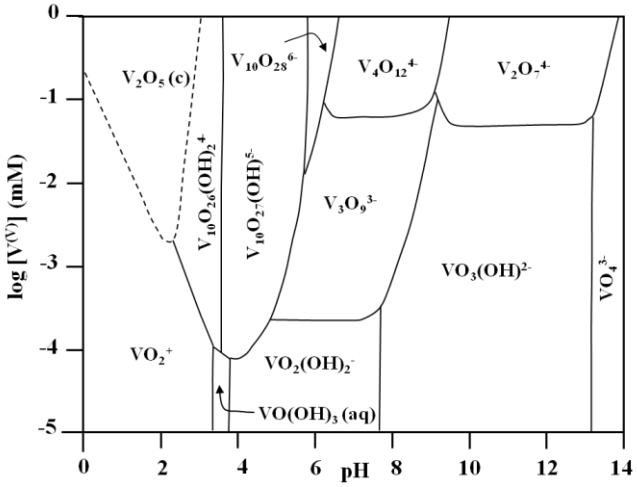

Fig.I.7: Predominance diagram of $V^{(V)}$ as a function of pH for a total ionic strength of 1 M and total vanadium concentration of 1 mM [Adapted from 77].

Although the concentrations used for the speciation diagram are much lower than those used in the VRFB, the dominant species in the VRFB electrolyte solutions can be considered to be VO_2^+ since the pH of the solutions is mostly closer to 0 and even negative, due to the high (2-3 mol.L^{-1}) concentration of acid used.

The studies of the vanadium (V) solubility were first performed by adding excess V_2O_5 powder to thermoregulated glass bottles containing an initial H_2SO_4 concentration [70]. The samples were left for 45 days to reach equilibrium with daily stirring before analyzing the dissolved fraction; results are presented in Fig.I.8. The effect of the studied parameters was already mentioned before: the solubility of $V^{(V)}$ decreases with temperature and increases with sulfuric acid concentration; concentrations of 3 mol.L^{-1} of $V^{(V)}$ can be reached in 9 mol.L^{-1} of H_2SO_4 at 10 °C but these conditions are not suitable for the other three species of the VRFB. The solubility of V_2O_5 at 30 °C and 3 M initial acid is only 0.5 mol.L^{-1} which is considered not sufficient for the functioning of the battery. The dissolution reaction (Rx.I.7) shows that the presence of protons in the solution (increased ratio of H^+ ions to $V^{(V)}$ ions) favors the equilibrium towards the left, i.e. the dissolution of the powder.

$$2\ VO_2^+ + H_2O \leftrightarrow\ V_2O_5 + 2\ H^+ \qquad \text{Rx.I.7}$$

The increase of the solubility at high sulfuric acid concentrations was explained also by the formation of vanadium-sulfate/bisulfate complexes and dimerisation/polymerisation of VO_2^+ ions ($V_2O_4^{3+}$ or $V_2O_3^{4+}$, reported by Madic et al. [78]).

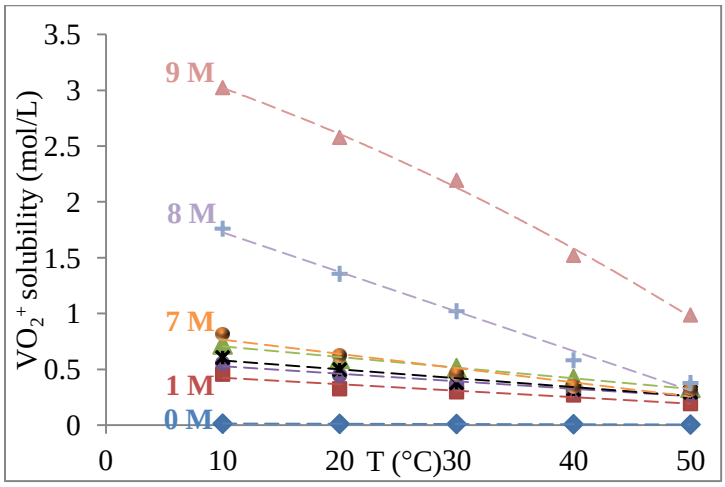

Fig.I.8: Effect of the temperature (10, 20, 30, 40 and 50 °C) on the solubility of vanadium (V), presented as VO_2^+, in various initial sulfuric acid concentrations (from 0 to 9 M) [Adapted from 70]

Similarly to the correlation of the solubility presented for the $V^{(IV)}$, Eq.I.11 gives the variation of the solubility of $V^{(V)}$, corresponding to the evolutions given in Fig.I.8 [70]. The average absolute deviation obtained was 16% with a maximum deviation of about 77% attributed to the difficulty of the interpretation of the V_2O_5 solubility data in the range 0 to 9 M of H_2SO_4. The maximum deviation can be reduced to 31 % if the sulfuric acid range taken into account is between 3 and 9 M. This equation is also presented in Eq.I.12.

$$logS = C1 + \frac{C2\sqrt{m}}{T^2} + \frac{C3 \times m^{1/3}}{T^3} + \frac{C4\sqrt{m}}{1+C5\sqrt{m}} + C6 \times m^2 + C7 \times m^3 \qquad \text{Eq.I.11}$$

$$logS = C1 + \frac{C2 \times m}{T} + \frac{C3 \times m}{T^2} + \frac{C4\sqrt{m}}{1+C5\sqrt{m}} + C6 \times m^2 + C7\sqrt{m} \qquad \text{Eq.I.12}$$

Where: S: solubility of the vanadium pentoxide (mol/L);

m: total sulfate concentration (mol/L);

T: Temperature (°C);

C1 to C7: regression constants (see table I.5)

Table I.5: Regression constants for solubility correlations of $VOSO_4$ and V_2O_5 in H_2SO_4 [70]

Regression constants	V_2O_5		$VOSO_4$
	0 – 9 M H_2SO_4	3 – 9 M H_2SO_4	
C1	-2.319	-20.442	-0.45
C2	65.05	2.995	0.017
C3	-656.9381	-18.698	-1.2
C4	2.6765	58.966	11.63
C5	0.7823	1.294	1.33
C6	-0.0593	0.0627	-3.5
C7	0.00614	-7.21	-0.04

Luckily, it was found that higher concentrations of VO_2^+ can be obtained differently from the electro-oxidation of concentrated $V^{(IV)}$ solutions [79].
To study the behavior of the concentrated vanadium (V) (from 2 to 5 M in VO_2^+, in 5 to 7 M total sulfate), solutions were prepared by electrolytic oxidation of corresponding $VOSO_4$ solutions [69]. The density, viscosity and conductivity of these solutions were studied and it was found that for a vanadium concentration greater than 3.5 M, the properties of the solutions are greatly altered: the viscosity exhibits a sudden steep increase and deviate the solution from the hydraulic flow region, i.e. exhibits a non Newtonian behavior. It was attributed to i) the formation of extended chains of polyvanadic molecules and ii) an increase of the ion-ion interactions, where the ion distribution at high supersaturation reaches a state looking like cristallinity. On the other hand, the conductivity was found to decrease with increasing $V^{(V)}$ concentration: at constant sulfate concentration, the increase of vanadium concentration will hold more sulfate/bisulfate ions, by the formation of ions pairs, which will induce a decrease of the free H_2SO_4 concentration, thus less free H^+ ions [69, 80].

On the other hand, the poor thermal stability of vanadium (V) solutions constitutes a problem as well. It was found that solutions of more than 2 M $V^{(V)}$ undergo thermal precipitation at temperatures above 40 °C when prepared in 2 M H_2SO_4 [80-81], but the precipitation, studied by Rahman [70], appeared to be slow as, for example, at 50 °C in 7 M total sulfate a 3.9 M $V^{(V)}$ solution did not show any sign of precipitation even after 60 days. However, this rate is not quantified and also studied at high sulfate concentrations (between 5 and 7 M) which are higher than to the amount used in the battery. In any case, the poor thermal stability of $V^{(V)}$ solutions was the subject of many studies in order to understand the problem. Kausar et al. [82-83] suggested that several $V^{(V)}$ complexes exist, formed by interactions with sulfate/bisulfate ions. In the absence of enough free H^+ ions, VO_2^+ transforms to VO_3^- which in turn forms HVO_3 that precipitates under high temperature to V_2O_5. Vijayakumar et al. [84] had a different explanation and they conducted Nuclear Magnetic Resonance (NMR) spectroscopy and density functional

theory (DFT) studies on 2 M VO_2^+ solutions in 5 M total sulfate between – 30 and 60 °C. They found that the hydrated $[VO_2(H_2O)_3]^+$ ion is stable for low temperatures but undergoes a deprotonation process to form neutral H_3VO_4 which in turn, through a condensation reaction of its hydroxyl groups, forms the precipitate V_2O_5, visible in solution as yellow-red particles. It can be confirmed that the precipitation process of $V^{(V)}$ is an endothermic reaction but it can be prevented by eliminating the deprotonation step by increasing the amount of free protons in solution, hence the stability of vanadium (V) solutions at high sulfuric acid concentrations.

The temperature effect on vanadium (IV) and (V) solutions was confirmed by Xiao et al. [73]. They studied the stability and reversibility of the precipitation in the same temperature range as performed for the $V^{(III)}$ and $V^{(II)}$ and they found that the precipitation of $V^{(IV)}$ at low temperatures (until – 35 °C) is reversible, i.e. re-heating the suspension leads to the dissolution of the precipitated powder. However, the thermal precipitation of $V^{(V)}$ at T > 40 °C appeared to be irreversible because cooling the solution did not lead to the re-dissolution of the precipitate. Authors assume that the precipitate is V_2O_5 with a very low solubility which explains its non-dissolution after thermal precipitation. Besides, electrochemical studies were performed in the temperature range from – 10 to 50 °C on a $V^{(IV)}$ solution at 1.5 M in 2.8 M H_2SO_4; results show that decreasing the temperature causes i) a decrease of the current density and ii) an increase of the irreversibility of the system (measured by the potentials difference between the anodic and the cathodic signals) [73]. The diffusion coefficients, calculated for both $V^{(IV)}$ and $V^{(V)}$, increase with the temperature, and the effect was more important in the case of $V^{(IV)}$.

In conclusion, the posolyte appears to be limited by the vanadium (V) poor thermal stability and needs the presence of high concentrations of acid to remain stable. Solutions of $V^{(IV)}$ at 2.8 M in 3 M H_2SO_4 can be reached at 50 °C and remain stable for several days.

I.3.2.3. Additives for improving the stability of the electrolytes

The analysis presented for the electrolytes clearly shows their instability towards two main and important factors: the sulfuric acid concentration and the temperature (the last makes the operating conditions of the battery restricted and limits its capacity). Researches have been done on the effect of adding stabilizing additives enabling to reach higher concentrations of vanadium in the electrolytes; however, the different properties of the four vanadium oxidation states, prevent finding a common additive [85].

The additives used for the stabilization of electrolyte solutions were classified on the basis of their function:

- precipitation inhibitors,
- immobilizing agents,

- kinetic enhancers,
- electrolyte impurities,
- chemical reductants.

A wide range of organic and inorganic additives have been proposed over the years [63, 85-88] but most of the organic proposed were found to be inadequate due to the oxidative nature of $V^{(V)}$. The impact of the added species on the overall performance of the battery should be studied in parallel with the total cost of the electrolytes. Since chemical additives do not enter in the scope of this work, we will develop this section further.

Other approaches for the optimization of electrolytes composition included the use of a mixed supporting electrolyte. The sulfuric acid, despite being found as suitable for the dissolution of the vanadium salts, appeared to be a key component for the optimization of the battery especially since its concentration had a different effect on $V^{(V)}$ than all other three oxidation states. Thus, a mixture of sulfuric and hydrochloric acid for the stabilization of vanadium (V) was introduced by Vijayakumar et al. [89]. The previously mentioned hydrated ion $[VO_2(H_2O)_3]^+$ exists in acidic solutions and depends on the vanadium and acid concentrations of the media. At vanadium concentrations greater than 1.75 M, they assume that it exists as the dimer $[V_2O_3.8H_2O]^{4+}$; the addition of HCl leads to the formation of $[V_2O_3Cl_2.6H_2O]^{2+}$ according to:

$$[V_2O_3.8H_2O]^{4+} + 2\ HCl \rightarrow [V_2O_3Cl_2.6H_2O]^{2+} + 2\ H_3O^+ \qquad \text{Rx.I.8}$$

The increase of the temperature for the mixture showed no precipitation of vanadium (V), contrary to what was observed earlier [84] and this was attributed to the formation of chloride based complexes: they assume that the de-protonation is harder for these species due to the electron donor ability of chloride molecule that increases the electron density of vanadium and reduces interactions with oxygen.
Using a mixed sulfate-chloride supporting electrolyte for the VRFB appeared to be beneficial for the four oxidation states [90]; only V^{3+} at 3 M in 2.5 M total sulfate and 6 M Cl^- showed precipitation after 8 days at – 5 °C. Also, in the presence of HCl, the solutions viscosity was found to be lower than for the solutions containing only sulfates, at the same temperature. An advanced vanadium redox flow battery utilizing mixed acid electrolytes was put in place by Kim et al. [91]; it supplies 1 kW/1 kWh for an energy efficiency of 82 % with no visible precipitation at electrolyte temperatures greater than 45 °C. It also allowed to reduce the cost of the battery by 50 $/kWh (average total cost between 150 and 450 $/kWh), compared to the conventional pure sulfate VRFB (200-500 $/kWh) [91].
Further development of the mixed acid VRFB should take into account the possible formation of chlorine gas or VCl_3 toxic powder.

I.3.2.4. Membrane and peripheral components

The membrane is the separator that divides the reactor into two compartments, separating the posolyte from the negolyte. Its main purpose is to prevent the cross-mixing of the electrolytes while allowing the protons to pass through and insure the ionic conductivity in the battery and maintain the electroneutrality of the system [92-93]. Thus, the chosen membrane should allow good selectivity, have chemical and mechanical stability and low electronic resistance and be of low cost. It should be also able to prevent the preferential transfer of water between compartments.
The most commonly used membrane for the VRFB is Nafion®, which is a high cost cationic exchange membrane [94-95]. The Teflon-based Nafion® 117 and the type 2 Selemion membranes offer the best performance in the vanadium cell with overall efficiencies of more than 85% [71]. However, in order to decrease the costs for separators, research teams started searching for alternative materials with optimized specifications.

The membranes for VRFBs are prepared by three main methods [96]:

1. Casting polymer solutions via their polycondensation with introduction of functional groups (anionic such as sulfonic acid or cationic like quaternary ammonium…) to increase the ionic conductivity of the membrane;
2. Reinforcing an existing ion conductive membrane: an ion exchange resin is introduced into a porous support, such as poly(ethylene) or polytetrafluoroethylene, followed by cross-linking to reinforce the material;
3. Grafting of polymerizable monomers to films to obtain grafted membranes.

The most challenging part for the membrane preparation is to find suitable material that could resist to the oxidative nature of $V^{(V)}$, which appear to be the most harmful component for the membrane [97], without reducing much the ionic conductivity of the material.

It is important to determine the values of the parameters influencing the performance of the VRFB, such as the diffusion coefficients of the species, the water permeability and the membrane resistance. The data from these studies can be found in the bibliography [98-100], and some of them will be used in chapter V for the mass balance studies during battery operation.

The other important parts of the battery to take into account for the optimization are [88]:

- The gasket (PTFE, PVC and silicone materials mostly used): their thickness defines the dimensions of the electrolytic compartment. They also help to prevent leakage from the reactor;
- Pumps: they determine the flow rate of the electrolytes in the reactor, thus, they can influence the residence time and the entire performance of the battery. The choice of the pumps should also take into account the power consumed during circulation, the heat generated as well as the corrosive nature of the electrolytes;

- The storage tanks: chosen as a function of the battery type, i.e. the circulation mode. If the battery works in recirculation mode, only two tanks are required, one for the posolyte and one for the negolyte, and this mode is more efficient, simpler and more economic. For the batch mode four tanks are needed: two for supply tanks and two for storage where the electrolytes are stored until they are drained through.

Therefore, all the constituent parts of the VRFB have an impact on its performance and energy efficiency and must be chosen correctly.

I.3.2.5. Vanadium solid-salt batteries

T. Yamamura et al. [101] presented the vanadium solid-salt battery (VSSB) as a new energy storage system based on the four vanadium oxidation states, aimed for electric vehicles and other mobile applications. The VSSB contains two sets of vanadium solid salts: $VOSO_4/(VO_2)_2SO_4$ solid in the positive half cell and $V_2(SO_4)_3/VSO_4$ solid in the negative half cell. The solid particles are supported on carbon felts with a minimal amount of H_2SO_4 added to moisten the ion-exchange membrane [102]. The energy density of the introduced VSSB reaches an average of 77 Wh/kg with an energy efficiency of 87 % and a cell voltage of 1.34 V, achieved at a current density of 5 mA/cm^2. The redox reactions taking place during the operation of the battery include the dissolution and the solidification of the active species. However, these systems are still in their early development stages and much work is needed to improve the acid to solid ratios, the sulfuric acid concentration (including the degree of moisture needed) and the membrane choice for optimal functioning.

I.3.3. Functioning of the VRFB during cycling

Performing charge/discharge cycles of the battery is an essential tool for studying its performance and the impact of the optimized parameters (electrode, membrane, electrolyte composition) on the energy and/or power density. The monitored parameter during cycling can be the variation of the cell voltage with time during numerous cycles at constant applied current (or potential) which allows calculating the energy efficiency and capacity decay of the VRFB.

The concentration variation of the four species is also usually monitored during the cycling which gives important insight on the SOC of the battery and more precision on where the problem might occur. In fact, S. Corcuera et al. [51] used the cycling to put in place a new technique for the SOC monitoring of the VRFB and determining the effect of electrolyte imbalances, due to crossover, on the capacity. The cell potential was kept constant between 1.8 V (during charge) and 0.8 V (during discharge) so the cycles duration starts to decrease with time due to losses from the crossover of electrolytes and the capacity drops from 1900 mAh to 250 mAh after 40 cycles.

Another approach, used by Li et al. [103], is the monitoring of the viscosity of the vanadium electrolytes for the monitoring of the state of charge during cycling and they developed an empirical model linking the SOC to the viscosity and temperature, by using the pressure, temperature and flow rate of the electrolytes as measurable parameters.

Numerous other methods are proposed for the monitoring of the performances of the battery during cycling [104-106], and in the present work, we propose to do so by a combination of the follow-up of the cell voltage with the titration of the four vanadium oxidation states. All the used methods will be developed in the upcoming chapters.

I.4. Conclusion

Energy storage systems have been, for the past decades, a global center of interest and worldwide studies are dedicated to their optimization and enhancement; the various existing systems were synthetically presented in this chapter with their pros and cons. Among the ESS, electrochemical storage and more specifically redox flow batteries appear to be a good candidate for large scale energy storage applications, but their main drawback is the cross-contamination of the electrolytes which leads to their poisoning and increases the overall maintenance costs of the system.

The all-vanadium redox flow battery emerged as a 'cleaner' RFB where the transport of species across the membrane does not deteriorate the solutions since the same element is used in both compartments. However, this battery suffers from low energy density (< 40 Wh/kg) due to the low solubility of the vanadium species in concentrated sulfuric acid and in a restraint temperature range (< 2 mol/L); the battery should operate between 10 and 40 °C to avoid the precipitation of $V^{(II)}$, $V^{(III)}$ and $V^{(IV)}$ at low temperatures and that of $V^{(V)}$ at high temperatures. Similarly, the sulfuric acid concentration should remain between 2 and 4 mol/L.
It was found that the thermal precipitation of vanadium (V) and its stabilization at high H_2SO_4 concentrations (9 mol/L) was the main reason for inability to work at high temperatures where the solubilities of the other oxidation states would increase; on the other hand, concentrated $V^{(V)}$ solutions (up to 5 mol/L) could be prepared from electrolytic oxidation of vanadium (IV) and these solutions, despite their viscosity would remain completely dissolved.

In this work, we propose to combine the principles of three systems together, by taking the best feature of each: the semi-solid flow cells, the vanadium solid-salt battery and the aqueous RFBs. In fact, the work will be based on an all-vanadium redox flow battery with suspensions as electrolytes, containing a mixture of dissolved vanadium in sulfuric acid solutions in addition to excess vanadium sulfate powders. The purpose is to increase the energy density of the battery

and be able to store more energy per unit volume, by the presence of a bigger amount of active species (with vanadium equivalent concentrations up to 3.5 mol/L in 2 mol/L initial sulfuric acid). These solid particles are thought to dissolve during the functioning of the battery by displacement of their equilibriums during conversions. In addition, the presence of carbon based additives (KB nanoparticles) is studied aiming to i) increase the power density of the battery by extending the electrode through a percolating network and ii) possibly creating nucleation sites for the precipitation of the vanadium salts.

The presented bibliography does not address the electrochemical studies of vanadium suspensions nor their cycling in a VRFB reactor. Thus, the present work aims to perform these studies, in addition to a series of analytical and physico-chemical methods for the characterization of the solutions and the suspensions.

References:

[1] A. Obadia, "Le stockage de l'énergie électrique : une dimension incontournable de la transition énergétique. Conseil économique social et environnemental", 2015
[2] BP Statistical Review of World Energy, 69th Edition, 2020
[3] D. Allart, "Gestion et modélisation électrothermique des batteries lithium-ion", Phd thesis, Génie électrique, Normandie, 2017
[4] E. Barbour, I.A. Grant Wilson, J. Radcliffe, Y. Ding, Y. Li, "A review of pumped hydro energy storage development in significant international electricity markets", Renewable and Sustainable Energy Reviews, 61, 2016, 421-432, doi: 10.1016/j.rser.2016.04.019
[5] S. Rehman, L.M. Al-Hadhrami, M. Alam, "Pumped hydro energy storage system: A technological review", Renewable and Sustainable Energy Reviews, 44, 2015, 586-598, doi: 10.1016/j.rser.2014.12.040
[6] R. Amirante, E. Cassone, E. Distaso, P. Tamburrano, "Overview on recent developments in energy storage: Mechanical, electrochemical and hydrogen technologies", Energy Conversion and Management, 132, 2017, 372-387, doi: 10.1016/j.enconman.2016.11.046
[7] M. Budt, D. Wolf, R. Span, J. Yan, "A review on compressed air energy storage: Basic principles, past milestones and recent developments", Applied Energy, 170, 2016, 250-268, doi: 10.1016/j.apenergy.2016.02.108
[8] G. Venkataramani, P. Parankusam, V. Ramalingam, J. Wang, "A review on compressed air energy storage – A pathway for smart grid and polygeneration", Renewable and Sustainable Energy Reviews, 62, 2016, 895-907, doi: 10.1016/j.rser.2016.05.002
[9] S.M. Mousavi G, F. Faraji, A. Majazi, K. Al-Haddad, "A comprehensive review of Flywheel Energy Storage System technology", Renewable and Sustainable Energy Reviews, 67, 2017, 477-490, doi: 10.1016/j.rser.2016.09.060
[10] M.E. Amiryar, K.R. Pullen, "A Review of Flywheel Energy Storage System Technologies and Their Applications", Appl. Sci., 7, 2017, 286, doi: 10.3390/app7030286
[11] IRENA (2017), Electricity Storage and Renewables: Costs and Markets to 2030, International Renewable Energy Agency, Abu Dhabi
[12] J. Xu, R.Z. Wang, Y. Li, "A review of available technologies for seasonal thermal energy storage", Solar Energy, 103, 2014, 610-638, doi: 10.1016/j.solener.2013.06.006.
[13] A. Sharma, V.V. Tyagi, C.R. Chen, D. Buddhi, "Review on thermal energy storage with phase change materials and applications", Renewable and Sustainable Energy Reviews, 13 (2), 2009, 318-345, doi: 10.1016/j.rser.2007.10.005
[14] S. Koohi-Fayegh, M.A. Rosen, "A review of energy storage types, applications and recent developments", Journal of Energy Storage, 27, 2020, 101047, doi: 10.1016/j.est.2019.101047
[15] X.D. Xue, K.W.E. Cheng, D. Sutanto, "A study of the status and future of superconducting magnetic energy storage in power systems", Superconductor Science and Technology, 19(6), 2006, R31–R39, doi:10.1088/0953-2048/19/6/r01
[16] P. Tixador, "Superconducting Magnetic Energy Storage: Status and Perspective", IEEE/CSC & ESAS European superconductivity news forum, No. 3, 2008

[17] V. Karasik, K. Dixon, C. Weber, B. Batchelder, G. Campbell, P. Ribeiro, "SMES For Power Utility Applications: A Review of Technical and Cost Considerations", IEEE Transactions On Applied Superconductivity, 9 (2), 1999, 541-546, doi: 10.1109/77.783354.
[18] M. Jayalakshmi, K. Balasubramanian, "Simple Capacitors to Supercapacitors - An Overview", Int. J. Electrochem Sci., 3, 2008, 1196-1217
[19] M. Winter, R. J. Brodd, "What are batteries, fuel cells, and supercapacitors?", Chem. Rev., 104(10), 2004, 4245–4270, doi: 10.1021/cr020730k
[20] R. Kötz, M. Carlen, "Principles and applications of electrochemical capacitors", Electrochimica Acta, 45 (15–16), 2000, 2483-2498, doi: 10.1016/S0013-4686(00)00354-6
[21] J. Larminie, A. Dicks, "Fuel cell systems explained", 2nd Edition, Wiley, 2003, ISBN: 0-470-84857-X
[22] TPE, "Piles à combustible 1er S", worldpress.com
[23] X. Cheng, Z. Shi, N. Glass, L. Zhang, J. Zhang, D. Song, Z.S. Liu, H. Wang, J. Shen, "A review of PEM hydrogen fuel cell contamination: Impacts, mechanisms, and mitigation", J. Power Sources, 165 (2), 2007, 739-756, doi: 10.1016/j.jpowsour.2006.12.012
[24] C. Ponce de Leon, A. Frias-Ferrer, J. Gonzalez-Garcia, D.A. Szanto, F.C. Walsh, "Redox flow cells for energy conversion", J. Power Sources, 160, 2006, 716-732, doi: 10.1016/j.jpowsour.2006.02.095
[25] X. Luo, J. Wang, M. Dooner, J. Clarke, "Overview of current development in electrical energy storage technologies and the application potential in power system operation", Applied Energy, 137, 2015, 511-536, doi: 10.1016/j.apenergy.2014.09.081
[26] L.H. Thaller, "Electrically rechargeable redox flow cell", US Patent 3,996,064, 1976
[27] P. Alotto, M. Guarnieri, F. Moro, "Redox flow batteries for the storage of renewable energy: A review", Renewable and Sustainable Energy Reviews, 29, 2014, 325-335, doi: 10.1016/j.rser.2013.08.001
[28] A.Z. Weber, M.M. Mench, J.P. Meyers, P.N. Ross, J.T. Gostick, Q. Liu "Redox flow batteries: a review", J. Appl. Electrochem., 41, 2011, 1137-1164, doi: 10.1007/s10800-011-0348-2
[29] F. Pan, Q. Wang, "Redox Species of Redox Flow Batteries: A Review", Molecules, 20(11), 2015, 20499-20517, doi: 10.3390/molecules201119711
[30] P. Leung, X. Li, C. Ponce de Leon, L. Berlouis, C.T. John Low and F.C. Walsh, "Progress in redox flow batteries, remaining challenges and their applications in energy storage", RSC Advances, 2, 2012,10125-10156, doi: 10.1039/c2ra21342g
[31] F. Gall, "The Corrosion of Centrifugal Pumps in Aqueous Environments", Pumps and Compressors Conference, 2013
[32] M. Skyllas-Kazacos, M.H. Chakrabarti, S.A. Hajimolana, F.S. Mjalli, M. Saleem, "Progress in Flow Battery Research and Development", Journal of the Electrochemical Society, 158 (8), 2011, R55-R79, doi: 10.1149/1.3599565
[33] A. Price, S. Bartley, S. Male, G. Cooley "A novel approach to utility scale energy storage", Power Engineering Journal, 13(3), 1999, 122–129, doi: 10.1049/pe:19990304

[34] M. Skyllas-Kazacos, M. Kazacos, A. Mousa, "Metal halide redox flow battery", patent, PCT/GB2003/001757, April 2003
[35] D. Kim, Y. Kim, Y. Lee, J. Jeon, "1,2-Dimethylimidazole based bromine complexing agents for vanadium bromine redox flow batteries", International Journal of Hydrogen Energy, 44 (23), 2019, 12024-12032, doi: 10.1016/j.ijhydene.2019.03.050
[36] M. Chakrabarti, S.A. Hajimolana, F.S. Mjalli, M. Saleem, I. Mustafa, "Redox Flow Battery for Energy Storage", Arab J. Sci. Eng., 38, 2013, 723-739, doi: 10.1007/s13369-012-0356-5
[37] H. Chen, T.N. Cong, W. Yang, C. Tan, Y. Li, Y. Ding, "Progress in electrical energy storage system: A critical review", Progress in Natural Science, 19, 2009, 291-312, doi: 10.1016/j.pnsc.2008.07.014
[38] Q. Huang, Q. Wang, "Next-Generation, High-Energy-Density Redox Flow Batteries", ChemPlusChem, 80, (2), 2015, 312-322, doi: 10.1002/cplu.201402099
[39] P. Leung, A.A. Shah, L. Sanz, C. Flox, J.R. Morante, Q. Xu, M.R. Mohamed, C. Ponce de León, F.C. Walsh, "Recent developments in organic redox flow batteries: A critical review", J. Power Sources, 360, 2017, 243-283, doi: 10.1016/j.jpowsour.2017.05.057
[40] M. Duduta, B. Ho, V.C. Wood, P. Limthongkul, V.E. Brunini, W.C. Carter, Y.M. Chiang, "Semi-Solid Lithium Rechargeable Flow Battery", Adv. Energy Mater., 1 (4), 2011, 511-516, doi: 10.1002/aenm.201100152
[41] Z. Li, K.C. Smith, Y. Dong, N. Baram, F.Y. Fan, J. Xie, P. Limthongkul, W.C. Carter, Y.M. Chiang, "Aqueous semi-solid flow cell: demonstration and analysis", Phys. Chem. Chem. Phys., 15, 2013, 15833-15839, doi: 10.1039/C3CP53428F
[42] K. Chayambuka, J. Fransaer, X. Dominguez-Benetton, "Modeling and design of semi-solid flow batteries", J. Power Sources, 434, 2019, 226740, doi: 10.1016/j.jpowsour.2019.226740
[43] M. Skyllas-Kazacos, M. Rychick, R. Robins, "All-vanadium redox battery", US Patent, 4,786,567, 1988
[44] M.F. Ashby, J. Polyblank, "Materials for Energy Storage Systems-A White Paper" Granta Design, 2012
[45] G.A. Blengini, D. Blagoeva, J. Dewulf, C. Torres de Matos, V. Nita, B. Vidal-Legaz, C.E.L. Latunussa, Y. Kayam, L. Talens Peirò, C. Baranzelli, S. Manfredi, L. Mancini, P. Nuss, A. Marmier, P. Alves-Dias, C. Pavel, E. Tzimas, F. Mathieux, D. Pennington, C. Ciupagea, "Assessment of the Methodology for Establishing the EU List of Critical Raw Materials – Annexes", Publications Office of the European Union, Luxemburg, 2017, ISBN: 978-92-79-70213-6, doi:10.2760/875135, JRC107008
[46] R.R. Moskalyka, A.M. Alfantazi, "Processing of vanadium: a review", Minerals Engineering, 16 (9), 2003, 793-805, doi: 10.1016/S0892-6875(03)00213-9
[47] D. Rehder, "The role of vanadium in biology", Metallomics, 7, 2015, 730-742, doi: 10.1039/C4MT00304G
[48] M. Petranikova, A.H. Tkaczyk, A. Bartl, A. Amato, V. Lapkovskis, C.Tunsu, "Vanadium sustainability in the context of innovative recycling and sourcing development", Waste Management, 113, 2020, 521-544, doi: 10.1016/j.wasman.2020.04.007

[49] B.V. Venkataraman, S. Sudha, "Vanadium toxicity", Asian J. Exp. Sci., 19 (2), 2005, 127-134
[50] M. Bisson, V. Bonnemet, G. Gay, F. Ghillebaert, D. Guillard, L. Lethielleux, K. Tack, "Vanadium et ses composés", INERIS, 2012
[51] Sara Corcuera, Maria Skyllas-Kazacos, "State-of-charge monitoring and electrolyte rebalancing methods for the vanadium redox flow battery", Eur. Chem. Bull., 1 (12), 2012, 511-519, doi: 10.17628/ECB.2012.1.511
[52] P. Nikolaidis, S. Chatzis, A. Poullikkas, "Life cycle cost analysis of electricity storage facilities in flexible power systems", International Journal of Sustainable Energy, 38 (8), 2019, 752-772, doi: 10.1080/14786451.2019.1579815
[53] A.J. Bard, L.R. Faulkner, "Electrochemical Methods: Fundamentals and Applications", 2nd Edition, Chapter 3, Wiley, 2001
[54] M. Gencten, Y. Sahin, "A critical review on progress of the electrode materials of vanadium redox flow battery", Int. J. Eng. Res., 44 (10), 2020, 7903-7923, doi: 10.1002/er.5487
[55] A. Parasuraman, T.M. Lim, C. Menictas, M, Skyllas-Kazacos, "Review of material research and development for vanadium redox flow battery applications", Electrochimica Acta, 101, 2013, 27-40, doi: 10.1016/j.electacta.2012.09.067
[56] M. Rychcik, M. Skyllas-Kazacos, "Evaluation of electrode materials for vanadium redox cell", Journal of Power Sources, 19 (1), 1987, 45-54, doi: 10.1016/0378-7753(87)80006-X
[57] B. Sun, M. Skyllas-Kazacos, "Chemical modification of graphite electrode materials for vanadium redox flow battery application-part II Acid treatments", Electrochimica Acta, 37 (13), 1992, 2459-2465, doi: 10.1016/0013-4686(92)87084-D
[58] K.J. Kim, M.S. Park, Y.J. Kim, J.H. Kim, S.X. Dou, M. Skyllas-Kazacos, "A technology review of electrodes and reaction mechanisms in vanadium redox flow batteries", J. Mater. Chem. A, 3, 2015, 16913-16933, doi: 10.1039/C5TA02613J
[59] B. Sun, M. Skyllas-Kazacos, "Modification of graphite electrode materials for vanadium redox flow battery application-I: Thermal treatment", Electrochimica Acta, 37 (7), 1992, 1253-1260, doi: 10.1016/0013-4686(92)85064-R
[60] L. Yue, W. Li, F. Sun, L. Zhao, L. Xing, "Highly hydroxylated carbon fibres as electrode materials of all-vanadium redox flow battery", Carbon, 48 (11), 2010, 3079-3090, doi: 10.1016/j.carbon.2010.04.044
[61] W.G. Zhang, J.G. Xi, Z.H. Li, H.P. Zhou, L. Liu, Z.H. Wu and X.P. Qiu, "Electrochemical activation of graphite felt electrode for VO^{2+}/VO_2^+ redox couple application", Electrochim. Acta, 89, 2013, 429-435, doi: 10.1016/j.electacta.2012.11.072
[62] M. Cheng, "Electrolyte optimization and studies for the vanadium redox flow battery", Master Thesis, UNSW, Australia, 1991
[63] M. Skyllas-Kazacos, L. Cao, M. Kazacos, N. Kausar, A. Mousa, "Vanadium Electrolyte Studies for the Vanadium Redox Battery – A Review", ChemSusChem, 9, 2016, 1521-1543, doi: 10.1002/cssc.201600102

[64] C. Choi, S. Kim, R. Kim, Y. Choi, S. Kim, H. Jung, J.H. Yang, H.T. Kim, "A review of vanadium electrolytes for vanadium redox flow batteries", Renewable and Sustainable Energy Reviews, 69, 2017, 263-274, doi: 10.1016/j.rser.2016.11.188
[65] Y. Zhao, L. Liu, X. Qiu, J. Xi, "Revealing sulfuric acid concentration impact on comprehensive performance of vanadium electrolytes and flow batteries", Electrochimica Acta, 303, 2019, 21-31, 10.1016/j.electacta.2019.02.062
[66] K.L. Chawla, J.P. Tandon, "Vanadium compounds in reductimetric titrations – I: Standardisation of vanadium (II) sulphate with iron (III) solution", Talanta, 12 (7), 1965, 665-669, doi: 10.1016/0039-9140(65)80090-X
[67] N.H. Choi, S.K. Kwon, H. Kim, "Analysis of the Oxidation of the V(II) by Dissolved Oxygen Using UV-Visible Spectrophotometry in a Vanadium Redox Flow Battery", J. Electrochem. Soc., 160 (6), 2013, doi: 10.1149/2.145306jes
[68] K. Ngamsai, A. Arpornwichanop, "Investigating the air oxidation of V(II) ions in a vanadium redox flow battery", J. Power Sources, 295, 2015, 292-298, doi: 10.1016/j.jpowsour.2015.06.157
[69] E. Sum, M. Skyllas-Kazacos, "A study of the V(II)/V(III) redox couple for redox flow cell applications", J. Power Sources, 15 (2–3), 1985, 179-190, doi: 10.1016/0378-7753(85)80071-9
[70] F. Rahman, "Stability and properties of supersaturated vanadium electrolytes for high energy density vanadium redox battery", PhD thesis, UNSW, Australia, 1998
[71] A. Mousa, "Chemical and Electrochemical studies of V(III) and V(II) Solutions in Sulfuric Acid Solution for Vanadium Battery Applications", PhD thesis, UNSW, Australia, 2003
[72] A. Mousa, M. Skyllas-Kazacos, "Kinetics of V^{III} and V^{II} Sulfate Precipitation Processes in Negative Half-Cell Electrolyte of the Vanadium Redox Flow Battery", ChemElectroChem, 4, 2017, 130-142, doi: 10.1002/celc.201600426
[73] S. Xiao, L. Yu, L. Wu, L. Liu, X. Qiu, J. Xi, "Broad temperature adaptability of vanadium redox flow battery-Part 1: Electrolyte research", Electrochimica Acta, 187, 2016, 525-534, doi: 10.1016/j.electacta.2015.11.062
[74] A. Fetyan, G.A. El-Nagar, I. Lauermann, M. Schnucklake, J. Schneider, C. Roth, "Detrimental role of hydrogen evolution and its temperature-dependent impact on the performance of vanadium redox flow batteries", Journal of Energy Chemistry, 32, 2019, 57-62, doi: 10.1016/j.jechem.2018.06.010
[75] M. Vijayakumar, S.D. Burton, C. Huang, L. Li, Z. Yang, G.L. Graff, J. Liu, J. Hu, M. Skyllas-Kazacos, "Nuclear magnetic resonance studies on vanadium(IV) electrolyte solutions for vanadium redox flow battery", J. Power Sources, 195 (22), 2010, 7709-7717, doi: 10.1016/j.jpowsour.2010.05.008
[76] F. Rahman, M. Skyllas-Kazacos, "Solubility of vanadyl sulfate in concentrated sulfuric acid solutions", J. Power Sources, 72 (2), 1998, 105-110, doi: 10.1016/S0378-7753(97)02692-X
[77] J. Guzman, I. Saucedo, R. Navarro, J. Revilla, E. Guibal, "Vanadium Interactions with Chitosan: Influence of Polymer Protonation and Metal Speciation", Langmuir, 18, 2002, 1567-1573, doi: 10.1021/la010802n

[78] C. Madic, G.M. Begun, R.L. Hahn, J.P. Launay, W.E. Thiessen, "Dimerization of Aquadioxovanadium (V) Ion in Concentrated Perchloric and Sulfuric Acid Media", Inorg. Chem., 23, 1984, 469-476, doi: doi.org/10.1021/ic00172a019
[79] E. Sum, M. Rychcik, M. Skyllas-Kazacos, "Investigation of the V(V)/V(IV) system for use in the positive half-cell of a redox battery". J. Power Sources, 16, 1985, 85-95, doi: 10.1016/0378-7753(85)80082-3
[80] F. Rahman, M. Skyllas-Kazacos, "Vanadium redox battery: Positive half-cell electrolyte studies", J. Power Sources, 189 (2), 2009, 1212-1219, doi: 10.1016/j.jpowsour.2008.12.113
[81] M. Skyllas-Kazacos, C. Menictas and M. Kazacos, "Thermal Stability of Concentrated V(V) Electrolytes in the Vanadium Redox Cell", J. Electrochem. Soc., 143 (4), 1996, L86, doi: doi.org/10.1149/1.1836609
[82] N. Kausar, R. Howe, M. Skyllas-Kazacos, "Raman spectroscopy studies of concentrated vanadium redox battery positive electrolytes", Journal of Applied Electrochemistry, 31, 2001, 1327–1332, doi: 10.1023/A:1013870624722
[83] N. Kausar, "Studies of V(IV) and V(V) species in vanadium cell electrolyte", PhD thesis, UNSW, Australia, 2002
[84] M. Vijayakumar, Liyu Li, Gordon Graff, Jun Liu, Huamin Zhang, Zhenguo Yang, Jian Zhi Hu, "Towards understanding the poor thermal stability of V5+ electrolyte solution in Vanadium Redox Flow Batteries", Journal of Power Sources, 196 (7), 2011, 3669-3672, doi: 10.1016/j.jpowsour.2010.11.126
[85] K. Lourenssen, J. Williams, F. Ahmadpour, R. Clemmer, S. Tasnim, "Vanadium redox flow batteries: A comprehensive review", Journal of Energy Storage, 25, 2019, 100844, doi: 10.1016/j.est.2019.100844
[86] L. Cao, M. Skyllas-Kazacos, C. Menictas, J. Noack, "A review of electrolyte additives and impurities in vanadium redox flow batteries", Journal of Energy Chemistry, 27 (5), 2018, 1269-1291, doi: 10.1016/j.jechem.2018.04.007
[87] J.H. Park, J.J. Park, H.J. Lee, B.S. Min, J.H. Yang, "Influence of Metal Impurities or Additives in the Electrolyte of a Vanadium Redox Flow Battery", J. Electrochem. Soc., 165 (7), 2018, A1263, doi: 10.1149/2.0491807jes
[88] J. Zhang, L. Li, Z. Nie, B. Chen, M. Vijayakumar, S. Kim, W. Wang, B. Schwenzer, J. Liu, Z. Yang, "Effects of additives on the stability of electrolytes for all-vanadium redox flow batteries", J. Appl. Electrochem., 41, 2011, 1215–1221, doi: 10.1007/s10800-011-0312-1
[89] M. Vijayakumar, W. Wang, Z. Nie, V. Sprenkle, J.Z. Hu, "Elucidating the higher stability of vanadium(V) cations in mixed acid based redox flow battery electrolytes", J. Power Sources, 241, 2013, 173-177, doi: 10.1016/j.jpowsour.2013.04.072
[90] L. Li, S. Kim, W. Wang, M. Vijayakumar, Z. Nie, B. Chen, J. Zhang, G. Xia, J. Hu, G. Graff, J. Liu, Z. Yang, "A Stable Vanadium Redox-Flow Battery with High Energy Density for Large-Scale Energy Storage", Adv. Energy Mater., 1, 2011, 394-400, doi: 10.1002/aenm.201100008

[91] S. Kim, E. Thomsen, G. Xi, Z. Nie, J. Bao, K. Recknagle, W. Wang, V. Viswanathan, Q. Luo, X. Wei, A. Crawford, G. Coffey, G. Maupin, V. Sprenkle, "1 kW/1 kWh advanced vanadium redox flow battery utilizing mixed acid electrolytes, J. Power Sources, 237, 2013, 300-309, doi: 10.1016/j.jpowsour.2013.02.045
[92] H. Prifti, A. Parasuraman, S. Winardi, T.M. Lim, M. Skyllas-Kazacos, "Membranes for Redox Flow Battery Applications", Membranes, 2, 275-306, 2012, doi: 10.3390/membranes2020275
[93] Y. Shi, C. Eze, B. Xiong, W. He, H. Zhang, T.M. Lime, A. Ukil, J. Zhao, "Recent development of membrane for vanadium redox flow battery applications: A review", Applied Energy, 238, 2019, 202-224, doi: 10.1016/j.apenergy.2018.12.087
[94] C. Minke, T. Turek, "Economics of vanadium redox flow battery membranes", J. Power Sources, 286, 2015, 247-257, doi: 10.1016/j.jpowsour.2015.03.144
[95] B. Jiang, L. Wu, L. Yu, X. Qiu, J. Xi, "A comparative study of Nafion series membranes for vanadium redox flow batteries", Journal of Membrane Science, 510, 2016, 18-26, doi: 10.1016/j.memsci.2016.03.007
[96] X. Li, H. Zhang, Z. Mai, H. Zhang, I. Vankelecom, "Ion exchange membranes for vanadium redox flow battery (VRB) applications", Energy Environ. Sci., 4, 2011, 1147, doi: doi.org/10.1039/C0EE00770F
[97] T. Sukkar, M. Skyllas-Kazacos, "Membrane stability studies for vanadium redox cell applications", Journal of Applied Electrochemisrty, 34, 2004, 137-145, doi: 10.1023/B:JACH.0000009931.83368.dc
[98] E. Agar, K.W. Knehr, D. Chen, M.A. Hickner, E.C. Kumbur, "Species transport mechanisms governing capacity loss in vanadium flow batteries: Comparing Nafion® and sulfonated Radel membranes", Electrochimica Acta, 98, 2013, 66-74, doi: 10.1016/j.electacta.2013.03.030
[99] K. Oh, S. Won, H. Ju, "A comparative study of species migration and diffusion mechanisms in all-vanadium redox flow batteries", Electrochimica Acta, 181, 2015, 238-247, doi: 10.1016/j.electacta.2015.03.012
[100] T. Sukkar, M. Skyllas-Kazacos, "Water transfer behaviour across cation exchange membranes in the vanadium redox battery", Journal of Membrane Science, 222, 2003, 235-247, doi: 10.1016/S0376-7388(03)00309-0
[101] T. Yamamura, X. Wu, I. Sato, H. Sakuraba, K. Shirasaki, S. Ohta, "Vanadium Battery", JP Patent, US 9.419,279 B2, 2016
[102] T. Yamamura, X. Wu, S. Ohta, K. Shirasaki, H. Sakuraba, I. Satoh, T. Shikama, "Vanadium solid-salt battery: Solid state with two redox couples", J. Power Sources, 196 (8), 2011, 4003-4011, doi: 10.1016/j.jpowsour.2010.12.010
[103] X. Li, J. Xiong, A. Tang, Y. Qin, J. Liu, C. Yan, "Investigation of the use of electrolyte viscosity for online state-of-charge monitoring design in vanadium redox flow battery", Applied Energy, 211, 2018, 1050-1059, doi: 10.1016/j.apenergy.2017.12.009

[104] M.J. Watt-Smith, P. Ridley, R.G.A. Wills, A.A. Shah, F.C. Walsh, "The importance of key operational variables and electrolyte monitoring to the performance of an all vanadium redox flow battery", J. Chem. Technol. Biotechnol., 88, 2013, 126-138, doi: 10.1002/jctb.3870
[105] S. Ressel, F. Bill, L. Holtz, N. Janshen, A. Chica, T. Flower, C. Weidlich, T. Struckmann, "State of charge monitoring of vanadium redox flow batteries using half cell potentials and electrolyte density", J. Power Sources, 378, 2018, 776-783, doi: 10.1016/j.jpowsour.2018.01.006
[106] A. Tang, J. Bao, M. Skyllas-Kazacos, "Dynamic modelling of the effects of ion diffusion and side reactions on the capacity loss for vanadium redox flow battery", J. Power Sources, 196 (24), 2011, 10737-10747, doi: 10.1016/j.jpowsour.2011.09.003

Chapter II – Characterization and analysis of vanadium solutions

Table of contents:

Introduction

The analysis and characterization of the different vanadium species in solution is important to understand their evolution and behavior during the functioning of the battery. In fact, there are two types of analysis that should be conducted separately, one for the electrochemical behavior of the electrolyte solutions to study the effect of numerous parameters (concentration, oxidation state, presence of particles…) on the resulting current from the oxidation and reduction of the electrolytes and the other for the physicochemical properties of the species, i.e. identification, quantitative analysis and physical properties.

The electrochemical methods put in place for this study are for the preparation of the various oxidation states in the form of solutions or powders, by using a U-shaped cell, and for the analysis of the electrochemical behavior of the redox couples in a classical three electrodes cell.

On the other hand, as indicated in the previous chapter, the vanadium redox flow battery (VRFB) is composed of four oxidation states (V^{2+}, V^{3+}, VO^{2+} and VO_2^{+}) of dissolved vanadium salts in sulfuric acid. Given that each one of these salts exhibits different properties, it is essential to implement the adequate techniques for each one in order to be able to have a quantitative follow-up of their respective concentrations during charge/discharge cycling of the battery and calculate the energy efficiencies and conversion rates to compare with theoretical established mass balances. Thus, this chapter will develop the techniques put in place for the titration of the four vanadium species (UV-Vis spectrometry, potentiometric titration and inductively coupled plasma), in addition to nuclear magnetic resonance for the characterization of the species structure to try to better understand their behavior.

This chapter is based on a bibliographic review, for the UV-Vis characterization, and on results obtained in this study and presents the techniques implemented for the vanadium salts analysis as well as their characterization.

II.1. Battery electrolytes preparation and experimental setups used

The commercially available vanadium salt is the vanadyl (IV) sulfate hydrate $VOSO_4.xH_2O$ and it is used for the preparation of $V^{(IV)}$ solutions by dissolution in sulfuric acid which are then employed in both sides of the battery to obtain the three other oxidation states of vanadium. In order to study the electrochemical behavior of each oxidation state of the vanadium and be able to optimize the composition of electrolyte solutions, it is essential to have pure salts of all the vanadium valences. A U–shaped electrochemical divided cell (refer to Appendix X1) was used for the preparation of vanadium salts, by electro–reduction or electro–oxidation of $V^{(IV)}$ solutions, as required.

The U–shaped electrochemical cell is thus composed by two compartments separated by a *Nafion*® 117 ion exchange membrane, held between two Viton® seals, to assure a minimum

leakage, and pressed with PTFE plastic plates. The different parts of the setup as well as the assembled cell are shown in Fig.II.1.

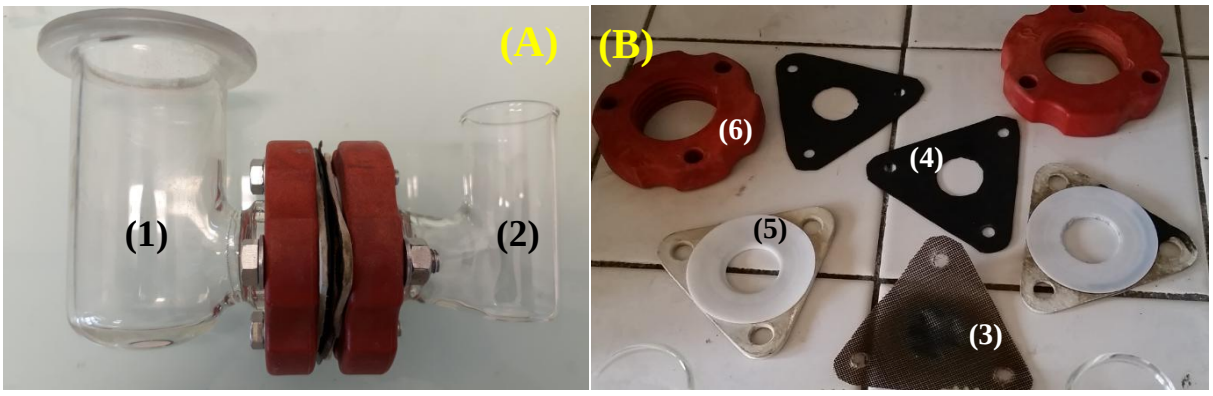

Fig.II.1: **(A)**: assembled U–shaped electrochemical cell with two non–symmetrical compartments: (1) electrolytic compartment of the working electrode (where the desired reaction occurs); (2) electrolytic compartment of the auxiliary electrode (filled with the supporting electrolyte alone here).
(B): dismantled junction bride (enabling to hold the ion exchange membrane and to ensure the separation of the two electrolytic compartments of the cell) (3) Nafion® 117 membrane; (4) Viton® joints with an open diameter of 2.5 cm; (5) PTFE plastic plates; (6) brides where the glass compartments are screwed.

A half-cell configuration was chosen to carry out the electro-synthesis of vanadium, according to the following reactions:

- Synthesis of VO_2^+

In the positive compartment: $VO^{2+} + H_2O \rightarrow VO_2^+ + 2\,H^+ + e^-$ Rx.II.1
In the negative compartment: $H^+ + e^- \rightarrow 1/2\,H_2$

- Synthesis of V^{3+}

In the negative compartment: $VO^{2+} + 2\,H^+ + e^- \rightarrow V^{3+} + H_2O$ Rx.II.2
In the positive compartment: $2H_2O \rightarrow O_2 + 4\,H^+ + 4e^-$

- Synthesis of V^{2+}

In the negative compartment: $VO^{2+} + 2\,H^+ + 2e^- \rightarrow V^{2+} + H_2O$; Rx.II.3
In the positive compartment: $2H_2O \rightarrow O_2 + 4\,H^+ + 4e^-$

The commercially available $VOSO_4.5H_2O$ was used for all the preparations ($V^{(V)}$, $V^{(III)}$ and $V^{(II)}$) and solvent decomposition occurred in the counter electrode compartment [1]. The bigger compartment of the cell (Fig.II.1-(A)-(1)) is used as working electrode compartment.

The vanadium will be used in excess to produce supersaturated solutions leading to precipitation to obtain the desired vanadium powder, but the starting material is 60 mL of a solution of vanadium (IV) at 1.5 M prepared in 3 M sulfuric acid added into the compartment of the working electrode, while the same volume of the same acid is introduced into the compartment of the

counter electrode. In order to reach supersaturated vanadium solutions, $VOSO_4.5H_2O$ powder was added gradually as the reaction progresses. During the electrolysis, aliquots of the vanadium solution were sampled and analyzed by UV–Vis spectrometry (see § II.3.1) to determine if the $V^{(IV)}$ is completely converted before adding more powder. The same analysis is performed to ensure the absence of $V^{(IV)}$ before ending the electrolysis.

The purpose of the electrolysis being only to obtain the different vanadium oxidation states, supplementary measurements were not undertaken to optimize the experimental conditions further, regarding the electrodes surface and activation, the stirring of the solvent compartment or the thermoregulation of the electrolytic cell. Also, the only parameter followed up during the electrolysis is the cell potential displayed on the power generator.

The working electrode is a graphite rod or graphite felt, depending on the experiment, while the counter electrode is always a platinum plate of 4 cm^2 geometrical surface. Electrolyses were performed under a constant current, and the stirring in the working electrode compartment was insured by a *Teflon*® magnetic bar. The temperature of the system was not controlled.
The obtained powder and solutions will be presented and further discussed in the next chapter.

II.2. Experimental setup used for the electrochemical analysis of the vanadium electrolytes

The electrochemical behavior of vanadium solutions should be studied separately for each oxidation state in order to understand the effect of the various operating parameters (vanadium concentration, electrode material, acid concentration…) and to be able to optimize their composition before using them in the VRFB. Performing current – potential curves for the different solutions/suspensions of vanadium was chosen as a suitable method for the study.

Current–potential curves, $I = f(E)$, are the basic tool of electrochemistry and are used for the characterization of redox systems (refer to Appendix X1). In order to draw these curves, it is necessary to have three electrodes in the electrochemical cell, containing the studied solution: the working electrode (WE), the reference electrode (RE) and the auxiliary or counter electrode (CE), as presented in Fig.II.2.

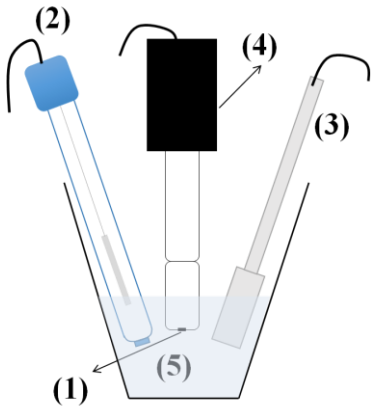

Fig.II.2: Three-electrode electrochemical cell used for the study of the electrochemical behavior of vanadium solutions: (1) working electrode disc; (2) reference electrode; (3) auxiliary or counter electrode; (4) rotating electrode body; (5) electrolyte solution.

In the case of this work, the $I = f(E)$ curves mostly used for the study of vanadium solutions are linear sweep voltammetry; they consist in the application of a varying potential to the working electrode, at constant time frequencies, which will result in oxidation or reduction reactions of electroactive species in solution, and the resulting current is recorded. The potentiostat used in this study is a PGSTAT30 from *Autolab*™, operated by NOVA 2.1.3 software.

Two different electrode materials were studied: solid graphite rods (GR) and graphite felt (GF), differentiated mainly by the aspect of the graphite composing the electrode. For the graphite rods, they consist of untreated graphite, shaped in the form of a cylindrical rod and are known for having somewhat a microporous structure between the carbon sheets constituting the structure. They need to be polished prior to being used, in order to have a reproducible surface of the electrode; its geometric surface is the sum of the surface of the lateral cylinder and that of the disc forming the base of the rod. To delimit the desired surface for our work, a *Teflon* tape is wrapped around the rod at the corresponding height and parafilm is rolled above it to maintain it in place, as shown in Fig.II.3-(A).

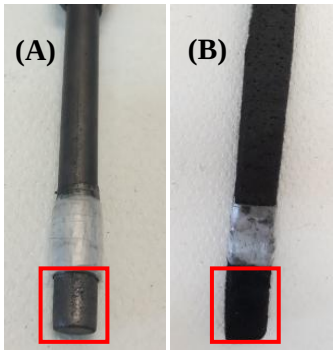

Fig.II.3: Electrodes used for the electrochemical characterization of vanadium solutions, the red squares correspond to the geometrical active surface of the electrode, immersed in the solution. **(A)**: graphite rod (diameter = 1 cm); **(B)**: graphite felt (thickness = 5 mm).

The graphite felt consists of entangled carbon fibers, forming a complex network constituting a macro-porous cloth. Unlike solid graphite, the felt absorbs the solution (as function of its surface oxidation state) and can get completely soaked by it; resin based polymer is used to delimit the surface to use: it is placed in enough quantity to fill completely the thickness of the felt on a length of 1 cm, above the desired surface, and is left to polymerize overnight. Then a piece of parafilm is wrapped above the glue in order to have a visual cue to immerse the electrode correctly in the solution. This method was proven to be adequate to block any soaking of the electrode above the desired surface; otherwise, the geometrical surface used for the analysis can change during the experiment. The electrode used in this work is provided from *Goodfellow*™, has a thickness of 5 mm and a specific surface greater than 1000 $cm^2.g^{-1}$. Another important aspect of the GF is that its bare surface exhibits low electrocatalytic activity and poor kinetic reversibility for the vanadium redox couples, and should be therefore activated to enhance its performance [2]. In this work, a simple treatment is applied to the GF systematically before its use in any solution: ten cycles of cyclic voltammetry were performed in 3 M sulfuric acid at a scanning rate of 25 $mV.s^{-1}$ with a scanning range between 2.5 and 1 V. This expects to form carbon oxides on the surface of the graphite used as positive electrode.

A saturated calomel electrode is used as reference and placed in a Luggin capillary filled with 3 M sulfuric acid. The counter electrode is a platinum plate of 4 cm^2 geometrical surface, as mentioned before. The electrochemical cell has a capacity of 25 cm^3 and the WE is placed as close as possible to the RE to reduce the resistance.

II.3. Analytical techniques for electrolyte characterization

II.3.1. UV-VIS spectroscopy

UV-Visible spectroscopy is used for quantitative evaluation of the concentrations of various species; it is based on the absorbance by these species of a beam of light in the ultra–violet (200–400 nm) and in the visible (400–800 nm) region of the spectrum [3-5]. The incident light of a certain intensity ($I°$) is partially absorbed by the lit sample, generating a transmitted light of a different intensity (I_T) that will be measured by the UV-VIS spectrophotometer detector. The absorbance A is defined as the logarithm of the ratio $I°/I_T$. The Beer–Lambert's law links the absorbance to the concentration of the analyzed species *j*, according to the equation:

$$A = -log\frac{I_T}{I°} = \varepsilon\, \ell\, C_j \qquad \text{Eq.II.1}$$

where:

ε = molar absorptivity or extinction coefficient (in $L.mol^{-1}.cm^{-1}$); ε is a quantity characteristic of the substance and depends on the wavelengths λ at which the sample absorbs;

ℓ = thickness of the lit sample (in cm) or optical path of the light (or the length the UV cell);

C_j = concentration of the analyzed substance (in $mol.L^{-1}$).

The Beer–Lambert's law is valid for dilute solutions (ideal mixtures) for which A is typically lower than 1 (i.e. $A \leq 1 \rightarrow I_T \geq 10*I°$). Depending on the instrument, if the absorbance is greater than 2, the error can reach 10 to 20 % [5] as a function of the value of ε.
A reference measurement should be done prior to a sample analysis, using the same cuvette and containing the blank solution that would ideally not absorb in the same spectral region of the studied substance. Then a calibration is required for each substance, in order to determine the corresponding value of the extinction coefficient ε.
UV-VIS spectroscopy can be used for the analysis of vanadium, thanks to the distinctive colors of each oxidation state in aqueous solutions; indeed, in acidic conditions the four salts of "$V^{(II)}$, $V^{(III)}$, $V^{(IV)}$ and $V^{(V)}$ are respectively violet, green, blue and yellow.
In Fig.II.4 are presented the spectra of the four vanadium oxidation states, plotted in this study, in the range of $250 < \lambda_{nm} < 1100$. All the species absorb in the UV range, however, only the three lower valances ($V^{(II)}$, $V^{(III)}$ and $V^{(IV)}$) exhibit characteristic bands in the visible range of spectrum. Conversely, the $V^{(V)}$ spectrum, even if it shows an absorption for $\lambda < 500$ nm, does not show a characteristic wavelength at which it can be detected alone or quantified.

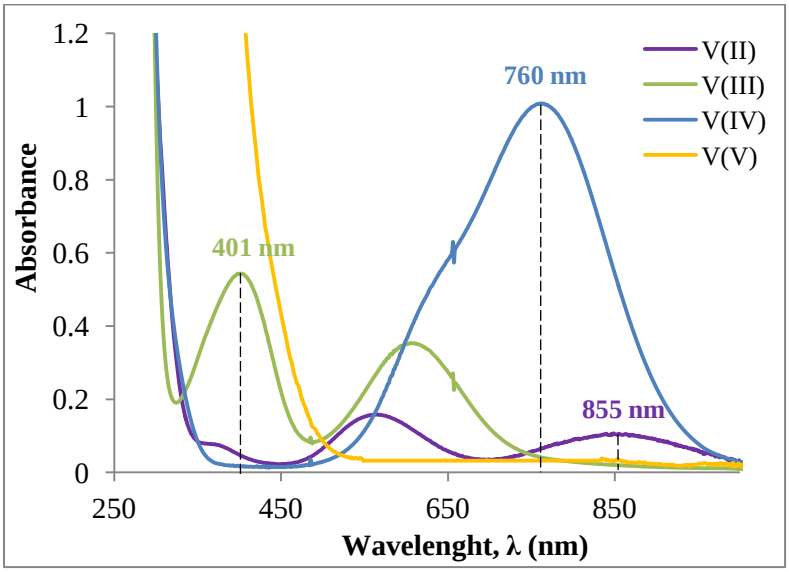

Fig.II.4: UV spectra of various vanadium electrolytes (0.05 M vanadium (V^{2+}, V^{3+}, VO^{2+} and VO_2^+) diluted in 3 M sulfuric acid)

As mentioned above, a calibration is necessary before using this technique and many researchers have determined the extinction coefficients for the different vanadium oxidation states. It was found that depending on the study, the value of ε varies for the same oxidation states; the extinction coefficients of $V^{(II)}$, $V^{(III)}$, $V^{(IV)}$ were found in the bibliography and are presented in the table II.1.

Table II.1. Extinction coefficients for vanadium solutions as found in the bibliography, compared to the values obtained in the calibration of this work

Reference	Solution media	Wavelength λ (nm)	$\varepsilon_{(V^{(II)})}$ (L.mol^{-1}.cm^{-1})	$\varepsilon_{(V^{(III)})}$ (L.mol^{-1}.cm^{-1})	$\varepsilon_{(V^{(IV)})}$ (L.mol^{-1}.cm^{-1})
Kim et al. [6]	aqueous H_2SO_4	855	1.73	0.11	–
		610	3.76	5.85	–
		765	–	–	13.4
Brooker et al. [7]		800	2.42	–	–
		760	–	–	17.17
Furman et al. [8]	aqueous $HClO_4$	400	–	8.3	–
		580	–	5.5	–
Present work	aqueous H_2SO_4	401	–	11.17	–
		610	–	6.97	–
		760	–	–	19.92
		855	2.04	–	–

II.3.1.1. Calibration of $V^{(II)}$, $V^{(III)}$ and $V^{(IV)}$

The UV-Vis spectroscopy calibration of the three oxidation states of the vanadium is essential for their quantification in the present work especially because the bibliography shows a wide range for the values of extinction coefficients.

The calibration for each oxidation state was performed in a concentration range between 0.01 and 0.5 M in vanadium by direct dissolution of the corresponding powder in 3 M sulfuric acid. The $V^{(IV)}$ powder, $VOSO_4.5H_2O$ is commercially available, while $V_2(SO_4)_3.9H_2O$ and $VSO_4.1.5H_2O$ were prepared by electrochemical reduction of a $V^{(IV)}$ solution and purified adequately. The powder preparation was described previously in this chapter. The spectrometer used in this study is a Hewlett–Packard 8453.

The extinction coefficient of $V^{(II)}$ was determined here (under Nitrogen atmosphere) at 855 nm (Fig. II.5), since it does not interfere with any absorbance of the other vanadium oxidation states, except $V^{(IV)}$ (Fig. II.4) but in general, in the negolyte there are not $V^{(IV)}$ nor $V^{(V)}$; in the same manner, in the posolyte there are not $V^{(II)}$ nor $V^{(III)}$. The linear evolution of the absorbance as a function of the vanadium concentration observed in graph (II) of Fig.II.5, enables the extinction coefficient of $V^{(II)}$ at 855 nm to be determined: $\varepsilon_{V^{(II)}\ at\ 855\,nm} = 2.04$ L.mol^{-1}.cm^{-1}. It should be noted that the point corresponding to a concentration of 0.1 M was not taken into account for the calculation of ε because it appears that it starts to deviate from linearity.
The calculated value is not in agreement with the ones found in the bibliography: the difference with the value determined by Brooker et al. ($\Delta\varepsilon = 0.38$ L.mol^{-1}.L^{-1}) can be due to the fact that the absorbance is not measured at the same wavelength and the difference with the work of Kim et al. at the same wavelength is $\Delta\varepsilon = 0.31$ L.mol^{-1}.L^{-1} (18 %). The observed discrepancy may be

due to the preparation of the solution; in this study the solutions are prepared by dissolution of a prepared $VSO_4.1.5H_2O$ and its dissolution and dilution in sulfuric acid while in their case a main solution is prepared by electrolytic reduction of a $V^{(III)}$ solution then the dilution is performed in ultra-pure water. Also, an additional difference is the spectrometer used which can have an impact as well on the results.

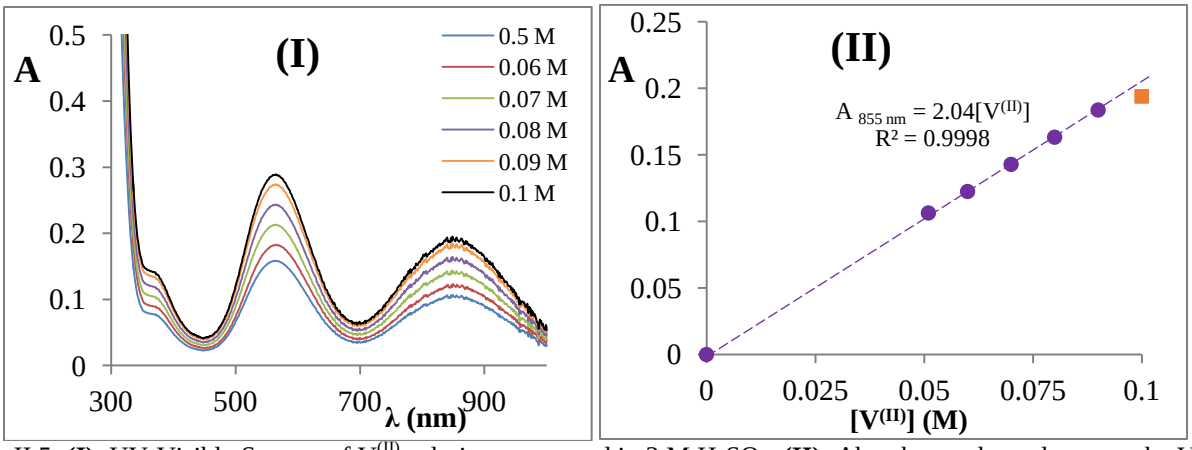

Fig.II.5: **(I)**: UV-Visible Spectra of $V^{(II)}$ solutions, prepared in 3 M H_2SO_4; **(II)**: Absorbance dependence on the $V^{(II)}$ concentration at the characteristic wavelength of 855 nm.

For the vanadium (III) calibration, the obtained spectra for the analyzed solutions (Fig.II.6-(I)) exhibits two different peaks (610 and 401 nm) and the two extinction coefficients were calculated, even though neither of the peaks can be used (directly, without deconvolution) for the quantification, since they overlap with the bands of the $V^{(II)}$. The calibration curves are presented in Fig.II.6, for a solution containing only $V^{(III)}$.

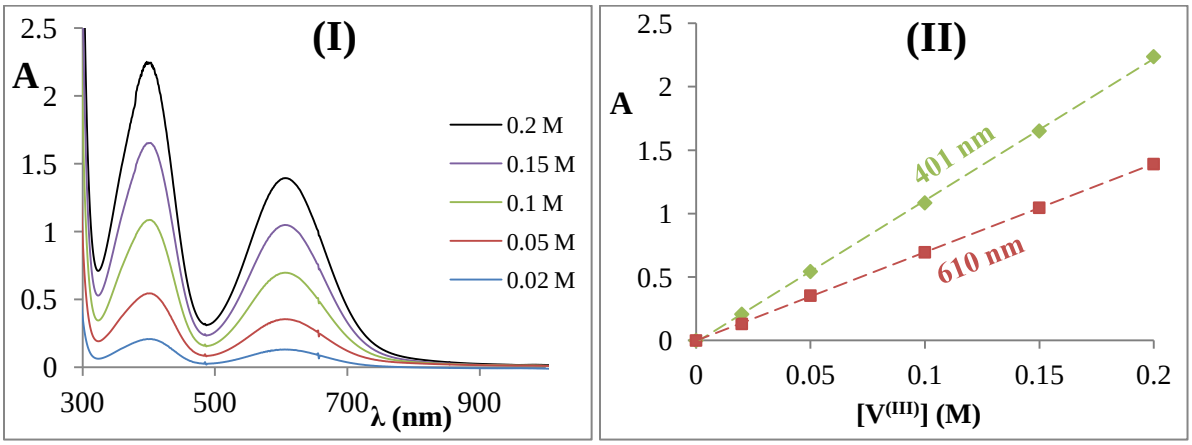

Fig.II.6: **(I)**: Spectra of $V^{(III)}$ solutions for concentrations from 0.02 to 0.2 M, prepared in 3 M H_2SO_4 from direct dissolution of $V_2(SO_4)_3.9H_2O$ powder; **(II)**: Absorbance dependence on the $V^{(III)}$ concentration at the characteristic wavelengths of: 401 nm (green, diamonds) and 610 nm (red, cubes).

The extinction coefficients correspond to the slopes of the straight lines:

- At 401 nm: $A_{401} = 11.17\left[V^{(III)}\right],\ R^2 = 0.999 \Rightarrow \varepsilon_{V^{(III)},401\,nm} = 11.17\ L.mol^{-1}.cm^{-1}$
- At 610 nm: $A_{610} = 6.97\left[V^{(III)}\right],\ R^2 = 0.999 \Rightarrow \varepsilon_{V^{(III)},610\,nm} = 6.97\ L.mol^{-1}.cm^{-1}$

The comparison of the obtained values of ε with the ones listed in table II.1 shows that for λ = 401 nm, ε from the study of Furman et al. is performed in perchloric acid, thus the discrepancy between the values ($\Delta\varepsilon$ = 2.87 L.mol^{-1}.cm^{-1}, equal to 34.6 %) can come from different interactions created in the solution as a result of using a different acid. As for λ = 610 nm, a difference of 1.47 L.mol^{-1}.cm^{-1} (27 %) is found with the value given by Furman et al. which can be attributed to the i) the different wavelength at which the value is measured and ii) to the solvent used for the preparation of the solution. Comparison with the value obtained by Kim et al. gives a difference of 1.21 L.mol^{-1}.cm^{-1} (19 %) and the same explanation given earlier for $V^{(II)}$ can also be applied here.

Similar experiments were conducted for vanadium (IV) and the results are presented in Fig.II.7. Similarly to the calculations of $V^{(II)}$, the value of the highest concentration (0.15 M) is not taken into account because it starts to deviate from the linearity of the curve.

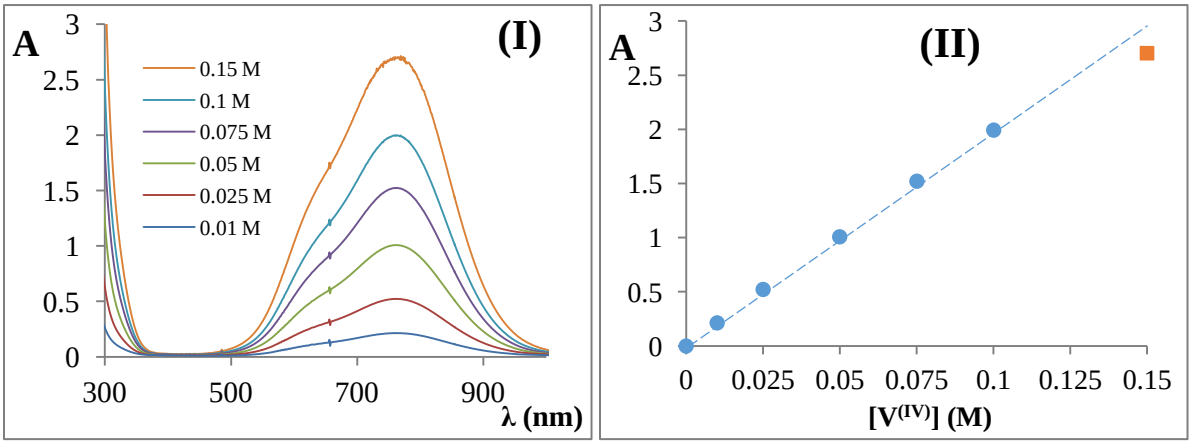

Fig.II.7: **(I)**: Spectra of $V^{(IV)}$ solutions for concentrations from 0.01 to 0.15 M, prepared in 3 M H_2SO_4 from direct dissolution of $VOSO_4.5H_2O$ powder; **(II)**: Absorbance dependence on the $V^{(IV)}$ concentration at the characteristic wavelengths of 760 nm.

The extinction coefficient corresponds to the slope of the straight line:

$$A_{760} = 19.92 \times \left[V^{(IV)}\right],\ R^2 = 0.999 \Rightarrow \varepsilon_{V^{(IV)},760\,nm} = 19.92\ L.mol^{-1}.cm^{-1}$$

Comparing the value of $\varepsilon_{V^{(IV)}}$ with those of the bibliography shows a difference of 49 % ($\Delta\varepsilon$ = 6.52 L.mol^{-1}cm^{-1}) with the value of Kim et al., explained by the different wavelength at which the value is calculated and a difference of 16 % ($\Delta\varepsilon$ = 2.75 L.mol^{-1}cm^{-1}) with the value obtained by Brooker et al. which can be attributed to the fact that the measurements performed in their study was done in plastic cuvettes instead of quartz and with a different UV-VIS spectrometer so these two factors could have contributed in the discrepancy observed.

It should be noted that for the quantification of the vanadium solutions ($V^{(III)}$ and $V^{(IV)}$), all the aliquots will be diluted to have an concentration below 0.1 M to stay in the linear domain of the calibration.

II.3.1.2. Limitations of the technique

The spectra of $V^{(II)}$ and $V^{(III)}$ overlap at two wavelengths around 400 and 600 nm, which is a limitation for the analysis of the $V^{(III)}$ in a solution containing both. In fact, the $V^{(II)}$ can be analyzed at 855 nm, thus a deconvolution of the two other peaks is necessary to access to the [$V^{(III)}$]. Note also that a linear evolution of the absorbance was observed [9-10] for mixtures of $V^{(II)}/V^{(III)}$ in the case of VRFB for a state of charge (SOC) greater than 0.2, and this information can be used for the determination of the concentrations ratio in the mixture. The deconvolution of the peaks by Python, by assimilating the peaks to a Gaussian curve, can be considered adequate to obtain the peaks separately. However, we tried this method but it was found impossible to separate the peaks corresponding to $V^{(II)}$ and $V^{(III)}$ at 400 and 600 nm because when they are in the same solution they form only one combined peak that cannot be distinguished into two. Therefore, another analytical method is necessary in order to validate the obtained values of the concentrations.

As indicated above, in general, in the posolyte of the VRFB there are no $V^{(II)}$ nor $V^{(III)}$, it contains only $V^{(IV)}$ and $V^{(V)}$. Thus, the band of the $V^{(IV)}$, at 760 nm, is not disturbed by the presence of others species, even $V^{(V)}$, and can thus be used for the quantification.

On the other hand, a dilution of the solution is necessary for the analysis as it was found that the linearity of the Beer-Lambert's law is valid for vanadium concentrations lower than 0.1 M [11] and the deviation from linearity above this concentration was shown in the study of Grossmith et al. to be largely due to a shift of the peak position from 760 to 750 nm.

In addition, contrary to $V^{(II)}/V^{(III)}$, a mixture of $V^{(IV)}/V^{(V)}$ (for a total vanadium concentration between 0.35 and 1.6 $mol.L^{-1}$ prepared in 3 or 4 $mol.L^{-1}$ sulfuric acid) exhibits a non-linear behavior of the absorbance with the mixture ratio [10, 12]. This was attributed to the formation of a complex constituted by both $V^{(IV)}$ and $V^{(V)}$ for which the UV-VIS spectrum appeared to be different from the individual spectrums of each oxidation state. In fact, since $V^{(V)}$ was found to absorb at $\lambda < 500$ nm at very high values of absorbance ($A > 3$) with no characteristic peaks, we would tend to say that in a mixedvalence solution, the only peak observed would be that of $V^{(IV)}$ at around 760 nm. However, it was shown in several studies that the shape of the curve changes for $V^{(IV)}/V^{(V)}$ mixtures and an excess absorbance was witnessed for different mixture ratios than what would have been expected for a $V^{(IV)}$ or $V^{(V)}$ solution [10]. After subtracting the expected absorbance from the excess, a parabolic curve was obtained with a maximum corresponding to

the 50 % mixture, therefore a 1:1 stoechiometry of VO^{2+}:VO_2^+ leading to assume the formation of the complex $V_2O_3^{3+}$. This complex was observed in a mixed acid solution [13] and the existence of a mixed-valence complex was supported by a V^{51} NMR study where the analysis showed the broadening of the NMR peak [14] for a solution prepared in perchloric acid. As a matter of fact, several structural studies have shown that the VO_2^+ group is bent and that the formation of the mixed valence compound can be considered as the substitution of one of the coordinated water molecules of the $VO^{2+}_{(aq)}$ cation by one of the oxygen atoms of the dioxovanadium (V) group playing the role of a ligand.

Such a behavior was not observed in the present study in the obtained UV-Vis spectra probably because all the analyzed samples are diluted in sulfuric acid and in diluted solutions, the formed complex decomposes to its individual salts. However, this does not exclude the fact that the complex can exist in the battery during its functioning.

II.3.2. Potentiometric titration

Potentiometric titration at zero current is also examined for the vanadium analysis (refer to Appendix X2).
The experiments were carried out using an automatic titrator *888 Titrando Metrohm*® equipped with a stirrer and the analysis could be monitored with the associated software *tiamo* ^{TM}. The used electrode is a combined platinum–silver/silver chloride electrode (Pt – Ag/AgCl/Cl^-). The titrant solution is stored in a bottle serving as a burette and enables automatic introduction of a flow of 0.1 $mL.s^{-1}$ into a beaker containing the continuously stirred analyte solution.

II.3.2.1. Titration of $V^{(V)}$ with $Fe^{(II)}$

The titration of the $V^{(V)}$ was performed in the present study by the Mohr's salt (ammonium iron (II) sulfate hexahydrate, 99%, Sigma Aldrich) dissolved in ultra–pure water acidified with H_2SO_4 at 3 M. The following reactions were involved:

$$VO_2^+ + 2\,H^+ + e^- \rightarrow VO^{2+} + H_2O \qquad E° = 1.00\ V/SHE \qquad \text{- Rx. II.1}$$

$$Fe^{(II)} \rightarrow Fe^{(III)} + e^- \qquad E° = 0.77\ V/SHE \qquad \text{Rx. II.4}$$

The global reaction will be:

$$VO_2^+ + Fe^{(II)} + 2\,H^+ \rightarrow VO^{2+} + Fe^{(III)} + H_2O \qquad \text{Rx. II.5}$$

Aliquots of dissolved $V^{(V)}$ at different concentrations are sampled in volumes between 0.2 and 1 mL for the analysis and a volume of 30 mL of ultra–pure water is added in order to submerge the electrode. A validation of the method has been done by comparing the results from titration with inductively coupled plasma ICP measurements for VO_2^+ solutions that were prepared by dissolution of the vanadium pentoxide V_2O_5 in 3 M sulfuric acid.

The potentiometric titration provides the S-shaped or sigmoid curve $\Delta E = f(V_{Fe(II)\ added})$.

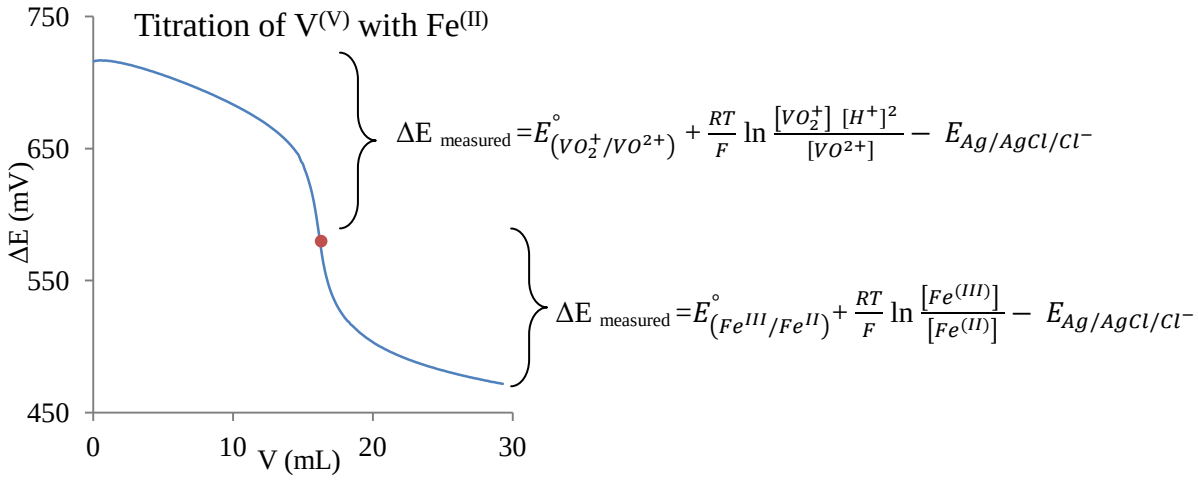

Fig.II.8: Evolution of the potential ΔE of a VO_2^+ solution as a function of the added volume of $Fe^{(II)}$ solution at 0.1 M; titration achieved using a combined "platinum indicator electrode and a silver/silver chloride reference electrode"

The obtained $\Delta E = f(V_{Fe(II)\ added})$ curve is reproducible for all the analyzed samples; an error of approximately 0.5 % was obtained between two repetitions of the same titration.

Another important point to take into account before validating the method, is the absence of interference of the $V^{(IV)}$ that would necessarily be present in the posolyte of the battery. A solution was prepared by dissolution of $VOSO_4.5H_2O$ in 2 M sulfuric acid and an aliquot of 0.22 mL of VO^{2+} at 1.7 M was used with 30 mL of water for the titration.

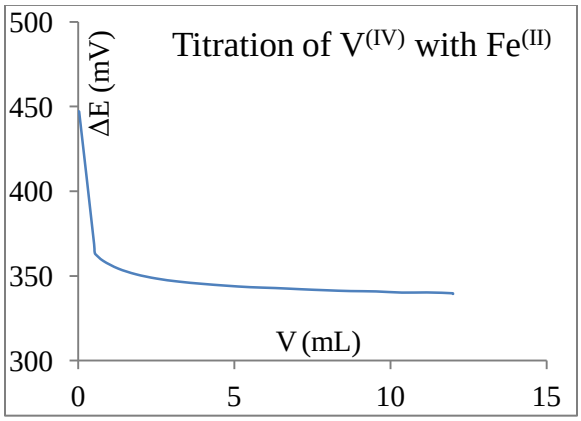

Fig.II.9: Evolution of the potential ΔE of a VO^{2+} solution as a function of the added volume of $Fe^{(II)}$ solution at 0.1 M; titration achieved using a combined "platinum indicator electrode and a silver/silver chloride reference electrode"

The titration curve presented in Fig.II.9 shows that the potential of the indicator electrode falls to the $Fe^{(II)}/Fe^{(III)}$ potential range, immediately as the first drops of Mohr salt solution are introduced

into the bulk. Therefore, the presence of VO^{2+} in a titrated solution of VO_2^+ does not interfere with the analysis.
Thereby this method can be considered as adequate and accurate, after comparison with ICP, for the quantification of the vanadium (V) during the operation of the redox flow battery.

II.3.2.2. Titration of $V^{(II)}$ and indirect titration of $V^{(III)}$ with I_2

The potentiometric titration of $V^{(II)}$ and $V^{(III)}$ does not seem to have had much attention in the recent years; as found for the $V^{(V)}$, most of the techniques were developed around the 1960s.
Even if the reaction seems to be slow, the $V^{(III)}$ reacts with the oxygen and oxidizes to vanadium (IV), that is why most of the attempts to titrate this species were carried out under inert atmosphere. Conversely, the reaction of the $V^{(II)}$ with the oxygen appears to be rapid (complete oxidation in a few minutes) that is why in this case the removal of the dissolved oxygen is mandatory.
Various attempts were made expecting to determine an accurate, rapid and reproducible method for the titration of $V^{(III)}$; all the methods which did not lead to the required results are presented in appendices X6 to X6. In the following, the method which enables effective, specific and precise titration of the vanadium is presented.

II.3.2.2.1. Potentiometric titration of the $V^{(II)}$ by iodine I_3^-

As indicated above, the vanadium (II) compounds are powerful reducing agents and have been employed for visual, potentiometric and amperometric titrations of various oxidizing agents [15-16]. $V^{(II)}$ can be oxidized by one, two, or three electrons, depending on the oxidation potential of the redox couple with which it reacts and on the mode of titration.

The redox systems and the reactions involved in the titration with the iodine are:

$$V^{2+} \rightarrow V^{3+} + e^- \qquad E° = -0.26 \text{ V/SHE} \qquad \text{Rx.II.6}$$

$$I_2 + 2\,e^- \rightarrow 2\,I^- \qquad E° = 0.54 \text{ V/SHE} \qquad \text{Rx.II.7}$$

The global reaction will be:

$$I_2 + 2\,V^{2+} \rightarrow 2\,I^- + 2\,V^{3+} \qquad \text{Rx.II.8}$$

The preparation of the iodine solution requires solid iodine (I_2 99 % from Fisher Scientific) and potassium iodide (Aldrich Chemicals, 99+ %) in order to dissolve the iodine (in deaerated ultra-pure water). The solution of the V^{2+} also deaerated was titrated according to Rx.II.8, and the potential of a platinum redox indicator electrode was monitored versus a silver/silver chloride electrode. The obtained curve (Fig.II.10) is a sigmoid shaped curve containing a simple jump of the potential corresponding to the oxidation of the vanadium. The curve enables to perform a quantitative analysis of the solution of the V^{2+} ions in the VRFB without any interference from

the presence of $V^{(III)}$ in solution given that there was no reaction between V^{3+} and I_2, validated as well (see appendix X6).

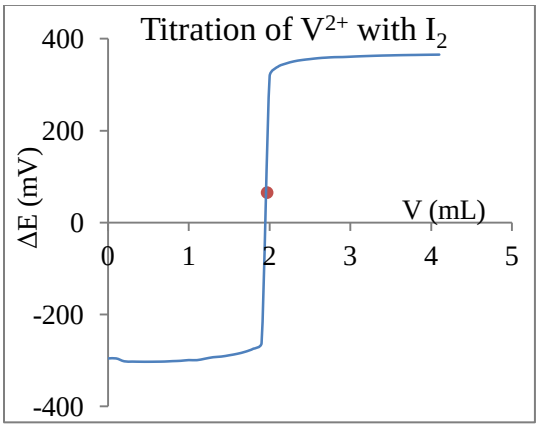

Fig.II.10: Evolution of the potential ΔE of a V^{2+} solution as a function of the added volume of I_2 solution at 0.1 M; titration achieved using a combined "platinum indicator electrode and a silver/silver chloride reference electrode"

II.3.2.2.2. Indirect potentiometric titration of the $V^{(III)}$ by iodine I_3^-

The vanadium (III) is first reduced by metallic zinc to V^{2+} which is titrated by iodine.

A solution of V^{3+} is prepared by dissolution of $V_2(SO_4)_3.9H_2O$ powder in 3 M sulfuric acid and an excess of zinc powder was added to reduce V^{3+} to V^{2+} with nitrogen bubbling through the erlenmeyer to avoid the re–oxidation of $V^{(II)}$.

The reactions taking place are:

$V^{3+} \rightarrow V^{2+} + e^-$ $\quad E° = – 0.26$ V/SHE - Rx.II.6

$Zn_{(s)} \rightarrow Zn^{2+} + 2\ e^-$ $\quad E° = – 0.76$ V/SHE Rx.II.9

The global reaction will be:

$Zn_{(s)} + 2V^{3+} \rightarrow Zn^{2+} + 2\ V^{2+}$ Rx.II.10

The reduction reaction Rx. II.10 takes less than 2 minutes for the V^{3+} to be completely transformed to V^{2+}. Then the suspension was filtered (under nitrogen) and the V^{2+} was titrated by the iodine (I_3^-) following the procedure indicated above.

II.3.2.3. Determination of the acid concentration

The electrolytes of the vanadium redox flow battery are prepared in aqueous media, usually by dissolving vanadium sulfate salts in concentrated sulfuric acid. During cycling of the battery, the concentration of protons is likely to change due to: i) the oxydo-reduction reaction at the positive electrode (- Rx.II.1), ii) the migration through the cationic membrane and iii) any eventual precipitation/dissolution of the vanadium salts that induce consuming or releasing sulfate groups that would inevitably impact the free protons in solution.

$$VO_2^+ + 2\,H^+ + e^- \leftrightarrows VO^{2+} + H_2O \qquad \text{- Rx.II.1}$$

As a matter of fact, as mentioned in the previous chapter, the sulfuric acid concentration is an important factor that controls the solubility of the vanadium salts. Increasing the total sulfate concentration shifts the equilibriums (11) to (14) towards the left, leading to a lesser dissociation of the vanadium sulfate salts [17] and eventually the precipitation of these salts in solution.

$$VSO_{4(s)} \leftrightarrows V^{2+} + SO_4^{2-} \qquad \text{Rx. II.11}$$
$$V_2(SO_4)_{3(s)} \leftrightarrows 2V^{3+} + 3SO_4^{2-} \qquad \text{Rx. II.12}$$
$$VOSO_{4(s)} \leftrightarrows VO^{2+} + SO_4^{2-} \qquad \text{Rx. II.13}$$
$$(VO_2)_2SO_{4(s)} \leftrightarrows 2VO_2^+ + SO_4^{2-} \qquad \text{Rx. II.14}$$

Therefore, the quantification of the total sulfate concentration in solution is also important and can be achieved by ICP analysis of the element sulfur, taking into account all the SO_4^{2-} and HSO_4^- coming from both the sulfuric acid dissociation and the vanadium dissolution-precipitation equilibriums.
The determination of the acidity of the electrolyte (i.e. the concentration of free protons) requires a specific method and this is described below.

The determination of the pH of a solution is usually achieved using a pH-meter calibrated in the appropriated pH range. However, the vanadium aqueous solutions could also behave as acids (they dissociate for example and release sulfate which can take from the free H^+ to form HSO_4^-), therefore the pH does not really represent solely the concentration of the sulfuric acid.

The acid–base reaction can be used to titrate by potentiometry the electrolytes and to examine if it is possible to distinguish the acidity of the sulfuric acid from that of the vanadium salts. A solution of sodium hydroxide at 1 M (NaOH, VWR, 100 %) is used for the preparation of the titrant solution. The titration is performed with a glass pH electrode.

First of all, a solution of 3 M H_2SO_4 solution is titrated to validate the method and have a reference to which can be compared the results obtained for H^+ titration in vanadium solutions. To that end, 1 mL of H_2SO_4 3 M is diluted in 30 mL of ultra-pure water in order to immerse the electrode. The result of the titration (Fig.II.11) is a classic sigmoid shaped curve corresponding to the following reaction:

$$H^+ + OH^- \rightarrow H_2O \qquad \text{Rx. II.15}$$

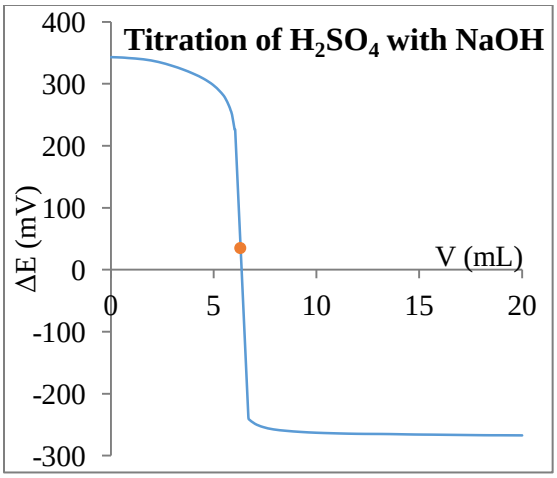

Fig.II.11: Evolution of the potential ΔE of a H_2SO_4 solution as a function of the added volume of NaOH solution at 1 M; titration achieved using a glass pH electrode

The curve presented in Fig.II.11 shows only one end-point corresponding to the total acidity i.e. to the first and second acidity of the H_2SO_4 dissociation to HSO_4^- and SO_4^{2-} respectively. Considering that the first dissociation of H_2SO_4 to HSO_4^- is total (high $K_{H_2SO_4/HSO_4^-}$), the second dissociation to SO_4^{2-} remains partial with an equilibrium constant $K_{HSO_4^-/SO_4^{2-}} = 0.013$ at 25 °C (the concentrations are in mol/kg for the calculation of ($K_{HSO_4^-/SO_4^{2-}}$)), therefore, the concentration of free H^+ in solution comes only from the first dissociation and is calculated from the potentiometric titration curve as:

$$[H^+] = \frac{[OH^-] \times V_{NaOH\ added}}{V_{H_2SO_4\ titrated}} \times \frac{1}{2} = \frac{1 \times 6.3}{1} \times \frac{1}{2} = 3.15\ M \qquad \text{Eq.II.2}$$

with a deviation of 5 % from the assumed concentration of 3 M; this error than come from the preparation of the solution.

After this, the titration of protons in vanadium (III) and (IV) solutions is performed. The vanadium (III) solution has an initial concentration of 0.1 M prepared in 3 M H_2SO_4, while the $V^{(IV)}$ solution has a concentration of 1.8 M and is prepared in 2 M H_2SO_4. The vanadium sample is diluted in 30 mL ultra-pure water to submerge the electrode. It was found that the acidity of H_2SO_4 is separated from that of V^{3+} and VO^{2+} as shown in Fig.II.12. The first equivalence point on each curve (orange disc) corresponds to the end point of the H^+ titration.
It can be noticed that the two curves do not exhibit the same shape, depending on the oxidation state of the vanadium in solution whereas the starting and ending values of the measured potential are the same.

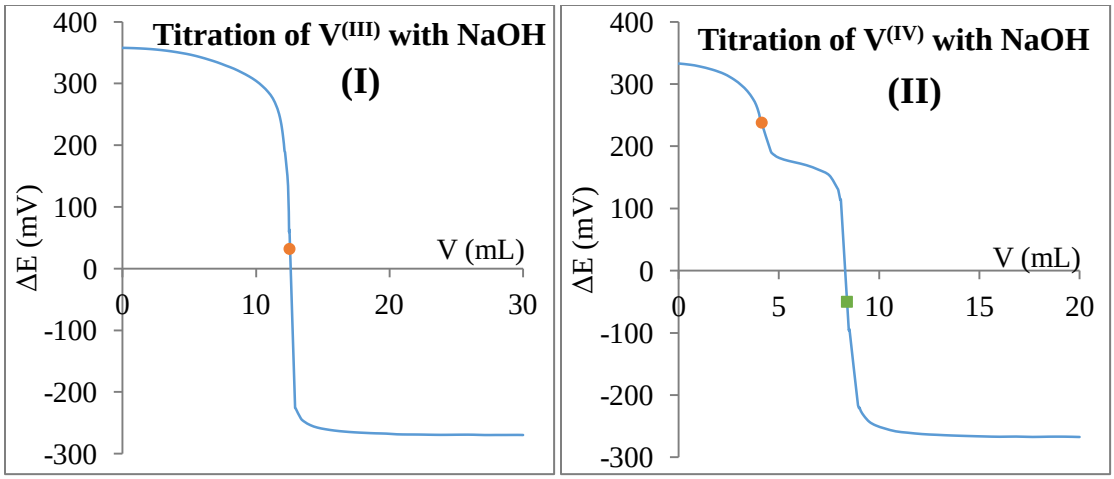

Fig.II.12: Evolution of the potential ΔE of a $V^{(III)}$ solution **(I)** and a $V^{(IV)}$ solution **(II)** as a function of the added volume of NaOH solution at 1 M; titration achieved using a glass pH electrode; the orange discs on each graph represent the end points corresponding to the titration of the total H^+ in solution and the green cube on the $V^{(IV)}$ titration curve corresponds to the end point of the titration of VO^{2+} by NaOH.

First, for the titration of the $V^{(III)}$ solution, it appears that only the sulfuric acid is titrated with only one equivalence point even after adding 30 mL of NaOH. The calculation of the H_2SO_4 concentration gives a deviation of 4.4 % with the concentration of the prepared solution. On another note, the aqueous chemistry of $V^{(III)}$ seems to be complicated (Fig.II.13-(I)) where it appears to exist under at least three forms between pH 0 and 5, according to its speciation diagram.

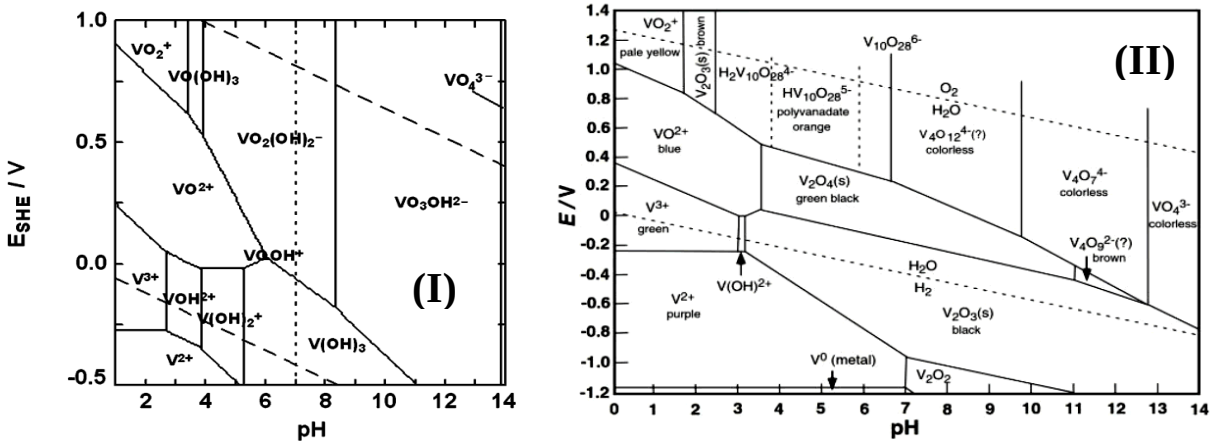

Fig.II.13: Theoretical E=f(pH) diagram of the vanadium: **(I)** in water for an ionic strength I = 0.038 M from ref. [18] and **(II)** in aqueous media from ref. [19]

As for the VO^{2+} titration by NaOH, two end points are visible on the curve. The first one corresponds to the acid titration and allows calculating the concentration of H_2SO_4 with a deviation of 3.75 % with the assumed concentration prepared. The second end-point (Fig.II.12-(II), green cube) must correspond to the titration of dissolved VO^{2+}. According to Fig.II.13-(II),

the predominant species until pH = 3.5 is VO^{2+}, after which it precipitates as V_2O_4 and the reaction taking place can be written as:

$$2\ VO^{2+} + 2\ OH^- \rightarrow V_2O_{4\ (s)} + 2\ H^+ \qquad \text{Rx.II.16}$$

Hence, calculating the concentration of $V^{(IV)}$ should be possible after subtracting the volume added to neutralize the H^+ ions from the total volume added until the end point of the vanadium.

To conclude:

- the vanadium (V) can be titrated by an iron (II) solution without any interference from vanadium (IV);
- the vanadium (II) can be titrated with a solution of iodine without interference from vanadium (III);
- concerning the $V^{(III)}$ titration, several redox couples were tested in order to find an adequate titrant but none of them appeared to be able to oxidize quantitatively the V^{3+} to VO^{2+}. Thereby, an indirect method of titration was proposed in which the $V^{(III)}$ solution is reduced to $V^{(II)}$ by reaction with solid zinc powder and the $V^{(II)}$ is titrated with iodine.

The potentiometric titration of $V^{(IV)}$ was not addressed in the present work.

As for the determination of the sulfuric acid concentration in vanadium solutions, and more precisely the free H^+, it was found that by potentiometric titration with a strong base such as NaOH, it is possible to determine the $[H^+]$ concentration without the interference of the acidity of the vanadium (III) or (IV). The effect of $V^{(II)}$ and $V^{(V)}$ on this titration were not studied herein.

II.3.3. Inductively coupled plasma

Inductively coupled plasma (ICP) is a powerful technique for the determination of metals and some non-metals in different sample matrices; the method is very sensitive and enables to determine low concentrations (theoretically until the ppb). The basics of ICP are presented in appendix X7.

In the present work, the ICP is coupled to an optical emission spectrometer as a detector; the device used is an ULTIMA 2 ICP–OES Spectrometer from Horiba Scientific® instruments.

This technique is known for its sturdiness, multi-elementary character and high linearity of its measuring range. These advantages are confronted to the disadvantage of not being able to differentiate between the different ions of an atom or more precisely its several oxidation states. It detects the ion as a chemical element no matter the oxidation state in which it is and gives the total concentration present in the solution. For example, when preparing a solution of vanadyl sulfate $VOSO_4$ in sulfuric acid H_2SO_4, the sulfate from the dissociation of the powder SO_4^{2-} and the sulfate from the acid solution HSO_4^- cannot be differentiated and will be seen as a total concentration of sulfate. Similarly, for the vanadium analysis, using ICP for the analysis of

electrolyte solutions would surely give accurate results but it will not be able to differentiate the vanadium oxidation states, which is crucial for the quantification of the electrolytes during the functioning of the battery. Therefore, only a total vanadium concentration can be measured in an analyte sample.
This technique is used in this work for the determination of exact concentrations of solutions used for the calibration of the UV–VIS spectrometry, the calculation of the water quantity in a hydrated powder and the determination of a total vanadium concentration in an electrolyte solution complimentary to the other analysis techniques (potentiometry and spectroscopy).

The vanadium is detected at two characteristic wavelengths in the ICP–OES: 292.402 and 327.612 nm. The measurements are made on both wavelengths and the concentration of the solution is determined by calculating the average between the values.
For example, to calculate the water content contained in the vanadium powder, an intermediate solution of 2000 ppm of ^{51}V is prepared by dissolving the $VOSO_4.xH_2O$ powder in 3 M sulfuric acid and then diluted to 10 and 20 ppm for analysis. Each solution was analyzed twice for a better reliability of the results, presented in Table II.2. For the solution preparation, "x" was considered to be equal to 0; therefore, the molar mass of the powder is 163 $g.mol^{-1}$ for $VOSO_4$.

Table II.2: ICP report for the analysis of the vanadyl sulfate solution to calculate its water content

Wavelengths (nm)	Estimated Concentration (ppm)	Obtained Concentration (ppm)	RSD* (%)	RU** (%)
292.402	10	6.3	2.5	2.01
	10	6.3	2.7	
	20	12.5	1.6	2.02
	20	12.3	2.1	
327.612	10	6.3	0.8	2.02
	10	6.2	1.6	
	20	12.3	1.7	2.01
	20	12.5	0.8	

*RSD: Relative Standard Deviation of the instrument, calculated for the three repetitions of each sample done by the instrument.
**RU: Relative Uncertainty, calculated between the values obtained for the two analyzed samples of each concentration.

The results show that there is approximately 40% difference between the prepared or estimated concentration and the obtained concentration from the analysis. This difference corresponds to the water content of the powder that was not taken into account when preparing the solution.

Using the concentration value obtained from the ICP, the exact molecular weight of the vanadium salt can be calculated and used to determine "x": the molecular weight is 253 g/mol instead of 163 g/mol written on the bottle and the powder is pentahydrated, $VOSO_4.5H_2O$.

Similar protocol and calculations are undertaken for all the ICP–OES analysis for water contact determination for the powders used in this work.

II.3.4. Nuclear magnetic resonance

Nuclear magnetic resonance (NMR) analysis (see appendix X7 for the basics of the technique) helps to identify the chemical structure of the active vanadium species composing the electrolyte of the redox flow battery [20] and thus helps understanding the redox chemistry of vanadium in different electrolyte solutions, such as water exchange mechanisms, complex formations and the existence of more than one form of the vanadium species involved. Naturally occurring ($_{23}V$) is composed of one stable isotope ^{51}V and one radioactive isotope ^{50}V, making its analysis by NMR possible through the ^{51}V isotope.

In the present study, the RMN device used is a BRUKER AVANCE III HD 500MHz equipped with a multi-core cryoprobe. The samples were prepared and diluted in 3 M aqueous sulfuric acid. To be able to analyze the sample by NMR, it is necessary to have a reference with ^2D molecules. Therefore, a sealed capillary tube containing only deutered water D_2O was inserted in the glass tube containing the sample so that the composition of the solution is not modified and the NMR analysis can be done.
The results of the NMR studies conducted on $V^{(V)}$ concentrated solutions will be discussed further in Chapter III.

II.4. Determination of some physical properties of vanadium solutions and suspensions: density and viscosity

The electrolytes of the vanadium battery are mostly prepared in concentrated sulfuric acid ($[H_2SO_4]$ = 2 – 3 M) and they contain vanadium concentrations ranging from 1.5 to 2.5 M. Their density and viscosity are likely to vary during the charge – discharge cycles, as a function of the solutions composition. Studying the variation of the viscosity of these solutions can be useful for understanding the phenomena happening in the battery.

The electrolytes studied in the present study are liquid/solid suspensions, i.e. mixtures of solid particles and dissolved species of one or two electroactive materials. Therefore, their physical properties would be modified compared to these of their solutions (below saturation), and this could affect on the one hand the maximum current through the modification of the effective diffusion coefficients of the different species and thus impact the state of charge of the battery,

and on the other hand the flow into the various elements of the battery (pipes, electrolytic compartments and storage tanks) might be modified from the set flow rate of the pump which is used for the calculations of the mass balance equations. Thus, a deviation between experimental and theoretical values can be observed so having at least the order of magnitude of the viscosity variation can help explain the phenomena taking place. Hence, a series of density and viscosity measurements are performed to try to determine the properties of the used suspensions.
The dynamic viscosity (μ) characterizes the resistance to laminar flow of a fluid. Measurements of a mass flow rate of a mixture in a tube make possible the estimation of the viscosity by using Poiseuille's law:

$$\Delta P = \frac{8\,\mu\,L}{\pi\,r^4}\left(\frac{m}{\rho t}\right) \qquad \text{Eq.II.3}$$

Where ΔP is pressure drop between the inlet and outlet of the tube (Pa), μ is the dynamic viscosity (Pa.s), L is the length of the tube (m), r is the radius of the tube (m), ρ is the density of the solution (kg.m^{-3}), t is the mass measurement duration (s) and $\frac{m}{\rho t}$ is the volumetric flow ($\frac{kg}{\frac{kg}{m^3}\,s}$).

The values of r and L are characteristic of the experimental setup and the values of ΔP, m and t are determined experimentally. The only missing value is the density ρ.
Note that, this law is valid for homogeneous and Newtonian (simple) fluids. Since the concentrated solutions used here do not belong to this kind of fluids, the measured viscosity with this method should be considered as "effective viscosity".

II.4.1. Apparatus used and calibration

The density values can be experimentally determined using an Anton-Paar *DMA 38* oscillating U-tube densimeter (Fig.II.14-(I)). The sample is inserted by using a syringe through hole **(1)** into the thermoregulated U-shaped tube **(2)** in which takes places the measurement of the density. The solution is discarded from hole **(3)** after the device finishes its acquisition and the value of the density is displayed on the screen **(4)**, which also serves to set the required temperature.

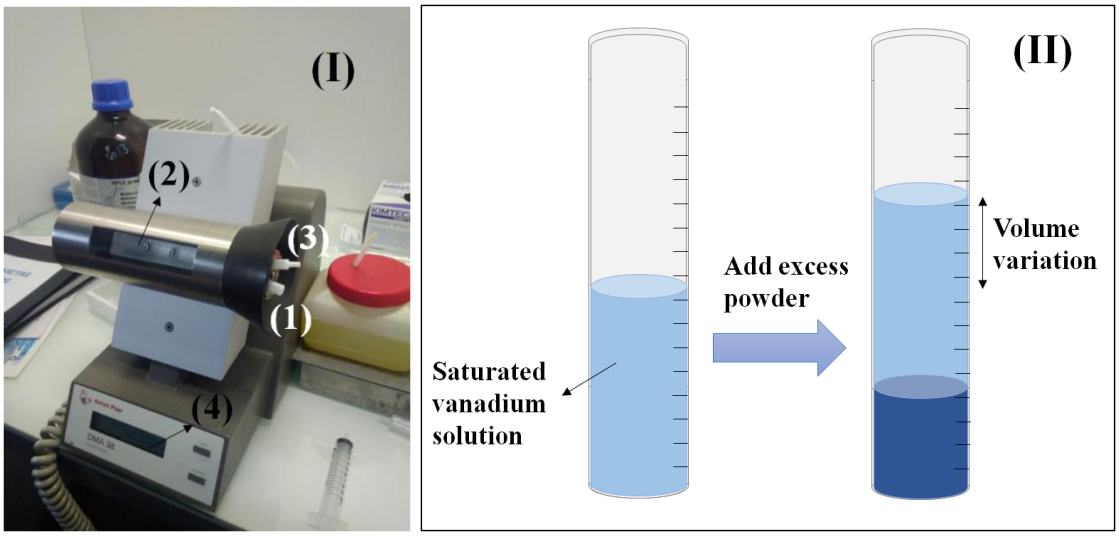

Fig.II.14: **(I)**: Photo of a Densimeter DMA 38 for measuring the density of vanadium solutions; **(II)**: schematic representation of the process of measuring the variation of the volume when adding excess vanadium powder to a saturated solution.

The density measurements were performed at four temperatures: 15, 20, 30 and 40 °C for the following vanadium solutions, dissolved in 3 M H_2SO_4:

- $V^{(IV)}$ concentrations in the range $0.5 < [VO^{2+}{}_{/in\ mol/L)}] < 2.5$;
- $V^{(III)}$ concentrations in the range $0.08 < [V^{3+}{}_{/in\ mol/L)}] < 0.8$;
- $V^{(V)}$ concentrations in the range $0.5 < [VO_2^{+}{}_{/in\ mol/L)}] < 5$;

The measurements of the density of vanadium (IV) suspensions, using the *Densimeter DMA 38* are difficult to carry out, because it is impossible to introduce the powder of the suspension into the capillary tube of the densimeter. In fact, the density of the $VOSO_4$ powder (d = 2.5) is higher than this of the liquid (d ≈ 1.35) and leads to a rapid sedimentation of the suspension. Therefore, for these suspensions a different method is implemented which consists in measuring the variation in mass and volume during successive additions of $VOSO_4$ in a graduated test tube containing a saturated $V^{(IV)}$ solution (Fig.II.14-(II)). The results are presented further below in this chapter.

In order to carry out the viscosity measurements, an experimental setup, entirely glass made, was conceived (Fig.II.15); in fact, because of the corrosive behavior of the vanadium suspensions/solutions used in this study, the classical rheometers (with metallic devices) are unusable. Besides it is difficult to use an ubbelohde tube because of the presence of solid particles. An apparent viscosity can then be calculated through Eq.II.3 after measuring the mass flow of the vanadium solutions/suspensions.

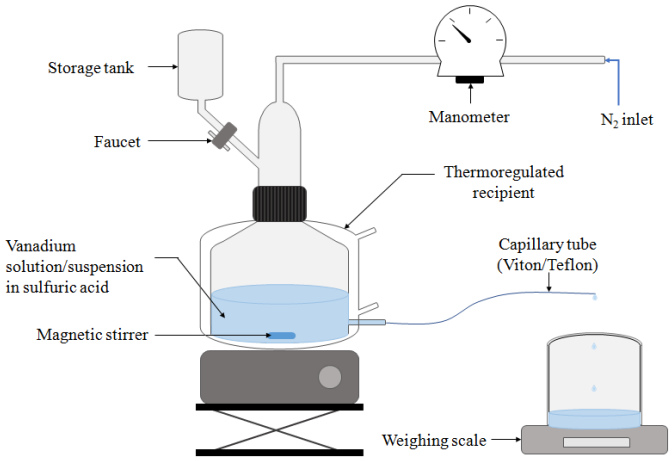

Fig.II.15: Experimental setup for measuring the mass flow rate of vanadium solutions/suspensions

The capillary tube used is in *Viton*®, a fluoroelastomer rubber, with an internal diameter of 0.75 mm and a length of 25 cm. The thermoregulated recipient has an internal diameter of 10 cm and the small glass tube at the exit of the recipient, allowing the connection with the capillary, has a length of 4 cm and an internal diameter of 2 mm.

Before using both devices (densimeter and viscosimeter) for the analysis of vanadium solutions/suspensions, they should be calibrated; solutions of sulfuric acid at different concentrations were used for that purpose and the results were compared to those found in the bibliography (Fig.II.16) [21].
An error of approximately 5 % is observed at higher H_2SO_4 concentrations, especially for the viscosity measurements, but the obtained results can be considered as accurate to validate the two experimental setups and use them for the measurements on the vanadium solutions.

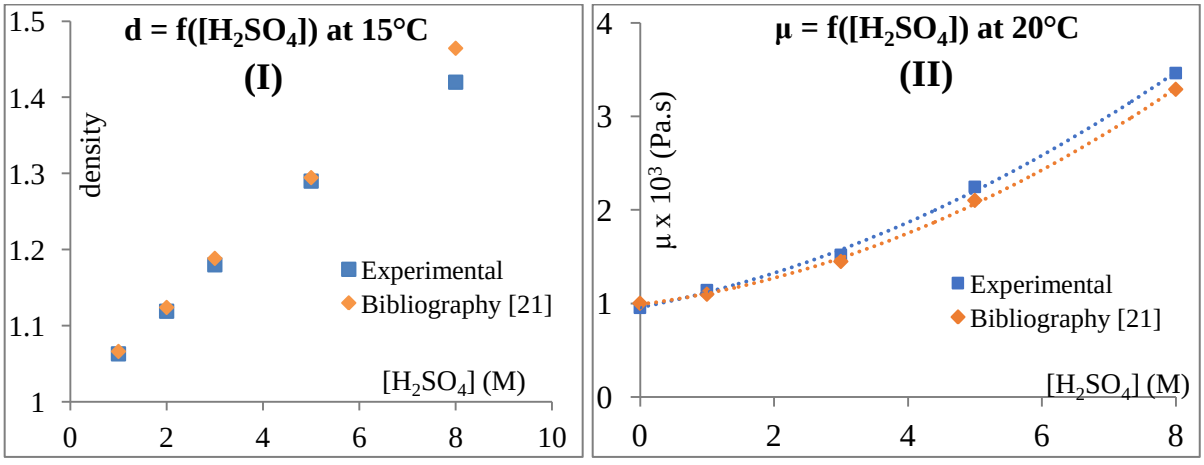

Fig.II.16: Calibration of the experimental setups (viscosimeter (Fig.II.15) and Densimeter (Fig.II.14-(I))) performed using sulfuric acid solutions at concentrations from 1 to 8 M; Curves in graph **(I)**: evolution of density as a function of $[H_2SO_4]$ at 15 °C; Curves in graph **(II)**: evolution of viscosity as a function of $[H_2SO_4]$ at 20 °C (capillary tube in *Viton*®, Φ_{intern} = 0.75 mm, L = 25 cm, 2000 < ΔP < 3000 Pa)

II.4.2. Density measurements

In this section the density of the different vanadium solutions was measured. The solutions of the $V^{(III)}$ and $V^{(IV)}$ were prepared by direct dissolution of $V_2(SO_4)_3.9H_2O$ and $VOSO_4.5H_2O$ respectively in sulfuric acid. Concerning the vanadium (V), the solutions were prepared by dilution of an initial solution (VO_2^+]= 5 M) obtained by electro-oxidation of a suspension of $V^{(IV)}$ (the experimental setup for this experiment was described previously in this chapter). Therefore, since the acid concentration in the 5 M $V^{(V)}$ solution is unknown, the diluted solutions do not have the same H_2SO_4 concentration, but this did not affect the behavior of the solutions density towards the variation of the temperature which exhibited the same tendency as the solutions of $V^{(III)}$ and $V^{(IV)}$ prepared in initial 3 M H_2SO_4.

The results, presented in Fig.II.17, show that the density varies linearly as a function of both the vanadium concentration and the temperature. In the examined range, the effect of the concentration to the density appears to predominate compared to the effect the temperature, meaning that the temperature variation does not create new solute–solvent interactions.

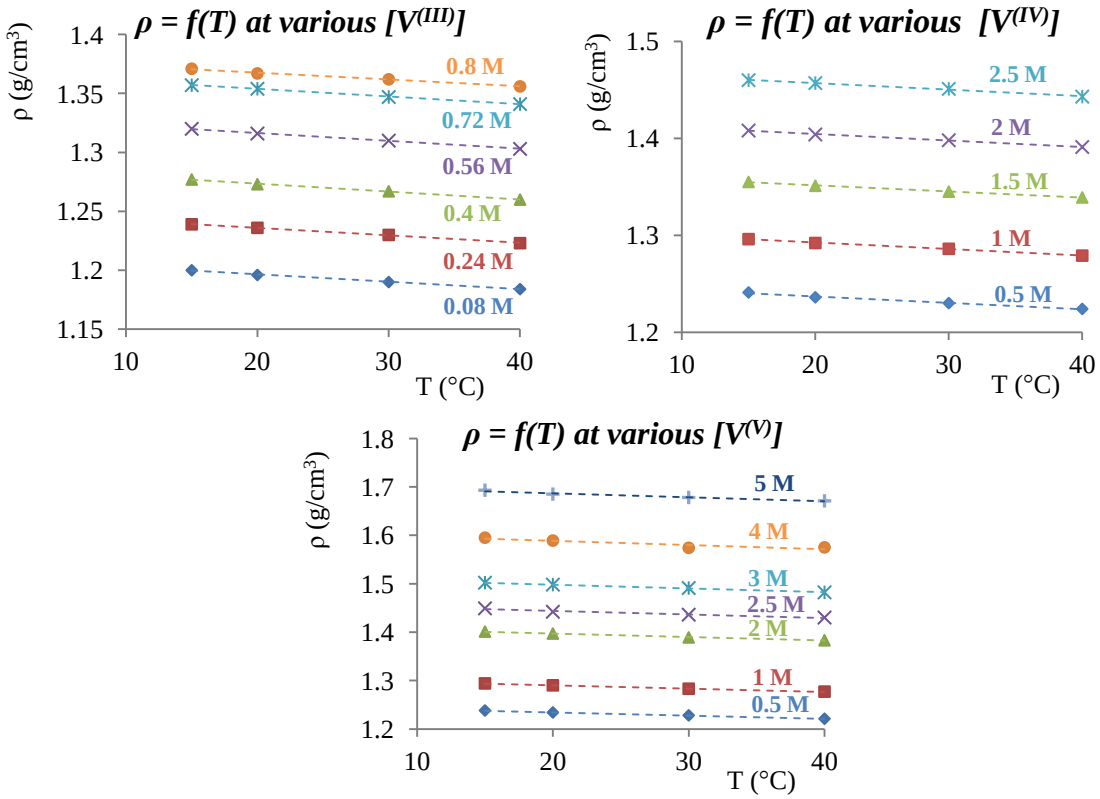

Fig.II.17: Temperature dependence of the density ρ of various solutions of vanadium in H_2SO_4 3 M, at various concentrations. Top left: $V^{(III)}$; examined concentrations range : $0.08 < [V^{(III)}]_{(\text{in mol/L})} < 0.8$;
Top right: $V^{(IV)}$; examined concentrations range : $0.5 < [V^{(IV)}]_{(\text{in mol/L})} < 2.5$; $[H_2SO_4]= 3$ M.
Bottom middle: $V^{(V)}$; examined concentrations range : $0.5 < [V^{(IV)}]_{(\text{in mol/L})} < 5$; $[H_2SO_4]= 3$ M.

As expected, the density increases with the vanadium concentration, for example, an increase from 1.2 to 1.37 g/cm^3 is observed when increasing the $V^{(III)}$ concentration from 0.08 to 0.8 M and this linear evolution leads to the following equation, applicable for all the vanadium solutions, for each studied temperature:

$$\rho = \alpha \times [Vanadium] + \rho_{H_2SO_4} \qquad \text{Eq.II.4}$$

It can also be noticed that the density values for a fixed vanadium concentration are very similar for the vanadium (IV) and (V) solutions but slightly higher for the $V^{(III)}$ solutions, even with lower concentrations and this can be verified in the Fig.II.18 below.

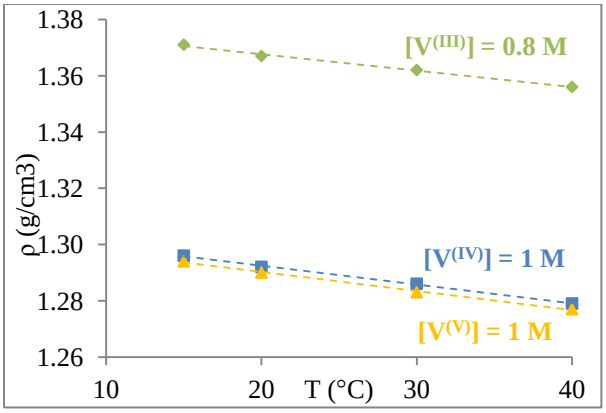

Fig.II.18: Curves showing the evolution of the density ρ (g/cm^3) as a function on the temperature (15, 20, 30 and 40 °C) for $V^{(III)}$, $V^{(IV)}$ and $V^{(V)}$ solutions at 0.8 M for $V^{(III)}$ and 1 M for $V^{(IV)}$ and $V^{(IV)}$ prepared in 3 M H_2SO_4.

The higher values of density of vanadium (III) solutions could be due to the important number of water molecules (9 H_2O for $V_2(SO_4)_3$) crystallizing with the vanadium salt, which means the need to introduce a higher mass to get the same concentration as for the $V^{(IV)}$ and $V^{(V)}$ solutions. Moreover, the dissociation of $V_2(SO_4)_3$ releases 1.5 SO_4^{2-} for each V^{3+} ion, which impacts the free H^+ in solution and thereby influences the density of H_2SO_4, leading to a modification of the density of the $V^{(III)}$ solution according to Eq.II.4.

Additional density measurements were performed, at constant temperature, on $V^{(IV)}$ solutions prepared in 5 M H_2SO_4, for vanadium concentrations in the range limited from 0.5 to 1.5 M due to the limited solubility of vanadium in concentrated sulfuric acid.
The results in Fig.II.19 show that the rate of increase of the density with temperature for solutions containing 5 M H_2SO_4 is the same to this observed with solutions at lower sulfuric acid concentration (3 M), thus validating the proposed Eq.II.4.

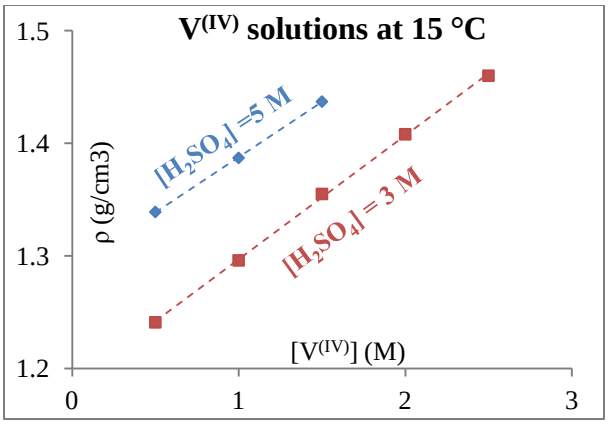

Fig.II.19: Vanadium ($V^{(IV)}$) concentration dependence of the density ρ (g/cm^3) of the resulting solution for two different sulfuric acid concentrations (3 and 5 M); T = 15 °C.

The results of the measurements for $V^{(IV)}$ suspensions are presented in Fig.II.20-(I) in terms of the variation of the total volume of the suspensions against the mass of $VOSO_4$ added. The zero on the X-axis corresponds to the saturated $V^{(IV)}$ solution.

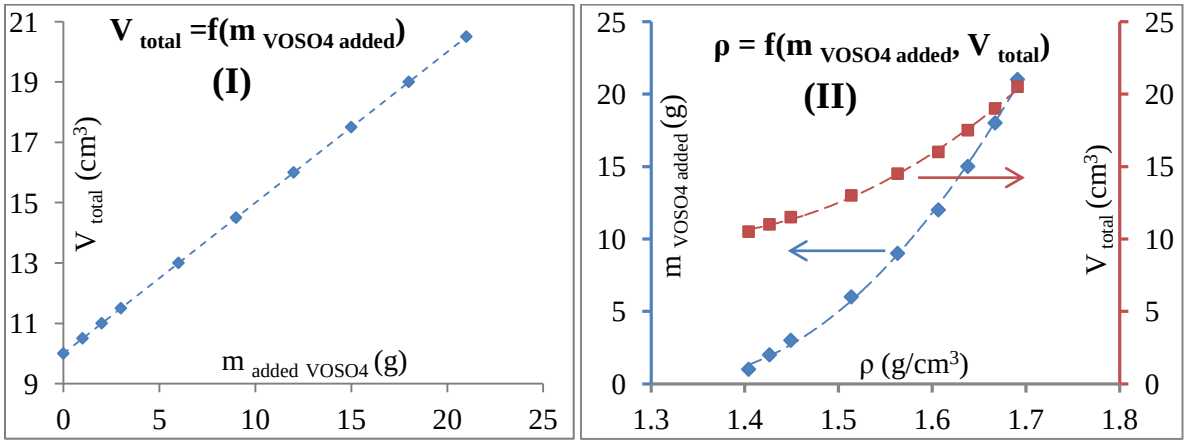

Fig.II.20: **(I)**: Evolution of the total volume of the suspension as a function of the added quantity of $VOSO_4$ powder in the saturated solution; **(II)**: evolution of the calculated density as a function of the added quantity of $VOSO_4$ powder and the total volume of the suspension.

The volume of the suspension increases linearly with the mass of the $VOSO_4$ powder added in the saturated solution (Fig.II.20-(I)). The graph on the right indicates the evolution of the density of the suspension, against the mass or the volume of the solid added. The following correlations can be extracted from Fig.II.22 to have a generalized evolution of V (linear) and ρ (polynomial):

$$V_{total} = 0.5 m_{added\ VOSO_4} + V_{saturated\ solution} \quad \text{Eq.II.5}$$

$$m_{added\ VOSO_4} = 152.16\rho^2 - 403.61\rho + 268.05 \quad \text{Eq.II.6}$$

$$V_{total} = 76.08\rho^2 - 201.8\rho + 144.02 \quad \text{Eq.II.7}$$

These results are useful for the calculation of exact concentrations of the suspensions of vanadium used in the VRFB electrolysis after adding a known vanadium excess, given that the total volume affects the final concentration of the active species involved.

II.4.3. Viscosity measurements

Various experiments, expecting the calculation of the dynamic viscosity, were performed using the experimental setup presented in Fig.II.15; the experiments consist in measuring the mass flow rate as a function of the applied pressure. However, given that the measured values depend on a variety of factors (length of the tube, pressure, measured time and weight) which can each introduce an error to the calculated viscosity in addition to the complications introduced with the solid particles, we will consider that the values obtained correspond to the 'apparent viscosity' of the solutions/suspension.

II.4.3.1. Apparent viscosity measurements of $V^{(IV)}$ solutions

First, the viscosities of solutions containing $V^{(IV)}$ at 0.5, 1,1.5 and 2 M in 3 M sulfuric acid are measured at 20 and 25 °C. Other temperatures were not tested due to the difficulty to thermoregulate the capillary tube. The obtained results (indicated in Fig.II.21) show a slight decrease in the viscosity, from 4.1 to 3.6 mPa.s for the 1.5 M solution, when increasing the temperature from 20 to 25 °C. It should be noted that the solubility of $V^{(IV)}$ at these temperatures in 3 M H_2SO_4 is around 1.8 M and the solution at 2 M was obtained by heating to dissolve all the vanadium powder.
The apparent viscosity appears to increase exponentially as a function of the vanadium concentration; the correlation obtained is given in Eq.II.8, where α is a constant that varies with temperature.

$$\mu_{apparent} = \alpha e^{0.75[VO^{2+}]} \qquad \text{Eq.II.8}$$

On the other hand, the evolution of $\mu_{apparent}$ with temperature at a fixed concentration appears to be linear ($\mu_{apparent} = \beta T_{(K)}$). Although it might be straightforward to think that the linear curves would have the same slope, it was found that this was not the case and the values of β for the concentrations of 0.5, 1,1.5 and 2 M are: - 1.29×10^{-2}, - 6.28×10^{-2}, - 7.71×10^{-2} and - 6.21×10^{-2} respectively.

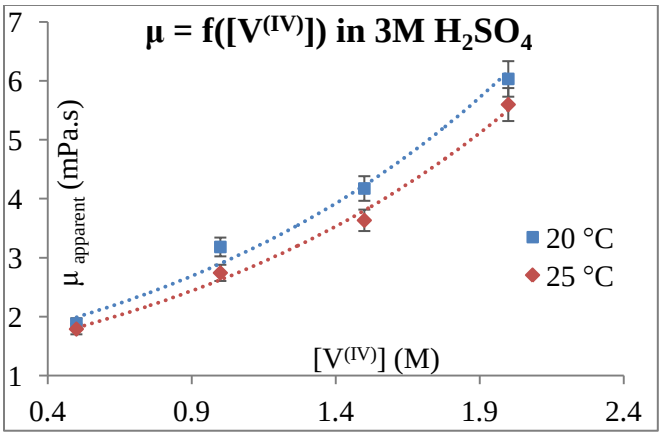

Fig.II.21: Evolution of the apparent viscosity μ as a function of dissolved vanadium (IV) in 3 M sulfuric acid at 20 et 25 °C; Capillary tube in *Viton*® ($\Phi_{internal}$ = 0.75 mm, L = 25 cm), 2000 < ΔP < 3000 Pa.

II.4.3.2. Apparent viscosity measurements of $V^{(V)}$ solutions

The following experiments expect to measure the apparent viscosity of a concentrated solution of $V^{(V)}$ (5 M) obtained by electrolysis and exempted of any solid. This solution appears to be more viscous than the concentrated solutions of $V^{(IV)}$. Moreover, the obtained measurements of the flow, when a *Viton*® capillary tube was used, are not constant and they vary with time. It should be noted that the tube is completely filled with solution before starting the measurements.

To exclude any effect of the tube material on this rheological behavior, the same measurements were performed after substituting the *Viton*® tube by another *Teflon*® tube ($\Phi_{internal}$ = 1.5 mm, L = 15 cm) and the same behavior was observed: under constant pressure, the mass flow of the solution decreased between successive measurements (Fig.II.22).

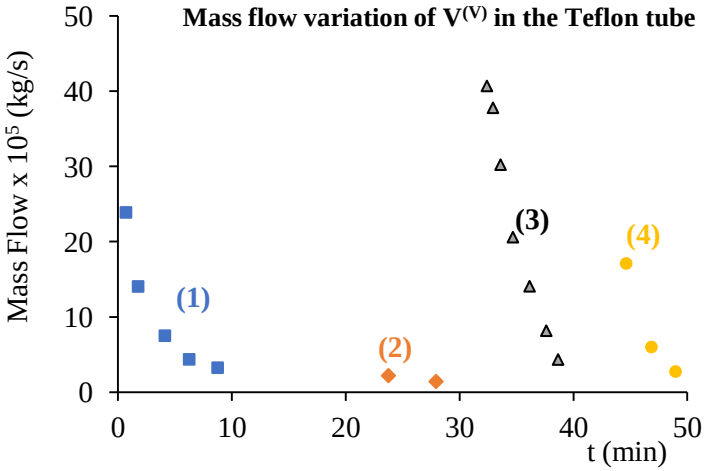

Fig.II.22: Evolution of the mass flow of the 5 M vanadium (V) solution in the *Teflon*® capillary tube ($\Phi_{internal}$ = 1.5 mm, L = 15 cm) as a function of time under a pressure drop ΔP = 5100 Pa, at T = 20 °C. (1): the first series of measurements conducted on a new capillary tube; (2): The solution was immobilized during 15 minutes into the pipe and then the measurements were made; (3): the capillary is removed, emptied and washed before conducting a new series of experiments; (4): the capillary is only slightly emptied.

Note that, nor the interruption of the flow (curve 2, Fig.II.22), nor the partial (curve 4) or the complete cleaning of the pipe (curve 3), enables to stabilize the flow. This behavior suggests a rheopexy of the solution, characteristic of a non-Newtonian fluid: the longer the fluid undergoes shearing force, the higher will be its viscosity, as observed in the present case.

Therefore, in order to carry out the flow measurements and to get an estimation of the viscosity (even a not rigorous value), it was decided to rinse and to dry with compressed air the *Teflon*® capillary tube before each measurement, and then to perform the mass flux measurement at the beginning of the flow (the first 10 s).
Operating this way enables to obtain the viscosity values (called 'apparent' because of the imprecision) indicated in Fig.II.23. The apparent viscosity was measured at three temperatures corresponding to the temperature measured at the outlet of the capillary tube, and the results indicate that the viscosity decreases when T increases (expected evolution). Note that the values of the viscosity of the solution containing 5 M of VO_2^+ are ~ 30 times greater than those obtained with a 2 M $V^{(IV)}$ solution at 20 °C.

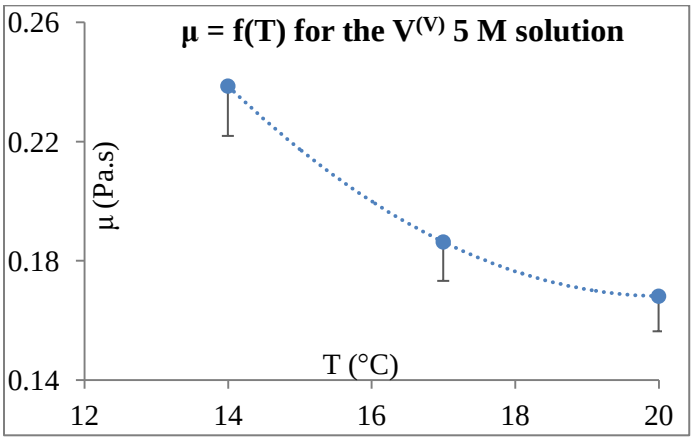

Fig.II.23: Temperature dependence of the apparent viscosity μ of a solution containing 5 M of VO_2^+; Capillary tube in *Teflon*® ($\Phi_{internal}$ = 1.5 mm, L = 15 cm), 3000 < ΔP < 5000 Pa.

The corresponding correlation of $\mu = f(T_{(K)})$ is a second order polynomial (Eq.II.9), different from the exponential evolution observed for the $V^{(IV)}$ solutions.

$$\mu_{apparent} = 1.9 \times 10^{-3} T_{(K)} - 1.11 T_{(K)} + 163 \qquad \text{Eq.II.9}$$

This equation is applicable only for a vanadium (V) concentration of 5 M. The viscosity of supersaturated $V^{(V)}$ solutions was studied by Rahman [22], among which a 5 M solution at different total sulfate concentrations: the viscosity in his study increases from 0.04 Pa.s in a 5 M total sulfate/bisulfate concentration to 0.2 Pa.s in a 7 M total sulfate/bisulfate concentration at 20 °C. The apparent viscosity calculated in our study at the same temperature (0.17 Pa.s) is close to that of the one obtained at 7 M total sulfate, which can lead to formulate two assumptions: i) the

concentration of sulfates during the preparation of the 5 M solution is close to 7 M due to the production of H^+ in solution on one hand and to the addition of $VOSO_4$ excess powder on the other hand and ii) if the previous statement is true, then the method put in place for measuring the apparent viscosities of vanadium solutions is valid.

II.4.3.3. Apparent viscosity measurements of $V^{(IV)}$ and $V^{(III)}$ suspensions

A suspension of $V^{(IV)}$ was prepared by adding 100 g of $VOSO_4.5H_2O$ in 23 g of sulfuric acid at 3 M. The mixture was stirred for 2 h in order to dissolve the maximum amount of the solid and to reach the saturation and leave the rest as excess powder in suspension. In addition, the experimental setup of Fig.II.15 was slightly modified to be adapted for the suspensions: the capillary tube was removed and the mass flow was measured according to the small glass tube ($\Phi_{internal}$ = 2 mm, L = 4 cm) directly attached to the recipient containing the stirred suspension. As a matter of fact, if the capillary tube is used, the suspension tends to sediment inside it and the flow stops. Moreover strong stirring into the vial and high velocity of the suspension into the capillary tube (several hundreds of cm per s) are required to avoid a funnel effect at the entrance of the pipe and the sedimentation into the pipe. In these conditions the suspension flowing at the outlet was assumed to be representative of the mixture contained in the thermoregulated reservoir. The measured value of the apparent viscosity for the $V^{(IV)}$ suspension is 18 Pa.s with an error of ~ 15 % between the performed measurements.

A similar study is undertaken for a vanadium (III) suspension: 28 g of $V_2(SO_4)_3.9H_2O$ was added to 25 g of saturated V^{3+} solution, initially prepared in 3 M sulfuric acid. The measured apparent viscosity value is 14 Pa.s with an error of ~ 10 % between the performed measurements.

These values are very high compared to the ones obtained for the solutions even for the 5 M $V^{(V)}$. The first thing to note is that the measured values for the suspensions are not extremely accurate due to the errors that could be generated by the non-homogeneity of the measured sample. In addition, they depend on the geometry of the system (diameter and length of the tube) and on the hydrodynamics of the system used. Nevertheless, the performed experiments can give at least an order of magnitude of the apparent viscosity of vanadium suspensions.

Given the high values observed, we can expect pressure drops generated during the circulation of such suspensions in the battery which will increase the energy consumption for the pumps. In addition, an increase in this apparent viscosity can have a negative impact on the current because of the decrease of the diffusion of the species and a slower actual flow rate. In all cases, the values for the suspensions will most likely be used for qualitative analysis of the behavior of the suspensions during the functioning of the battery.

In conclusion, the density and viscosity of vanadium solutions have been estimated using the two methods described herein. In the case of suspensions the measurements are very sensitive because of the tendency of the solid particles to sediment and to form colloidal mixtures (as a function of the granulometry which is susceptible to change during cycles 'charge/discharge').
However, the obtained data (ρ and μ) are important to understand and to optimize the performances of a battery (i.e. limiting current, pressure drops, energy consumption because of the flow, or even additional ohmic drops).

II.5. Conclusion

As a conclusion for the present chapter, various analytical techniques were described for the characterization and quantification of vanadium solutions used as electrolytes in the VRFB. First, the setup for the preparation of the vanadium powders or solutions is presented; it consists of a U-shaped cell in which vanadium (IV) suspensions undergo electrolytic conversions to form $V^{(II)}$ and $V^{(III)}$ powders and $V^{(V)}$ solutions.
After preparing the required initial material in vanadium, they can now be analyzed for their electrochemical behavior and their physico-chemical properties:

- The electrochemical three-electrode cell is composed of a graphite working electrode, a saturated calomel reference electrode and a platinum counter electrode for plotting I = f(E) curves to study the vanadium redox systems;
- The physico-chemical properties consist in measuring the density and viscosity of vanadium solutions and suspensions which can be useful for the interpretation of the phenomena during functioning of the battery. The experimental setups, put in place in the lab, are presented along with the obtained results.

It was found that the apparent viscosity of a 5 M vanadium (V) solution is about 30 times higher than that of a 2 M vanadium (IV) solution at 20 °C ($\mu_{apparent, V(IV)} = 6x10^{-3}$ Pa.s << $\mu_{apparent, V(V)}$ = 0.17 Pa.s). The variation of $\mu_{apparent}$ with temperature is a second order polynomial for $V^{(V)}$, studied at 14, 17 and 20°C and varies exponentially as a function of the vanadium (IV) concentration.
Measuring the density and apparent viscosity of vanadium suspensions was found to be harder than the solutions; for the density an evolution of the variation of the total volume of a saturated solution with addition of excess powder gave a correlation of $V_{total} = 0.5m_{added\ VOSO_4} + V_{saturated\ solution}$. The apparent viscosity of suspensions, found to be more than 80 times higher than that of $V^{(V)}$ solutions and 2500 times higher than $V^{(IV)}$ solutions, should be carefully interpreted as it is greatly influenced by all the experimental conditions of the setup.

On another note, the characterization of vanadium solutions is also an important criterion for the VRFB as it allows a quantitative follow-up of the concentrations. The UV–Vis spectrometry is efficient when only one of the oxidation states is present in solution, especially for the negolyte,

because of the overlapping of the characteristic peaks at several wavelengths. The $V^{(II)}$ can be analyzed at the characteristic wavelength of 855 nm with $\varepsilon = 2.04$ L.mol^{-1} cm^{-1}, $V^{(III)}$ at λ_{chosen} = 401 nm with $\varepsilon = 11.17$ L.mol^{-1} cm^{-1}, $V^{(IV)}$ at $\lambda_{chosen} = 760$ nm with $\varepsilon = 19.92$ L.mol^{-1} cm^{-1}, while $V^{(V)}$ did not appear to have a characteristic peak in the UV-Vis spectrum.

This lead to searching for a complimentary method for the quantification, and potentiometric titration was found to be adequate: $V^{(V)}$ can be titrated with $Fe^{(II)}$, $V^{(II)}$ with I_2 and $V^{(III)}$ can be indirectly titrated with I_2 after chemically reducing it to $V^{(II)}$ by reaction with solid Zn. The acidity, or free H^+ concentration, can be determined separately from the vanadium (III) and (IV) by titration with a NaOH solution. In addition, ICP–OES appears to be essential for the determination of exact total vanadium concentrations and water content and can be also used for the analysis of total sulfate in solution.
The NMR was also addressed as a characterization technique, allowing the analysis of vanadium solutions for the determination of the presence of different species of the same oxidation state.

In the next chapter, the electrochemical characterization of vanadium solutions will be detailed as a function of the vanadium oxidation state and the effect of different parameters to try to find the optimal conditions for the preparation of the electrolyte solutions.

References:

[1] W. Moura De Carvalho Jr, L. Cassayre, D. Quaranta, F. Chauvet, R. El-Hage, T. Tzedakis, B. Biscans, "Stability of highly supersaturated vanadium electrolyte solution and characterization of precipitated phases for Vanadium Redox Flow Battery", J. Power Sources, 2020, Under review

[2] A. Hassan, T. Tzedakis, "Enhancement of the electrochemical activity of a commercial graphite felt for vanadium redox flow battery (VRFB), by chemical treatment with acidic solution of $K_2Cr_2O_7$", Journal of Energy Storage, 26, 2019, 100967, doi: 10.1016/j.est.2019.100967

[3] M.H. Penner, "Basic Principles of Spectroscopy", in book "Food Analysis", Springer International Publishing, 2017, pages: 79-88

[4] C. De Caro, C. Haller, "UV/VIS Spectrophotometry - Fundamentals and Applications", book, Metler-Toledo publication, 2015

[5] H.H. Perkampus, "UV-VIS Spectroscopy and Its Applications", book, Springer, 1992.

[6] N.H. Choi, S.k. Kwon, H. Kim, "Analysis of the Oxidation of the V(II) by Dissolved Oxygen Using UV-Visible Spectrophotometry in a Vanadium Redox Flow Battery", J. Electrochem. Soc., 160 (6), 2013, A973-A979, doi: 10.1149/2.145306jes

[7] R.P. Brooker, C.J. Bell, L.J. Bonville, H.R. Kunz, J.M. Fenton., "Determining Vanadium Concentrations Using the UV-Vis Response Method", J. Elechtochem. Soc., 162 (4), 2015, A608-A613, doi: 10.1149/2.0371504jes

[8] S.C. Furman, C.S. Garner, "Absorption Spectra of Vanadium (III) and Vanadium (IV) Ions in Complexing and Non-complexing Media', J. Am. Chem. Soc., 72 (4), 1950. 1785-1789, doi: 10.1021/ja01160a105

[9] Z. Tang, D.S. Aaron, A.B. Papandrew, T.A. Zawodzinski, Jr, "Monitoring the State of Charge of Operating Vanadium Redox Flow Batteries", ECS Transactions, 41 (23), 2012, 1-9, doi: 10.1149/1.3697449

[10] X. Gao, R.P. Lynch, M.J. Leahy, D.N. Buckley, "Spectroscopic Study of Vanadium Electrolytes in Vanadium Redox Flow Battery (VRFB)", ECS Transactions, 45 (26), 221st ECS Meeting, 2013, doi: 10.1149/04526.0025ecst

[11] F. Grossmith, P. Llewellyn, A. Fane, M. Skyllas-Kazacos, "Proceedings of Symposium on Energy Storage: Load Levelling and Remote Applications", Electrochem. Soc. Proceedings, Electrochem. Soc., 88 (11), 1988

[12] C. Petchsingh, N. Quill, J.T. Joyce, D.N. Eidhin, D. Oboroceanu, C. Lenihan, X. Gao, R.P. Lynch, D.N. Buckley, "Spectroscopic Measurement of State of Charge in Vanadium Flow Batteries with an Analytical Model of V^{IV}-V^{V} Absorbance", Journal of The Electrochemical Society, 163 (1), 2016, A5068-A5083, doi: 10.1149/2.0091601jes

[13] P. Blanc. C. Madic, J. P. Launey, "Spectrophotometric identification of a mixed-valence cation-cation complex between aquadioxovanadium (V) and aquaoxovanadium (IV) ions in perchloric, sulfuric, and hydrochloric acid media", Inorg. Chem., 21, 8, 1982, 2923-2928, doi: 10.1021/ic00138a003

[14] K. Okamoto, W.S. Jung, H. Tomiyasu, H. Fukutomi, "Vanadium-51 NMR Line-broadening in the Mixture of Dioxovanadium (V) and oxovanadium (IV) Ions in Perchloric Acid Solution", Inorganica Chimica Acta, 143, 1988, 211-221, doi: 10.1016/S0020-1693(00)83692-0

[15] K.L. Chawla, J.P. Tandon, "Vanadium compounds in reductimetric titrations-I: Standardisation of vanadium (II) sulphate with iron (III) solution", Talanta, 12 (7), 1965, 665-669, doi: 10.1016/0039-9140(65)80090-X
[16] K.L. Chawla, J.P. Tandon, "Vanadium compounds in reductimetric titrations-III: Applications of vanadium (II)", Talanta, 13 (6), 1966, 859-862, doi: 10.1016/0039-9140(66)80292-8
[17] F. Rahman, M. Skyllas-Kazacos, "Solubility of vanadyl sulfate in concentrated sulfuric acid solutions", J. Power Sources 72 (2), 1998, 105–110, doi: 10.1016/S0378-7753(97)02692-X
[18] F. Aureli, S. Ciardullo, M. Pagano, A. Raggi, F. Cubadda, "Speciation of vanadium (IV) and (V) in mineral water by anion exchange liquid chromatography-inductively coupled plasma mass spectrometry after EDTA complexation", Journal of Analytical Atomic Spectrometry, 23 (7), 2008, 1009-1016, doi: 10.1039/b805234b
[19] El-Sayed A Manaa, "Selective Leaching of Vanadium from Boiler Oiled Ash Residue Using Sodium Carbonate-Bicarbonate Binary Solution", Chem Technol Ind J., 13 (1), 2018, 124
[20] M. Vijayakumar, S.D. Burton, C. Huang, L. Li, Z. Yanga, G.L. Graff, J. Liu, J. Hu, M. Skyllas-Kazacos, "Nuclear magnetic resonance studies on vanadium (IV) electrolyte solutions for vanadium redox flow battery", J. Power Sources, 195, 2010, 7709-7717, doi: 10.1016/j.jpowsour.2010.05.008
[21] O.T. Fassulo, "Sulfuric acid: Use and handling", McGraw-Hill, 1965, page 304
[22] F. Rahman, "Stability and properties of supersaturated vanadium electrolytes for high energy density vanadium redox battery", Phd Thesis, University of New South Wales (Australia), 1998

Chapter III – Elucidation of the effect of electrode material and solid particles on the limiting current of vanadium using a three electrodes cell

Table of contents:

Introduction

The aim of this work is to increase the energy density of the battery through increasing the quantity of active species in the electrolytes. Since the vanadium electrolytes are limited by the solubility of the different salts as a function of the sulfuric acid concentration and the operating temperature, as discussed in chapter I, it is proposed here to increase the amount of active species by operating with vanadium suspensions, i.e. adding excess vanadium solid particles to the electrolytes. In addition, a carbon based additive (Ketjen black – KB) is considered for two main reasons: 1) it could create a percolating network in the suspension, extending by that the surface of the electrode to the bulk and enhancing the electronic transfers and 2) it could play the role as a crystallization site during the precipitation of the vanadium salts during the functioning of the battery, as a function of their solubilities, leading to the formation of smaller crystals.
Thus, the effect of the different solid particles should be addressed in order to understand their effect on the electrochemical behavior of the two redox systems and on the resulting limiting current.

In addition, the electrode material is a key component of the VRFB and the choice of the adequate electrode, in combination with the composition of the electrolytes is important.

Thus, the present chapter deals with the study of the effect of various parameters on the limiting current, expecting to enable the choice of the adequate combination of electrodes and electrolytes composition leading to an increase of the energy density of the battery. These parameters include: the electrode material, the vanadium and sulfuric acid concentrations, the oxidation state of vanadium and the presence of solid particles in solution such as vanadium powder and carbon nanoparticles (Ketjen Black – KB). The electrodes studied in this work are, as described in chapter II, graphite rods and graphite felt; they are differentiated mainly by the graphite structure that induces a major impact on the response of the system in current and reversibility. On the other hand, the suspensions, studied for the three oxidation states of vanadium ($V^{(III)}$, $V^{(IV)}$ and $V^{(V)}$), exhibit different behaviors as a function of the nature (vanadium and/or KB) and the quantity of added powder.
The vanadium system is characterized by electrochemical methods, mainly linear sweep voltammetry in a half cell (three electrodes cell), and the results are presented in the following chapter.

The classical three electrodes cell described in chapter II (Fig.II.2) is used. Two models of working electrode (WE) are used:

- a graphite disk (and cylinder both tested) mounted on a rotating body;
- immobile graphite cylinder or carbon felt immersed into the solution and the stirring is performed by a magnetic bar.

It should be reminded that the reference and the auxiliary electrodes are a saturated calomel electrode (SCE) and a platinum plate ($S_{geometrical}$ = 4 cm^2) respectively.

III.1. Characterization of the $V^{(IV)}/V^{(V)}$ system (posolyte)

This study is structured in two parts, the first examines the oxidation of $V^{(IV)}$ to $V^{(V)}$ and the second discusses the reduction of $V^{(V)}$ to $V^{(IV)}$. In the first part, three main sections address the electrode material, the presence of solid particles (vanadium powder and KB particles) and the vanadium oxidation state ($V^{(IV)}$ and $V^{(V)}$).
The study of vanadium (IV) solutions on the two graphite electrodes at different concentrations in the presence of KB will be presented. In this part, the solid graphite is used in two different geometries: a rotating disc and an immobile rod. Then, solid vanadium particles with or without carbon nanoparticles are added to a concentrated $V^{(IV)}$ solution and their effect on the current is analyzed, on both electrodes. In this section, a new experimental setup is introduced; it is constituted of a rotating graphite cylinder (working electrode) and a cross-shaped stirrer (used to enhance the stirring of the powder in suspension).
Finally, the behavior of the vanadium (V) is discussed, starting from the preparation of solutions at 5 mol/L of $V^{(V)}$, to their analysis by linear sweep voltammetry and expecting to understand the effect of the high concentrations on the resulting current, and the addition of KB to the mixture.

All the experiments are performed under ambient temperature (between 20 and 25 °C).

III.1.1. Effect of the electrode material on the oxidation current of $V^{(IV)}$ to $V^{(V)}$ in the absence or presence of KB particles

III.1.1.1 Graphite felt used as working electrode

The electrochemical behavior of the graphite felt is not reproducible (either over time or depending on its history) if no treatment is applied on it [1]; this is due to the presence of different carbon oxygen groups on its surface that are susceptible of being electroactive and interfere with the active species in solution in addition to its important hydrophobic character. The graphite is usually treated with several methods (thermally, chemically, electro-chemically) in order to create oxygenated groups; it appears that these groups have a bigger affinity with vanadium ($V^{(IV)}/V^{(V)}$) and would improve the electrocatalytic behavior of the graphite felt in the positive electrode compartment. Hence, a treatment is necessary in order to obtain reproducible results and a protocol is defined, as described in the previous chapter, for a pre-treatment of the graphite felt (GF). For the purpose of this work involving graphite felt, a standard procedure was adapted for all the used electrodes (one electrode used per solution), in order to activate the surface of the felt and also decrease its hydrophobic state. As a reminder, the graphite felt used has a thickness of 5 mm and the geometrical surface is determined by the length and width of the part of the electrode immersed in the solution.

III.1.1.1.1. Study of the blank solution

Ten cycles of cyclic voltammetry are performed at 50 $mV.s^{-1}$ with the electrode immersed in a 3 M sulfuric acid solution, in the absence of stirring, between 2.5 and - 1 V. It can be seen (Fig.III.1) that as the number of cycles increases, the current increases as well as the appearance of oxidation and reduction peaks, relative to the formation and reaction of oxygenated groups on the surface of the electrode. Moreover, the aspect of the electrode is modified during its treatment: in fact, a non-treated electrode is unable to be soaked by an aqueous solution and the fibers practically repel the water from the surface, conversely, the treated electrodes becomes less hydrophobic and absorbs the sulfuric acid solution.

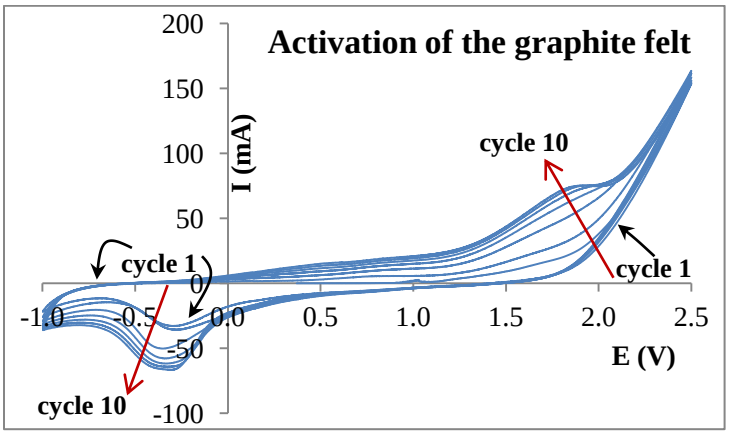

Fig.III.1: Cyclic voltammetry curves plotted on a graphite felt electrode (S_g = 2 cm^2) in 50 mL of a 3 M H_2SO_4 solution for the activation of the electrode; WE = GF, RE = SCE, CE = Pt plate, no stirring, r = 50 $mV.s^{-1}$, 10 cycles from 2.5 to – 1 V.

The activated electrode was used to draw current–potential I= f(E) curves for the different solutions. Fig.III.2 presents two consecutive curves obtained with blank i.e. the supporting electrolyte alone. The first curve (1) exhibits an oxidation peak in the range from 0.4 to ~ 1.8 V, identical to the ones formed during the activation cycles and is followed by the exponentially shaped curve attributed to the water oxidation to O_2. This peak is attributed to the functional groups formed on the surface of the felt during the treatment process.

At the end of the first linear sweep, the electrode is depolarized for one minute and curve N°2 is plotted in the same potential range. The peak observed on the first curve disappears from the second one which means that the C–O groups formed on the surface of the GF electrode are being oxidized. This oxidation being total, curve N°2 shows only the residual current of the solvent, followed by its oxidation. This result is interesting because the presence of such additional peaks is detrimental to the purpose of the study, as the $V^{(IV)}/V^{(V)}$ couple would oxidize in the potential range between 0.8 and 1.5 V (E° = 1 V/SHE). Note also that no reaction occurs in the potential range from 0.5 to 1.1 V, and at 1.5 V the residual current is lower than 3 mA. Yet, the amount of surface groups is low and does not significantly affect the faradaic yield. In

fact, calculating the charge Q by integrating the surface under the curve between curves (1) and (2) allows calculating the number of active sites on the surface of the electrode by assimilating the surface to a Platinum plate which is considered to have 10^{15} atoms/cm^2:

$$N_{sites/cm^2} = \frac{N_{atoms}}{10^{15}} = \frac{n_{mol} \times N_A}{10^{15}} = \frac{Q \times N_A}{F \times 10^{15}}$$

This equation is valid if all the sites are assumed as active. The number of sites per geometric cm^2 N_{sites/cm^2} of electrode surface is found to be equal to 32. The platinum atomic radius is around 1.35 Å while that of the carbon is approximately the half, at 0.7 Å; hence 1 Pt atom is equivalent to 2 carbons. Thus, comparatively, we can say that the real surface area of the graphite electrode is 16 times greater than the corresponding geometrical surface considered.

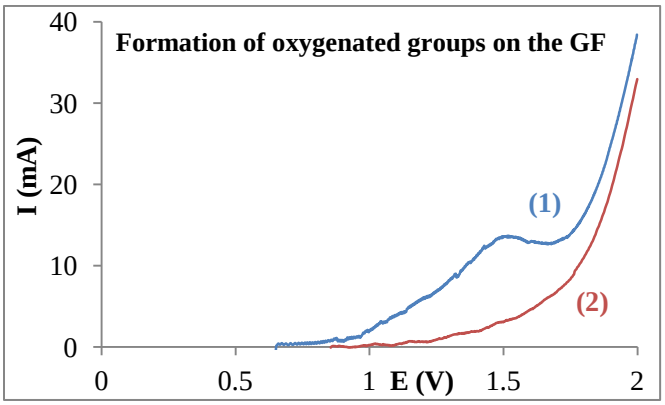

Fig.III.2: Current–potential curves plotted on an activated GR electrode (S_g = 2 cm^2) in 50 mL of a 3 M H_2SO_4 solution, showing the formation of an oxidation peak; (1): first sweep on the electrode and (2) second sweep; WE = GF, RE = SCE, CE = Pt plate, ω ≈ 500 rpm (magnetic bar), r = 5 mV.s^{-1}.

Therefore, for all the upcoming curves on GF electrodes, two consecutive curves were drawn and only the second one will be shown, as it corresponds to the active species in solution without the interference of the oxidation of the C–O groups.
The same phenomenon was observed in reduction in a deaerated solution, but since the system studied in this section is the oxidation of $V^{(IV)}$ to $V^{(V)}$, the results of the reduction of the protons from a sulfuric acid solution on GF are not presented here.

The reproducibility of the I = f(E) curves on graphite felt for the sulfuric acid solutions was validated by drawing and overlaying several curves in the same conditions; a deviation of 1.5 % in the value of the obtained residual current was observed between the different plotted curves and was considered to be acceptable for the study.

In the next part, the effect of the presence of carbon nanoparticles on the oxidation current is studied. The quantity of added KB is a mass percentage of the used solution: for example, in 25 mL of sulfuric acid, adding 1 % in weight of KB corresponds to adding 0.25 g of carbon powder,

with the assumption that 1 mL of sulfuric acid weights 1 g. The KB powder is highly hydrophobic [2], so when putting it in an aqueous solution, it floats on the surface and does not get soaked easily. Hence, to prepare the studied solutions, the KB is added to the aqueous media and subjected to stirring for several hours prior to the analysis. To make sure that all of KB powder is completely wet, no powder should remain on the surface and when left at rest, in the absence of stirring, the powder will eventually sediment at the bottom of the vessel.

Since the effect of KB on the oxidation current of $V^{(IV)}$ to $V^{(V)}$ will be studied, the same amounts are added to the sulfuric acid and the results (I = f(E) curves) are presented in Fig.III.3-(I). The KB is added to 50 mL of initial sulfuric acid at 3 $mol.L^{-1}$, at the following weight fractions: 0.5 % (0.25 g), 1 % (0.5 g), 2 % (1 g) and 5 % (2.5 g).

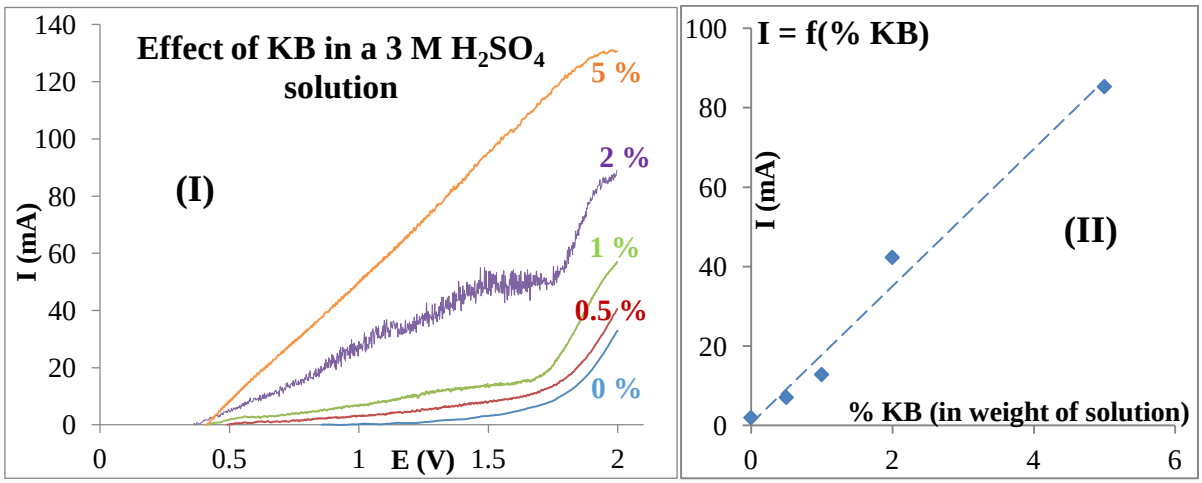

Fig.III.3: **(I)**: I = f(E) curves plotted for 50 mL of 3 M sulfuric acid solution containing, in weight, different quantities of KB powder: 0 % (blue), 0.5% (red), 1 % (green), 2 % (violet) and 5 % (orange); WE = GF (S_g = 2 cm^2), RE = SCE, CE = Pt plate, ω ≈ 500 rpm (magnetic bar), r = 5 $mV.s^{-1}$; **(II)**: Evolution of the current measured at E = 1.4 V as a function of the amount of added KB in weight of solution.

The I = f(E) curve of H_2SO_4 without KB shows the absence of signals in the potential range between 0.5 and 1.5 V; the exponential (E > 1.7 V) corresponds to the oxidation of water. The addition of KB clearly causes the current to increase and the curves show a 'plateau' with a limiting current between 1.2 and 1.6 V.

For the first three curves (0, 0.5 and 1 % (M/M) KB), an increase of the residual current, from practically 0 in the absence of KB to 13 mA for the 1 % suspension, is observed. Then the current increases more drastically for the two higher fractions: 45.8 mA for 2 % KB and 95 mA the 5 % suspension.

These current magnitudes are relatively high compared to those expected for the $V^{(IV)}$ oxidation; the current due to the presence of KB, could be of two types: capacitive (adsorption of SO_4^{2-} anions on the surface of the KB particles) or faradaic due to the oxidation of C–O groups on the surface of KB.

The nanoparticulate nature of KB would explain the absence of peak-shaped signals (typical of surface reactions).

It should be noted that for the 5 % suspension, the obtained mixture is very thick and viscous: it constitutes a kind of paste, the stirring becomes difficult and in this state, the mixture is not suitable for use in circulation in the battery. Therefore, the vanadium solutions will not be studied for this KB fraction.

III.1.1.1.2. Study of the vanadium solutions

After performing the analysis on the supporting electrolyte, vanadium could be added to the solution. It was chosen to start with a low concentration of $V^{(IV)}$ (0.1 M in 3 M H_2SO_4) in order to understand better the effect of the presence of KB particles before increasing the quantity of the active species. It should be noted that for each solution a new graphite felt electrode was activated and used, so that no effect of further activation would be dragged along between solutions and conceal the desired studied effect. Also, as mentioned in the case of sulfuric acid, two consecutive curves were always plotted to remove the effect of the oxidation of C–O groups due to the activation of the felt, but it appears that each two consecutive curves are reproducible without the appearance of the peaks observed in curve (1) of Fig.III.2. This could mean that the amplitude of the peak is negligible compared to the current obtained from the oxidation of the vanadium.

The simplified oxidation reaction of $V^{(IV)}$ to $V^{(V)}$ could be written as:

$$VO^{2+} + H_2O \rightarrow VO_2^{+} + 2\,H^{+} + 1\,e^{-} \qquad E° = 1.00\ V/SHE \qquad Rx.III.1$$

The I = f(E) curves presented in Fig.III.4 (I) shows that in the absence of KB (blue curve), the curve exhibits a classic shape with a diffusion plateau which occurs at higher potentials than the ones observed in the presence of KB. This can be attributed to an important ohmic drop due to the configuration in which the graphite felt is used, which consists in using a 10 cm long band with the electronic connection placed at the end, far from where the electrode touches the solution. The addition of KB in the bulk causes the following changes:

- The overall current decreases when KB nanoparticles are added (Fig.III.4-(II));
- The curves exhibit a peak at around 1.4 V.

A low stirring could be the reason of the presence of these peaks. Here, the magnetic bar turns at 500 RPM and the suspensions were sufficiently stirred; however, it is possible that the KB accumulates within the felt and the $V^{(IV)}$ solution becomes more or less stagnant. In this case, the electrochemical answer of the system could give a peak.

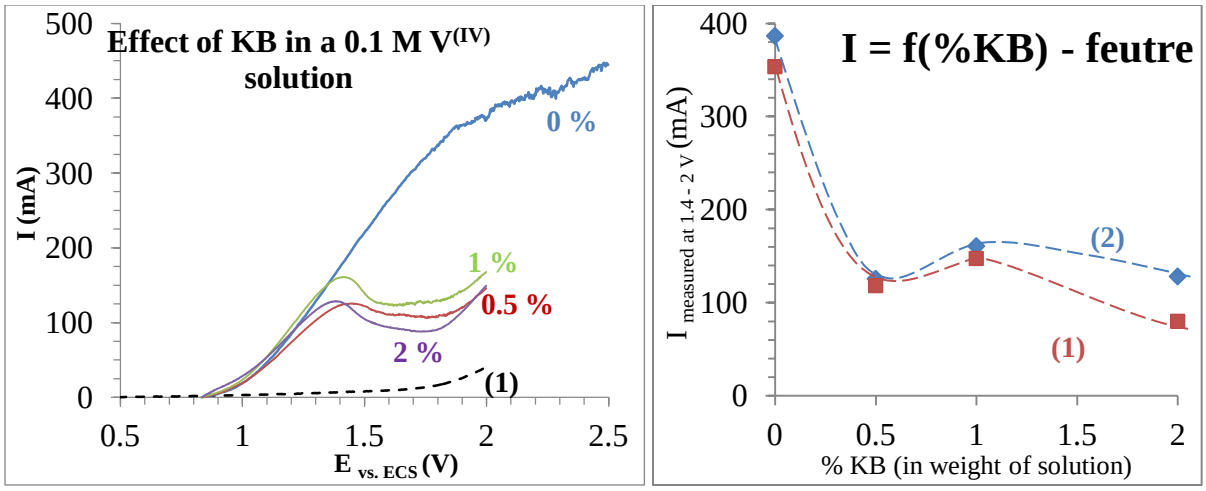

Fig.III.4: **(I)**: Dependence of the I = f(E) curves on the KB %, obtained for the oxidation of a 0.1 M $V^{(IV)}$ solution in 3 M H_2SO_4 into a 50 mL solution: 0 % (blue), 0.5% (red), 1 % (green) and 2 % (violet); curve 1 = blank (0.5 % KB) extracted from Fig.III.3; WE = GF (S_g = 2 cm^2), RE = SCE, CE = Pt plate, ω ≈ 500 rpm (magnetic bar), r = 5 $mV.s^{-1}$; **(II)**: Evolution of the current as a function of the amount of added KB in weight of solution: (1, blue): total current of vanadium and residual current from the solvent; (2, red): net current exempted from the residual current.

The peak shaped curves obtained in the presence of KB can also be explained by the adhesion of carbon nanoparticles on the surface of the graphite felt, or simply "sticking" on the fibers, probably prohibiting the renewal of the active species in the diffusion layer. In the case of this study, it appears that starting from 0.5 % in weight of KB, the amount of nanoparticles is enough to cause the slogging of the fibers and decrease the current. The expected percolation effect from the KB, with stirring of the solution, is not observed which was supposed to extend the actual surface of the GF electrode into the bulk; the oxidation reaction of vanadium could have occurred in solution with electronic exchanges happening on the surface of the KB particles, instead of diffusing to the surface of the electrode (Fig.III.5); however, it appears that the clogging effect is more pronounced.

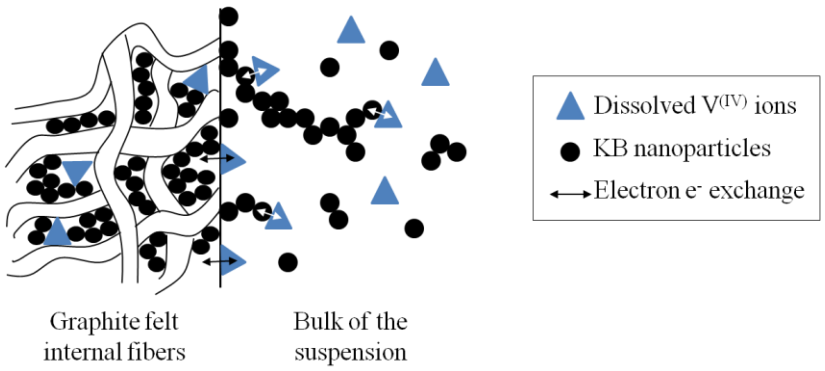

Fig.III.5: Schematic representation of the KB particles percolation in solution: the exchange of the electrons in the bulk occurs on the surface of the KB (white arrow) as well as on the electrode surface (black arrow); it also shows KB nanoparticles accumulated between the GF fibers (it should be noted that the real geometrical proportions are not respected for the scheme)

As a matter of fact, the nanoparticles present in higher quantities could limit the transport of vanadium by diffusion inducing an overall lower current. Another assumption could be that the nanoparticles could agglomerate thus reducing their specific surface area in the bulk and consequently the percolation to the surface of the electrode.

To sum up, the use of KB nanoparticles in the presence of a graphite felt electrode is susceptible to cause a clogging of the surface by sticking on and inside of the carbon fibers, and this would impact negatively the resulting current, even though it does not cancel it completely.

III.1.1.2 Solid graphite used as working electrode

Carbon based electrodes are widely used in the domain of vanadium redox flow battery since they fulfill three of the most important required criteria: high active surface area, low cost and good resistivity against acids. The graphite felt discussed above checks the three categories but requires significant activation to increase the electro-affinity of the carbon fibers to vanadium, make it hydrophilic and improve the reversibility of the system. Moreover, in the presence of KB nanoparticles, clogging of its surface reduces its performances. Therefore, in the present work another carbon based electrode was studied: low cost solid graphite which is resistant to acid media, and also mechanically more resistant than the graphite felt. In the following part of this chapter, two configurations of solid graphite electrodes will be studied for the oxidation of $V^{(IV)}$ to $V^{(V)}$: a disc and a cylinder.

III.1.1.2.1 Effect of a graphite disc mounted on a rotating electrode body

The first study was carried out using disc of graphite (Φ = 3 mm) a working electrode surrounded by a Teflon rod. The tip is fixed on a rotating body to form the rotating disc electrode (RDE). The experimental setup corresponds to the one described in Fig.II.2 of chapter II.
Unlike the GF, the graphite disc (GD) electrode appears to have a better affinity to the vanadium system and does not need a special treatment before use, even though its response can be enhanced if the surface is treated. For the purpose of this work, no prior processing was inflected on the electrode and the same disc was used for the analysis of several solutions. On the other hand, using solid graphite requires a polishing step in order to have a reproducible surface.

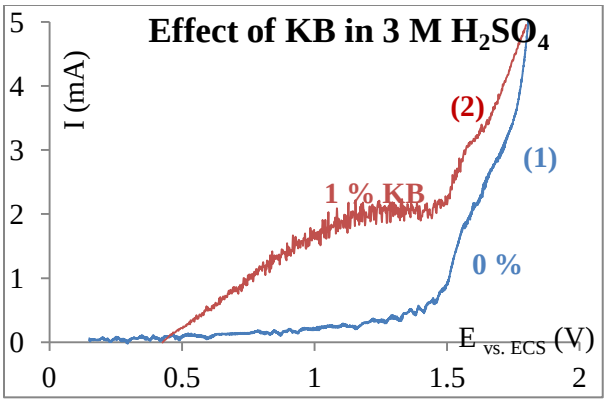

Fig.III.6: I = f(E) curves plotted on a rotating disc electrode immersed in a 50 mL solution of 3 M sulfuric acid without (1, blue) and with 1 % of KB powder (2, red); WE = RDE (S_g = 0.07 cm^2), RE = SCE, CE = Pt plate, ω = 500 rpm (RDE), r = 5 $mV.s^{-1}$.

The curves in Fig.III.6 were obtained with the supporting electrolyte without (1) and with (2) KB. The addition of KB to the sulfuric acid causes the current to increase 8 folds from 0.2 to 1.6 mA at 1 V.

Note that the oxidation wave observed after 1.5 V corresponds to the oxidation of chloride ions that could have been released from the internal solution contained in the reference electrode (KCl at saturation to maintain the potential of the saturated calomel electrode constant).

The curves in Fig.III.7 show the current – potential curves obtained with vanadium (IV) solutions at two concentrations: 0.1 M (red curve) and 1 M (green curve). Both curves exhibit a diffusion plateau corresponding to a VO^{2+} mass transfer limitation and located in the potential range between 1.1 and 1.5 V. then the curves show the exponential of the solvent starting at around 1.8 V.

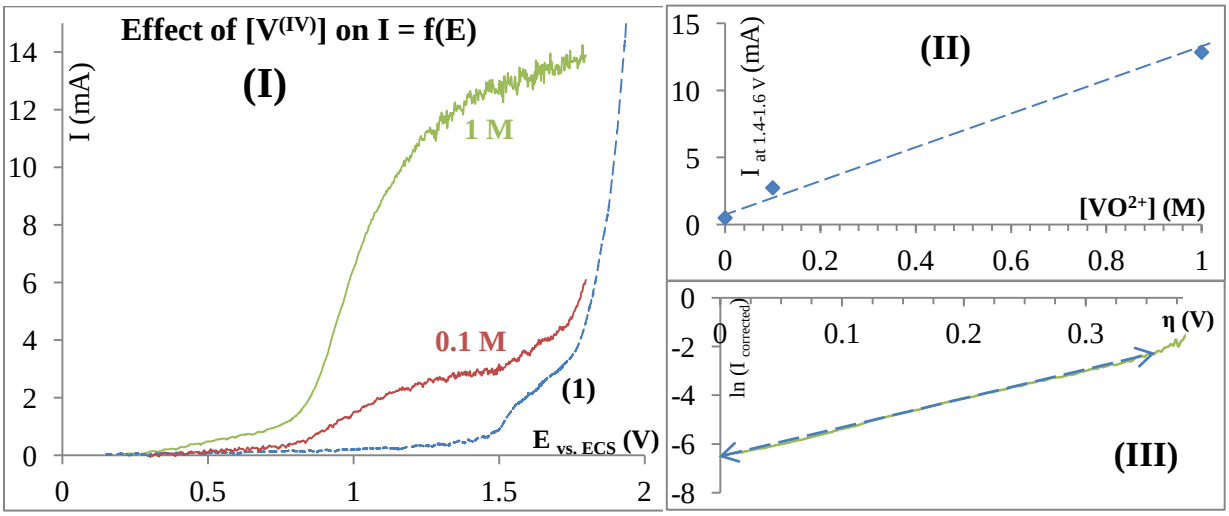

Fig.III.7: **(I)**: I = f(E) curves plotted on a rotating disc electrode immersed in a 50 mL solution of 0.1 M (red) and 1 M (green) of $V^{(IV)}$ in 3 M sulfuric acid solution ((1), blue); WE = RDE (S_g = 0.07 cm^2), RE = SCE, CE = Pt plate, ω = 500 rpm (RDE), r = 5 $mV.s^{-1}$; **(II)**: linear evolution of the limiting current as a function of the vanadium concentration; **(III)**: evolution of *ln* ($I_{corrected}$) as a function of the over potential for the 1 M solution

The analysis of the kinetic properties and reversibility of the $V^{(IV)}/V^{(V)}$ redox system through the oxidation curves of $V^{(IV)}$ can be performed with the Butler-Volmer equation (Eq.III.1), corrected from the diffusion (both the electronic and mass transfer limitations exist), which allows to access to intrinsic heterogeneous electronic transfer kinetic constant for oxidation $k°$ and the anodic electronic transfer coefficient α.

$$I = nFSk°C\frac{I_{lim}-I}{I_{lim}}\exp\left[\frac{\alpha nF}{RT}(E - E_{I=0})\right] \qquad \text{Eq.III.1}$$

The logarithmic study of the previous equation gives the corrected current:

$$\ln I_{corrected} = \ln\left(\frac{I\times I_{lim}}{I_{lim}-I}\right) = \ln(nFSk°C) + \frac{\alpha nF}{RT}\eta \qquad \text{Eq.III.2}$$

(See "Nomenclature" for the different parameters)

The value of the over-potential η = 0 is taken at E = 0.8 V where the reaction appears to start. Plotting $\ln I_{corrected} = f(\eta)$ allows calculating α and $k°$ from the slope and Y-intercept respectively. In Fig.III.7-(III), the dashed arrows delimit the linear part of the curve which served for the calculations.

Table III.1: Values of $k°$ and α obtained for the $V^{(IV)}$ solution at 1 M

	Slope	α	Y-intercept	$k°$ (m/s)
1 M	11.922	0.30	-6.46	$2.32\text{x}10^{-6}$

The value of α is different from 0.5 which means that the studied system is not symmetrical and that it involves complex mechanisms during the reactions at the electrode. In fact, as presented in chapter I, the Rx.III.1 involves oxygen transfers, which certainly complicates the system, in addition to the ion transfer at the surface of the electrode and this leads to a low value of α.

On the other hand, even though the curves in this study are plotted on a solid, untreated graphite electrode, they will be compared to what was found in the bibliography for studies performed on a glassy carbon (GC) electrodes for the $V^{(IV)}/V^{(V)}$ system. E. Sum et al. [3] obtained a value of $k°$ of $7.5\text{x}10^{-6}$ m/s for a vanadium concentration of $5.5\text{x}10^{-2}$ M, on a 3 mm GC disc while Yamamura et al. [4] found $k° = 0.68 \times 10^{-6} m/s$ for a vanadium concentration of $5\text{x}10^{-2}$ M on a 1 mm GC disc. The $V^{(IV)}/V^{(V)}$ system is generally described as a quasi-reversible or irreversable system [3-5] and it appears that even in the bibliography the values do not match and vary in a wide range. This could be attributed to the preparation of the graphite electrode even without applying an activation treatment. Thus, the obtained value for this study will be compared with the upcoming calculation performed in the presence of 1 % of KB.

The increase of the current with the vanadium concentration is presented in Fig.III.7-(II); after deducting the residual current from the supporting electrolyte, the increase in current due to the

vanadium concentration is around 5.2 folds when passing from 0.1 to 1 M (current measured at E = 1.4 V); however, the concentration ratio is equal to 10 and does not correspond to the ratio of the current increase. An assumption for this discrepancy is the decrease of the diffusion coefficient with the increase of the vanadium concentration.

The Fig.III.8 presents the curves obtained in the presence of KB at 1 % in the VO^{2+} solutions.

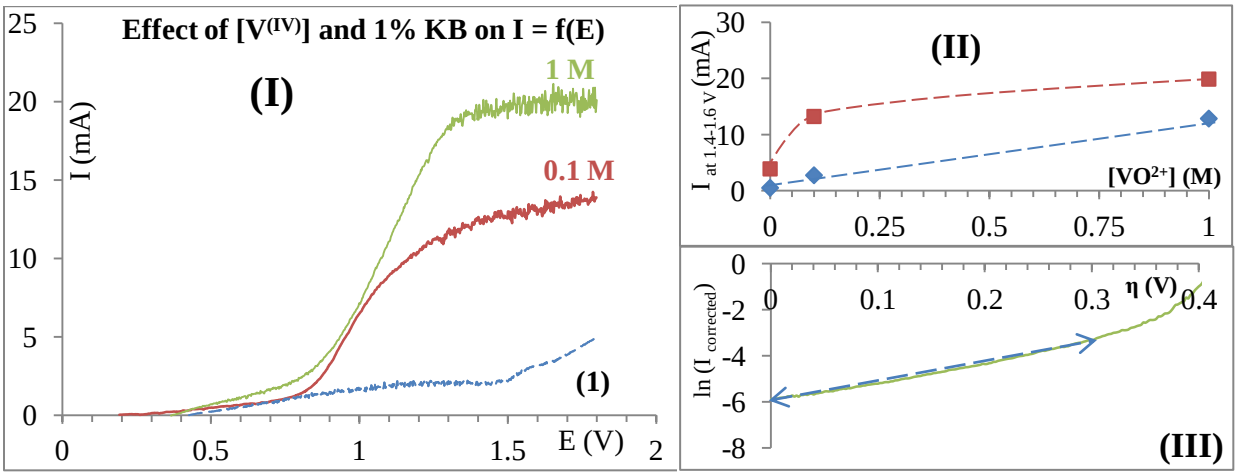

Fig.III.8: **(I)**: I = f(E) curves plotted on a rotating disc electrode immersed in a 50 mL solution of 0.1 M (red) and 1 M (green) of $V^{(IV)}$ in 3 M sulfuric acid (+ 1%KB) solution ((1), blue); WE = RDE (S_g = 0.07 cm^2), RE = SCE, CE = Pt plate, ω_{RDE} = 500 rpm, r = 5 $mV.s^{-1}$; **(II)**: evolution of the limiting current (red cubes), at 1.7 V, as a function of the vanadium concentration, compared to the current obtained without KB (blue diamonds) exported from Fig.III.7-(II); **(III)**: evolution of *ln* ($I_{corrected}$) as a function of the over potential for the 0.1 M solution (red), and the 1 M solution (green)

The addition of KB appears to have a positive effect on the resulting current. For the 0.1 M $V^{(IV)}$ solution, the increase of the net current at 1.7 V brought by the presence of the nanoparticles is around 1.53 times while it is 1.45 folds for the 1 M vanadium (IV) solution, comparatively to the results obtained in Fig.III.7-(I). This effect is opposite to what was observed on the graphite felt electrode (Fig.III.4); here, the presence of KB appears to enhance the electronic transfers and extends the surface of the electrode to the bulk, which corresponds to the desired effect.

The same analysis performed without KB is applied here to see if the presence of carbon nanoparticles affects the kinetic properties of the redox system. The obtained values are presented in table III.2.

Table III.2: Values of $k°$ and α obtained for the $V^{(IV)}$ solution at 1 M in the presence of 1 % in weight of KB

	Slope	α	Y-intercept	$k°$ (m/s)
1 M	8.30	0.21	-5.87	4.18×10^{-6}

As performed for the calculations in the absence of KB, the value of the $\eta = 0$ is taken at E = 0.8 V. It appears that the presence of KB induced a decrease of the value of α by more than 40 % and this means that the system becomes more complex in the presence of KB. However, the value of $k°$ doubles and this allows confirming that the KB nanoparticles enhance the electronic transfers.

It is important to note that the behavior of the system, with or without KB, is not identical for all the vanadium concentrations, thus the values of α and $k°$ can vary significantly. This can be attributed to several parameters:

- Modification of the sulfate concentration;
- Modification of the interactions between the dissolved vanadium and the KB nanoparticles inducing a modification of the percolation network;
- Depending on the vanadium concentration, complex chemical reaction can take place.

To confirm the effect of KB on the increase of the current, another quantity of KB (3 % in weight) was studied for the solution at 1 mol.L^{-1} of VO^{2+} and the results, reported in Fig.III.9-(I), show another increase of the current that was not observed on the graphite felt for 2 % in weight of KB. The difference here is the electrode material and the stirring: the felt keeps the carbon particles between its fibers without being removed by the stirring of the magnetic bar at the bottom of the cell. In the case of the RDE, the only visible surface of the electrode is a 0.07 cm^2 rotating disc exhibiting a smooth surface which does not allow to the KB nanoparticles to accumulate. Thus, the electronic percolation is more effective and enables the enhancement of the current.

Moreover, the presence of carbon particles causes the curves to shift to higher potentials: for the curve at 3 % in weight of KB, the diffusion plateau is not yet completed. In addition, a slight increase of the half-wave potentials can be observed: it increases from 0.988 V to 1.055 V and 1.118 V for 0 %, 1 % and 3 % in weight of KB respectively. This is probably due to the increase of the ionic resistance of the solution, so the observed shift of the curves results from the ohmic drop. This is confirmed also by the decrease of the values of α for the 1 % KB observed in table III.2. The presence of KB also affects the shape of the curves from the beginning (E = 0.5 V), because of the oxidation of the oxygenated groups of the electrode.

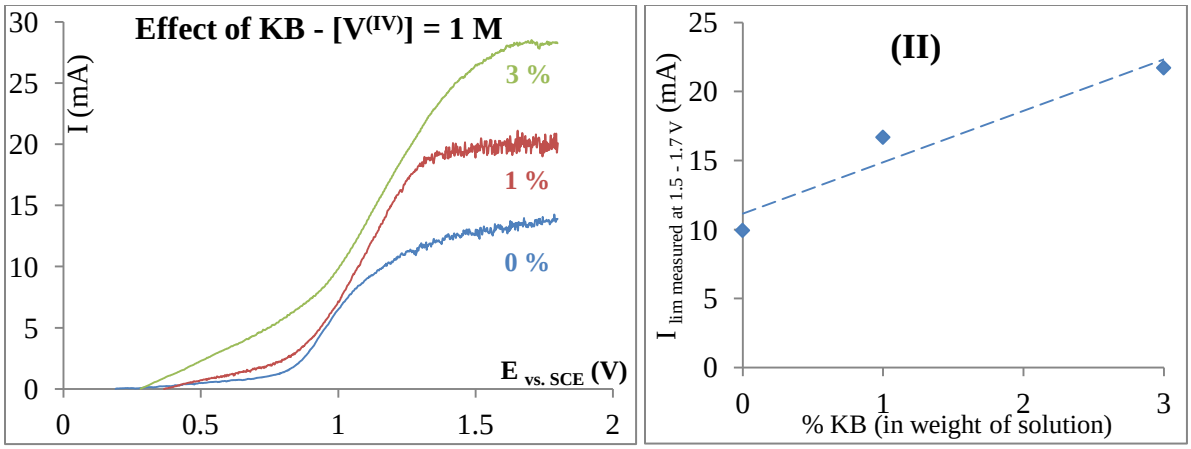

Fig.III.9: **(I)**: Effect of the KB quantity on the I = f(E) curves of the oxidation of 1 M of $V^{(IV)}$ prepared in 3 M H_2SO_4; the curves 0% (blue) and 1 % (red) were imported from Fig.III.6-(I) and III.8-(I); WE = RDE (S_g = 0.07 cm^2), RE = SCE, CE = Pt plate, ω_{RDE} = 500 rpm, r = 5 $mV.s^{-1}$; **(II)**: evolution of the limiting current as a function of the percentage of KB in weight.

The increase of the limiting current with the percentage of KB is linear, with a_{KB} the amount of KB in solution:

$$I_{lim} = 3.73 \times a_{KB} + 11.15 \qquad R^2 = 0.93$$

Another study was performed on the KB suspensions to examine a possible effect of the method of preparation of the KB suspension. Until now, the wetting of the KB was achieved by keeping the solution under stirring for several hours prior to the analysis. The second method consists in introducing the KB nanoparticles into a solution at 70 °C; this appeared to be more efficient and less time consuming for the wetting process. One possible reason of the easier wetting in a heated solution is that at higher temperature, the water molecules are more dissociated in solution and are susceptible of creating easier bonds with the surface oxides of the carbon black leading to its wetting. Another reason could be the fact that the increase of the temperature enables easier removal of the air present in the pores of the KB.

Anyhow, the wetting of the KB by heating the solution could have induced changes in the properties and surface groups of the KB which would in turn impact the response of the vanadium oxidation current. Therefore, two solutions were prepared separately: 1 % in weight of KB nanoparticles were added to two separate solutions of $V^{(IV)}$ at 1 $mol.L^{-1}$ prepared in 3 $mol.L^{-1}$ of H_2SO_4; one solution was left under stirring overnight in order to be sure that all the KB are incorporated correctly into the liquid and the other vanadium solution was heated to 70 °C and then the KB was slowly added and was immediately soaked inside the solution.
Then, current – potential curves were plotted for both solutions using the RDE at 500 RPM and in the same conditions as above. The idea is to examine if the preparation impacts the response of the system. The results (Fig.III.10) show no significant difference between the two curves which means that the activity of the KB in the suspension is not affected by our proposed preparation methods. However, to avoid any alteration of the vanadium solutions due to heating

(possible precipitation for $V^{(V)}$ solutions, water evaporation…) the suspensions will always be prepared by agitation of the KB.

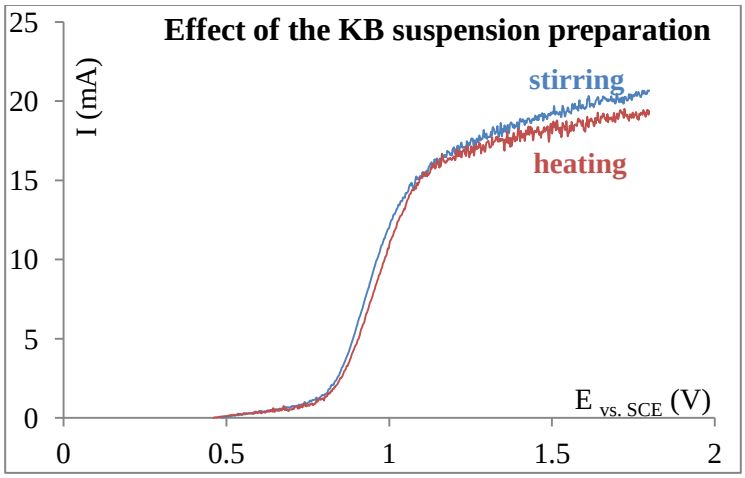

Fig.III.10: Effect of the KB suspension preparation on the I = f(E) curves obtained for the oxidation of 1 M of $V^{(IV)}$ in 50 mL of 3 M sulfuric acid solution in the presence of 1 % in weight of KB particles; the KB suspension was prepared by stirring (blue) or prior heating of the solution (red); WE = RDE (S_g = 0.07 cm^2), RE = SCE, CE = Pt plate, ω = 500 rpm (RDE), r = 5 $mV.s^{-1}$.

Lastly, the effect of the stirring rate of the RDE was examined for a 1 $mol.L^{-1}$ VO^{2+} solution containing 1 % in weight of KB particles. The results (Fig.III.11-(I)) show that the I = f(E) curves exhibit a classical form, with a plateau ($1.1 < E_{(V)} < 1.5$) corresponding to a mass transfer limitation. Increasing the angular velocity in the range from 0 to 2500 RPM causes the current to increase more than eight times:

- For $\omega_{RDE} \leq 50$ RPM, the curves present a peak typical of a concentration depletion at the diffusion layer; increasing the stirring causes the peak to disappear
- For $\omega_{RDE} \geq 1000$ RPM, the curves are deformed, where the slope of the plateau increases with the rotation frequency. One possible explanation could be the modification of the ionic resistance of the interfacial solution during the plotting of the I = f(E) curves. In fact, the modification of the composition of the solution, especially at high currents, creates ohmic drops which deform the curves.

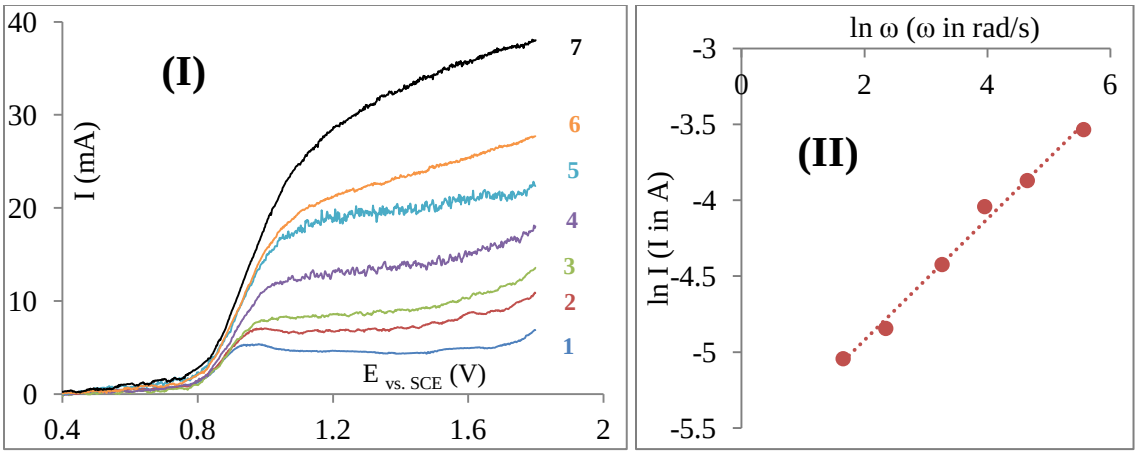

Fig.III.11: **(I)**: Effect of the stirring rate of the working electrode on the shape of the current-potential curves obtained at the quasi-steady state for the oxidation of a suspension of $V^{(IV)}$ to $V^{(V)}$ containing 1 % in weight of KB; Primary data: angular velocity of the electrode ω = 0, 50, 100, 250, 500, 1000 and 2500 RPM for the curves I = f(E) 1 to 7 respectively. $[V^{(IV)}]$ = 1 mol.L^{-1} in $[H_2SO_4]$ = 3 mol.L^{-1}; r = 5 mV.s^{-1}; WE = rotating disc electrode (RDE); S_{WE} = 0.07 cm²; CE = Pt plate. **(II)**: Evolution of ln (I) as a function of ln (ω); the currents were extracted from graph (I) at E = 1.4 V with subtraction of the corresponding residual current for each ω.

The Fig.III.11-(II) clearly shows a linear evolution of the natural logarithm of the current (picked at E = 1.4 V for all curves, thus considered as a limiting current), against the natural logarithm of the angular velocity ω. The values of I correspond to the faradic oxidation current of $V^{(IV)}$ after subtracting the H_2SO_4 + 1 % KB at the different stirring rates studied.

$$ln\ I_{\ at\ 1.4\ V,in\ A} = -5.72 + 0.4 \times ln\ \omega_{rad/s} \qquad R^2 = 0.99 \qquad \text{Eq.III.3}$$

The magnitude of the obtained slope (0.4) is lower than that predicted by Levich's correlation ($I_{\ lim} = f(\omega^{0.5})$) for a rotating disc electrode in "homogeneous solutions". In the case of the studied suspensions, the presence of solid KB particles might compromise the stability of the flow by colliding on the surface of the electrode. Besides, the Reynolds number, characteristic of the flow regime, is function of the kinematic viscosity ν of the liquid; the studied solutions to which the Levich law is applied are rather diluted and do not contain solid particles and this factor can contribute therefore to the deviation of the slope from the '0.5' normal value.

In conclusion, it was found that the increases of the concentration of vanadium (IV) as well as the quantity of added KB particles have a positive impact on the oxidation current, studied on a 0.07 cm^2 graphite disc mounted on a rotating electrode body. Compared to the results obtained on the graphite felt in the presence of KB, i) the magnitude of the current is $\sim\frac{160}{13} = 12$ folds higher in the case of graphite felt compared to a graphite RDE, ii) the curves exhibit a more 'classic' shape compared to these on the GF which exhibits a peak characteristic of a depletion of active species at the electrode surface and iii) in the presence of KB, the current did not decrease as in the case of the GF probably due to the difference between the structure of the two electrodes.

However, adding KB nanoparticles was found to increase the irreversibility of the system on the RDE, observed by a decrease of more than 40 % of the value of the anodic electronic transfer coefficient α.
The preparation of the KB suspensions was also addressed; no significant impact was observed on the resulting current between the two preparation methods; the mode of preparation chosen for all the suspensions in this work is the agitation until complete wetting of the particles.

III.1.1.2.2 Immobile graphite rod used as working electrode

In this part of the work, the same analysis performed on the graphite felt (section **III.1.1.1**) is repeated but on an immobile graphite rod (GR): the electrode is immobile, the stirring is ensured by a magnetic stirrer at the bottom of the cell and the working surface of the electrode is formed by a lateral cylinder in addition to the disc forming the base, hence, the flow of the solution on the electrode is not identical to that observed for the RDE. As mentioned before, no activation treatment was performed on the solid graphite and the same electrode was used as is for all the studied solutions.
This solid graphite electrode was chosen as the working electrode material for the study of the effect of the presence of vanadium solid particles in the electrolyte solutions.

After performing the analysis on the supporting electrolyte, the effect of the presence of 3 amounts of KB nanoparticles (0.5, 1 and 2 % in weight) in a 0.1 M vanadium solution was studied. The curves presented in Fig.III.12-(I) show an increase in the current with the increasing amount of KB even for the highest fraction of 2 %. After subtracting the residual current of the supporting electrolyte, it appears that the increase of the current is mostly significant for the highest percentage of 2 %.

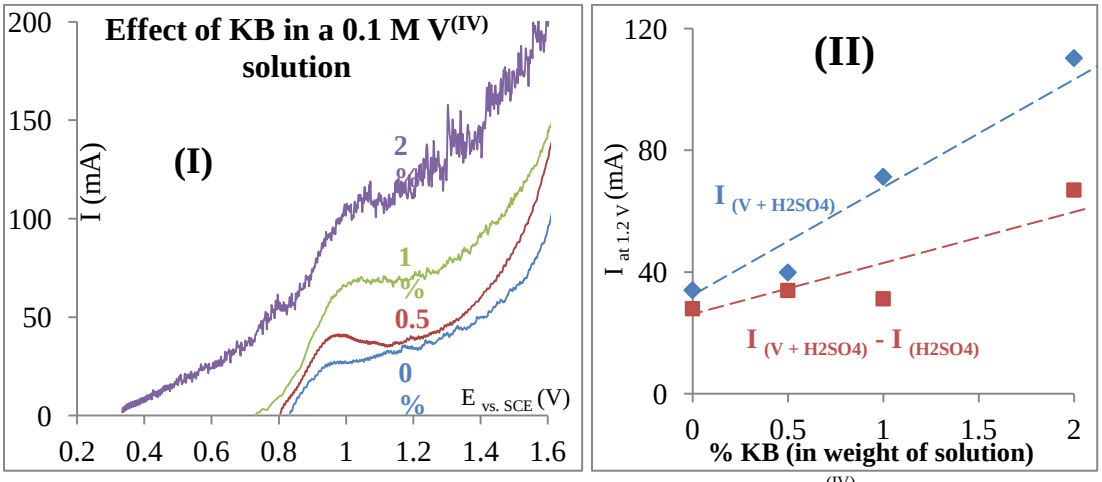

Fig.III.12: **(I)**: Effect of the KB on the I = f(E) curves of the oxidation of 0.1 M $V^{(IV)}$ in 3 M sulfuric acid solution containing, in weight, different quantities of KB powder: 0 % (blue), 0.5% (red), 1 % (green) and 2 % (violet); WE = GR (S_g = 2 cm^2), RE = SCE, CE = Pt plate, ω ≈ 500 rpm (magnetic bar), r = 5 $mV.s^{-1}$; **(II)**: Evolution of the current at 1.2 V as a function of the amount of added KB in weight of solution: blue: total current of vanadium and residual current from the solvent, red: current corresponding only to the vanadium oxidation after subtraction of the residual current.

However, the current obtained on the GF was still higher (~ 85.6 mA compared to ~ 67 mA on the GR) for the 2 % fraction even though the current decreased and the felt was clogged with KB particles. This shows clearly that the real active surface of the felt is greater than that of the solid graphite electrode. In fact, as determined from Fig.III.2, the ratio of $S_{real}/S_{geometric}$ for the graphite felt is approximately 15 while that of the graphite rod is close to 1.

In order to discuss further this point, a more concentrated solution of VO^{2+} was prepared: 1.5 M in 3 M of H_2SO_4, and it was studied on both electrode materials with a smaller electrode geometrical surface (0.5 cm^2 for the GF and 1 cm^2 for the GR). The curves obtained on the two electrodes exhibit the same 'classical' shape (Fig.III.13): a diffusion plateau is observed on both with a higher current on the graphite felt even though its surface is smaller, so for comparison, a theoretical curve is placed in a black dashed line and corresponds to what would have been obtained on a 0.5 cm^2 graphite rod. The limiting current is increased by about 3 folds on the graphite felt used as working electrode (from ~ 75 mA on the supposed GR, S_g = 0.5 cm^2 to ~ 217 mA on the GF, S_g = 0.5 cm^2).

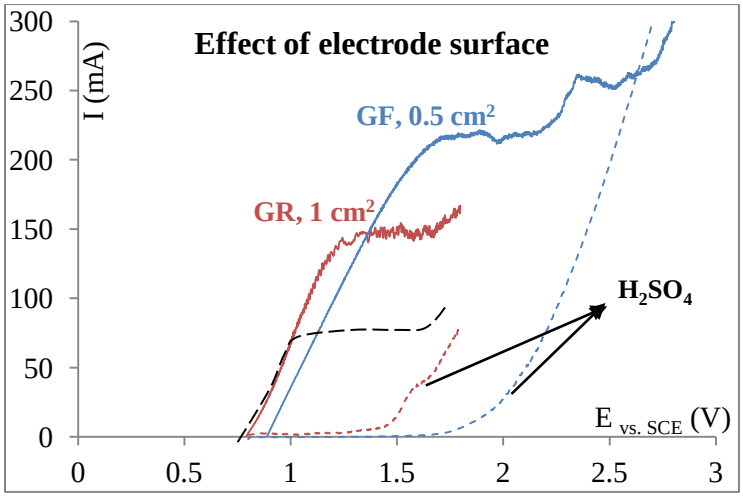

Fig.III.13: Comparison of the I = f(E) curves performed on two electrodes (GF, S_g = 0.5 cm^2 (blue)) and GR, S_g = 1 cm^2 (red). The black dashed line corresponds to a schematic representation of a possible curve performed on a GR, S_g = 0.5 cm^2; [VO^{2+}] = 1.5 M; [H_2SO_4] = 3 M on the corresponding electrode: dashed curves; RE = SCE, CE = Pt plate, ω ≈ 500 rpm (magnetic bar), r = 5 $mV.s^{-1}$.

All the results obtained on the graphite felt suggest a better efficiency through a higher generated current for the same analysis conditions between the two studied electrode materials. However, it must not be forgotten that the purpose of this study is to increase the energy density of the battery by increasing the electrolyte solutions concentrations through the addition of vanadium solid particles (with or without carbon black). Therefore, the effect of solid particles should be studied on both electrodes before choosing the adequate material for the reactor, and this part will be addressed in the following section.

III.1.2. Effect of the presence of vanadium solid particles ($VOSO_4$) on the oxidation current of $V^{(IV)}$ to $V^{(V)}$

For the preparation of the vanadium suspensions, an important parameter to know is the total volume of the slurry. As seen in the study of the density of vanadium suspensions in chapter II, an amount of X grams of added $VOSO_4$ powder to a vanadium saturated solution increases the volume of the suspension of a value of X/2 mL.
The equivalent $V^{(IV)}$ concentrations of the studied suspensions in the next part of the study are: 2.73, 3.57 and 4.5 mol/L prepared separately by adding the required amount of $VOSO_4.5H_2O$ powder into 25 mL of a vanadium solution at 1.6 mol/L in 3 mol/L H_2SO_4. The increase of the concentration increases the viscosity of the suspension; the 4.5 mol/L suspension appears to me more of a paste than a fluid and stirring using a magnetic bar becomes difficult.
Each suspension was studied on both electrode materials discussed above: the graphite felt (thickness = 5 mm) and the immobile graphite rod (diameter = 7 mm; S_g = 1 cm^2). However, for the graphite felt it was already seen with the KB nanoparticles that the fibers of the electrode were clogged by the powder and it would be the same behavior in the presence of vanadium particles. The study was performed anyway but the results are presented in appendix X8.

III.1.2.1 Effect of solid particles studied on a GR used as electrode

For the graphite rod (S_g = 1 cm^2), the $V^{(IV)}$ curves start at ~ 0.8 V) and exhibit a mass transfer limitation highlighted by the diffusion plateau (1.1 to 1.8 V, depending on the suspension, Fig.III.14-(I)).

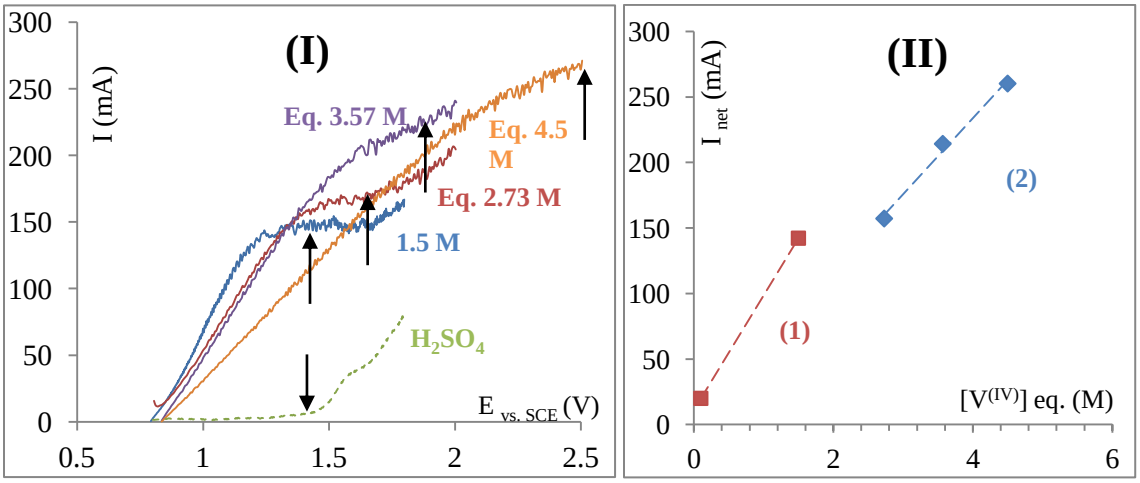

Fig.III.14: **(I)**: $V^{(IV)}$ concentration dependence on the I = f(E) curves obtained on a GR electrode (S_g = 1cm^2); the $V^{(IV)}$ equivalent concentrations are indicated in the figure; [H_2SO_4] = 3 M; RE = SCE, CE = Pt plate, ω ≈ 500 rpm (magnetic bar), r = 5 $mV.s^{-1}$;
(II): Evolution of the net current, picked at the potentials indicated by the arrows, as a function of the vanadium (IV) equivalent concentration in the studied suspensions

For solutions of $V^{(IV)}$ at C < 1.5 M, the current increases linearly with a slope of 87.3 mA/(mol.L^{-1}) (Fig.III.14-(II-1)). When the solid particles are added, the current increases as well but at a lower rate highlighted by a lower slope of 58 mA/(mol.L^{-1}) (Fig.III.14-(II-2)).

The value of the limiting current increases with the $V^{(IV)}$ equivalent concentration with a leaning of the curve towards higher potentials. Back to the increase of the current, given that the saturation concentration of $V^{(IV)}$ is around 1.8 M at the studied temperature ($20 < T_{(°C)} < 25$) [6-7], the increase of the current does not come from an increase of the concentration (C is constant = solubility) nor from the direct reactivity of the solid particles. The grains circulating in solution by stirring can strike the surface of the graphite rod and have as a direct effect an increase in the mass transfer and consequently on the current; statistically, the particles motion reduces the thickness of the diffusion layer. Another assumption can be made: the particles, when hitting on the rod, can erode the surface which would increase the active surface of the electrode by creating microscopic scratches and increase I consequently.

It should be noted that, even though the applied stirrer rotation remains constant, the efficiency of the stirring decreases when the mass fraction of the added powder increases, taking into account that: i) the friction caused by a gradual increase in the number of grains of the $VOSO_4$ powder and ii) the power of the stirrer is constant.
Besides, increasing the amount of the powder makes the system slower/more irreversible, certainly due to the introduction, by the solid particles, of an additional ionic resistance inducing additional ohmic drop.

Concerning the curve relative to $[V^{(IV)}]_{eq.}$ = 4.5 M, the increased amount of particles induced a higher ohmic drop and the diffusion plateau is shifted to potentials higher than 2 V.

Further analysis will be performed on a solid graphite electrode and will be presented in section "1.3" of this chapter to understand more the effect of solid particles by studying the effect of the stirring of the electrode in addition to a cross-shaped stirrer at the bottom of the cell instead of the magnetic bar.

III.1.2.2 Additional studies on the 4.5 M suspension

As mentioned in the previous part, the most particle-loaded suspension exhibits an important viscosity; the apparent viscosity of an equivalent concentration of 5.6 M is 18 Pa.s (see chapter II). This quantity of vanadium can generate circulation problems such as clogging of the inlet/outlet of the reactor and even inside the electrode compartment and add additional power cost to the pumping system. This suspension was studied to try to understand the effect of the stirring on the current and also the effect of a 1 % in weight fraction of KB. The KB was added

in order to create a percolation network inside the suspension that would enhance the electronic transfers where the stirring is not efficient.

Concerning the stirring, a bigger magnetic bar is used (length = 2.5 cm and diameter = 0.8 cm) with a more powerful stirring device (P = 40 W) capable of driving the suspension. The results obtained for the solid graphite are presented in Fig.III.15. (Refer to appendix X8 for the GF)

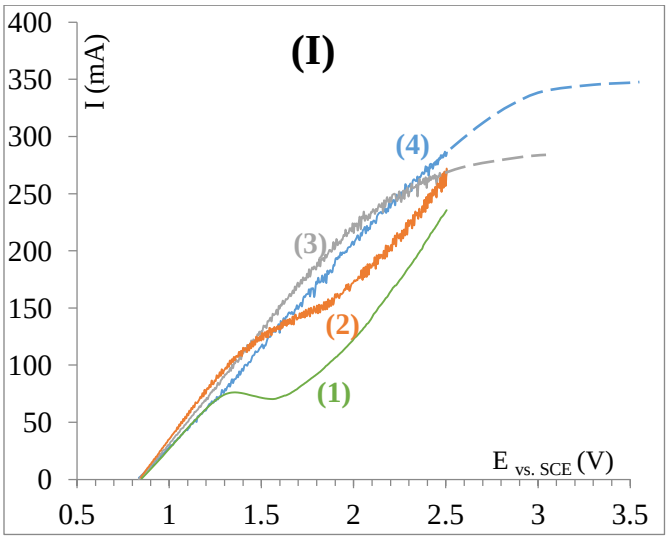

Fig.III.15: **(I)**: Effect of the stirring of a vanadium (IV) suspension with an equivalent concentration of 4.5 M at different stirring rates: (1, green): 0 RPM, (2, orange): 250 RPM, (3, grey): 500 RPM, extrapolated, and (4, blue): 1000 RPM, extrapolated; $[H_2SO_4]$ = 3 M; WE = GR, S_g = 1 cm^2; RE = SCE, CE = Pt plate, r = 5 $mV.s^{-1}$

The effect of stirring is well marked on the graphite rod:

- In the absence of stirring, a classic curve (1) was obtained: the first exponential part corresponds to the activation, followed by the peak translating a partial depletion of $V^{(IV)}$ in the interfacial solution;
- The curve (2, orange) obtained with a stirring of 250 RPM exhibits a higher limiting current and the plateau is shifted to higher potentials;

In fact, in general, increasing the angular velocity ω causes both the current to increase and the curve to shift to more anodic values of E. Indeed, at ω = 1000 RPM, the curve does not show a plateau even with reaching 2.5 V. The curve was voluntarily stopped at this potential since beyond that, the response of the system is not useful for the battery.

It should be noted that the current obtained on the GR remains lower than that obtained on the GF, although the ohmic drop is not corrected.

The next experiment concerns the study of the effect of the addition of 1 % in weight of KB particles to the suspension containing 4.5 M of $V^{(IV)}$. The curves of the residual current with and without KB were discussed previously.

On the solid graphite rod, the presence of 1 % of KB causes the decrease of the current, contrary to what was observed for the 0.1 M solution of $V^{(IV)}$ (Fig.III.12). Moreover, the curve obtained in the presence of KB does not show a diffusion plateau but exhibits a peak, thus translating that the interfacial solution is depleted from VO^{2+} ions during the monitoring of the curve.

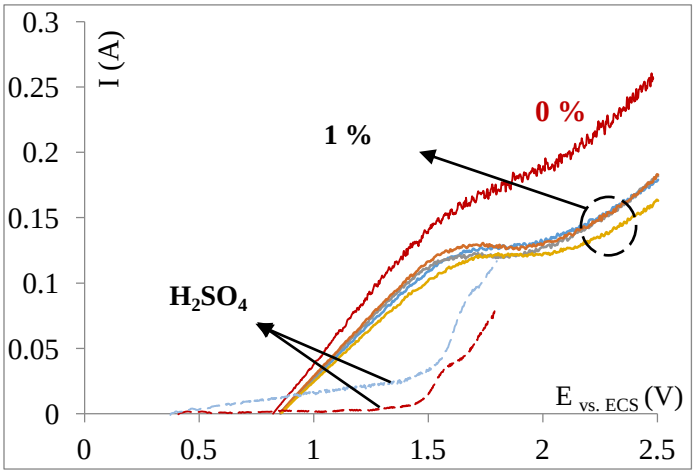

Fig.III.16: Effect of the presence of 1 % in weight of KB on the I = f(E) curves performed on a graphite rod electrode (S_g = 1 cm^2) immersed in a solution of H_2SO_4 3 M containing $V^{(IV)}$ at an equivalent concentration of 4.5 M; ω ≈ 500 RPM (magnetic bar) RE = SCE, CE = Pt plate, r = 5 $mV.s^{-1}$.

A possible explanation of the current decrease is that the KB could surround the vanadium particles thus inducing a decrease of their motion and consequently of the mass transfer close to the interface.

Consequently, the desired effect from the addition of KB particles, i.e. the increase of the current by electronic percolation, is not observed here, or its effect is probably minor compared to the effect of the $VOSO_4$ collisions. However, the effect of electronic percolation was clearly demonstrated in the two I = f(E) curves obtained for the supporting electrolyte alone.

III.1.2.3 Study of the presence of Gum Arabic in the suspensions

Gum arabic (GA) or acacia gum is the best known and oldest of all the tree gum exudates and it originated from the *Acacia Senegal* and *Acacia seyal* trees. It is a mixture of polysaccharides and glycoproteins and has been widely used for its emulsifying, stabilizing, thickening, and binding properties in applications in multiple fields (food additive, ceramics, paintings, pharmacology…) [8-9]. Carbon black, as mentioned before, is hydrophobic, difficult to wet in an aqueous solution. For the purpose of this work, two methods were tested to put the KB in solution (stirring and pre-heating the solution), they were discussed above and they showed no difference in the behavior of the suspension in the plotted *I = f(E)* curves. However, gum arabic enables the stabilization of emulsions and the dispersion of nanoparticles in aqueous solutions [9]; it was decided to check its effect for the suspensions of for the carbon black particles in sulfuric acid.

For that purpose, 0.5 % in weight of gum arabic powder (from VWR, d = 1.35 g/cm^3) and two KB fractions (1 and 2 % in weight) were added to 25 mL of a H_2SO_4 3 M solution and the resulting suspension was stirred for 10 minutes. The KB appeared to be completely soaked. When the suspension was left at rest, the KB nanoparticles sediment in less than an hour. The sedimentation was not observed for the suspensions prepared by the two previous methods (Fig.III.17). This interaction between the KB particles and the GA comes from the structure of the latter which is constituted by a chain containing a hydrophobic and hydrophilic function. In addition, having an important molecular weight (thanks to the polysaccharide chain) leads to its sedimentation, taking the attached KB with it. In fact, in the presence of the GA, the KB nanoparticles agglomerates, probably because their interactions decrease in the presence of GA, and the weight of the resulting adducts becomes greater than the Archimedean thrust leading to the precipitation of the KB.

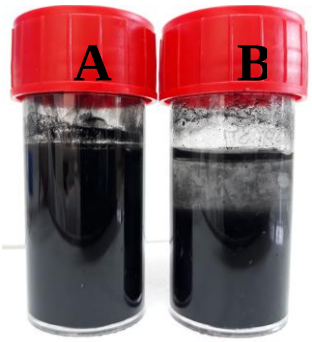

Fig.III.17: photo of the two prepared mixtures of 25 mL H_2SO_4 with 2 % in weight of KB nanoparticles, taken one hour after stopping the stirring; (A): without GA and (B): with 0.5 % in weight of GA.

Current – potential curves were plotted on a 1 cm^2 graphite rod immersed in the prepared suspension. It should be noted that the electrode was polished once before starting the analysis but not between the different suspensions studied. In the absence of vanadium, the results show that the presence of GA does not affect the I = f(E) curves of the 3 M sulfuric acid solution. The capacitive current induced by KB on the residual current on the GR completely disappear. This means that the percolation effect created by the KB particles disappears in the presence of GA, playing the role of coagulant and is placed, on the one hand, between the KB particles, and on the other hand, between the particles and the electrode as shown in the schematic representation below (Fig.III.18-(II)).

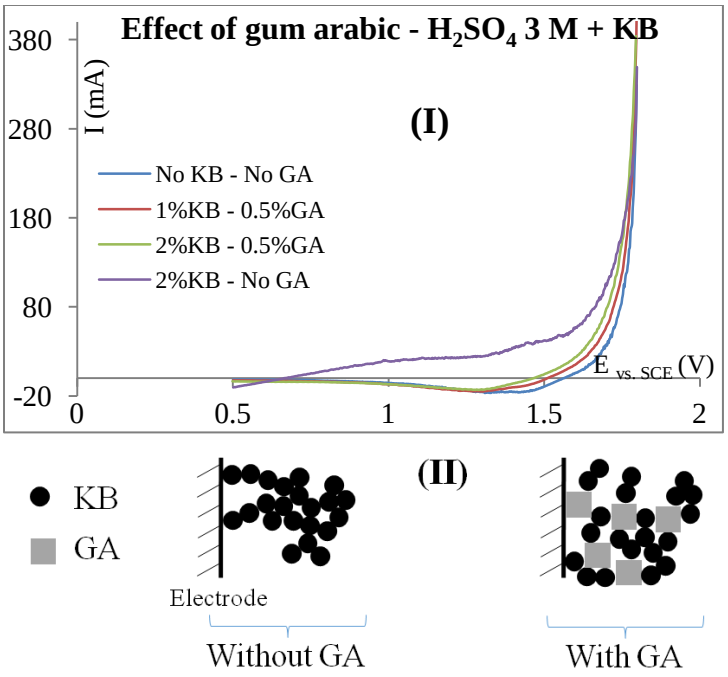

Fig.III.18: **(I)**: Comparison of I = f(E) curves (forward scan only) performed on a graphite rod (S_g = 1 cm^2) immersed in a H_2SO_4 3 M solution containing: blue: no KB and no GA; red: 1 % KB and 0.5 % GA; green: 2 % KB and 0.5 % GA; violet: 2 % KB and no GA; RE = SCE, CE = Pt plate, r = 5 $mV.s^{-1}$; **(II)**: schematic representation of the possible behavior of GA in the KB suspension.

The GA is electrochemically inert, since it did not show any characteristic peaks; besides it seems able to weaken the electronic conduction assured by the percolation of the KB. The effect of GA is studied further in a vanadium (IV) suspension containing KB to i) see if it helps reduce the viscosity of the suspension by dissociating possibly formed aggregates and ii) study its effect in the presence of vanadium dissolved active species and solid particles.

A 25 mL suspension of $V^{(IV)}$ is prepared at an equivalent concentration of 4.35 $mol.L^{-1}$ to which a 0.5 % in weight fraction of gum arabic is added and the mixture is left for 10 minutes under stirring before plotting the curves. The performed I = f(E) curves on this suspension are not reproducible and the current appears to decrease with the number of curves performed (the electrode was depolarized between each curve.

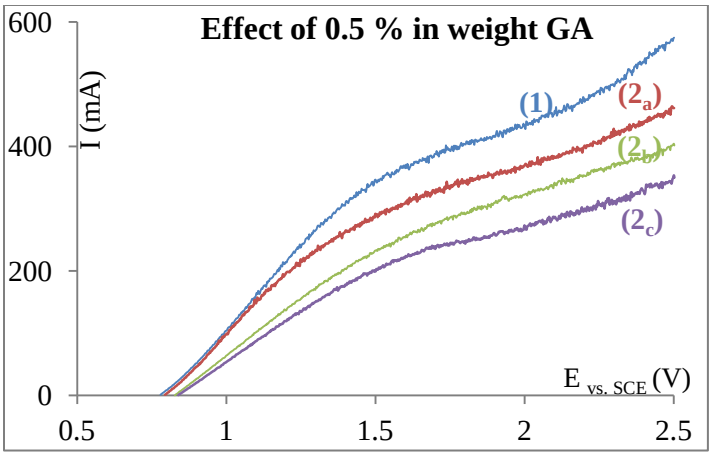

Fig.III.19: Comparison of I = f(E) curves obtained on a GR (S_g = 1 cm^2) immersed in a 3 M H_2SO_4 solution containing: (1) suspension of $V^{(IV)}$ at $C_{eq.}$ = 4.35 M; (2) = (1) + 0.5 % in weight of GA; (2_a), (2_b) and (2_c): curves plotted successively after a simple depolarization of the electrode for the reproducibility study; ω ≈ 500 RPM (magnetic bar); RE = SCE, CE = Pt plate, r = 5 $mV.s^{-1}$.

The decrease of the current observed for the suspension containing GA could be possibly due to the adsorption of the polysaccharide on the surface of the graphite electrode reducing thereby its surface which leads to the decrease of the current. In fact, the carbon, being always slightly hydrophobic, will attract the GA to its surface in order to create a more favorable environment around the electrode in the aqueous media.

In an attempt to increase the current by enhancing to electronic percolation, 2 % in weight of KB was added to the mixture; the resulting suspension is a paste impossible to mix. To reduce the viscosity of this resulting mixture, higher percentages of GA (0.5 to 2 %) were added and the results are presented in Fig.III.20.

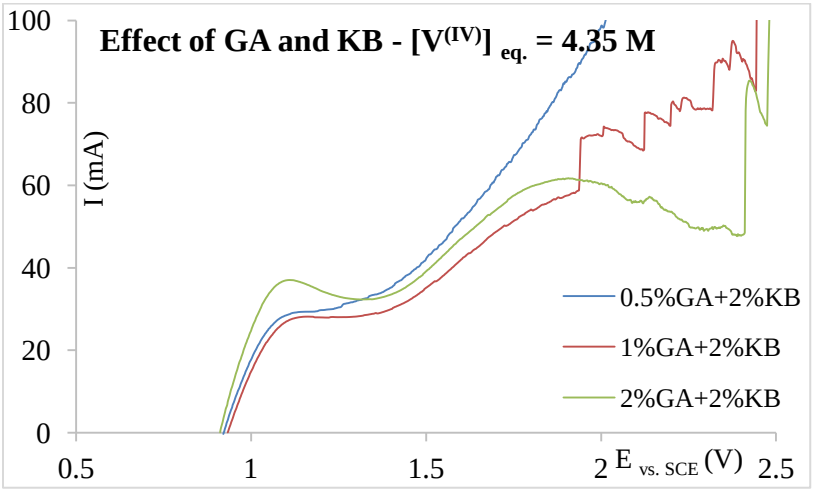

Fig.III.20: Comparison of I = f(E) curves obtained on a GR (S_g = 1 cm^2) immersed in a 3 M H_2SO_4 solution containing a suspension of $V^{(IV)}$ at $C_{eq.}$ = 4.35 M and different fractions of GA and KB: blue/ 0.5%GA-2%KB; red/ 1%GA-2%KB; green/ 2%GA-2%KB; $\omega_{stirrer}$ = 0 RPM; RE = SCE, CE = Pt plate, r = 5 $mV.s^{-1}$.

These results, although they do not give the exact operating mode of the gum arabic on the graphite rod, but they allow formulating the following explanation: as discussed previously, the GA could have adsorbed on the surface of the electrode, reducing by that its active surface and its efficiency. Since the suspension is a paste-like media, the KB should normally create a percolation network leading to the increase of the current but that effect was not observed and could be explained by the masking of the surface by the surfactant.

To summarize, it was found that the oxidation of a vanadium (IV) solution on a graphite felt electrode gives a higher current, at equivalent geometrical surfaces, than on a solid graphite rod, and this is due to the structure of the felt which, thanks to its macroporous carbon fibers network, has a bigger real active surface. However, the addition of vanadium particles to the solution led to the clogging of the felt. This not only had important consequences on the oxidation current which decreased, but could also induce the decrease of the flow and a pressure drop. A stagnant layer of inert powder, covering the working electrode, would impact negatively the power density of the VRFB.
In addition, since a specific activation of the felt was not addressed in this work, the active oxygenated groups that would improve the response of the system on this electrode were probably not fully operating.
Therefore, the solid graphite was chosen to be the working electrode of the reactor for the VRFB. This part of the work will be addressed in chapter V.

As for the KB, its effect in the presence of vanadium solid particles appeared to be detrimental and led to the decrease of the current of about 40 %; this was attributed due to the additional viscosity that it brought to the suspension and the effect of possible coating of the vanadium particles, decreasing the mass transfer. However, the KB nanoparticles are not yet discarded from the present work, as they are assumed to have a role in the nucleation during the eventual precipitation of the powders during the functioning of the battery, which is expected to yield small crystals, easier to circulate. Also, the gum arabic was not examined further.

III.1.3. Effect of the $VOSO_4$ solid particles studied on a graphite cylinder rotating electrode

After performing a series of electrochemical kinetic experiments on vanadium (IV) suspensions, it appeared that a graphite solid electrode was more suitable as an electrode material than the GF. However, the stirring of suspensions containing $[V^{(IV)}]_{eq.} > 3.5$ M and more than 1 % of KB was still a matter of interest since the obtained results did not give a clear conclusion regarding to the effect of a good mixing of the suspension.

Therefore, an improved experimental device is conceived. In addition to a rotating graphite cylinder, a cross-shaped stirrer (referred as CSS in the following) was used in order to insure a

homogeneous distribution of the particles. The CSS is a PTFE-made stirrer with a 3 cm diameter, and 4 mm thick blades. The experiments were carried out in a conventional three electrode cell (Fig.III.21) having 100 cm^3 of capacity and the following electrodes were used:

- working electrode: graphite cylinder screwed on the body of a classical rotating electrode assembly to form a RCE. The used rotation frequencies are in the range 300 - 1500 RPM. The geometric surface area of the working electrode is 7.07 cm^2 (sum of both the lateral area of the cylinder and the surface of the disc forming its base).
- a saturated calomel electrode (SCE) was used as reference electrode for all the experiments; it is immersed into a Luggin capillary tube containing the supporting electrolyte (3 M H_2SO_4). Because of the particular shape of the working electrode, we chose to locate the extremity of the Luggin capillary at ~ 1 mm of the middle of the lateral area of the graphite cylinder for all experiments (see Fig.III.21).
- a platinum plate with 2.25 cm^2 / face of geometrical surface area was used as auxiliary electrode and located in front of the RCE. The used potentiostat is powerful enough, enabling to manage the system without any limitation caused by the relatively small surface of the counter electrode compared to that of the working electrode.

Special care is taken to keep always the same positions of the electrodes for all the experiments. Besides, ohmic drop compensation was performed on the basis of the value of the resistance of the solution between WE and RE; this resistance was measured by electrochemical impedance at the OCP.

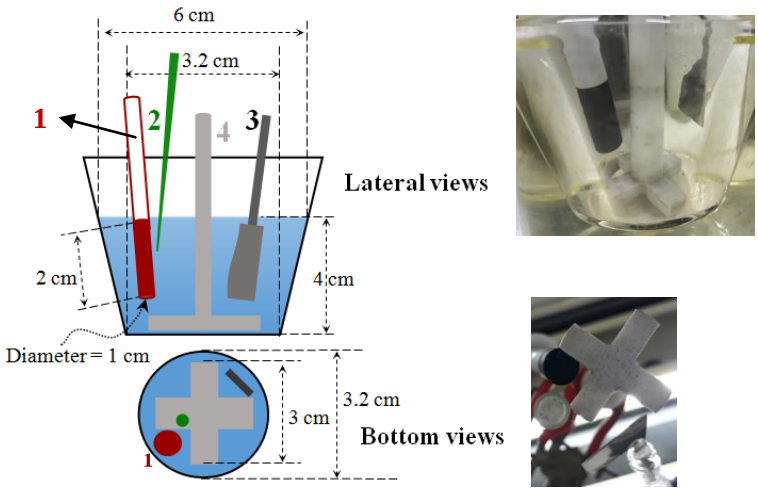

Fig.III.21: **Left**: Sketch of the experimental setup as seen directly through the cell (lateral view) and from the bottom of the cell (bottom view); 1 = working electrode, 2 = Luggin capillary containing the reference electrode (SCE), 3 = counter electrode, 4 = additional cross shaped stirrer. **Right:** Photos of the setup

The simplified oxidation reaction, presented in Rx.III.1, which occurs at the working electrode can be also written more completely as:

$$VOSO_4.5H_2O + H_2O \rightarrow ½\ \{(VO_2)_2SO_4.1.5H_2O\} + e^- + (½\ HSO_4^- + ½\ H^+) + H^+ + 4.25\ H_2O \quad \text{Rx.III.2}$$

Note that this reaction releases 5 molecules of water from the dissociation of the $VOSO_4.5H_2O$ and captures 1.5 for the $(VO_2)_2SO_4.1.5H_2O$ [10]. The reduction of the proton occurs at the counter electrode.

This section is structured in two parts: the first one (§ III.1.3.1) concerns the study of the effect on the vanadium oxidation current, of the stirring of vanadium solutions by both the RCE and the CSS. A similar study was carried out in the second part (§ III.1.3.2) in the presence of three different types of solid particles (each one devoted to the study of the effect of one parameter): i) inert glass spheres, ii) solid particles of the $VOSO_4.5H_2O$ and iii) Ketjen black nanoparticles.

III.1.3.1. Characterization of the dissolved $V^{(IV)}$ oxidation current without solid

III.1.3.1.1. Effect of the stirring rate of the working electrode on the current – potential curves for the V(IV) oxidation without particles

Since the experimental setup contains two elements (RCE and CSS) that are not usually used for electrochemical studies, it is important to understand the effect, on the current of the vanadium oxidation, of the coupled stirring. First, the effect of the stirring rate of the RCE was studied without rotation of CSS from the current-potential curves of a saturated vanadium solution at 10 °C.

In Fig.III.22-(I), it appears that increasing the angular velocity in the range from 300 to 1800 RPM causes the current to increase more than twice. For angular rates lower than 600 RPM, the I = f(E) curve exhibits a classical form, with a plateau ($1.08 < E(V) < 1.4$) corresponding to a mass transfer limitation. Increasing the angular velocity of the electrode causes the curves to be deformed; the slope of the plateau is not constant. The latter increases with the rotation frequency (see also Fig.III.22-(II)), thus suggesting that the (average) mass transfer coefficient depends not only on the stirring intensity but also on the applied potential or the flowing current. This seems strange, because the $V^{(IV)}/V^{(V)}$ is reversible in these conditions (as seen in the curves plotted for more diluted solutions which exhibited a constant limiting current). One plausible explanation could be the modification of the resistance of the solution during the plotting of the I = f(E) curves. In fact, the increase of the mass transfer causes the 'pseudo-limiting' current to significantly increase and this leads to an important production of the $V^{(V)}$ at the anode and also an important flux of gaseous H_2 (0.12 cm^3/s) at the cathode interface. Both phenomena contribute to increase the ionic resistance: the $V^{(IV)}$ oxidation releases 5 molecules of water and consequently modifies the interfacial pH and the H_2 bubbles also negatively affects the ionic conductivity of the solution. To sum up, the increase of the stirring causes the reaction rate to increase and to create an additional ohmic drop which contributes to deform the curve.

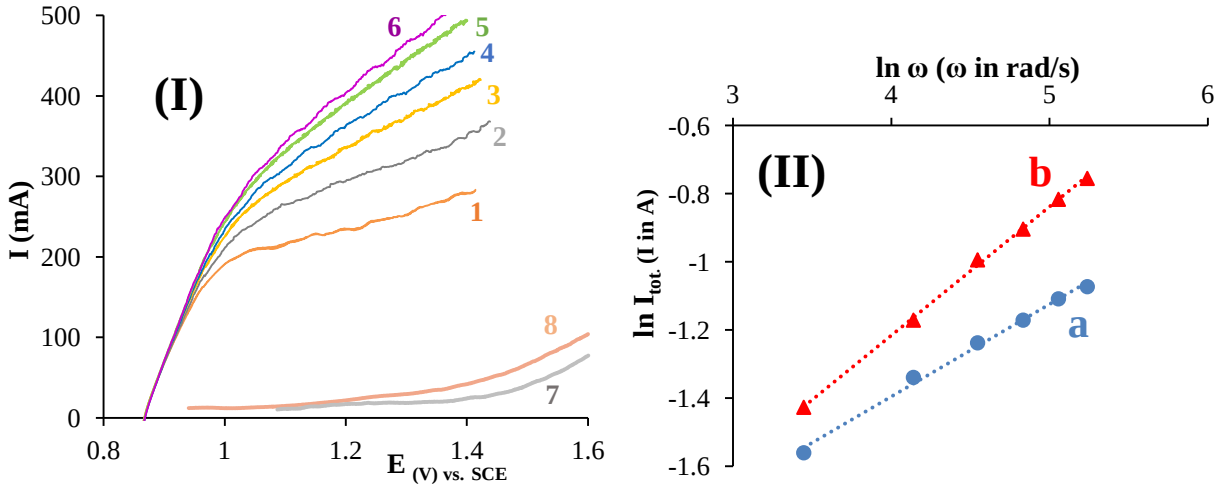

Fig.III.22: **(I)**: Effect of the stirring rate of the working electrode on the shape of the current-potential curves obtained at the quasi-steady state for the oxidation of a solution of $V^{(IV)}$ to $V^{(V)}$. ω = 300, 600, 900, 1200, 1500, 1800 RPM for the curves I = f(E) 1 to 6 respectively. Curves 7 and 8: residual current at respectively 1200 and 1800 RPM. Primary data: $[V^{(IV)}]$ = 1.5 mol.L^{-1} in $[H_2SO_4]$ = 3 mol.L^{-1}; S_{WE} = 7.07 cm^2; r = 10 mV.s^{-1}; T = 10 °C; WE = rotating cylindrical electrode graphite made (RCE) (*diameter 1 cm, height 2 cm)*; AE = Pt. Ohmic drop corrected (EIS).

(II): Evolution of *ln (I)* as a function of *ln (ω),* where *ω* is the angular velocity of the electrode; the currents were extracted from graph (I) without subtraction of the residual current. **a**: $ln\, I_{\,at\ 1.1\,V,in\,A} = f(ln\,\omega)$; **b:** $ln\, I_{\,at\ 1.3V,in\,A} = f(ln\,\omega)$.

The Fig.III.22-(II) clearly shows a linear evolution of the natural logarithm of the current (picked at two different potentials of the I = f(E) curves, thus considered as a limiting current, Eq.III.4), against the natural logarithm of the angular velocity ω. As indicated above, the slopes of the straight lines increases when the potential where the current was read increases.

$$\textbf{a:}\ ln\, I_{\,at\ 1.1\,V,in\,A} = -2.48 + 0.27 \times ln\,\omega_{rad/s} \qquad R^2 = 0.995 \qquad \text{Eq.III.4}$$

$$\textbf{b:}\ ln\, I_{\,at\ 1.3V,in\,A} = -2.73 + 0.38 \times ln\,\omega_{rad/s} \qquad R^2 = 0.999 \qquad \text{Eq.III.5}$$

It is important to mention that:

- The current picked at two different potentials of the I = f(E) curves can be considered as a limiting current $I_{lim} = n\,F\,S\,k\,C_{V^{(IV)}}$, where k is mass transfer coefficient, expressed as a power law of the angular velocity of the stirrer:

$$k = a' + b' \times \omega^{\gamma} \implies I_{lim} = a'' \times S + b'' S \times \omega^{\gamma} \text{ (See appendix X9)} \quad \text{Eq.III.6}$$

The magnitudes of these slopes (0.27 and 0.38) are lower than the slope predicted by the Levich correlation ($I_{lim} = f(\omega^{0.5})$) for a rotating disc electrode in very well defined conditions [11-13].

- The working electrode is a rotating cylinder having *two electroactive areas:* the bottom section which is a disc and its peripheral/cylindrical area. The measured limiting current is a

contribution of both faces of the electrode, and the relative contribution of each part needs to be determined.
We will try to get a better understanding of the electrodes' behavior in the following sections.

III.1.3.1.2. Respective contributions of the disc and the cylinder faces of the working electrode on the $V^{(IV)}$ oxidation current

Current potential curves were plotted for various conditions (Fig.III.23) in order to examine independently the effects of both the disk and the cylinder surfaces of the working electrode, on the mass transfer under stirring conditions. The solution used is the $V^{(IV)}$ at saturation (1.5 M). To that end the RCE was prepared in two ways:
* The disk was insulated with a thin adhesive scotch tape and the curves *I= f(E)* were plotted for the external cylindrical surface, see Fig.III.23-(I) curves 1C to 6C.
* The external cylindrical surface was isolated with the same thin adhesive tape, trying to avoid any modification of the geometry of the cylinder (i.e. no roughness, the whole tape surface is completely smooth); then the *I= f(E)* curves were plotted on the disk active face and presented in Fig.III.23-(I), curves *I= f(E)* 1D to 6D.
The first observation is that the magnitude of the current measured with the cylinder alone (curves 1C to 6C) is about 5 to 6 times higher than the current measured with the disc alone (curves 1D to 6D). Besides, the surface ratio (S_c / S_d) between the cylinder and the disc is equal to ~ 8. Taking into account that the limiting current is proportional to the surface area and to the mass transfer coefficient of the $V^{(IV)}$, these results evidence the need to determine and to compare the equations linking the mass transfer and the angular velocity for both geometries, the disc and the cylinder. It seems that the transfer is more efficient for the disc than for the cylinder, but this needs to be confirmed. The current was measured at two different potentials (1.1 and 1.3 V) for both the cylinder and the disc; then the curves $ln\ I = f(\ln \omega)$ were plotted and presented in Fig.III.23-(II). The graph exhibits linear relations for all the examined cases:

C_1: Cylinder at 1.1 V $\leftrightarrow ln\ I_{\ at\ 1.1\ V,in\ A} = -3.14 + 0.37\ ln\ \omega_{rad/s}$ $R^2 = 0.98$ Eq.III.7
C_2: Cylinder at 1.3 V $\leftrightarrow ln\ I_{\ at\ 1.3\ V,in\ A} = -3.13 + 0.42\ ln\ \omega_{rad/s}$ $R^2 = 0.99$ Eq.III.8
D_1: Disc at 1.1 V $\leftrightarrow ln\ I_{\ at\ 1.1\ V,in\ A} = -4.15 + 0.22\ ln\ \omega_{rad/s}$ $R^2 = 0.99$ Eq.III.9
D_2: Disc at 1.3 V $\leftrightarrow ln\ I_{\ at\ 1.3\ V,in\ A} = -4.24 + 0.29\ ln\ \omega_{rad/s}$ $R^2 = 0.99$ Eq.III.10

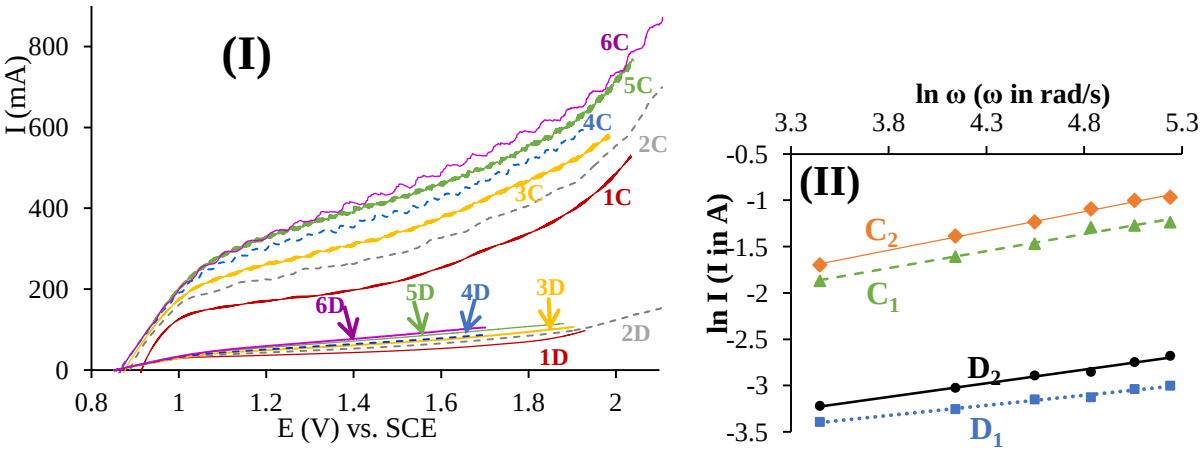

Fig.III.23: **(I)**: Effect of the stirring rate of the working electrode (RCE) on the shape of the current-potential curves obtained at the quasi-steady state for the oxidation of a solution of $V^{(IV)}$ to $V^{(V)}$. Angular velocity ω = 300, 600, 900, 1200, 1500, 1800 RPM respectively for the curves I = f(E) 1 to 6. Top/group C: Curves obtained with the cylinder alone while the disc is masked; Bottom/group D: Curves obtained with the disc alone while the cylinder is masked. WE = rotating graphite (disc or cylinder, diameter 1 cm, height 2 cm); $[V^{(IV)}]$ = 1.5 mol.L^{-1} in $[H_2SO_4]$ = 3 mol.L^{-1}; $S_{cylinder}/S_{disc} = \left(\sim \frac{6.3}{0.78}\right) \sim 8$; r = 10 mV.s^{-1}; T = 10 °C; AE = Pt. Ohmic drop corrected with the initial value of the solution resistance (EIS).
(II): Plots of ln I = f (ln ω); the currents were extracted from the Fig.III.23-(I), without subtraction of the residual current. C_1 and C_2 correspond to the cylinder at respectively 1.1 and 1.3 V; D_1 and D_2 correspond to the disc at respectively 1.1 and 1.3 V.

Note that, considering the disc alone, the slope found (~ 0.2 to 0.3 as function of the potential used) is practically the half of the theoretical value predicted by the Levich law ($I_{lim} = \lambda\, \omega^{0.5}$) for a rotating disc electrode. This discrepancy is attributed to the fact that our operating conditions do not fulfil all criteria (indicated below) required for the application of the law:

- the ratio of "the diameter of an inert surface around the disk" to "the diameter of the electroactive surface of the disc" needs to be at the least equal to 10, to enable the correct flow of the solution. Here, because of the chosen form of the graphite cylinder, the whole surface of the disc is reactive, instead of a small disc surrounded by a Teflon non-reactive area, enabling the establishment of a stabilized and defined interfacial flow [12];
- the ratio of "the vessel diameter" to "the electrode diameter" needs to be at least equal to 10 to avoid border effects (here the ratio is (~ 3)).

Concerning the cylinder, the slope found (~ 0.35 to ~ 0.42) is also practically the half of the theoretical value predicted in the bibliography ($I_{lim} = \lambda' \omega^{0.7}$ [13]). Note that, the exponent of 0.7 was obtained with a metallic cylinder inserted between two inert cylinders of the same diameter and a cylindrical form counter electrode having a larger diameter than the WE. The discrepancies could be caused by:

i) a non-uniform electrical field because of the particular geometry of the chosen system: the CE is a plane plate of platinum and the current density to the rear surface area of the cylinder is very low, thus reducing its effective electroactive surface area, and,

ii) a non-uniform flow around the bottom border of the cylinder (similarly to the disc). Here, if we assume an upward flow from the bottom of the electrochemical cell to the disc, we can conclude that the solution arriving to the disc (i.e. the basis of the cylinder) is deviated far from the cylinder, thus reducing the flux arriving to the lateral area of the electrode (possible eddies near lateral wall).

Another parameter which can influence the answer of the electrode could be the activation of the surface area of the graphite [1]. As a matter of fact, oxygenated groups (C-O) at the surface of the graphite seem to enhance the electrocatalytic activity of the graphite, as discussed in the previous part for the graphite felt electrode.

In the present study the electrode has been polished (as much as possible in the same conditions for all the plots), but no extra activation was performed before any recording of the current. Thus a part of its surface could remain covered by oxygenated groups while the other part is not and this is difficult to be controlled, because of the easy oxidation (chemical or electrochemical) of the graphite.

A comparison of the sum of the individual currents (surface of the disc and lateral surface of the cylinder) to the current obtained with the whole electrode (RCE) was performed and the results (Fig.III.24) shows practically no difference for high stirrings ($\omega > 1000$ RPM). However, a slight difference appears at lower angular velocities, the general evolution is that the current is higher for the entire WE than for the sum of the two redesigned ones, especially for the lowest examined angular velocities. This difference can be explained by the creation of a vortex at the ends of a non-perfectly masked surface which displaces the solution away from the electrode.

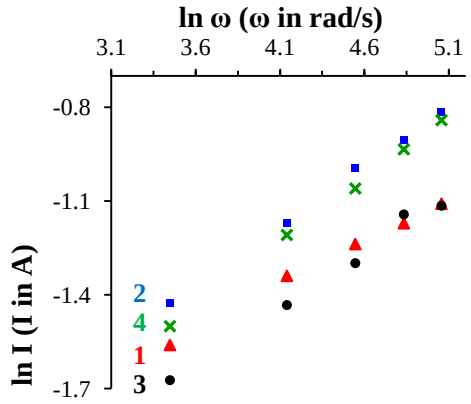

Fig.III.24: Comparison of the logarithmic evolutions of the $V^{(IV)}$ oxidation currents (measured at 1.1 and 1.3 V) as a function of the logarithm of the angular velocity of the graphite WE (RCE), obtained in the two following cases:
- the whole electrode surface is operative; curves: 1-▲ (I at 1.1V); 2-■ I at 1.3V (results extracted from Fig.III.22-(I)).
- the magnitude of the current corresponds to the sum of both the magnitudes of the currents obtained with the disc and the cylinder; curves: 3-● (I at 1.1V) and 4-× (I at 1.3 V) (results extracted from Fig.III.23-(I)).

To sum up, the stirring affects the current but its effect is lower than the effect theoretically predicted by the correlation found in bibliography [12-13], because the operating conditions are different from those made to establish the theoretical laws used for comparison.

III.1.3.1.3. Effect of the coupled stirring rates of both the working electrode and the cross-shaped additional stirrer on the current – potential curves for the $V^{(IV)}$ oxidation

The second step is to study the effect of the cross-shaped additional stirrer on the magnitude of the current as well as on the mass transfer. To that end, several current-potential curves were plotted in various stirring conditions (not shown here). Their general form is similar to the one shown in Fig.III.22 and 23.
The magnitude of the limiting current of the oxidation of the $V^{(IV)}$ to $V^{(V)}$ was determined as a function of the angular velocity for both RCE and CSS (in the range from 300 to 1500 RPM; both stirrers turn in the same direction), and the results are presented in Fig.III.25. The graph (I) in this figure presents the limiting current dependence on the angular velocity of the CSS, obtained for various angular velocities of the RCE. The general tendency shows that increasing the stirring causes the current to increase for both the RCE and CSS. However, a closer examination of the current evolutions shows two different areas, attributed to two behaviors:

- For angular velocities of the cross shaped stirrer ω CSS $\lesssim$ 600 RPM, and for values of the ω RCE $\lesssim$900 RPM (i.e. the first two points of the curves 1 to 3), the limiting current: i) increases when ω RCE increases, and ii) remains practically constant or even very slightly decreases when ω CSS increases. For these low angular velocities, the effect of the rotation of the CSS is not perceptible by the RCE, because the effect of its agitation predominates.

- Staying at angular velocities of the CSS $\lesssim$ 600 RPM, the increase of the rotation of the RCE (1000 $\lesssim$ ω RCE in RPM $\leq$ 1500 RPM), (i.e. the first two points of the curves 4 and 5) causes the limiting current of the vanadium oxidation: i') to increase when ω RCE increases, and ii') to significantly decreases when ω CSS increases.

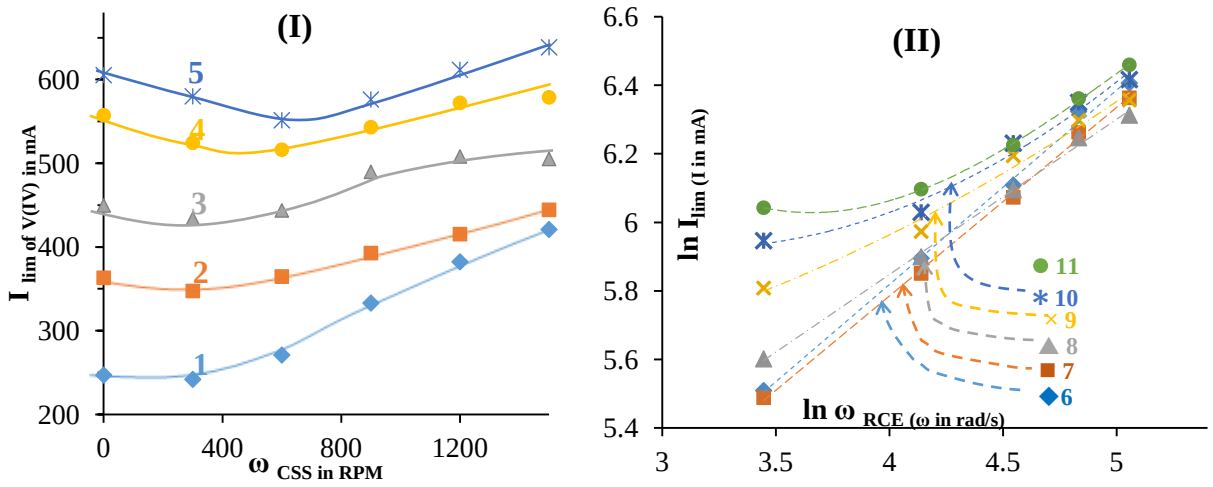

Fig.III.25: **Graph (I)**: Dependence of the limiting current of the oxidation of $V^{(IV)}$ (at E ~ 1.1 V) versus the angular velocity of CSS ($\omega_{CSS\ in\ RPM}$), for various angular velocities of the graphite RCE (each curve was obtained at constant ω_{RCE}, respectively curve N° / $\omega_{RCE\ in\ RPM}$: 1: ◆300; 2: ■ 600; 3: ▲900; 4: ●1200; 5: ✱ 1500).
Graph (II): Logarithmic evolution of the limiting current as a function of the logarithm of the angular velocity of the graphite RCE ($\ln \omega_{RCE}$), for various stirring rates ω_{CSS} of the cross shaped stirrer (each curve was obtained at constant ω_{CSS}, respectively curve N° / $\omega_{CSS\ in\ RPM}$: 6: ◆ 0; 7: ■ 300; 8: ▲600; **9: × 900;** 10 ✱1200; 11: ● 1500).
Primary data concerning the I = f(E) curves: WE = rotating graphite; $[V^{(IV)}]$ =1.5 mol.L^{-1} in $[H_2SO_4]$ = 3 mol.L^{-1}; r = 10 mV.s^{-1}; T = 10 °C; AE = Pt. ohmic drop corrected (EIS).

It seems that the effect of the stirring of the RCE on the $V^{(IV)}$ mass transfer (so on the current) is partially compensated by the agitation created by the CSS. The rotation of the CSS causes a partial decrease of the convective flux of the $V^{(IV)}$ arriving at the interface of the RCE, and therefore to a partial decrease of the resulting current (from ~ 0.6 A to ~ 0.52 A). Assuming that the RCE causes an upward flow from the bottom of the vessel to the disc, we can conclude that the rotation of the CSS prevents this motion and the solution is drifted far from the electrode, thus reducing the global flux of the $V^{(IV)}$. However, it is important here to consider this effect because when studying the suspensions, strong agitation of the CSS is necessary to supply the required power enabling the motion of the solid particles, which constitutes a goal of this study.

The right side of the curves in graph (I) of Fig.III.25, (ω > 600 RPM) corresponds to the evolution of the limiting current as function of the angular rates of the CSS, for several rotation frequencies of the RCE. Conversely to the lower ω_{CSS}, here the magnitude of the current increases with the angular rate of the CSS, whatever the rotation of the RCE; the effect observed for ω_{CSS} < 600 RPM seems to be damped. Moreover, this positive effect of the CSS (enhancement of the limiting current) is an interesting result because these 'high' angular velocities (ω_{CSS} > 600 RPM) are required to allow the fluidization of the suspension. Besides, note that for these 'high' rotations the current also increases with the stirring of the RCE (~ 0.35 to ~ 0.6 A).

The graph (II) in Fig.III.25 reports the $ln\ I_{lim} = f(\ln \omega_{RCE})$ for the various angular velocities of the cross shaped stirrer ($0 \leq \omega_{CSS\ in\ RPM} \leq 1500$). Each curve in this graph (II) reports the points obtained for one ω_{CSS} in graph (I) i.e. the points found on each perpendicular line passing through an angular velocity of the cross shaped stirrer. The curve 6 for example presents the points (current) read on graph (I), on the vertical Y-axis, at the origin of the horizontal X-axis i.e. immobile CSS, $\omega_{CSS} = 0$.

The graph clearly shows two different shapes for the curves: the curves 6, 7 and 8, obtained at low angular rates of the stirrer (ω_{CSS} is respectively equal to 0, 300 and 600 RPM), are practically identical on the graph, and exhibit a linear evolution. This confirms the above conclusion about the 'low effect' of the agitation of the CSS on the limiting currents for $\omega_{CSS} \leq$ 600 RPM. The curves 9, 10 and 11 were obtained at higher angular rates of the stirrer (ω_{CSS} equals 900, 1200 and 1500 RPM respectively). They exhibit two different domains: on the left side the limiting current is practically constant, meaning that the stirring of the CSS cancels the effect of the stirring by the RCE. On the right side of the curves, the $ln\ I_{lim}$ increases linearly with $ln\ \omega_{RCE}$, meaning that the mass transfer enhancement produced by the RCE predominates.
Note also that in this graph (II) the effect of the stirring of the CSS on the limiting current can be observed by the points found on each perpendicular line passing through an angular velocity of the RCE.

Table III.3 provides the slopes γ of the curves $ln\ I_{lim} = f(ln\ \omega_{RCE})$ according to Eq.III.6 (for both ranges $\omega_{RCE} < 600$ RPM and $\omega_{RCE} > 600$ RPM) obtained for a given angular velocity of the CSS. In the absence of stirring of the CSS ($\omega_{CSS} = 0$ RPM), the exponent γ is found to be equal to ~ 0.6 which is intermediate between 0.5 (disc) and 0.7 (cylinder).
For all the carried out experiments, this exponent γ decreases as the angular velocity of the CSS increases. For angular rates of the RCE lower than 600 RPM, the exponent γ is strongly affected by the rotation of the CSS, and is almost cancelled for ω_{CSS} = 1500 RPM meaning that the agitation of the CSS completely compensates that of the RCE: there are antagonistic effects between the cross shaped stirrer and the rotating electrode.

Table III.3: Slope values obtained from the linear regression of Eq.III.6: $\ln (I) = \text{const.} + \gamma \times ln\ (\omega)$ for the curves of Fig.III.25 – graph (II).

Cross shaped stirrer (RPM)		0	300	600	900	1200	1500
Fig. 5 graph (II), curve N°		6	7	8	9	10	11
γ	$\omega_{RCE} < 600$ RPM	0.57	0.55	0.43	0.28	0.11	0.07
	$\omega_{RCE} > 600$ RPM	0.57	0.55	0.47	0.44	0.42	0.40

Conversely, for angular rates of the RCE higher than 600 RPM, even if the coefficient γ is affected (slightly decreases from 0.47 to 0.4), the low observed decrease translates the fact that

the effect of the RCE on the flux of the vanadium transferred to the interface predominates against the effect of the CSS.
Even if the coefficient γ informs about the effect of the rotation of each element (RCE and CSS) on the vanadium transferred flux, what is important to note is that the rotation of both stirrers contributes to increase the mass transfer.
The effect of the rotation of the CSS is more significant for high (> 600 RPM) angular rates, and this:
- is typical of the geometry of the used electrochemical cell,
- will be very important to ensure the motion of concentrated suspensions of the vanadium.
The results, obtained for a saturated solution of $V^{(IV)}$, will be used as reference in the study of the impact of solid particles on the response of the system.

III.1.3.2. Study of the solid – liquid suspensions

The presence of solid particles in the posolyte (but also in the negolyte) can significantly affect positively or negatively the performances of the battery. Indeed, as a function of the rate of the discharge or recharge of the system, precipitates can appear and as a function of their size they can stick on the electrodes and cause some passivation. Moreover, the motion of the bigger size particles close to the interface 'electrode-suspension' could contribute to enhance the molar flux of the active species, increasing therefore the current. In other words, the shock of the particles at the interface can be assumed to contribute to statistically reduce the thickness of the diffusion layer, thus enhancing the mass transfer. Another effect of the solids could be the decrease of the effective diffusion coefficient, and both parameters will be examined in the next section.

III.1.3.2.1. Effect of the fraction of the solid: glass spheres

Current-potential curves were plotted in suspensions constituted by a 0.75 mol/L solution of the $V^{(IV)}$ and various contents of solid inert glass hollow spheres (specific gravity of ~1.1 g/cm^3 and a granulometry in the range of $9 < d_{\text{glass spheres in } \mu m} < 13$ (average $d$iameter =11 μm)). Because their specific gravity is 'lower than this of the vanadium acidic solution' most of the glass spheres float, and this requires therefore a strong stirring to obtain a uniformly distributed suspension. The I = f(E) curves (not shown here) have a similar shape to these obtained above. Fig.III.26 shows the evolution of the current of the oxidation of $V^{(IV)}$ versus the mass percent of the solid inert glass spheres.
The measured current (0.3 to ~ 0.05 A) is in the same order of magnitude than half of the one measured on curve 5, Fig.III.22-graph (I) (in the absence of rotation of the CSS and with a concentration of $V^{(IV)}$ of 1.5 M).
The figure contains only 'four measurements' and it is possible that the shape of the curve could be slightly different in the first part (possible presence of a peek for solid fractions lower than 15 %). The curve shows a strong influence of the solid glass spheres on the current. Indeed, for low

mass fraction of the spheres (≲ 20 %) the current lightly increases (≲ 15 %), probably because an enhancement of the mass transfer of the vanadium arriving at the interface is caused by the motion of the spheres into the diffusion layer.

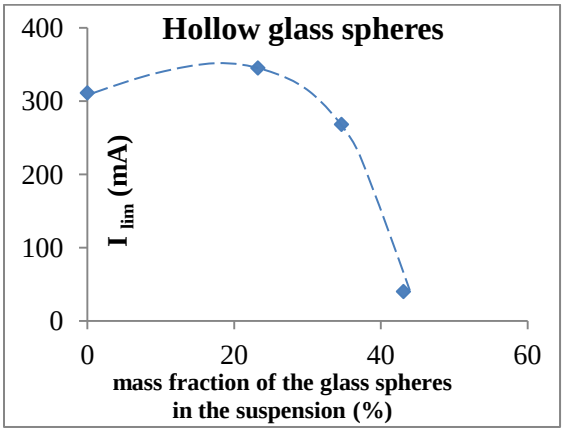

Fig.III.26**:** Curve showing the evolution of the vanadium oxidation limiting current measured at E= 1.3 V as a function of the mass fraction of added glass spheres into a 60 mL solution of $V^{(IV)}$ at 0.75 M; [H_2SO_4] = 3 M. Hollow glass beads with a specific gravity of ~1.1 g/cm^3 and a granulometry in the range of 9 < $d_{\text{glass spheres in µm}}$ < 13 (average diameter =11 µm).
Primary data for the monitoring of the *I=f(E)* curves; r = 10 mV/s; T = 10 °C; WE = graphite cylinder; RE = ECS; AE = Pt plate, CSS at 1500 RPM; RCE at 1500 RPM.

However for higher fractions (≳ 30 %) of the solid particles the current dramatically decreases until being practically cancelled for 45 % of solid particles into the suspension.

This evolution could be due to the decrease of the effective diffusion coefficient of the $V^{(IV)}$, because of the decreasing space to diffuse in the bulk.
Indeed, 50 g of the glass spheres represents a volume of solid of 45.4 mL into 60 mL of the liquid. Assuming the additivity of the volumes is applicable (total volume of the suspension =105.4 cm^3) and the mean diameter of the glass spheres is d_g = 11 µm (their granulometry ranges from 9 to 13 µm) then, the number of particles (6.52×10^{10} particles) represents a volumetric fraction of the solid ϕ_{max} = 0.43 and the volume fraction available for the diffusion is ε = (1- ϕ_{max}).
If the glass spheres are equally dispersed into the electrochemical vessel, that represents N_g= 641 glass spheres per cm of distance, in a direction between the wall of the cell and the axis of the RCE.

Then, the tortuosity (Eq.III.11) is equal to 1.4, and enables to access the effective diffusion coefficient D_{eff} (Eq.III.12).

$$\tau = 1 + (\pi - 2) \times d_g \times \frac{N_g}{2} \qquad \text{Eq.III.11}$$

$$D_{eff} = \frac{\varepsilon}{\tau} D = 0.41 \times D \qquad \text{Eq.III.12}$$

This result shows that the diffusion coefficient falls at about 60% of its initial value, which could partially explain the current decrease, but not its complete cancellation. Note that the masking of the electrode's accessible surface by the glass spheres could also significantly affect the current.

Indeed assuming roughly a thickness of the diffusion layer in the range from 50 to 100 µm it is possible to stack maximum about ten glass spheres, which represent an important barrier, even if these spheres have an important size and could relatively be easily removed from the electrode's surface.
Note that similar results were obtained by using full beads (Sigma Aldrich) having a specific gravity of ~2.3 g/cm^3 and a granulometry in the range of 425 < $d_{\text{glass spheres in µm}}$ < 600 (Fig.III.27).

The current decreases at a lower rate than what was observed previously, from 1.5 to 1 A in a $V^{(IV)}$ solution at 1.5 M in 3 M H_2SO_4, and the current is not canceled even after adding a bigger mass fraction of spheres (63 %). This may be due to the fact that the hollow spheres have a smaller diameter, thus, a 50 g of glass spheres contains more particles (6.52×10^{10} particles) than the same weight of the full spheres (1.5×10^{7} particles). Therefore, the effective diffusion coefficient is more impacted in the first case and has a bigger influence on the current.

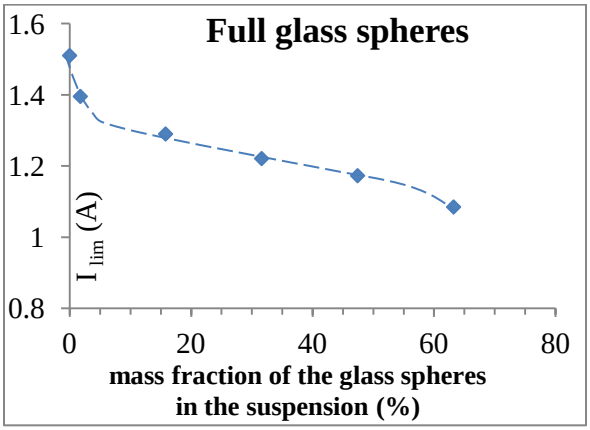

Fig.III.27**:** Curve showing the evolution of the vanadium oxidation limiting current as a function of the mass fraction of added glass spheres into a 60 mL solution of $V^{(IV)}$ at 1.5 M; [H_2SO_4] = 3 M. Hollow glass beads with a specific gravity of ~2.5 g/cm^3 and a granulometry in the range of 425 < $d_{\text{glass spheres in µm}}$ < 600 (average diameter = 500 µ*m*).
Primary data for the monitoring of the *I=f(E)* curves; r = 10 mV/s; T = 10 °C; WE = graphite cylinder; RE = ECS; AE = Pt plate, CSS at 1500 RPM; RCE at 1500 RPM.

To summarize, the enhancement in the vanadium molar flux arriving at the interface (by the motion of the spheres into the diffusion layer) is not really significant for the low fractions of the solid spheres. Furthermore, the current decreases rapidly when the fraction of added glass spheres increases, mainly because of the reduction of the available space for the diffusion of the vanadium.

III.1.3.2.2. Effect of the fraction of the solid: $VOSO_4$ solid particles

Various *I=f(E)* curves were plotted on a graphite rotating cylinder used as anode and immersed into a suspension containing a solution saturated in $V^{(IV)}$/1.5 M and various mass fractions of solid particles of $VOSO_4$; the results are indicated in Fig.III.28.

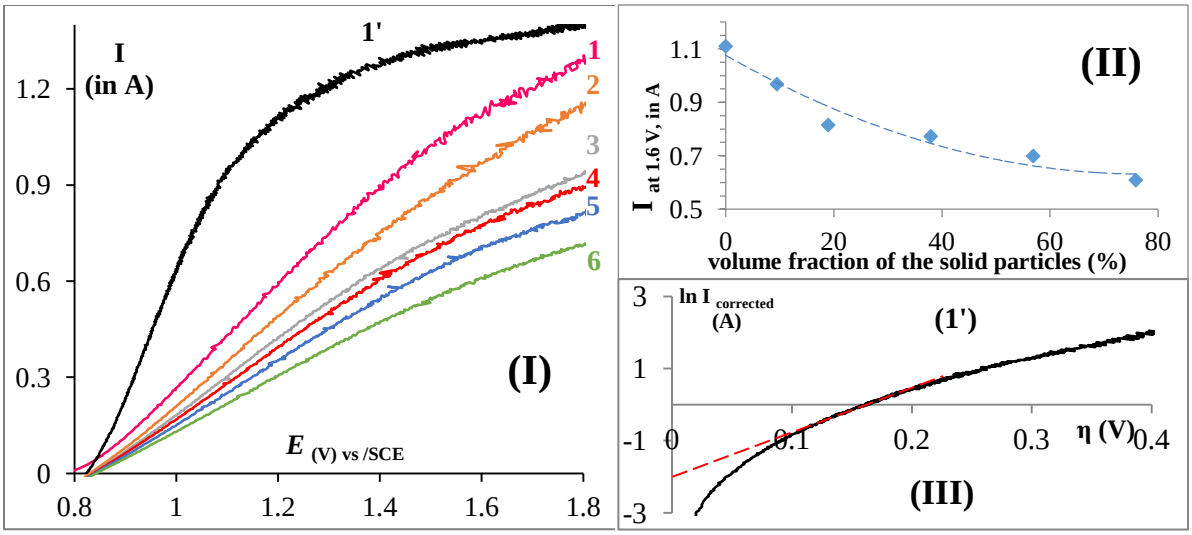

Fig.III.28: **(I):** Current potential curves obtained on a graphite RCE, immersed in Liquid-Solid suspensions containing dissolved $V^{(IV)}$ (60 cm^3, at saturation i.e. 1.5 mol/L) and various mass fractions of the solid $VOSO_4.5H_2O$ as indicated: 1/Pink : 0 g; 2/brown: 5.7 g; 3/grey: 11.4 g; 4/red: 22.8 g; 5/blue: 34.2 g; 6/green: 45.5 g (total molar quantity of the $V^{(IV)}$ in equivalent mol/L of suspension: 1.5, 1.79, 2.05, 2.5, 2.88, 3.21). Curves 1 to 6 obtained without correction of the ohmic drop. Curve 1' = the same solution than for curve 1, with corrected ohmic drop (EIS). WE = graphite RCE; CE = Pt plate; $[H_2SO_4]$ = 3 M; r = 10 mV/s; T= 10 °C; $\omega_{RCE(RPM)} = \omega_{CSS(RPM)}$= 1500 RPM. **(II)**: Evolution of the current measured at 1.6 V as a function of the added solid particles of $VOSO_4.5H_2O$; **(III)**: evolution of *ln ($I_{corrected}$)* as a function of the over potential plotted for curve (1').

Curve 1 was obtained with the saturated solution of the dissolved $V^{(IV)}$ at 1.5 M (in $[H_2SO_4]$ = 3 M). The curve exhibits a large range of overpotential (from ~0.8 to ~1.6 V) before reaching the beginning of a plateau and the corresponding limiting current. The strong shift of the I = f(E) curve could be attributed i) to a slow/partially irreversible system, but also ii) to the significant ohmic drop because of the important current flow (I_{max}~1.3 A → 1.8 kA/m²). The curve 1′, obtained at the same conditions, but with correction of the ohmic drop, exhibits a classical shape, showing i) a limited activation overpotential range (from ~0.8 to ~1 V), and ii) a 'diffusion-plateau' corresponding to a mass transfer limitation for the $V^{(IV)}$. This shape clearly indicates that the corresponding redox system ($V^{(IV)}/V^{(V)}$) is rapid/quasi-reversible. The analysis of the obtained I = f(E) curves by Butler-Volmer, as performed before (§ III.1.1.2.1), allows to obtain the following results by considering η = 0 at E = 0.8 V: the values of the anodic electronic transfer coefficient α and $k°$ are calculated for curve (1') for which the effect of the ohmic drop is corrected; we find α = 0.287 and $k° = 1.42 \times 10^{-6}$ m/s. The value of the transfer coefficient is identical to what was obtained on the immobile graphite rod for a vanadium concentration of 1 M (§ III.1.1.2.1) while the value of $k°$ is lower in this case. Since the same redox system is studied, the values should have been identical but the obtained difference might be due to the different experimental conditions between the two cases.

The curves 2 to 6 of Fig.III.28-(I), obtained by adding into the saturated solution of $V^{(IV)}$ increasing quantities of the solid $VOSO_4.5H_2O$, show that the current, measured at 1.6 V

decreases as the amount of the added powder increases, and the decrease (until ~ 46 %) reaches a pseudo-plateau for solid particles fractions higher than ~ 30 %. Moreover, as the solid fraction increases, the curve deformation is amplified, even with an ohmic drop correction using the initial measured resistance of the solution. The decrease of the current can be fitted to a second order polynomial curve, where f_s is the volume fraction of the solid particles:

$$I = 7 \times 10^{-5} {f_s}^2 - 1.15 \times 10^{-2} f_s + 1.08 \qquad R^2 = 0.95$$

Except the fact that no increase of the current was observed for the very low fractions of solid added (not examined in fact), this behavior appears to be similar to the one observed in the case of inert glass spheres (Fig.III.26 and 27), and the same conclusion can be made: the solid contributes to reduce the volume of the liquid into which the $V^{(IV)}$ diffuses, thus reducing its flux arriving to the electrode. However, because of the extended size range of the solid vanadium particles (~3 < $d_{p\ in\ \mu m}$ < ~ 600) it is not easy to carry out a rigorous and deep quantitative analysis of the system.

These results show that, at constant stirring, the increase of the fraction of the solid particles of the vanadium does not seem to significantly enhance the current. This means that, under these conditions, nor the collisions of the particles on the electrode surface, nor the dissolution of the solid particles, contribute to significantly increase the rate of the vanadium oxidation. In addition to that, for the higher fractions of the solid in the suspension (> 30 %) a negative effect was observed and the current decreases, that is why it seems important to avoid operating with a liquid/solid suspension in the electrochemical reactor.

III.1.3.2.3. Effect of the stirring of the L-$VOSO_4$ suspension

The effect of the stirring of a suspension containing a constant quantity of the $VOSO_4$ powder, on the limiting current of the vanadium oxidation, was examined and the results were indicated in Fig.III.29. The curves 1a to 3a were obtained under various angular rates of the RCE keeping the CSS immobile, while for the curve 4a both the RCE and the CSS are used. The curves 1 to 3 were imported from Fig.III.22 for comparison.

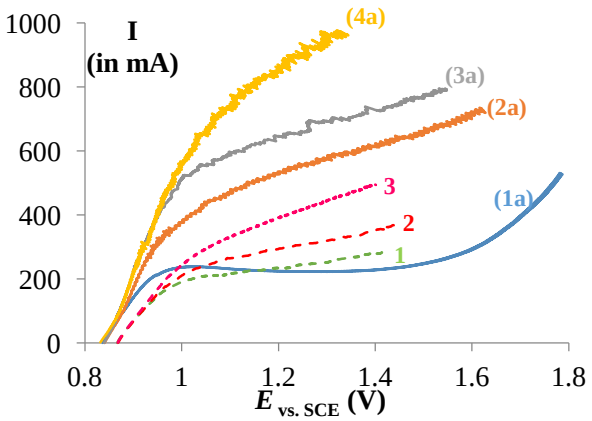

Fig.III.29: *I=f(E)* obtained for various stirring on a graphite RCE, immersed in Liquid-Solid suspension containing dissolved $V^{(IV)}$ at 1.5 mol/L and solid $VOSO_4$, the total vanadium concentration in the suspension is equivalent to 2.35 mol of $V^{(IV)}$ /litre of suspension (which corresponds to 80 % of the solubility in solid form); for the curves 1a to 3a the angular velocities ω_{RCE} are 300, 600 and 1500 RPM respectively and ω_{CSS} = 0 RPM. For the curve 4a, $\omega_{RCE} = \omega_{CSS}$ = 1500 RPM; Curves 1, 2 and 3 are imported from Fig.III.22 for ω_{RCE} = 300, 600 and 1500 RPM respectively. WE = graphite RCE; CE= Pt plate; [H_2SO_4] = 3 M; r = 10 mV/s; T = 10 °C; Curves obtained with correction of the ohmic drop (EIS).

The curves (2a) and (3a) exhibit a classical shape with a diffusion plateau of which intensity increases with the stirring; the curve (1a) obtained with an angular rate of 300 RPM exhibits the same features, except that the limiting current slightly decreases for applied potentials higher than 1 V/SCE. This decrease is due to the depletion of active material in the diffusion layer; in fact, the applied stirring is insufficient to renew the interfacial layer solution, nor to lift the solid particles. This phenomenon disappears for higher stirring rates (curves 2a and 3a).
Increasing the angular rate of the RCE causes the current to increase in all the examined cases.
As a matter of fact, for the liquid-solid suspension, the logarithmic analysis of the current taken on the curves 2a and 3a led to the correlation (Eq.III.13). The same analysis performed for the curves 2 and 3 (from Fig.III.22) led to the correlation (Eq.III.4) for which the slope is very close to the previous one: 0.27 against 0.25 (but the magnitude of the current was lower).

$$ln\ I_{at\ 1.1\ V,in\ A} = -1.78 + 0.25 \times ln\ \omega_{\ rad/s} \qquad \text{Eq.III.13}$$

The limiting current is enhanced when the CSS is activated (curve 4a): at 1. 4 V, the current is 0.95 A, 0.7 A and 0.48 A for the curves 4a, 3a and 3 respectively. Here, the effect of the coupled stirrings at high angular velocities ($\omega_{RCE} = \omega_{CSS} = 1500$ RPM) appears to be synergistic.
To conclude, at a constant solid mass fraction of the suspension, the stirring appears to have a positive effect on the current, even if this effect is lower than what is theoretically expected (see previous discussion). In addition, the comparison of the magnitude of the limiting currents, (curve 2 and 2a, or 3 and 3a) shows that in presence of solid particles the current is ~ 80 % higher than without particles. Under strong stirring, the vanadium mass transfer appears to be enhanced compared to the one measured in the absence of solid in the saturated solution. This behavior is confirmed with the introduction of the additional stirring (CSS/1500RPM/curve 4b). Besides, to avoid any decrease in the transferred flux of the vanadium, during a preparative electrolysis carried out under mass transfer limiting conditions such as the condition in 1a), it is necessary to ensure sufficient stirring of the suspension.
These results are not contradictory with the results observed when studying the effect of the solid fraction on the current; indeed, here the solid fraction remains constant and the stirring enhances the transfer, while in the previous situation the stirring remains constant and the fraction of the solid increases thus decreasing the available volume for the diffusion of the vanadium ions.
Note that another objective of this study was to examine if the dissolution of the solid particles of the vanadium could eventually compensate its depletion in the vicinity of the interface, thus enabling an increase of the oxidation current. The obtained results do not allow concluding on this point because the effect of the strong stirring (required to maintain a uniform/fluidized suspension) predominates and it is no ease to observe the dissolution of the vanadium.

III.1.3.2.4. Influence of Ketjen Black (KB) on the oxidation current

This part aims to study, by plotting the I=f(E) curves, the effect of KB on the vanadium $V^{(IV)}$ oxidation limiting current. As mentioned before, the addition of KB is expected to extend the surface of the electrode in the bulk (exploiting the adhesion of KB aggregates on the current

collector) [14]. The carbon nanoparticles are suspected to induce an increase of the current by a percolation phenomenon enabling to carry out the reaction (1) or (1') in any point of the suspension. Thus the electron released by the vanadium would be driven from KB grain to KB grain up to the interface.

The following procedure was applied in order to monitor the *I = f(E)* curves: a certain mass fraction of the KB was added into a saturated solution of $V^{(IV)}$; then, the effect of the mass fraction of the solid particles of the $VOSO_4.5H_2O$ was studied and the current was measured at 1.6V.

The curve (1) in Fig.III.30 obtained (without KB) for suspensions containing various mass fractions of $VOSO_4.5H_2O$, shows that the magnitude of the current decreases when the mass fraction of the solid increases, a similar behavior to this observed above (Fig.III.28, §III.3.2.2.1). The introduction of a low mass fraction of the KB (0.1 g/0.12 mass %, Curve (2)) in the saturated solution ($[V^{(IV)}]$ = 1.5 mol.L^{-1}, first point on the left) causes the current to increase of ~40 %, thus confirming that at low fractions the KB acts as an electronic conductor enabling electronic percolation i.e. the electrons produced by the $V^{(IV)}$ oxidation can be driven by the KB aggregates from the bulk to the RCE surface in some extent length.

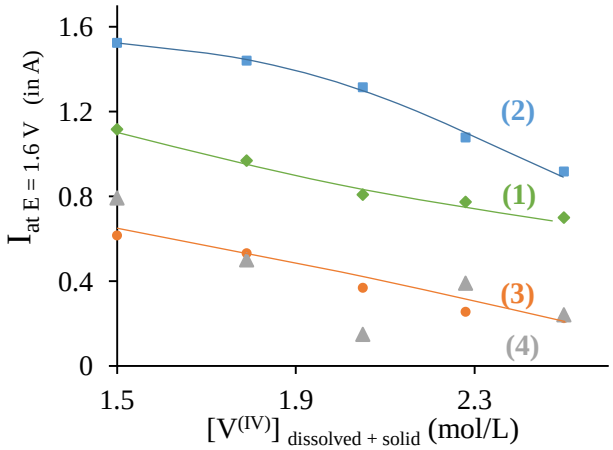

Fig.III.30: Evolution of the $V^{(IV)}$ oxidation current measured at 1.6 V as a function of the added mass of the solid $VOSO_4.5H_2O$, for various mass fractions of the ketjen black (KB). The origin of the abscises correspond to a saturated solution of the $V^{(IV)}$ (1.5 mol/L). Curves number- KB mass/ mass %: 1- 0 g/ 0 %; 2- 0.1 g/0.17 %; 3- 0.25 g/0.42 %; and 4-0.7 g/1.17%; Points: experimental results; lines: interpolated evolutions. Primary data for *I= f(E)* (curves not shown here): WE = graphite RCE; CE = Pt plate; $[H_2SO_4]$ = 3 M; T= 10 °C; $\omega_{RCE} = \omega_{CSS}$ = 1500 RPM; r = 10 mV/s; $V_{initial}$ = 60 cm^3. Curves obtained without correction of the ohmic drop. The suspensions were prepared as indicated in section 2.2.

When $VOSO_4.5H_2O$ solid particles are added into the saturated solution (in absence/curve (1) or in presence/curve (2) of KB), the current decreases and the decrease is enhanced as the mass fraction of the vanadium solid added increases. The previously involved problem of the decrease of the flux of VO^{2+}, created by the solid particles of the vanadium, could again be a possible explanation. In addition, here, the introduced solid particles of the vanadium can interact with the KB nanoparticles, thus leading to solid adducts (KB-Vanadium). These particles could possibly

'break' the KB aggregates thus preventing the electron driving to the collector. Note that even if the current decreases in the curve 2, its magnitude remains higher than this measured without KB (curve 1) for all the examined fractions of the solid vanadium.

Besides, for higher fractions of KB (0.25 g/0.42 % for curve 3 and 0.7 g/1.17 % for curve 4) the observed current decreases: a "concentrated" suspension of the KB negatively affects the vanadium oxidation current, while a "low" fraction has a beneficial effect. This strange behavior would require further studies; a possible explanation could be that in a concentrated suspension of KB nanoparticles, in the absence of any surfactant, an agglomeration of the KB nanoparticles can occur, thus creating higher sizes aggregates which are consequently less efficient against the electronic conduction in the bulk, they can even constitute more effective barriers to the $V^{(IV)}$ mass transport.

To sum up, a low percentage of the KB has a noticeable beneficial effect (increase of 40 %) on the $V^{(IV)}$ oxidation current, but higher contents of KB become a drawback and leads to the decrease of this current.

Note that, perfect reproducibility of these results is difficult to obtain because there are various operating factors difficult to control *(polishing of the RCE, ohmic resistance of the suspension containing KB and solid $VOSO_4.5H_2O$, perfect mixture of KB and solid $VOSO_4.5H_2O$).* So the uncertainties of these results (Fig.III.30) are estimated in the range from 10 to 15 %.

In conclusion, the new introduced setup with an additional stirring device allowed the study of the mass transfer coefficient against the angular velocity of the graphite rotating cylinder and of the CSS and it was found that the determined exponent γ of the power law ($k=f(\omega^{\gamma})$) is always lower than the theoretical predicted value. The main reason of the discrepancy is the non-rigorous respect of the fixed and required operating conditions, initially set for the Lévêque correlation.

Regarding the uplifting of the solid particles by the CSS, it appears that the stirring by the CSS alone will be preferred instead of the electrode (RCE), since it seems that (in the case of a solution) its motion partially compensates the effect of the rotation of the working electrode, especially for angular rates of the CSS > 900 RPM.

As for the study of the effect of solid particles on the oxidation current, no significant increase of the anodic current was observed when adding low mass fraction of the vanadium particles; conversely, the solid negatively affects the anodic current (Fig.III.28); the latter decreases rapidly (until ~ 46 %) when the introduced solid fraction reaches ~30 %, which was also observed with the introduction of inert glass spheres. This was attributed to shrinkage of the available space for vanadium diffusion, by the occupation of the solid particles causing the diffusion coefficient to decrease. Note that, the strong stirring hides any possible increase of the current due to the dissolution of the salt and that the curves are strongly deformed because of the important ohmic drop (increased as the solid fraction increases), which could be also responsible for the drop of the current at constant potential.

Lastly, the presence of low mass fractions of KB nanoparticles (0.17 %) appears to be beneficial to the vanadium oxidation current (increase of 40 %) thanks to the electronic percolation created by the KB aggregates which ensure the electrons transport to the collector. However, this benefice is attenuated when: i) solid particles of the $VOSO_4$ were introduced into the suspension, and ii) higher mass fraction of the KB nanoparticles were involved. Attractive interactions between $VOSO_4$ solid particles and KB nanoparticles, or even between KB nanoparticles among themselves (in absence of any surfactant) are probably responsible of the destruction of the KB aggregates and the disruption of the electronic conduction in the bulk.

This effect between the KB and the vanadium particles was also observed before on the immobile graphite rod (§ III.1.2.2, Fig.III.16) and at a higher KB content.

III.1.4. Study of the effect of concentrated $V^{(V)}$ solutions on the reduction current of $V^{(V)}$ to $V^{(IV)}$

The characterization of the redox couple constituting the posolyte requires the study of the reduction of the $V^{(V)}$ to $V^{(IV)}$ with the effect of the different parameters examined above (electrode material, effect of vanadium inert solid particles, presence of a carbonated additive). The solubility of the vanadium (V) oxide V_2O_5 is very low ($s_{VO_2^+ at\ T=25°C} < 0.6\ mol/L$ in 3 mol/L sulfuric acid) and its dissolution is slow (cf. chapter IV).
After the preparation of concentrated $V^{(V)}$ solution, the electrochemical study in the classical three-electrodes cell was undertaken for the two working electrodes studied above (GF and GR), in addition to the presence of KB nanoparticles.

III.1.4.1. Preparation of $V^{(V)}$ concentrated solutions

The experimental setup (U-shaped electrochemical cell) used for the preparation was described in chapter II. The working electrode is an inactivated graphite felt (thickness = 5 mm; immersed surface S_g = length of 4 cm x width of 2 cm = 8 cm^2), chosen for its larger active surface area which would decrease the electrolysis time. The suspension was stirred by the cross-shaped stirrer. The counter electrode is a platinum plate (S = 4 cm^2) and there is no stirring in the negolyte. The suspension studied was constituted by 50 mL of $VOSO_4.5H_2O$ at an equivalent concentration of ~ 4.5 M in 3 M sulfuric acid.

A current of 0.3 A roughly estimated as the 1/10 of the initial limiting current was applied to carry out the electrolysis and to prepare the solution.
The total electrolysis time was 30 h and the amount of charge supplied is 32 400 C, which corresponds to 1.5 times the required charge for a complete conversion ($\frac{50\times4.5}{1000}\times 96500 = 21.7\ kC$.

The obtained solution was analyzed by potentiometric titration and validated by ICP analysis and the concentration of VO_2^+ was found to be 5 mol/L ($[V^{(IV)}]_{t=0}$ = 4.5 M); the discrepancy can be explained by a decrease of the initial volume of the posolyte. In fact, various parameters could contribute to decrease this volume which is relatively difficult to determine precisely at the end of the electrolysis:

- The half reaction ($VO^{2+} + H_2O \leftrightarrows VO_2^+ + 2\ H^+$) consumes 1 mole of H_2O per electron;
- To insure the ionic conduction across the Nafion 117 membrane, H_3O^+ migrates ($t_{H/Nafion} \approx 0.94$) from the posolyte to the negolyte; this means that ~ 0.9 molecules are transported from a compartment to the other;
- Because of the long duration of the electrolysis (30 h), a fraction of the solution can evaporate, contributing to the decrease of the volume of the posolyte.

Note that the obtained posolyte is totally homogeneous without any solid. The whole $V^{(V)}$ obtained was dissolved and the resulting viscosity (μ = 0.16 Pa.s), also due to the increase of the H_2SO_4 concentration during the electrolysis. The faradaic yield, assuming a conversion of 95 %, is estimated as the following:

$$y_f = \frac{0.95 \times 96500 \times 0.225}{32400} = 0.636$$

The amount of charge lost (> 35 %) can be explained by the galvanostatic mode and the fact that, during the electrolysis, the applied current was kept constant and at a certain time it becomes higher than the limiting current. The excess of charge was used to oxidize water.

The obtained supersaturated solution of $V^{(V)}$ is then stored at 4 °C. The $V^{(V)}$ is stable at low temperatures and no precipitation was observed for more than 6 months as long as the solution was stored in the refrigerator (very slow precipitation kinetics). Extensive studies (NMR) were performed to determine the hydrated form of the $V^{(V)}$ species prepared by electrolysis.

III.1.4.2. Current – potential curves for $V^{(V)}$ solutions at 2.5 and 5 M

The vanadium (V) needs special care because it could be responsible of various problems in the VRFB: its oxide V_2O_5 exhibits low solubility, it is unstable with increasing temperature [15-16] and its requirement of concentrated acidic media. However, obtaining concentrated VO_2^+ solutions via electro-oxidation of concentrated $V^{(IV)}$ suspensions appeared to be successful and generates stable solutions.

The electrochemical study of this solution was undertaken in the classic three electrodes cell on the two electrode materials discussed through the chapter. Two concentrations were chosen to perform this study, 5 mol/L and 2.5 mol/L diluted from the latter in 3 mol/L H_2SO_4. A significant drop in the viscosity of the solution was noticed after the dilution, but it was not studied in the viscosity measurements (chapter II).

The current – potential curves were first performed on the graphite felt electrode and the results are presented in Appendix X10.

The I = f(E) curves obtained on the graphite rod with the vanadium (V) solutions are presented in Fig.III.31 where two concentrations are examined (2.5 and 5 M). Compared to the curve obtained with the supporting electrolyte, the curve of the vanadium at 2.5 M exhibits at least two signals (0.9 to 0 V and -0.1 to -0.5 V) plus the exponential part of the solvent. In the posolyte, the only redox couple involved is the $V^{(IV)}/V^{(V)}$; thus the analysis of the curves does not need to go beyond the first signal (~ 0.5 V), but we propose to try to identify and explain the phenomena taking place above that potential. The first signal exhibits a plateau in a large range of the potential (0.9 – 0 V) and the second signal appears as a peak and its magnitude is lower than that of the latter.

The ratio of the currents of these two signals ($\frac{\sim 150}{\sim 50} \approx 2.7$) is not in agreement with the ratio of the electrons. In fact, we assume that the product obtained after reductions at a potential of ~ 0.5 V is $V^{(II)}$; thus, we can attribute the first signal to the bielectronic reduction of:

$$VO_2^+ + 4H^+ + 2e^- \rightarrow V^{3+} + 2H_2O \qquad \text{Rx.III.3}$$

Then the monoelectronic reduction of V^{3+} to V^{2+} occurs (0 to -0.5 V).

Two parameters at least could explain the discrepancies between the ratio $\frac{I_{lim\,(0.9,0)}}{I_{\mathrm{lim}\,(0,-0.5)}}$ and the ratio $\frac{n^{e-}{}_{V^{(V)}\rightarrow V^{(III)}}}{n^{e-}{}_{V^{(III)}\rightarrow V^{(II)}}}$:

- The first parameter is the acidity at the interface; the reduction of 1 mol of VO_2^+ to V^{2+} requires 4 H^+; this means that during the measurement, ($0.9 \geq E_{(V)} \geq 0$) the interface is impoverished from acid. This can affect the vanadium forms and favor hydroxylated forms of the various species;
- The second parameter is the diffusion coefficient of the vanadium (V) which is dependent on the viscosity of the solution, i.e. the concentration of H_2SO_4.

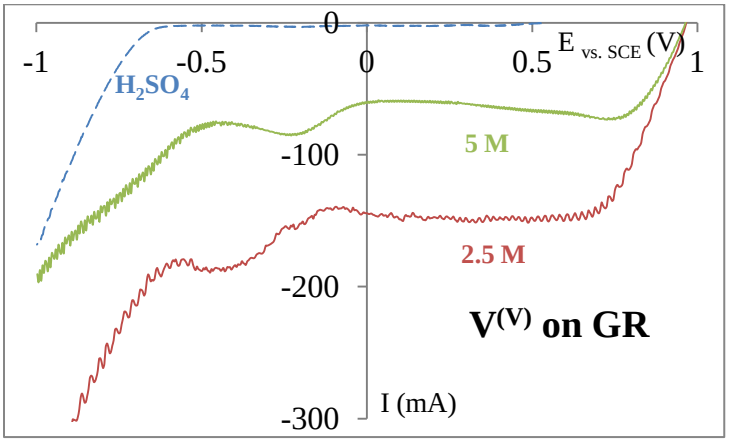

Fig.III.31: Comparison of I = f(E) curves performed on a graphite rod electrode (S_g = 1 cm^2) immersed in 20 mL of two $V^{(V)}$ deaerated solutions: green/ $[V^{(V)}]$ = 5 M, obtained from electrolysis; red/ $[V^{(V)}]$ = 2.5 M obtained from the dilution of the latter in 3 M H_2SO_4 (blue curve); RE = SCE, CE = Pt plate, ω ≈ 500 RPM (magnetic bar), r=5 $mV.s^{-1}$.

Another fact is the absence of a signal specifically devoted to the reduction of the $V^{(IV)}$ to $V^{(III)}$. The electrochemical behavior of $V^{(IV)}$ as a function of pH is unknown and chemical and disproportionate reactions could occur, for example:

$$V^{(V)} \xrightarrow{e-} V^{(IV)} \Longrightarrow V^{(IV)} \xrightarrow{e-} V^{(III)} \; and \; V^{(III)} + V^{(V)} \longrightarrow V^{(IV)} \qquad \text{Rx.III.4}$$

Such electrochemical/chemical sequence can modify the overall form of the voltammograms.

Concerning the curve I = f(E) obtained with the solution of $V^{(V)}$ at 5 M, the current seems to be reduced to half when the concentration is doubled, which is what was also observed on the graphite felt (appendix X10). There are at least two main reasons which explain this behavior:

- At a higher concentration, the $V^{(V)}$ exists at least in two forms in equilibrium; the electrochemical behavior of these forms of the $V^{(V)}$ is different and not sufficiently studied; however, what is obvious is that the individual concentration of each form is lower than 5 M;
- Increasing the concentration of $V^{(V)}$ by electrolysis also generates sulfuric acid; both increases of concentrations cause the viscosity of the solution to increase (from ~ 0.01 Pa.s for 2 M $V^{(V)}$ in 5 M total sulfate to ~ 0.18 Pa.s for 5 M $V^{(V)}$ in 7 M total sulfate [15]) and this is disastrous for the magnitude of the current (decrease of the diffusion coefficient).

Note also the presence of an additional signal in the potential range of -0.5 to -0.9 V probably due to the reduction of a hydrated form of vanadium.

The presence of various equilibriums between species of $V^{(V)}$ in concentrated solution was also discussed by C. Madic et al. [17] who discussed the formation of $V^{(V)}$ complexes in high sulfuric acid media. Also, F. Rahman et al. [15] studied by cyclic voltammetry the effect of vanadium (V) concentration (2 to 5 M) in 6 M total sulfate/bisulfate on the current and peaks position. It was found that the magnitude of the peak current increases linearly as the $V^{(V)}$ concentration increases from 2 to 3.5 M; however, for higher concentrations, the peak height decreases and the authors attributed this decrease to the sharp increase in viscosity of the $V^{(V)}$ concentrated solution resulting in a decrease of the diffusion coefficient and then of the peak current. Another explanation found by this research team was that changes in the interfacial tension properties of the more concentrated solution may reduce the wettability of the glassy carbon electrode in the solution, thereby reducing the effective surface area and decreasing peak currents.

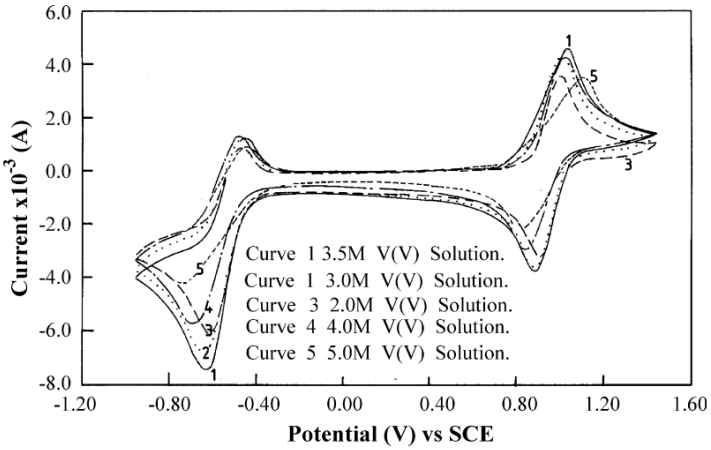

Fig.III.32: Cyclic voltammogram of $V^{(V)}$ solution in 6 M total sulfate/bisulfate [15], obtained using a glassy carbon electrode at a scan rate of 0.02 V/s.

However, we assume that there is an additional explanation to this evolution, and we presented earlier the assumption of the existence of more than one species of $V^{(V)}$ in concentrated solutions.
The presence of two different $V^{(V)}$ species impacting the current will be addressed in the next section (§ III.1.4.4)

III.1.4.3. Effect of KB nanoparticles in concentrated $V^{(V)}$ solutions

The effect of KB nanoparticles added to the $V^{(V)}$ solutions was studied for two fractions (1 and 2 % in weight) on a graphite rod and the results are presented in Fig.III.33.

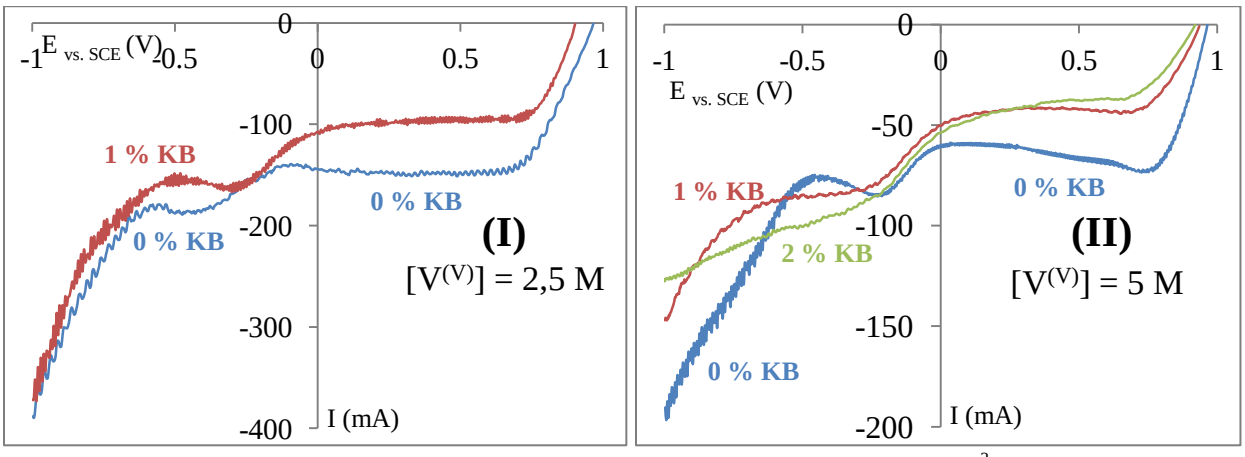

Fig.III.33: Comparison of I = f(E) curves performed on a graphite rod electrode (S_g = 1 cm^2) immersed in 20 mL of two $V^{(V)}$ deaerated solutions, containing 1 and 2 % in weight of KB: **(I)** $[V^{(V)}]$ = 2.5 M, and **(II)** $[V^{(V)}]$ = 5 M; RE = SCE, CE = Pt plate, ω ≈ 500 RPM (magnetic bar), r = 5 $mV.s^{-1}$.

Adding the carbon nanoparticles in these solutions increases the viscosity of the mixture and decreases the current for both $V^{(V)}$ concentrations; the decrease of the diffusion coefficient of the

$V^{(V)}$ because of the decrease of the viscosity is the proposed explanation even if this is not completely satisfactory. The effect of electronic percolation is not observed, contrary to what was observed for diluted vanadium (IV) solutions where the current increases. The shape of the curve for the 2.5 M solution is not modified by the presence of the KB particles and the decrease of the current is observed for both reduction waves (100 instead of 150 mA at 0.5 A). For the 5 M solution, the presence of KB also affects the current of the reduction of $V^{(V)}$ to $V^{(IV)}$. In fact, the current, lower than that obtained for the 2.5 M vanadium solution, also decreases of about 45 % whatever the percentage of KB added, for the same reason as above.

III.1.4.4. Investigation on the existence of two species of $V^{(V)}$

The presence of more than one species of $V^{(V)}$ ions in solution was suspected from the beginning; indeed, the low solubility of the V_2O_5 oxide which could not provide concentrations higher than 0.6 mol/L, obtaining a 5 mol/L solution of vanadium (V) through electro-reduction of vanadium (IV) enables to consider more than one form of the dissolved $V^{(V)}$. Numerous studies were conducted on the stability of $V^{(V)}$ as a function of the temperature and the sulfuric acid concentration, as discussed in chapter I.

The following study consists in comparing the electrochemical behavior of $V^{(V)}$ solutions (at 0.1 mol/L in 3 mol/L sulfuric acid) resulting from both preparations, i.e. dissolution of the oxide or reduction of the $V^{(IV)}$ Analysis were carried out by linear voltammetry, potentiometric titration and UV-Vis spectrometry, to try to better understand the content of the solutions.

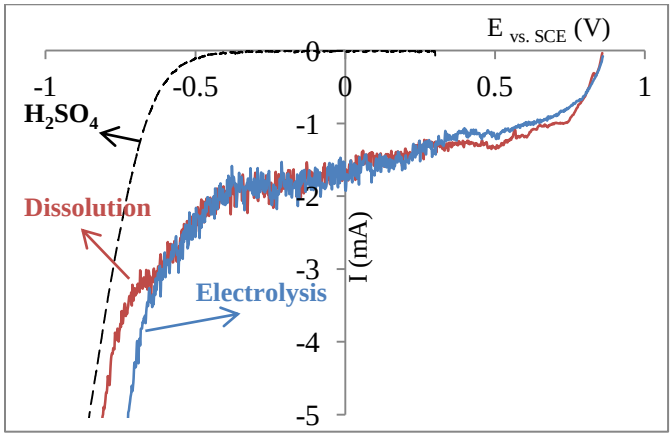

Fig.III.34: Comparison of I = f(E) curves obtained on a rotating disc graphite electrode (S_g = 0.07 cm^2), immersed in a deaerated 3 M H_2SO_4 solution (black curve) containing 0.1 M VO_2^+, prepared either by dissolution of the V_2O_5 oxide (red) or electro-oxidation of $V^{(IV)}$ in a U-shaped electrochemical cell (blue); RE = SCE, CE = Pt plate, ω = 500 rpm (RDE), r = 5 $mV.s^{-1}$.

Comparison of the voltamperometric curves shown in Fig.III.34 does not indicate any significant difference: both start at the same potential at 0.86 V for the reduction of $V^{(V)}$ to $V^{(IV)}$ and then to $V^{(III)}$ which in turn reduces to $V^{(II)}$ at around -0.5 V. The limiting current is identical for both

solutions and taking into account that the solutions are at the same concentration, we can conclude that they contain the same species.
On the other hand, the potentiometric titration by $Fe^{(II)}$ gave identical curves (having a sigmoid shape) for both solutions. As for the UV-Vis spectrometry, it has been established in chapter II that the $V^{(V)}$ does not have any characteristic peak, thus the aim of this analysis is to see if the presence of a different form of $V^{(V)}$ in solution induces any new additional absorption band. However, that was not the case and here again the spectra were identical for both solutions.

To validate the assumption that either the species formed by dissolution and electrolysis are identical, NMR analysis of solutions of $V^{(V)}$ at various concentrations were performed. The examined range is from 0.33 M to 4.6 M of $V^{(V)}$ diluted from the latter in 3 M H_2SO_4.

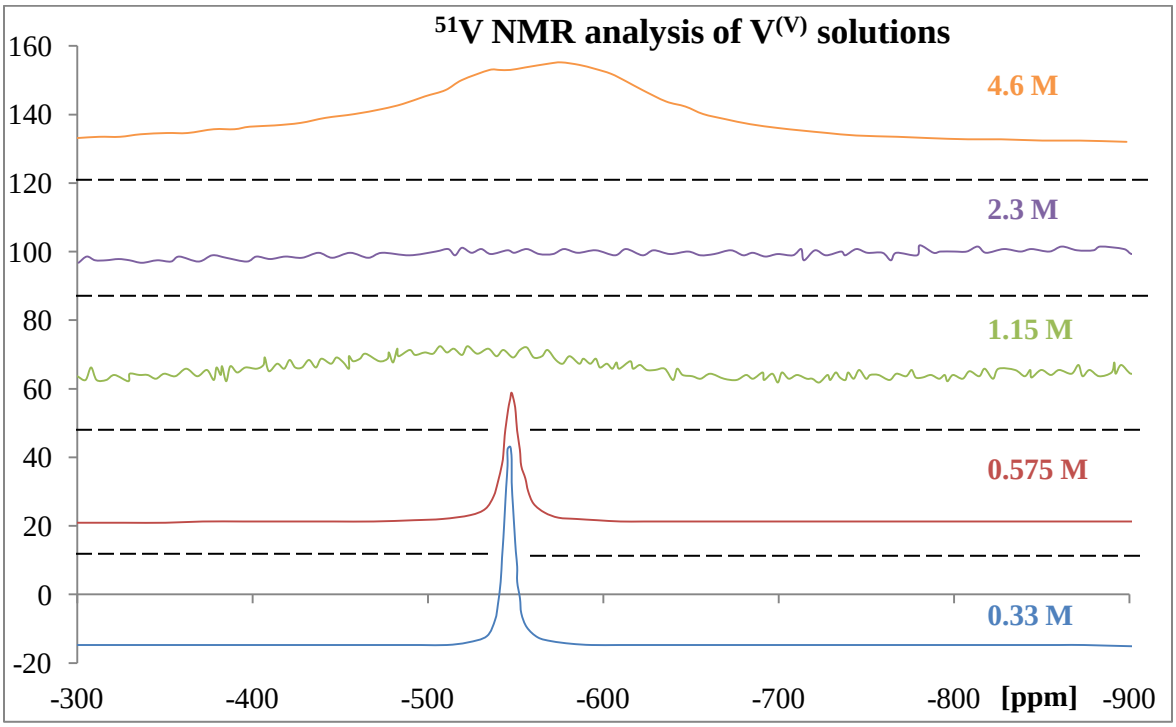

Fig.III.35: NMR spectrums of $V^{(V)}$ solutions obtained from the dilution of the initial 4.6 M concentration in 3 M sulfuric acid; $T_{analysis}$ = 25 °C; D_2O in capillary tube inside the NMR tube sample; orange/ 4.6 M; violet/ 2.3 M; green/ 1.15 M; red/ 0.572 M and blue/ 0.33 M.

The obtained results show a wide shape of spectrums, different for each concentration:

- for the more concentrated solution (4.6 M, orange curve), the signal appears to be broad, with a non-dissociated double peak. This shape is not usual for an NMR analysis and could be interpreted as corresponding to two different species interacting together in the same media;
- when the solution is diluted by half (2.3 M in 3 M sulfuric acid, violet curve), the previous signal becomes practically flat; one possible explanation could be that the

equilibrium between the forms existing at higher concentrations shifts to an intermediate state not detectable by NMR;

- the third curve (1.15 M, green curve) exhibits a small restitution of the signal between –500 and –600 ppm with a band wider than the first, implying the formation of new equilibrium in solution;
- the last two curves (red and blue) have the same shape: a thin peak is obtained at around –550 ppm. This same peak was observed for analysis performed for a temperature range between 10 and 40 °C for diluted solutions (0.33 M) (results not presented here) and was attributed to one species: VO_2^+ ions, considered as the dominant species in diluted acid solutions (ph 0.8-1) [18].

The first conclusion that can be drawn from these results is that indeed there are more than one species of $V^{(V)}$ present in the most concentrated solution. However, the NMR analysis obtained herein does not allow obtaining the exact formulation of each form. On the other hand, the disappearance of the "shoulder" corresponding to the second form at low vanadium concentrations is due to the modification of the vanadium/acid ratio, lost during the dilutions since the initial H_2SO_4 concentration was not determined and the dilutions were performed with a constant 3 M solution, making each sample at a different [H_2SO_4] from the others.
In fact, the concentration of sulfuric acid appears to have the most important impact on the formation of the $V^{(V)}$ complexes. C. Madic et al. [17] studied the dimerization of $VO_2(H_2O)_4^+$ ions in concentrated (> 7 M) perchloric and sulfuric acid. It was found that the dimerization in H_2SO_4 depends on the concentration of the acid, even at low $V^{(V)}$ concentrations: in a 13 M H_2SO_4 solution, the ^{51}V NMR spectrum of a 0.05 M $V^{(V)}$ solution shows a clear formation of the dimer given that the VO_2^+ signals disappeared, usually clearly present at -540 ppm (as seen in the analysis performed in this work, Fig.III.35, red and blue curves). The dimerization leads to the formation of $V_2O_4(H_2O)_7^{2+}$ or $V_2O_3(H_2O)_8^{4+}$, depending on the media involved.

The dependence of the dimer formation on the acid concentration can be explained by [17]:

- the low activity of water at these high acid concentrations implies that the elimination of water molecules is a part of the dimerization process;
- the stability of the dimer in sulfuric acid is due to the complexation with HSO_4^- and/or SO_4^{2-} ions which are involved in the structure of the dimer (Rx.III.5 and 6);
- the interference of free protons is essential for the dimerization reaction.

$$2\ VO_2(H_2O)_4^+ + x\ HSO_4^- \leftrightarrows V_2O_4(H_2O)_{(7-2x)}(SO_4)_x^{(2-2x)} + x\ H^+ + (2x+1)\ H_2O \qquad \text{Rx.III.5}$$

$$2VO_2(H_2O)_4^+ + xHSO_4^- \leftrightarrows V_2O_3(H_2O)_{(8-2x)}(SO_4)_x^{(4-2x)} + (x-2)H^+ + (2x+1)H_2O \qquad \text{Rx.III.6}$$

The NMR results [17] showed broad signals for the vanadium (V) dimer in concentrated H_2SO_4. Generally, broad signals are observed when the studied nucleus is in an unsymmetrical

environment and leads to a quadrupole relaxation. In the case of ^{51}V in concentrated acid, the viscosity of the solution constitutes an additional source for the broadening of the peak, since high viscosities prevent fast relaxation of the molecules. In addition, a very negative chemical shift implies a higher positive charge than that of VO_2^+, which would suggest that the dimer formed is more consistent with the formulation $V_2O_3^{4+}$ (Rx.III.5) rather than $V_2O_4^{2+}$ (Rx.III.6).

In addition, the stability of each of these dimers comes from the original species from which they have been made: $V_2O_4^{3+}$ is the result of the combination of two identical VO_2^+ ions resulting in a high-energy charge-transfer transition, whereas $V_2O_3^{4+}$ generates from one VO_2^+ linked to a VO^{3+} (generated by strongly acidic media) and has a low-energy charge-transfer transition [17].

On the other hand, N. Kausar et al. [18] studied the complex formation by RAMAN spectroscopy and they suggest that in concentrated $V^{(V)}$ and sulfate solutions, the $V^{(V)}$ is linked bidentately with SO_4^{2-}/HSO_4^- groups in a six coordinate vanadium environment under distorted symmetry and they propose the following formed structures for the $V_2O_3^{4+}$ and $V_2O_4^{2+}$:

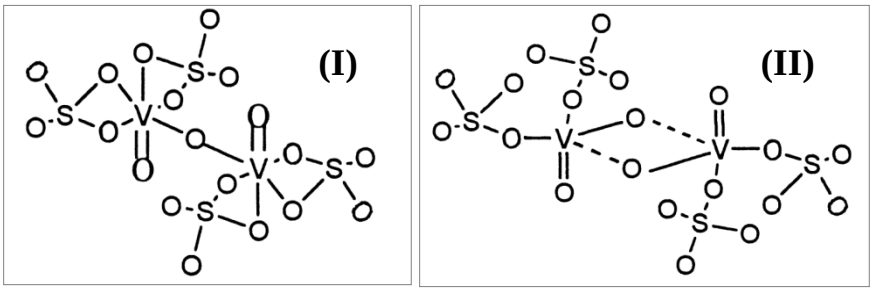

Fig.III.36: Proposed configurations for the $V_2O_3^{4+}$ **(I)** and $V_2O_4^{2+}$ **(II)** as suggested by N. Kausar et al. [18]

The electrochemical studies of such species would also involve the study of the mixed-valence cation complex $V_2O_3^{3+}$ formed between $V^{(IV)}$ and $V^{(V)}$ during the electrochemical reaction. However, such complex has a rapid decomposition because its equilibrium concentration is very low in such acidic media.

The modification of the vanadium/acid ratio leads to the formation of complexes (dimers or polymers) which could form an important steric blockage, as seen from the suggested configurations, inducing the disappearance of a peak in NMR due to the fast relaxation of the spins (violet curve). Therefore, in order to see the impact of the concentration on the existing forms of $V^{(V)}$ in this study, a constant ratio of vanadium/acid concentrations should have been maintained.

On the other hand, the effect of temperature on these two forms was studied for the 4.6 M solution: it was found that when increasing the temperature from 25 to 40 °C the whole peak disappears (Fig.III.37) and only a small artifact remains around 525 ppm, where the second peak should have been. However, the process is reversible and the whole peak is restored when decreasing the temperature back to 25 °C. This means that one of the forms is not stable at high

temperatures and it might be the one responsible for the instability of concentrated vanadium (V) solutions at high temperatures.

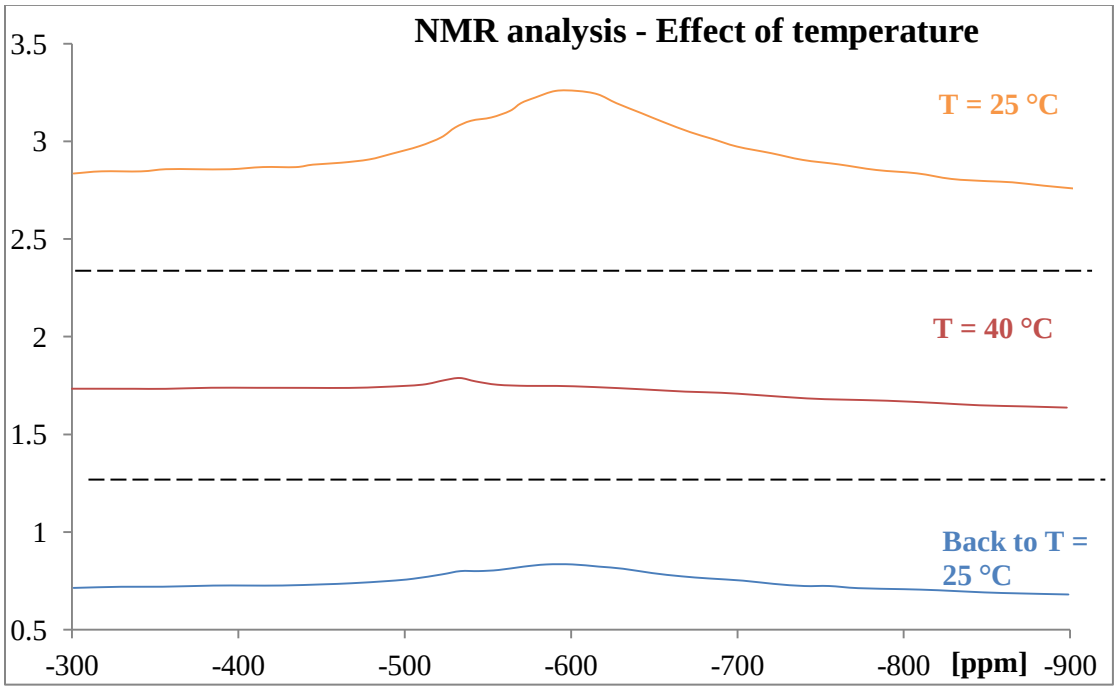

Fig.III.37: Effect of temperature on the NMR spectrums of the 4.6 M $V^{(V)}$ solution obtained from electro-oxidation of $V^{(IV)}$; D_2O in capillary tube inside the NMR tube sample; orange/ 4.6 M at 25 °C; red/ T is increased to 40 °C and blue/ T is decreased to the initial 25 °C.

Taking into account the findings of [17], [18] and the obtained NMR results of this work, we can conclude that when high vanadium (V) concentrations are prepared by electro-oxidation of $V^{(IV)}$, the resulting solution contains concentrated sulfuric acid leading to the dimerization of $V^{(V)}$ in solution. The formation, stability and reactivity of this dimer is closely related to the [H_2SO_4], this is why the effect of the concentration on the current in the I = f(E) curves was significant and different from what is usually obtained. Since, the 2.5 M solution was prepared in relatively diluted acid (3 M compared to more than 7 M in the bibliography), the equilibriums of the dimers were favored towards their dissociation, which is what also observed in the NMR spectrums (Fig.III.35).

In conclusion, stable and concentrated $V^{(V)}$ solutions (up to 5 M) can be obtained by electro-reduction of $V^{(IV)}$ and they can remain completely dissolved when stored under 4 °C. However, their viscosity and the existence of $V^{(V)}$ in different forms in concentrated sulfuric acid could generate problems during the functioning of the battery by a decrease of the generated current, inducing losses in the power density of the battery.

III.2. Electrochemical characterization of the $V^{(II)}/V^{(III)}$ system (negolyte)

The following section of this chapter will address the reduction of the $V^{(III)}$ to $V^{(II)}$ in the negolyte of the VRFB. The pure $V^{(III)}$ powder studied by electroreduction of the commercial $VOSO_4$ as indicated in Chapter II. The effect, on the reduction current, of the parameters such as the vanadium (III) concentration, the presence of solid particles and the concentration of sulfuric acid will be developed.

III.2.1. Preparation of $V^{(III)}$ powder

The preparation of the $V^{(III)}$ powder, by electro-reduction of a $V^{(IV)}$ suspension (Rx.III.7), was undertaken in the same U-shaped electrochemical cell described in chapter II and already used for the preparation of vanadium (V). Several problems were encountered during the preliminary preparation of $V^{(III)}$, which were not observed previously.

$$VO^{2+} + 2\ H^{+} + 1\ e^{-} \rightarrow V^{3+} + H_2O \qquad \text{Rx.III.7}$$

The initial vanadium (IV) and sulfuric acid concentrations were 4.5 and 3 M respectively. A graphite felt working electrode and the cross-shaped stirrer were used for the electrolysis and a current of 0.3 A was applied. However, it was noticed during the electrolysis that:

- the volume of the sulfuric acid in the anodic compartment was decreasing and approximately 20 mL (from the 60 mL initially used) were lost. Various phenomena could explain this evolution: first, in this system as previously, migration occurs mainly by transport of protons ions H_3O^+ from the posolyte to the negolyte. When one H^+ moves through the membrane to the negolyte, one molecule of water leaves the posolyte and accumulates in the opposite compartment. Second, the osmotic pressure induces losses of sulfuric acid towards the negolyte and third, the evaporation of water due to the exothermic reaction;
- the reaction is very exothermic; the temperature of the cell, which was not designed for thermoregulation, could reach 70 °C during the electrolysis, thus, it was necessary to decrease the temperature of the electrolytes. To that end, the cell was cooled under cold running water until the temperature drops to ~ 40 °C before continuing the experiment;
- after 18 h of electrolysis (~ half of the total electrolysis time), the cell potential increased to 30 V (maximum voltage delivered by the used power supply) and the experiment was interrupted. This increase of the cell voltage was attributed mainly to the decrease of the acid concentration during the electrolysis leading to an important ohmic drop of the system.

As a matter of fact, the reduction reaction shows that each vanadium (IV) ion consumes 2 H^+ in order to form one V^{3+} ion. To this consumption, we must add the migration of H^+ through the

membrane to the negolyte compartment. Therefore, starting with an initial vanadium concentration greater than that of the acid implies at a certain time the depletion of free protons in solutions, and causes the decrease of the conductivity and the impossibility to continue the reaction. Thus, a small volume (~ 5 mL) of pure H_2SO_4 (95 %) is added to the cathodic compartment and the cell potential decreased to around 10 V almost instantly; the electrolysis was able to be continued.
It should be also noted that the vanadium (III) precipitates before the conversion of $V^{(IV)}$ reaches 100 %; its solubility is low and decreases when the sulfuric acid concentration increases [19]. Thus, the addition of pure H_2SO_4 along the electrolysis (to decrease the voltage) would provoke the precipitation. Nevertheless, the electrolysis was always pursued even with a suspension.

It was also found that it could be better to start with a vanadium (IV) solution in 5 M sulfuric acid, and add $VOSO_4.5H_2O$ powder along the way; this enables 1) to facilitate the stirring and 2) to increase to 1 A the applied current in order to decrease the electrolysis time.

At the end of the electrolysis, the suspension is analyzed by UV-Vis spectrometry, by taking a representative sample of the negolyte from the cell. Then, the aliquot was diluted in order to completely dissolve the withdrawn solid and analyze it by UV-Vis. The suspension is left for 2 days in the cell until complete precipitation of the $V^{(III)}$ occurs then it is recovered for filtration. The mixture is filtrated using a classic Buchner setup, linked to an air pump, and filter paper. During the filtration the collected wet-solid is rinsed with ethanol (97 %) to remove the excess ions remaining in the suspension. Ethanol was chosen over water since the $V^{(III)}$ powder is more soluble in the latter.
After filtration, the wet-solid is dried in the oven at 60 °C for around 5 hours. The obtained powder has a light green-grey color and corresponds to $V_2(SO_4)_3.xH_2O$ [10] which is analyzed by ICP to determine its water content systematically for each new powder preparation and was found to vary between 9 and 12 molecules of water.

Having prepared the powder, it can now be used for the preparation of $V^{(III)}$ solutions or suspensions for the electrochemical analysis.

III.2.2. Study of the electrochemical behavior of the $V^{(III)}$ in solution or in suspension on a graphite rod

III.2.2.1. Effect of the $V^{(III)}$ and sulfuric acid concentrations

The solutions of V^{3+} were prepared by dissolution of the prepared powder of $V_2(SO_4)_3.xH_2O$ in 2 M sulfuric acid. The first experiments were performed with three solutions: 0.25, 0.5 and 1 M of V^{3+} on a 1 cm^2 graphite rod used as a working electrode; the solutions were deaerated since i) the reaction of interest, reduction of $V^{(III)}$ to $V^{(II)}$, occurs at relatively low potentials ($E^0_{(V2+/V3+)}$ = -0.26 V/SHE), lower than the reduction potential of the dissolved oxygen (E < 0.3 V/SCE) and ii)

the $V^{(II)}$ is easily oxidized by oxygen. In fact, Choi et al. [20] studied the oxidation of $V^{(II)}$ by dissolved oxygen and they found that the capacity of the VRFB decreases by 71 % after 10 cycles if the reservoir of the negolyte is not sealed while it was only 3.8 % loss for a sealed reservoir.

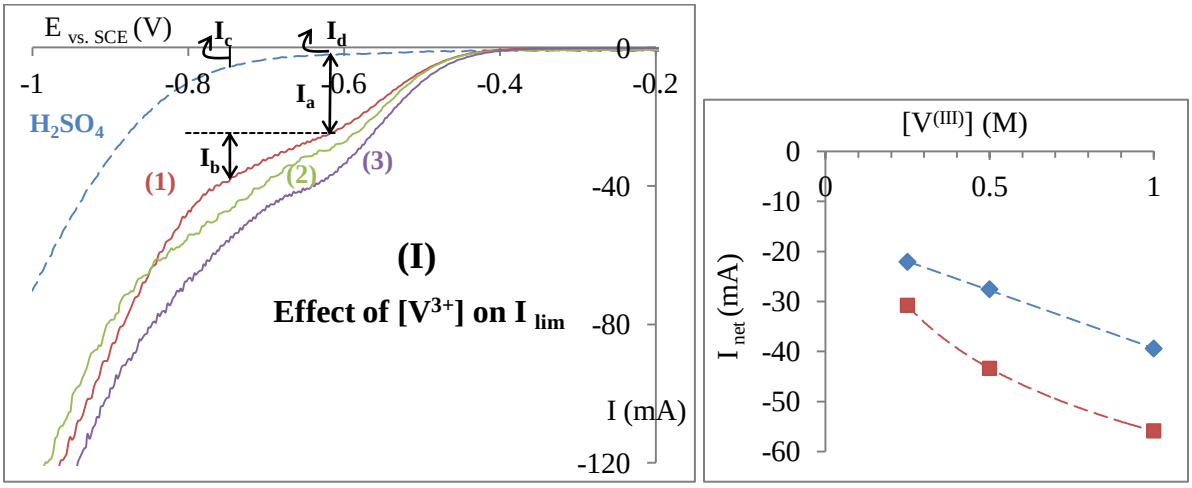

Fig.III.38: **(I)**: I = f(E) curves plotted on a graphite rod electrode (S_g = 1 cm^2) for various concentrations of $V^{(III)}$; blank: 2 M H_2SO_4 solution (blue curve); curves 1 (red), 2 (green) and 3 (violet): [V^{3+}] at 0.25, 0.5 and 1 M respectively; $V_{solution}$ = 20 cm^3; RE: SCE, CE: Pt plate; ω ≈ 500 rpm (magnetic bar); r = 5 mV/s. **(II)**: evolution of the net current as a function of $V^{(III)}$ concentration: (1) values of I picked around - 0.6 V and (2) values of I picked around - 0.75 V.

The obtained curves are presented in Fig.III.38-(I). Comparison of these curves with the blank show two signals of unequal magnitude, both attributed to the $V^{(III)}$ reduction. This means that the solution contains at least two different forms of the vanadium, probably V^{3+} and $V(OH)^{2+}$. The magnitude of these signals increase with the concentration of $V^{(III)}$ but the variation is not linear. In fact, the dissolution of $V_2(SO_4)_3$ consumes acid following the reaction:

$$V_2(SO_4)_3 + 3\ H^+ \rightarrow 2\ V^{3+} + 3\ HSO_4^- \qquad \text{Rx.III.8}$$

Consequently, the following reaction takes place:

$$V^{3+} + H_2O \leftrightarrows V(OH)^{2+} + H^+ \qquad \text{Rx.III.9}$$

From the curve (1), it is possible to estimate the concentration by operating as follows:

$$C_{V^{3+}} + C_{V(OH)^{2+}} = C_a + C_b = 0.25\ M \qquad \text{Eq.III.14}$$

$$\frac{I_a - I_d}{I_b - I_c} = \frac{nFSk_{V^{3+}}C_a}{nFSk_{V(OH)^{2+}}C_b} \qquad \text{Eq.III.15}$$

Assuming that $k_{V^{3+}} = k_{V(OH)^{2+}}$, it becomes possible to solve this system and to determine [V^{3+}]. Knowing that value, it becomes possible to determine the kinetic parameters for the V^{3+} reduction:

$$ln\frac{I\times I_{lim}}{|I_{lim}-I|} = \ln(nFSk°C) - \frac{\beta nF}{RT}\eta \qquad \text{Eq.III.16}$$

For the $V(OH)^{2+}$ analysis, a more complicated approach should be performed in order to apply the Butler-Volmer equation: the limiting current (I_a) found for the V^{3+} is deducted from the I = f(E) curve for E < -0.6 V in addition to the residual current to determine the net current relative to the $V(OH)^{2+}$. After that, the same calculation can be performed and the results are presented in table III.4. It should be noted that η = 0 is taken at – 0.4 and – 0.6 V respectively for V^{3+} and $V(OH)^{2+}$. The value of α is very close for both considered species and is greater than 0.5, which means that the system in both cases is simple. Concerning the values of $k°$, compared to the values obtained in the case of the $V^{(IV)}/V^{(V)}$ system, a difference of 10^3 is observed here which means that the $V^{(II)}/V^{(III)}$ redox system is more reversible. However, an increase of 1.5 times is observed between the V^{3+} and $V(OH)^{2+}$ which is normal considering that it is not the same system that is being studied on the electrode, but it would have been thought that the system containing the V^{3+} ion would be more reversible.

Table III.4: Comparison of the values of $k°$ and α obtained for the $V^{(III)}$ solution at 0.25 M for the V^{3+} and $V(OH)^{2+}$

	Slope	α	Y-intercept	$k°$ (m/s)
V^{3+}	-27.33	0.69	-0.4139	$0.69x10^{-3}$
$V(OH)^{2+}$	-24.58	0.62	1.0971	$1.03x10^{-3}$

E. Sum et al. [21] studied the $V^{(II)}/V^{(III)}$ redox system on a glassy carbon electrode and they found that the reversibility is strongly influenced by the preparation method of the surface of the electrode, with a value of $k° = 0.17 \times 10^{-6} m/s$ at pH = 0 with α = 0.67. On the other hand, Oriji et al. [22] found a much lower value (10^{-8} m/s with α = 0.5) and they attributed this difference to the different experimental conditions between the studies.

The cyclic voltammetry curves were plotted for these solutions (even if the concentrations are high) under the same conditions to see if the additional wave could be better resolved. The curves presented in Fig.III.39 exhibit high overvoltage, because of the high concentrations involved; the reduction of the V^{3+} occurs during the first peak, while the reduction of $V(OH)^{2+}$ occurs after – 0.75 V. also, the oxidation of the product of the reduction of $V(OH)^{2+}$ seems to occur in the potential range between – 0.25 and – 0.1 V.

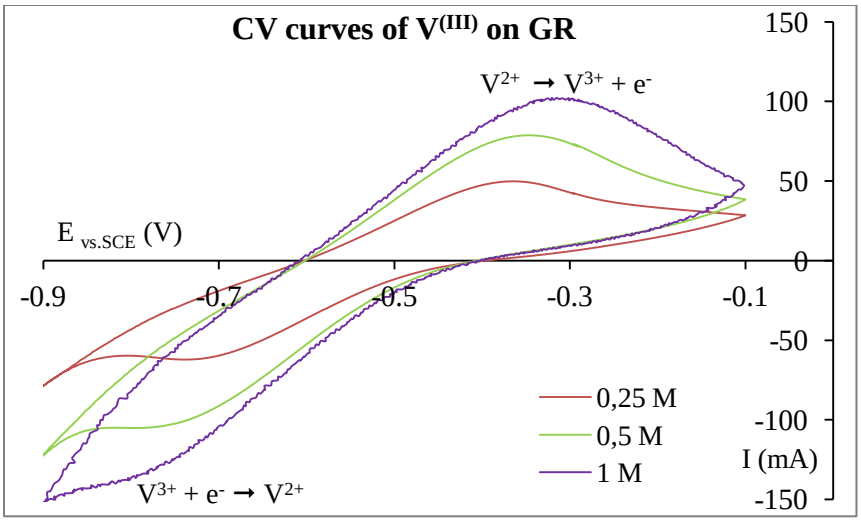

Fig.III.39: Comparison of the I = f(E) cyclic voltammetry curves performed on a graphite rod electrode (S_g = 1 cm^2) immersed in 20 mL of a 2 M H_2SO_4 solution containing dissolved V^{3+} at: (1-red): 0.25 M; (2-green): 0.5 M and (3-violet): 1 M; RE: SCE, CE: Pt plate; ω = 0 rpm; r = 50 mV/s.

It can be also noticed that the ratio between of the anodic peak current I_{anodic} to the cathodic peak current $I_{cathodic}$ is less than 1 which confirms the presence of more than one species.

Table III.5: Analysis of the CV curves of $V^{(III)}$ from Fig.III.39.

$[V^{(III)}]$ (M)	I_{anodic} (mA)	$I_{cathodic}$ (mA)	$I_{anodic}/I_{cathodic}$	E_{anodic} (mV)	$E_{cathodic}$ (mV)	ΔE (mV)
0.25	49.73	62.1	0.8	-0.366	-0.739	-1.105
0.5	78.77	104.25	0.76	-0.347	-0.767	-1.114
1	102.33	136.51	0.75	-0.321	-0.795	-1.116

The suggested assumption is the presence of two distinct forms of dissolved $V_2(SO_4)_3$ in solution, as a function of the quantity of free protons in solution. In fact, the dissolution of the powder releases 1.5 SO_4^{2-} ions per ion of V^{3+}, which will need 1.5 free H^+ from the solution to be linked. Also, the decomposition of $V_2(SO_4)_3$ is susceptible of releasing species such as $V_2SO_4^+$ and $V_2(SO_4)^{2+}$ in addition to the V^{3+} ion. This assumption can be consolidated by the Pourbaix diagram E = f(pH) of the vanadium species [23]. As it appears in the delimited domain in red, the predominance domain of the V^{3+} ion is limited for pH values between 0 and 2, above which the domain of the oxides begins.

Therefore, experiments were undertaken to study the effect of the sulfuric acid concentration on the reduction wave of $V^{(III)}$ for a chosen concentration of 0.5 M where the presence of the second wave was clear.

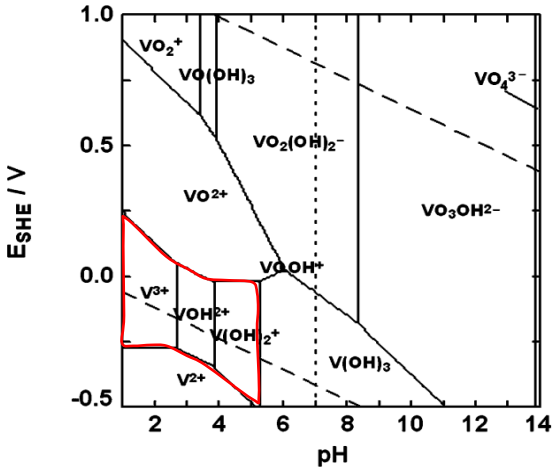

Fig.III.40: Pourbaix diagram of vanadium in water for an ionic strength I = 0.038. In red is highlighted the domain of interest for the $V^{(III)}$ species [23].

To that end, an initial 25 mL vanadium (III) solution was prepared at a concentration of vanadium of 0.5 mol/L by dissolution of the $V_2(SO_4)_3.xH_2O$ powder in a 0.2 mol/L sulfuric acid solution. The subsequent solutions at higher H_2SO_4 concentrations were prepared by adding corresponding amounts of 95 % H_2SO_4 directly into the initial solution in order to see the dissociation effect, if any, on the same species already present.

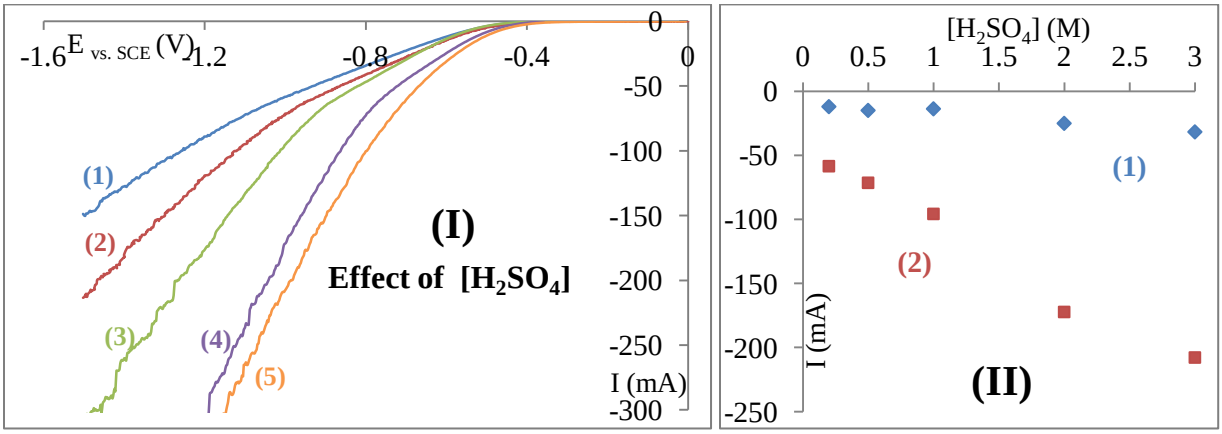

Fig.III.41: **(I)**: Comparison of the I = f(E) curves performed on a graphite rod (S_g = 1 cm^2), immersed in a 0.5 M $V^{(III)}$ solution while varying the sulfuric acid concentration: (1, blue): 0.2 M, (2, red): 0.5 M, (3, green): 1 M, (4, violet): 2 M and (5, orange): 3 M; RE: SCE, CE: Pt plate; ω ≈ 500 rpm (magnetic bar); r = 5 mV/s. **(II)**: Evolution of the current as a function of the sulfuric acid concentration: (1) (blue diamonds) for I measured at E = - 0.6 V; (2) (red cubes) for I measured at E = - 1 V.

The obtained curves exhibit a single signal of low resolution; compared to the curves of Fig.III.38, this signal could be attributed to the reduction of a hydrated form ($V(OH)^{2+}$ for example). In fact, starting with a low H_2SO_4 concentration causes the $V^{(III)}$ to be present in its hydrated form (see Fig.III.40); then, adding H_2SO_4 does not enable in the available time (~ 10

min of stirring) to shift the equilibrium (- Rx.III.9) to the right, that is why the first signal (curves of the Fig.III.38, - 0.7 , $E_{(V)}$ < - 0.4) was not observed.

$$V(OH)^{2+} + H^{+} \leftrightarrows V^{3+} + H_2O \qquad \text{- Rx.III.9}$$

Theoretically, when the concentration of the supporting electrolyte increases in solution, the reduction current of a cation (V^{3+} or $V(OH)^{2+}$ for example) decreases because the migration flux of the cation to the cathode decreases. In this case the increase of the current with the concentration can be due to the increase of the concentration of the solvent, i.e. the current is due to the H^{+} reduction and not to the $V^{(III)}$ reduction.

These results do not allow concluding on the nature of the different forms of $V^{(III)}$ nor their formation mechanisms but they confirm that the equilibrium between them is slow and that there is more than one species of $V^{(III)}$ reacting electrochemically and that not all of them have the same reactivity and/or reversibility which would have an impact on the functioning of the VRB especially if the dissociation does not favor the formation of the reversible species leading to the reduction to the corresponding $V^{(II)}$.

III.2.2.2. Effect of the presence of vanadium solid particles

The effect of the presence of $V_2(SO_4)_3.xH_2O$ powder was examined in this section. The bibliography states that in a 2 M sulfuric acid concentration, the solubility of V^{3+} is equal to 2.26 M at 20 °C [19]. However, in this work, we could not dissolve more than 0.55 M of $V_2(SO_4)_3.9H_2O$, prepared electrochemically, in 2 M sulfuric acid. For the preparation of the $V^{(III)}$ suspensions, a solution of 1 M of completely dissolved V^{3+} was prepared, and the quantity of solid was added to prepare the equivalent concentration of the suspension.

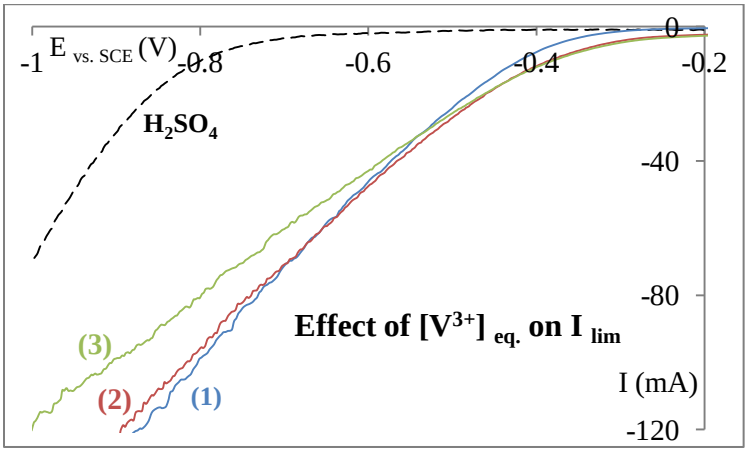

Fig.III.42: **(I)**: I = f(E) curves plotted on a graphite rod electrode (S_g = 1 cm^2) for various quantities of $V^{(III)}$ in a solid liquid suspension: (1, blue) 1.4 M; (2, red): 1.8 M; (3, green): 2.35 M; [H_2SO_4] = 2 M for all the curves; RE: SCE, CE: Pt plate; stirring: ω ≈ 500 rpm (magnetic bar); r = 5 mV/s.

The curves obtained with the suspensions are presented in Fig.III.42. It appears that in the presence of solid particles the diffusion plateau does not appear on the curves and a net evolution of the current as a function of the amount of added powder cannot be seen. This could be explained by a possible masking of the surface by the solid particles. Nevertheless, comparing the curves of the vanadium suspensions with that of the residual current of the supporting electrolyte shows that there is a significant current (~ – 40 mA at – 0.6 V) that can be attributed to the vanadium reduction.
Thus the presence of the powder might have an antagonist effect were they do not allow to differentiate the effect of different amounts of particles but at the same time they do not completely block the electrode and the reduction of dissolved V^{3+} can take place.

The electrochemical analysis of $V^{(III)}$ was undertaken on the graphite felt as well. The increase of the vanadium concentration in completely dissolved solutions showed an increase of the current but without the appearance of a reduction wave. This could be explained by an insufficient activation of the felt and a low affinity to the $V^{(II)}/V^{(III)}$ system. The addition of the powder exhibited a clogging of the felt: the real active surface area of the electrode is indeed increased compared to the graphite rod but the presence of solid particles, as explained before for the KB (§ III.1.1.1) and the $VOSO_4$ powder (appendix X8), is detrimental to the felt because of the clogging. The results obtained on the GF for the $V^{(III)}$ reduction are presented in Appendix X11.
This problem could be overcome by using a more 'aerated' geometry of the felt by creating micrometric holes between the fibers which would allow the circulation of the powder through the electrode without clogging it and keeping the characteristic high surface area.

III.3. Conclusion

In this chapter, the two active species of the posolyte ($V^{(IV)}$ and $V^{(V)}$) and the oxidant from the negolyte ($V^{(III)}$) were studied with the effect of different parameters on the resulting current of oxidation and reduction. It was found that the electrode material has an important impact on the response of the system as well as on the current; even if the graphite felt exhibits a real active surface area ($S_{real}/S_{geometric} \approx 15$) greater than that of a solid graphite rod, inducing in a bigger current ($I_{GF}/I_{GR} \approx 3.7$), it was not properly activated through an adequate process and therefore, the response of all the studied systems on the felt was not optimal. In addition, using a porous electrode with carbon fibers was not suitable for the study of suspensions as the solid particles (KB and/or vanadium powder) would clog the fibers and induce a negative impact on the resulting current. Therefore, the graphite rod was chosen as the working electrode of the VRFB.

The analysis of the kinetic properties of the $V^{(IV)}/V^{(V)}$ redox system through the oxidation curves of $V^{(IV)}$ was performed with the Butler-Volmer equation on a graphite disc for a vanadium (IV)

solution of 1 M in 3 M H_2SO_4. The value of $k°$ was found to double (from $2.32x10^{-6}$ to $4.18x10^{-6}$ m/s) when 1 % of KB nanoparticles were added to the solution while α decreased by ~ 40 % (0.30 to 0.21) which means that in the presence of the carbon additive the electronic transfers are enhanced but the mechanisms of the redox system becomes more complex.

The presence of solid particles during the oxidation of $V^{(IV)}$ to $V^{(V)}$ appeared to have a negative impact on the current: the system was studied on a graphite cylinder rotating electrode with an additional cross-shaped stirrer able to lift the particles and keep them in suspension. The solid particles leaded to a decrease of the current but did not cancel it which is considered as a benefice for the purpose of the study. The decrease of the current as a function of the volume fraction of the solid f_s is given by:

$$I = 7.10^{-5} {f_s}^2 - 1.15.10^{-2} f_s + 1.08$$

In fact, since the aim is to increase the energy density, the presence of solid particles in excess would be beneficial for that effect and does not deteriorate completely the performance of the battery; however, it will have an impact on the power density since the current would be lower.
As for the carbon black nanoparticles, the general tendency showed a decrease of the current in the presence of important quantities of KB, especially in the presence of vanadium particles as well in the suspension; the current decreases linearly at constant K fractions while increasing the amount of $VOSO_4$ particles. However, one fraction (0.17 % in weight) appeared to have a positive effect on the current: the value of I increases by 1.3 times compared to the suspensions containing only vanadium particles. This KB percentage could be possibly used for the electrolysis and cycling of the VRFB.

Concerning the study of $V^{(V)}$, the preparation of this oxidation state from the $V^{(IV)}$ lead to obtaining a very concentrated (5 M) and viscous solution (0.17 Pa.s) of $V^{(V)}$ without the precipitation of the species. The study of this solution at 5 and 2.5 M (diluted from the former) resulted in a decrease of the current by half when the concentration of the solution is doubled. This was attributed in part to the important viscosity of the 5 M solution, impacting the diffusion coefficient of the active species, but also to the dimerization of the $V^{(V)}$ at high acid concentrations leading to the formation of more than one species in solution which might not have the same reactivity. The presence of two species was discussed through an NMR analysis and a comparison of the bibliography: the $V_2O_3^{4+}$ dimer is susceptible to form in concentrated sulfuric acid and vanadium solutions. In conclusion, the $V^{(V)}$ would not create precipitation problems in the battery (for at least 1000 hours at 3 M of $V^{(V)}$ in 6 M total sulfate at 40 °C [14]) when used/formed at high concentrations but it would impact the resulting current and decrease it.

Lastly, the study of the negolyte was limited to the oxidation state $V^{(III)}$ because of the difficulties encountered for the production and storage of $V^{(II)}$ to protect it from oxidation by air. The study of the reduction curves of $V^{(III)}$ solutions at concentrations lower than 1 M showed two

signals translating two acid-based species (V^{3+} and $V(OH)^{2+}$) which distribution seems to be strongly conditioned by the concentration of sulfuric acid. The Butler-Volmer analysis for both species at a total vanadium concentration of 0.25 M showed that the value of α is close for both of them (0.69 and 0.62) while the value of $k°$ increases from $0.69x10^{-3}$ to $1.03x10^{-3}$ m/s for the $V(OH)^{2+}$. These values of $k°$ are relatively high compared to what was obtained in the bibliography.

On the other hand, the I = f(E) curves of $V^{(III)}$ suspensions, performed on the graphite rod, did not show any characteristic wave or increase of the current between different fractions of added solid but the reduction $V^{(III)}$ to $V^{(II)}$ is taking place on the electrode and this was confirmed by the presence of a cathodic current greater than the residual current.

References:

[1] A. Hassan, T. Tzedakis, "Enhancement of the electrochemical activity of a commercial graphite felt for vanadium redox flow battery (VRFB), by chemical treatment with acidic solution of $K_2Cr_2O_7$", Journal of Energy Storage, 26, 2019, 100967, doi: 10.1016/j.est.2019.100967

[2] G. Buxbaum, G. Pfaff, "Industrial inorganic pigments", 3rd Edition, Chapter 4, Wiley, 2005

[3] E. Sum, M. Rychcik, M. Skyllas-kazacos, "Investigation of the V(V)/V(IV) system for use in the positive half-cell of a redox battery", J. Power Sources, 16 (2), 1985, 85-95, doi: 10.1016/0378-7753(85)80082-3

[4] T. Yamamura, N. Watanabe, T. Yano, Y. Shiokawa, "Electron-Transfer Kinetics of Np^{3+}/Np^{4+}, NpO_2^{+}/NpO_2^{2+}, V^{2+}/V^{3+}, and VO^{2+}/VO_2^{+} at Carbon Electrodes", J. Electrochem. Soc., 152, 2005, A830, doi: 10.1149/1.1870794

[5] S. Zhong, M. Skyllas-Kazacos, "Electrochemical behavior of vanadium (V)/vanadium (IV) redox couple at graphite electrodes, J. Power Sources, 39, 1992, 1-9, doi: 10.1016/0378-7753(92)85001-Q

[6] F. Rahman, M. Skyllas-Kazacos, "Solubility of vanadyl sulfate in concentrated sulfuric acid solutions", J. Power Sources, 72 (2), 1998, 105-110, doi: 10.1016/S0378-7753(97)02692-X

[7] R. El Hage, F. Chauvet, B. Biscans, L. Cassayre, L. Maurice, T. Tzedakis, "Kinetic study of the dissolution of vanadyl sulfate and vanadium pentoxide in sulfuric acid aqueous solution", Chemical Engineering Science 199, 2019, 123-136, doi: 10.1016/j.ces.2019.01.024

[8] A.M. Islam, G.O. Phillips, A. Sljivo, M.J. Snowden, P.A. Williams, "A review of recent developments on the regulatory, structural and functional aspects of gum arabic", Food hydrocolloids, 11 (4), 1997, 493-505, doi: 10.1016/S0268-005X(97)80048-3

[9] S. Patel, A. Goyal, "Applications of Natural Polymer Gum Arabic: A Review", International Journal of Food Properties, 18 (5), 2015, 986-998, doi: 10.1080/10942912.2013.809541

[10] W.M. Carvalho Jr, L. Cassayre, D. Quaranta, F. Chauvet, R. El-Hage, T. Tzedakis, B. Biscans, "Stability of highly supersaturated vanadium electrolyte solution and characterization of precipitated phases for Vanadium Redox Flow Battery", J. Power Sources, 2020, Under review

[11] M. Eisenberg, C. W. Tobias, C. R. Wilke, "Ionic mass transfer and concentration polarization at rotating electrodes", J. Electrochem. Soc., 101 (6), 1954, 306-319, doi: 10.1149/1.2781252

[12] B. Trémillon, "Electrochimie analytique et réactions en solution", Dunod, 1993, Tome 1- ISBN : 978-2-225-84177-4 ; Tome 2- ISBN : 978-2-225-84255-9

[13] D.R. Gabe, F.C. Walsh, "The rotating cylinder electrode: a review of development", Journal of Applied Electrochemistry, 13, 1983, 3-21, doi: 10.1007/BF00615883.

[14] L. Madec, M. Youssry, M. Cerbelaud, P. Soudan, D. Guyomard, B. Lestriez, "Electronic-vs-Ionic Limitations to Electrochemical Performance in $Li_4Ti_5O_{12}$ Based Organic Suspensions for Lithium Redox Flow Batteries", Journal of The Electrochemical Society, 161(5), 2014, A693-A699, doi: 10.1149/2.035405jes

[15] F. Rahman, M. Skyllas-Kazacos, "Vanadium redox battery: Positive half-cell electrolyte studies", J. Power Sources, 189, 2009, 1212-1219, doi: 10.1016/j.jpowsour.2008.12.113

[16] F. Rahman, "Stability and properties of supersaturated vanadium electrolytes for high energy density vanadium redox battery", PhD thesis, UNSW, Australia, 1998
[17] C. Madic, G.M. Begun, R.L. Hahn, J.P. Launay, W.E. Thiessen, "Dimerization of Aquadioxovanadium(V) Ion in Concentrated Perchloric and Sulfuric Acid", Inorg. Chem., 23, 1984, 469-476, doi: 10.1021/ic00172a019
[18] N. Kausar, R. Howe, M. Skyllas-Kazacos, "Raman spectroscopy studies of concentrated vanadium redox battery positive electrolytes", Journal of Applied Electrochemistry, 31, 2001, 1327-1332, doi: 10.1023/A:1013870624722
[19] M. Skyllas-Kazacos, L. Cao, M. Kazacos, N. Kausar, A. Mousa, "Vanadium electrolyte studies for the vanadium redox battery – a review", ChemSusChem, 9, 2016, 1521-1543, doi: 10.1002/cssc.201600102
[20] N.H. Choi, S.k. Kwon, H. Kim, "Analysis of the Oxidation of the V(II) by Dissolved Oxygen Using UV-Visible Spectrophotometry in a Vanadium Redox Flow Battery", J. Electrochem. Soc., 160, 2013, A973, doi: 10.1149/2.145306jes
[21] E. Sum, M. Skyllas-Kazacos, "A study of the V(II)/V(III) redox couple for redox flow cell applications", J. Power Sources, 15 (2–3), 1985, 179-190, doi: 10.1016/0378-7753(85)80071-9
[22] G. Oriji, Y. Katayama, T. Miura, "Investigations on V(IV)/V(V) and V(II)/V(III) redox reactions by various electrochemical methods", J. Power Sources, 139 (1–2), 2005, 321-324, doi: 10.1016/j.jpowsour.2004.03.008
[23] F. Aureli, S. Ciardullo, M. Pagano, A. Raggi, F. Cubadda, "Speciation of vanadium (IV) and (V) in mineral water by anion exchange liquid chromatography-inductively coupled plasma mass spectrometry after EDTA complexation", Journal of Analytical Atomic Spectrometry, 23 (7), 2008, 1009-1016, doi: 10.1039/b805234b

Chapter IV – Kinetic study of the dissolution of vanadyl sulfate and vanadium pentoxide in sulfuric acid aqueous solution

Table of contents:

Introduction

The energy density of the battery is largely depending on the volume and concentration of the vanadium electrolytic solutions and numerous authors studied the effect of the composition of electrolyte solutions [1-2] on the performance of the battery, as presented in chapter I. Stable solutions with vanadium concentrations higher than 2 M could not be achieved in the working conditions of the VRFB, limiting the quantity of stored energy to around 40 kWh/m^3.
The electrolyte in the negative electrode compartment does not seem to exhibit major limitations related to the solubility of $V^{(III)}$ and $V^{(II)}$, but one important limitation encountered by the vanadium battery appears to be related to the precipitation of compounds in the positive electrode: precipitation of the $V^{(IV)}$ at low temperature and precipitation of the $V^{(V)}$ compounds at high temperature.
This fact limits the working temperature range of the VRFB between 10 and 40°C [3]. Precipitation of various vanadium salts and oxides was studied by several research groups and it was found that higher sulfuric acid concentrations stabilizes the $V^{(V)}$ solutions [4] but decreases the solubility of $V^{(II)}$, $V^{(III)}$ and $V^{(IV)}$.

Numerous works exist on the field of the vanadium battery, and one important objective is to avoid the vanadium pentoxide precipitation. Indeed, according to [4] and [5], vanadium (V) oxide dissolution is difficult, in addition to being an endothermic dissolution [6-7]. However, neither the understanding of the dissolution phenomena of the vanadium compounds, nor elucidation of the corresponding mechanisms was significantly explored; the published studies do not exhibit the determination of the physical limitations in order to act upstream. Hence, the present chapter deals with the study of the dissolution mechanisms of two common vanadium compounds: in 3 M sulfuric acid, at various temperatures (0 to 40°C), stirring rates and initial particles size. Apart from being the most common concentration used for an operating battery with 2 M $VOSO_4$, the sulfuric acid concentration (3 M) is chosen here, as a compromise between its positive effect on the dissolution of the vanadium pentoxide and its negative effect on the dissolution of vanadium sulfate [4].

To sum up, the general purpose of this study is to understand the phenomena governing the dissolution of vanadyl sulfate $VOSO_4$ and vanadium pentoxide V_2O_5 and to establish the corresponding kinetic laws, in order to have a better control on the accidental precipitation during VRFB operations. Simple models are proposed (diffusion/accumulation for $VOSO_4$ and kinetic rate for V_2O_5) and their resolution leads to theoretical kinetic equations describing the temporal evolution of these concentrations with satisfactory agreement with the experimental curves. Solubility's data and their temperature dependence are determined for both vanadium compounds involved.

In addition, given that in the present work the aim is to work in the VRFB with vanadium suspensions to increase the energy density of the battery, the obtained results are essential to understand the behavior of the posolyte containing excess vanadium solid particles.

IV.1. Material and methods

IV.1.1. Dissolution protocol

The chemicals used are vanadium (IV) sulfate oxide hydrate $VOSO_4.xH_2O$ (99.9%), vanadium (V) pentoxide V_2O_5 (99.6%) from Alfa Aesar, NormaPur H_2SO_4 from Sigma Aldrich, and deionized water.

Dissolution experiments were achieved in a thermo regulated reactor (cylinder of an internal diameter = 2 cm) at constant temperature. An adequate volume of aqueous solution 3 M sulfuric acid is poured in the reactor and stirred with a 1.5 cm magnetic bar until reaching the selected temperature. Then, an excess of vanadium compound is added ($m_{(vanadyl\ sulfate)}$ = 4.559 g and $m_{(vanadium\ pentoxide)}$ = 1.461 g), marking the initial time of the experiment. Stirring rate is kept constant during the experiment. At regular time intervals, aliquots are withdrawn from the solution with plastic syringes and are directly filtered twice with filters resisting to the acid media. The first filtration is performed using a polyether sulfone (PES) filter with a pore diameter of 0.23 µm, and the second one a polytetrafluoroethylene (PTFE) membrane filter (Millipore ready-to-use filters in plastic assembly) with a pore diameter of 0.1 µm.

The recovered filtrate is diluted and analyzed with the appropriate methods described in chapter II (UV-Vis spectrophotometry for the $V^{(IV)}$ and potentiometric titration by $Fe^{(II)}$ for the $V^{(V)}$).

The vanadium compounds dissolution occurs according to reactions (Rx.IV.1) and (Rx.IV.2) for $VOSO_4$ and V_2O_5 respectively.

$$VOSO_{4\,(s)} \rightleftharpoons VO^{2+} + SO_4^{2-} \qquad \text{Rx.IV.1}$$

$$V_2O_{5\,(s)} + 2H^+ \rightleftharpoons 2VO_2^+ + H_2O \qquad \text{Rx.IV.2}$$

These reactions were taken into account because the species involved at the chosen concentration of H_2SO_4 (3 M) are in agreement with the E-pH diagram indicated by K.Post et al. [8], and with the $V^{(V)}$ species distribution calculated from constants given by Baes and Mesmer [9].

IV.1.2. Morphology and particle size distribution of the powders

The scanning electron microscope (SEM) used to observe the grains morphology is a PhenomWorld XL SEM. The solid powders (V_2O_5 and $VOSO_4.xH_2O$) were coated with a thin gold layer (using an Emiteck K550X device) prior to SEM observation.

A laser diffraction particle sizing technique, using a Malvern Mastersizer 3000, was used to get the size distribution of the grains. The Malvern Mastersizer is usually used for materials ranging from hundreds of nanometers to several millimeters in size [10]. The particle size is reported as a volume equivalent sphere diameter.

IV.2. Dissolution of vanadium (IV) sulfate

IV.2.1. Characterization of the initial powder

The commercial vanadyl sulfate powder $VOSO_4.xH_2O$ used for the dissolution experiments is partially hydrated. Its water content x was determined by ICP at different concentrations, according to the method of determination of the vanadium concentration in an aqueous solution. The results of three analyses are found to be in the range from 5.4 to 5.6; thus taking into account the uncertainties of the analysis, the retained value of x is 5. Note that this result is in agreement with an octahedral geometry, and also with the fact claimed by J. Selbin [11], the hydrated vanadyl sulfate exists as $[VO(H_2O)_5]^{2+}$, 'the vanadyl ion', in acidic solutions. In the following, $VOSO_4.xH_2O$ is thus indicated as $VOSO_4.5H_2O$.

In Fig.IV.1 are presented the SEM micrographs of the commercial powder. These images display aggregated and multi-shaped particles of all sizes. Their dispersion during the dissolution in a stirred solution is expected to be easy, because of the dislocation occurring after the dissolution of the smallest particles.

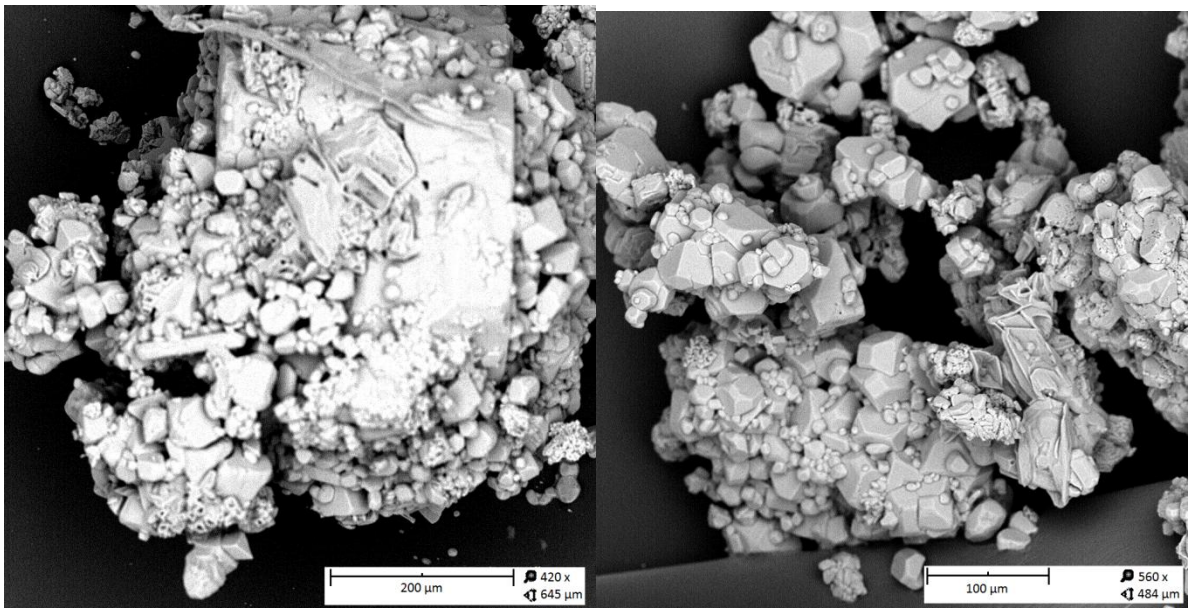

Fig.IV.1: SEM images of the vanadyl sulfate $VOSO_4.5H_2O$ commercial powder; 15 kV-Point; BSD full

The $VOSO_4.5H_2O$ particle size distribution is presented in Fig.IV.2. The first graph (Fig.IV.2-(I)) provides the particle size distribution of the commercial powder and clearly shows two distinct ranges: from 5 to 350 µm and from 350 µm to 4 mm. The commercial powder was sieved at 315 µm and separated into two fractions, for which particle sizes are presented in Fig.IV.2-(II) and Fig.IV.2-(III). They confirm two distinct populations of particle diameter: $d_p <$ 315 µm and $d_p >$ 315 µm.

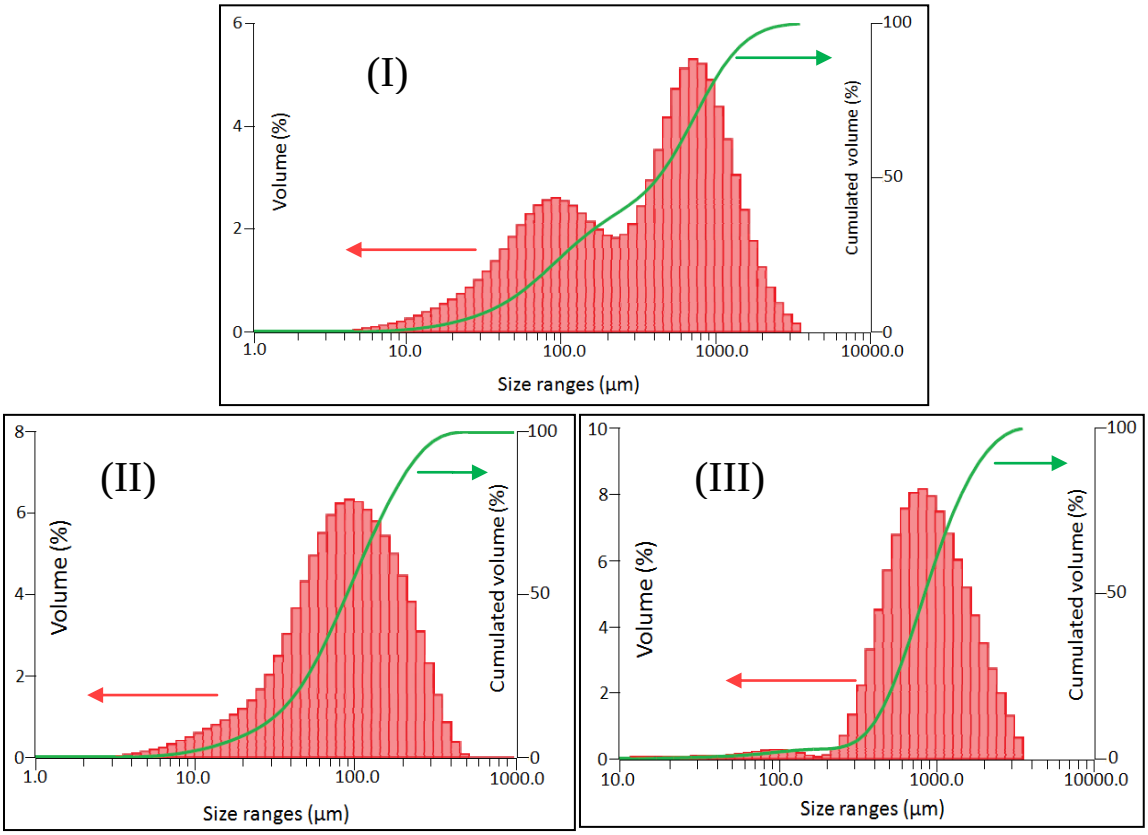

Fig.IV.2: Laser diffraction analysis (P = 3 bar; dry mode) showing the $VOSO_4.5H_2O$ size distribution: (I) commercial powder; (II) sieved powder d_p < 315 µm; (III) sieved powder d_p > 315 µm.

IV.2.2. Temperature dependence of the dissolution kinetics

Fig.IV.3 gathers experimental measurements of the VO^{2+} concentration in the suspension during the dissolution, for temperatures in the range from 5 to 30°C. For all the examined temperatures, a similar temporal evolution of the concentration of VO^{2+} was observed: the concentration increases rapidly at short reaction times (t < 3 min) and then the dissolution slows down until equilibrium is reached, after around 10 minutes. When the temperature increases from 5 to 30°C the initial dissolution rate increases as well.

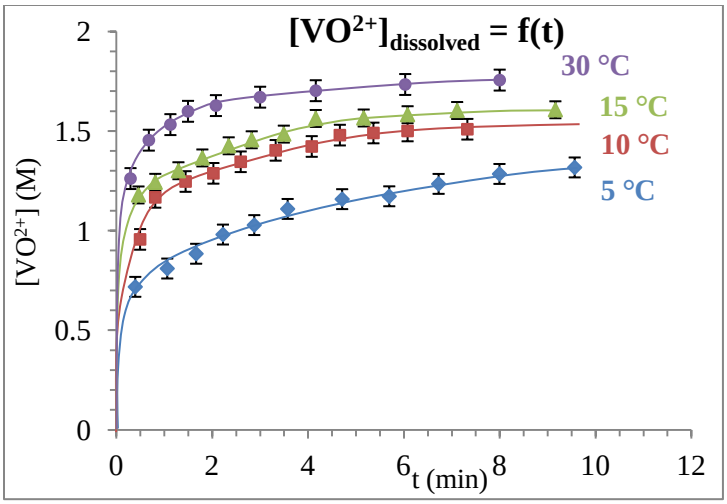

Fig.IV.3: Temporal evolution of the concentration of VO^{2+} released by the dissolution of a $VOSO_4.5H_2O$ commercial powder, for various temperatures; $[H_2SO_4]$ = 3 M; stirring 500 rpm; aliquots filtered by 0.23 and 0.1 µm filters.

The first concentration reported on the graph corresponds to 20 seconds after the introduction of the solid into the stirred solution. For this first measurement, at 5 °C the vanadium concentration reaches 0.7 M and this value doubles (1.3 M) at 30°C.

The concentration of the VO^{2+} measured at 20 s, will be used to determine the initial dissolution rate r° (defined as the ratio $\frac{[VO^{2+}]_{20\,s}}{20\,s}$). Assuming that the kinetic constant of the initial dissolution rate follows the Arrhenius law, Eq.IV.1 gives the initial dissolution rate r°:

$$r° = k \times f = A \times e^{-E_a/RT} \times f \qquad \text{Eq.IV.1}$$

where f is a function of the various operating parameters (activity of the solid vanadyl sulfate, diffusion coefficient of VO^{2+}, size of solid particles…).

Some of these parameters depend on the temperature but here, in order to get a rough order of the magnitude of the activation energy, the experimental data were analyzed (assuming the function f independent of T) and leads to the following linear regression:

$$\ln r°_{\left(\frac{mol}{L.s}\right)} = -\frac{2266.7}{T_{(K)}} + 4.8579 \qquad \text{Eq.IV.2}$$

This relation leads to an approximation of the activation energy of 18.8 kJ/mol for the dissolution of $VOSO_4.5H_2O$ in 3 M sulfuric acid, a value relatively low compared to the activation energy of a classical chemical reaction.

IV.2.3. Effect of stirring rate and particle size on dissolution kinetics

Several dissolution experiments were achieved by applying three stirring rates (500, 100 and 15 rpm), corresponding respectively to i) a well stirred-homogeneous suspension, ii) a minimum stirring rate enabling to uplift the particle and iii) partially decanted solid. Besides, these

experiments were carried out for two different particles size d_p (< 315 µm and > 315 µm). The corresponding time evolution of VO^{2+} concentration is presented in Fig. 4.

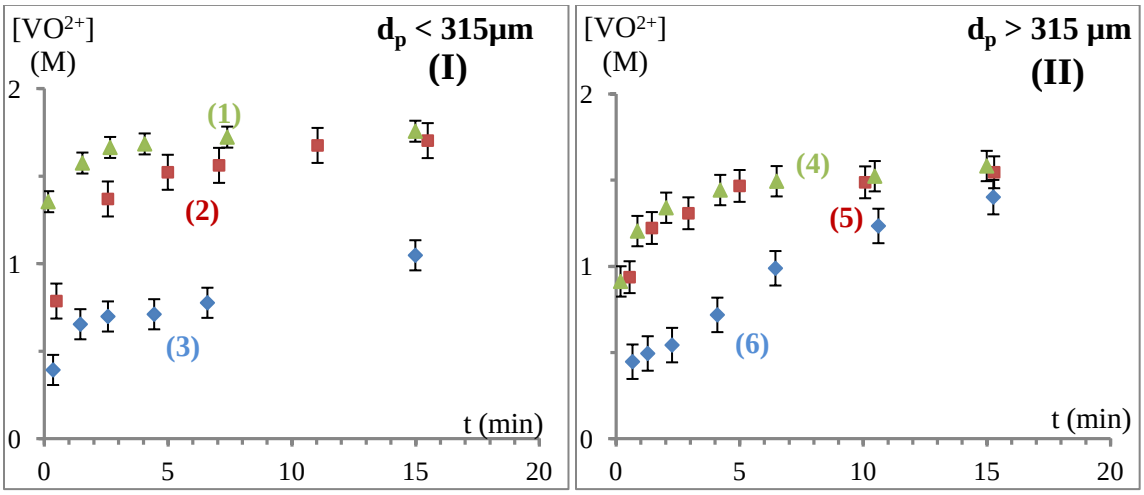

Fig.IV.4: Temporal evolution of the concentration of VO^{2+} released by the dissolution of a $VOSO_4.5H_2O$ commercial powder, for suspensions containing two different particle sizes and subjected to various stirring rates ω; T = 25°C, $[H_2SO_4]$ = 3 M, $VOSO_4.5H_2O$ powder; **(I)**: d_p < 315 µm: ω (in rpm) for (1), (2) and (3) are 500/triangles, 100/squares and 15/diamonds respectively; **(II)**: d_p > 315 µm: ω (in rpm) for (4), (5) and (6) are 500/triangles, 100/squares and 15/diamonds respectively.

For a defined range of particles size (d_p < 315 µm - curves 1-2-3 or d_p > 315 µm - curves 4-5-6, Fig. 4), it appears that a higher stirring rate increases the dissolution kinetics, since higher concentrations are achieved in a shorter time. For instance, $[VO^{2+}]_{(dp<315\ \mu m;\ \omega= 500\ rpm;\ t= 1')}$ = 1.5 M and $[VO^{2+}]_{(dp<315\ \mu m;\ \omega=100\ rpm;\ t= 1')}$ = 1.0 M.
Under constant stirring, the dissolution rate increases by decreasing the particles size. Thus, for a given dissolution time, and before reaching equilibrium, higher salt concentrations were measured with smaller particles. Indeed comparison of curves (1) and (4) obtained in two "well-stirred" suspensions show that the concentration of VO^{2+} after 1 min reaction time increases from ~ 1.2 to ~ 1.5 M when the size decreases from d_p > 315 µm to d_p < 315 µm.

A different shape is obtained for curves (3) and (6), which corresponds to the lowest stirring rate; they exhibit the slowest dissolution rate for both particle sizes. The slow agitation does not enable the motion of the particles which sediment at the bottom of the vessel, forming a 'coagulated' powder paste. Around each grain of this paste, the VO^{2+} concentration reaches rapidly the saturation concentration. These facts are in agreement with a dissolution rate limited by mass transfer. For long reaction time, all the curves tend to converge to the same saturation concentration (~ 1.7 to 1.8 M).

IV.2.4. Equilibrium data

After a certain time of stirring (between 5 and 10 minutes), the solution is saturated and the concentration of VO^{2+} is constant. The equilibrium values are reported in Fig. 5, along with data from M. Skyllas–Kazakos et al. [2] and F. Rahman et al. [12].
A satisfactory agreement is observed between our results and those of previous works, which confirms that the solubility of VO^{2+} increases with temperature. For the highest comparable temperature (30°C), a significant difference of around 20% is observed. This could be attributed to the difficulties encountered in the measurement of a precise volume at this temperature.
The results show that the solubility of VO^{2+} increases with temperature. The equilibrium constant of the $VOSO_4.5H_2O$ dissolution (reaction (3)) can be written as following:

$$K_{(3)} = \left(\frac{a_{VO^{2+}} \times a_{SO_4^{2-}}}{a_{VOSO_4\ solid}}\right)_{at\ the\ equilibrium} \qquad \text{Eq.IV.3}$$

Even if the first dissociation of H_2SO_4 to HSO_4^- is total (high $K_{H_2SO_4/HSO_4^-}$), the second dissociation to SO_4^{2-} remains partial with an equilibrium constant $K_{HSO_4^-/SO_4^{2-}} = 0.013\ at\ 25°C$ (the concentrations are in mol/kg) [13]. However, the released quantity of sulfate ions from HSO_4^- dissociation is not significant compared to the quantity released from the dissolution of $VOSO_4$; this implies that $[VO^{2+}]$ can be assumed equal to $[SO_4^{2-}]$.

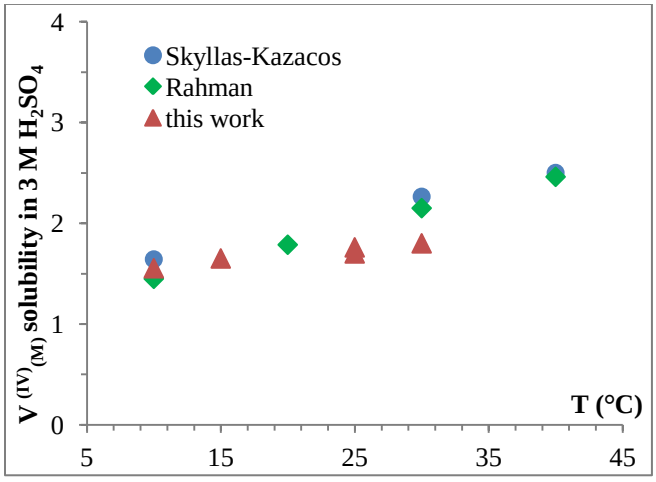

Fig.IV.5: Influence of temperature on the solubility of $V^{(IV)}$. Triangles: this work; circles: M. Skyllas-Kazacos et al. [2]; diamonds: F. Rahman et al. [12]

Concerning the activity of the solid powder of $VOSO_4$, we will assume it equal to 1. Thereby, the above equation can be written as follows:

$$K_{(3)} = \frac{\gamma_{VO^{2+}} \times \gamma_{SO_4^{2-}}}{a_{VOSO_4\ solid}} \times [VO^{2+}] \times [SO_4^{2-}] \Rightarrow K_{(3)} = \lambda \times \left([VO^{2+}]_{at\ equilibrium}\right)^2 \qquad \text{Eq.IV.4}$$

Where $\lambda = \frac{\gamma_{VO^{2+}} \times \gamma_{SO_4^{2-}}}{a_{VOSO_4\ solid}}$.

Because the concentrations of VO^{2+} at saturation are relatively high (1.2 to 1.7 M), the activity coefficients depend on the concentration, while the activity of the vanadyl sulfate solid is equal to 1; in a future work, the Pitzer model will be used in order to express these activity coefficients. Here, in order to get a rough estimation of the sensitivity of vanadyl sulfate solubility against temperature, the logarithm of the VO^{2+} saturation concentration was plotted versus 1/T, assuming λ independent from the concentration of the various species.
The linear regression analysis leads to the following relation:

$$ln\,[VO^{2+}]_{(sat,in\,M)} = -\frac{982.2}{T_{(in\,K)}} + 3.8$$

with a relatively low correlation coefficient (R^2=0.91) with the experimental results, explaining the uncertainties due to the dependence of the activity coefficients on the concentration.
From the slope of the above equation ($-982.2 = k/(2R)$), we deduce the value of k = 16.3 kJ/mol. The obtained value is i) positive showing the endothermic character of the vanadyl sulfate dissolution, and ii) a relatively low value, compatible with the dissociation of an ionic salt weakly bonded.

IV.2.5. Elucidation of the mechanism of the vanadyl sulfate dissolution

The results of this study show that, at constant temperature, the dissolution of vanadyl sulfate in 3 M sulfuric acid is limited by mass transport and that two main parameters (stirring rate and particle size) affect the dissolution rate.
Let us consider the following mechanism for the dissolution of the solid salt $VOSO_4.5H_2O$:

$VOSO_4$ (solid) ⇆ $VOSO_4$ (solvated/dissolved on the surface) Rx.IV.3

$VOSO_4$ (solvated/dissolved on the surface) ⇆ (VO^{2+} + SO_4^{2-}) both species dissociated on the surface Rx.IV.4

VO^{2+} (dissociated on the surface) ⇆ VO^{2+} (bulk) Rx.IV.5

Taking into account the results related to the effect of stirring (§ IV.2.3), the limiting step in the vanadyl sulfate dissolution will be assumed to be the transport of the VO^{2+} from the surface of the particles to the bulk i.e. Rx.IV.5. Besides, in the absence of an electric field, the transport of ions produced in reaction Rx.IV.4 is assumed to occur both by diffusion and by convection.
The mass balance for VO^{2+} in the area between the surface of the particle and the bulk could be written, (using m as the $V^{(IV)}$ molar concentration), as following:
Dissolution flux $_{(3)}$ ≈ dissociation flux $_{(4)}$ ≈ diffusion flux $_{(5)}$ = accumulation of VO^{2+} flux into the bulk

$$\left(\frac{\partial m}{\partial t}\right)_{bulk} = -S \times D \times (grad\ C)_{surface\ of\ particle} \quad \text{Eq.IV.5}$$

(Fick's Ist law)

To simplify, the $VOSO_4.5H_2O$ solid particles are considered spherical and a simple film model around the particle is creating the limitation to mass transfer (i.e. one direction transfer), the previous equation can be simplified as following:

$$\left(\frac{\partial m}{\partial t}\right)_{bulk} = -S \times D \times \left(\frac{\partial C}{\partial R}\right)_{surface\ of\ particle} \Rightarrow$$

$$\left(\frac{\partial m}{\partial t}\right)_{bulk} = -S \times D \times \frac{C_{bulk} - C_{surface}}{(R_{(t)} + e_{(t)}) - R_{(t)}} = S \times k_{(t)} \times (C_{sat} - C_{bulk}) \qquad \text{Eq.IV.6}$$

The effect of the convection was examined on the mass transfer coefficient $k_{(t)}$, using the expression of Ranz and Marshall relative to a forced convection around a solid sphere [14] (also known as the Leveque correlation providing the Sherwood number).

$$Sh = Sherwood\ number = \frac{k_{(t)} \times d_p}{D} = 2 + a \times Re^{1/2} \times Sc^{1/3} \qquad \text{Eq.IV.7}$$

This correlation is appropriated for spherical particles having the same size. In order to improve its applicability on the present case, some assumptions will be considered:

- The calculations will be achieved assuming the presence of four separated size ranges of the solid particles having an initial radius R° = 20, 40, 500 and 1000 µm representing respectively 20%, 35%, 35% and 10% of the total solid volume (see curve of Fig.IV.2-(I), cumulated volume);
- All the particles of the powder will be assumed spherical, despite the various shapes observed (Fig.IV.1). Considering Eq.IV.7, the constant "a" is generally assumed equal to 0.6. However, in the present study and because of the large size distribution, "a" will be taken as an adjusting factor, which effect will be examined.

The molar quantity of the dissolved VO^{2+} "m" for N particles of initial radius R° can be expressed as:

$$m = \frac{\rho \times V}{M} = N \times V_{one\ particle} \times \frac{\rho}{M} = N \times \frac{4}{3}\pi \times (R^{\circ 3} - {R_{(t)}}^3) \times \frac{\rho}{M} \qquad \text{Eq.IV.8}$$

(Refer to notation and symbols)

The concentration of VO2+ in solution can be written as $C_{bulk} = \frac{m}{V_l}$; V_l being the total volume of the suspension (including both the liquid and the solid).

Combining Eq.IV.6, Eq.IV.7 and Eq.IV.8 leads to Eq.IV.9 describing the variation of the radius R of the solid particles as a function of time, and representing the dissolution rate r of the vanadyl sulfate:

$$r \Rightarrow \frac{dR}{dt} = \frac{A_1 - A_2(R^{\circ 3} - {R_{(t)}}^3) + A_3\sqrt{R_{(t)}} - A_4(R^{\circ 3} - {R_{(t)}}^3)\sqrt{R_{(t)}}}{-R_{(t)}} \qquad \text{Eq.IV.9}$$

Where A_1 to A_4 are constants (refer to **Appendix X12** for their developed expressions).

Eq.IV.9, written as $r \Rightarrow \frac{dR}{dt} = f(R)$, is solved numerically using the Euler method ($R_{j+1} = R_j + step \times f(R,t)$) and enables to calculate a theoretical radius at time t, given that at t° = 0, R = R°.

Note that the step used is: $\frac{reaction\ time}{number\ of\ iterations\ j} = \frac{10}{100} = 0.1\ min$

The value of the radius R of a certain particle of $VOSO_4.5H_2O$, obtained at a certain time t, from the resolution of Eq.IV.9 enables to obtain the theoretical values of the dissolved quantity of VO^{2+} i.e. the moles number, using Eq.IV.8.

Note that Eq.IV.9 is resolved 4 times, each for one of the chosen initial R° (20, 40, 500 and 1000 µm) of the solid particles and the total concentration of the dissolved vanadium sulfate (VO^{2+}) in solution is deduced (sum of the four obtained values of molar quantity divided by V_l). Also, for each R°, a different value of the adjusting factor "a" (Eq.IV.7) was determined.
Fig.IV.6 shows two examples of the iterative determination, at 30°C, of the optimal value of two parameters (the constant "a" in the Leveque equation and the percentage of each particle size range which directly affects the number of total particles N of each R°). The optimized value of "a" or "N", is the one leading to a curve of the concentration of the dissolved vanadium sulfate which fits best with the experimental data curve.

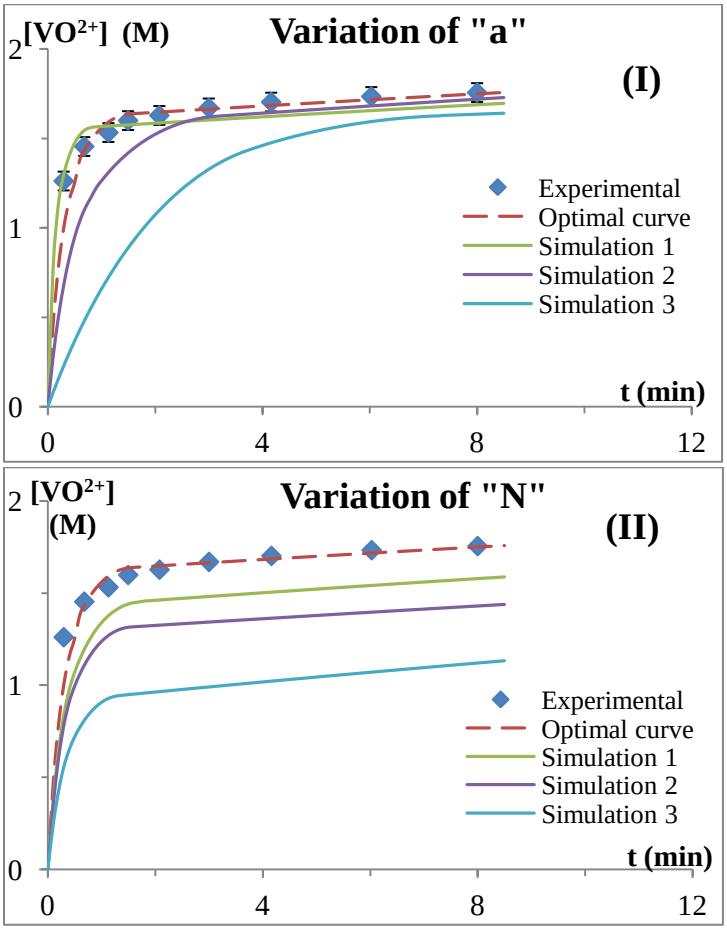

Fig.IV.6: Temporal evolution of the concentration of VO^{2+} released by the dissolution of the $VOSO_4.5H_2O$ commercial powder: dots=experimental curve; Continuous lines=simulated curves obtained with the non optimized parameter value, i.e. the constant "a" in the Leveque equation (figure **(I)**), and the percentage of each particle size range which directly affects the number of total particles "N" of each R° (figure **(II)**); Broken lines=simulated curves obtained with the optimized parameters of "a" (figure **(I)**), and "N" (figure **(II)**).

Following this iterative mode enables to evaluate the calculated curves at each temperature and the results are presented in Fig.IV.7 comparatively to the experimental data. Note that the viscosity was calculated for each temperature [15], while the value of the diffusivity at 25°C [16] was used for all the examined temperatures.

A relatively good agreement ($\frac{\Delta C}{C} = \pm$ 0.1M/~ 1.5M) is observed between the results of the model and the experimental ones. Discrepancies are observed for short durations of the dissolution (t < 1 min) because of the difficulty to standardize rapidly the suspension and to achieve precise measurement at the first few seconds after the stirring begins.

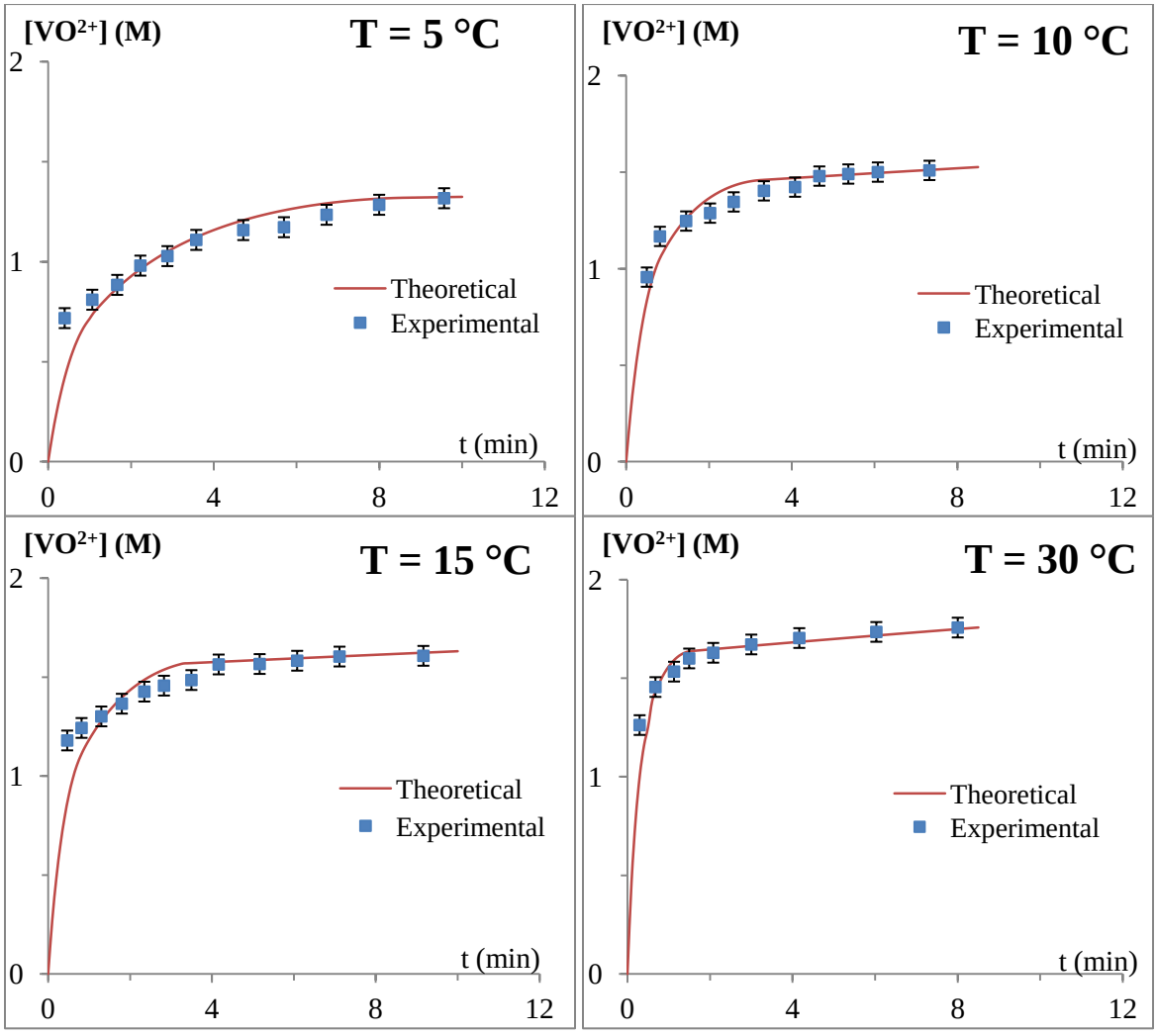

Fig.IV.7: Comparison between the experimental data (reported from Fig.IV.3) and the model (calculated using Eq.IV.9) of the temporal evolution of the concentration of VO^{2+} released by the dissolution of a $VOSO_4.5H_2O$ commercial powder, at various temperatures.

Another difficulty comes from the dissolution of the smallest particles, which exhibit fast kinetics. In fact, compared to the bigger particles, this introduces additional uncertainties because the number of small particles of powder was not exactly taken into account.

To sum up, the obtained results lead to the following conclusions:

- Regarding the effect of temperature: the initial dissolution rate increases with temperature. The solubility of the vanadyl sulfate at saturation (when the equilibrium of dissolution is reached) increases slightly with the temperature in the examined range of 5 to 30 °C, and this is compatible with the dissociation of an ionic salt weakly bonded.
- Both the stirring of the suspension and the size of the particles strongly affect the dissolution rate (mainly for dissolution times lower than 5 min), proving that the dissolution kinetics of the vanadyl sulfate (to VO^{2+}), is limited by the mass transfer of VO^{2+} from the solid powder surface to the bulk, while the chemical reaction with the proton is not limiting.

IV.3. Dissolution of vanadium pentoxide

IV.3.1. Characterization of the initial powder

The commercial powder of V_2O_5 was characterized by SEM and laser diffraction particle sizing technique. The SEM micrograph in Fig. 8-1 shows that the V_2O_5 particles form agglomerated sticks of various sizes. The size distribution (Fig. 8-2) shows a large dispersion of particle size from 120 nm to 4 mm.

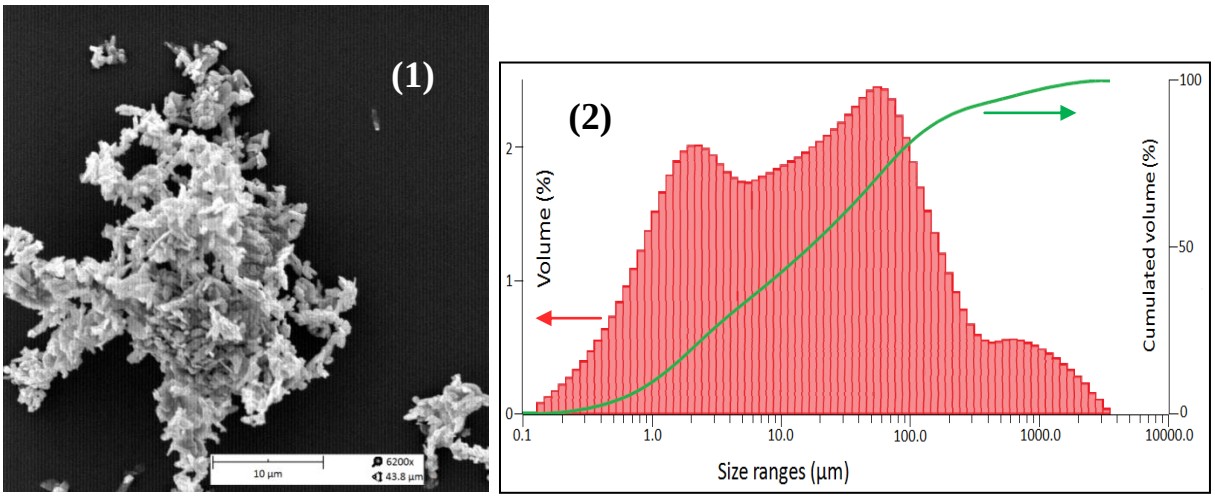

Fig.IV.8: (1) SEM pictures (10kV-Point; SED) and (2) size distribution obtained (by laser diffraction sizing technique; P = 3 bar, dry mode) of the vanadium pentoxide V_2O_5 commercial powder.

The graph exhibits three peaks located respectively at 2, 80 and 900 µm; therefore, in order to study the effect of particles size on the dissolution kinetic, the initial powder was sieved using four different cut off threshold sieves: 315 µm; 200 µm; 120 µm and 80 µm. Thus, five different

diameter ranges of powder were obtained: $d_p > 315\mu m$; $315 > d_{p\ (\mu m)} > 200$; $200 > d_{p\ (\mu m)} > 120$; $120 > d_{p\ (\mu m)} > 80$ and $d_{p\ (\mu m)} < 80$, three of which were used to carry out dissolution experiments.

IV.3.2. Effect of temperature on dissolution kinetics

The effect of temperature on the dissolution of vanadium pentoxide was studied in the range 0 to 40°C and the temporal evolution of the dissolved VO_2^+ concentration is presented in Fig.IV.9.

The behavior is rather similar for each temperature: a rapid dissolution occurs at "short" reaction times (less than 1 h) and then the concentration tends to reach a constant value. Note that, for all the examined temperatures (except 0°C), the dissolution equilibria of the vanadium pentoxide to VO_2^+ is achieved after 5 h of stirring; for the dissolution at 0 °C a higher reaction time is required to reach the saturation.

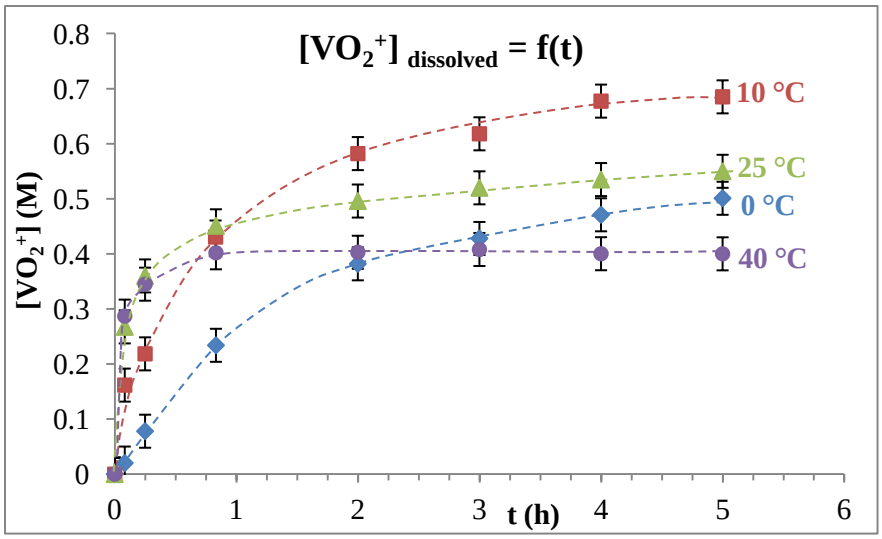

Fig.IV.9: Temporal evolutions of the concentration of the VO_2^+ (released by the dissolution of a V_2O_5 commercial powder), at various temperatures; $[H_2SO_4] = 3$ M; stirring 500 rpm.

Several differences can be observed compared to the dissolution features of $VOSO_4$:

- The saturation concentrations ($C_{sat.}$) of VO_2^+ are about three times lower than those of the VO^{2+}; in addition, the C_{sat} decreases when the temperature increases (contrary to the case of the $V^{(IV)}$, where C_{sat} increases with T). This point will be analyzed in the next section.
- For the stronger stirring (500 rpm), the time required to dissolve the oxide and to reach the saturation concentration of VO_2^+ is more than fifty times higher than that required for the VO^{2+}. Typical comparative values are 5 min to reach a concentration of VO^{2+} of 1.5 M, while 3 h were required to reach a concentration of VO_2^+ of 0.5 M. Moreover, at 40°C, the saturation concentration of VO_2^+ is reached for $t < 20$ min, while at 0°C the solution is not saturated, even after 5 h. Another experiment was carried out at 0°C where the suspension of vanadium pentoxide was left under stirring for one day. The concentration of the dissolved VO_2^+ was determined and the following values were obtained: $[VO_2^+]_{23\ h} = 0.788$ M and

$[VO_2^+]_{25\ h}$ = 0.783M. This last result tends to show that the mass transport is not the limiting step.

The concentration of the VO_2^+ measured for reaction times lower than five minutes (named $t_{initial}$), will be used to estimate approximatively the initial rate of the V_2O_5 dissolution r° (defined as the ratio $\frac{[VO_2^+]_{t_{initial}}}{t_{initial}}$).

Assuming, as for the vanadyl sulfate, that i) the kinetic constant of the initial dissolution rate follows the Arrhenius law, and ii) the other terms of the expression of the dissolution rate are independent of the temperature, then, the logarithmic analysis of the evolution of the initial rate with the temperature leads to the following correlation:

$$\ln r^{\circ}_{(r^{\circ}\ in\ \frac{mol}{L.s})} = 22.7 - \frac{8727.3}{T_{(in\ K)}} \qquad \text{Eq.IV.10}$$

The slope of this linear relation enables the determination of a roughly estimated value of the activation energy of the dissolution process: $E_a = 73\ kJ/mol$.

This energy is more than four times higher than the value obtained for the dissolution of $VOSO_4$ (18.8 kJ/mol). This could be explained by the fact that the hydration of the vanadium pentoxide (V_2O_5 which exhibits covalent bonds) followed by its reaction with H^+ ions is energetically more difficult to achieve, comparatively to the simple dissociation of the ionic salt $VOSO_4$.

IV.3.3. Effect of available surface area on dissolution kinetics

The effect of the particle size on the dissolution rate of V_2O_5 was examined at 40°C and 500 rpm stirring rate and the results are shown in Fig.IV.10.

Practically the same concentrations were measured for the three different size ranges of the solid particles ($80 < d_p < 120$ µm, $120 < d_p < 200$ µm and $200 < d_p < 315$ µm). These results tend to show that the dissolution rate does not depend on the solid/liquid exchange surface. Theoretically, the particle size affects the initial rate of the dissolution that should increase. However, in our case, owing to the low values of these dissolution rates, the curves do not have enough resolution to show any difference. Moreover, these results support our previous conclusion: the mass transfer does not represent a limitation to the dissolution of V_2O_5 but it is rather the chemistry of the system.

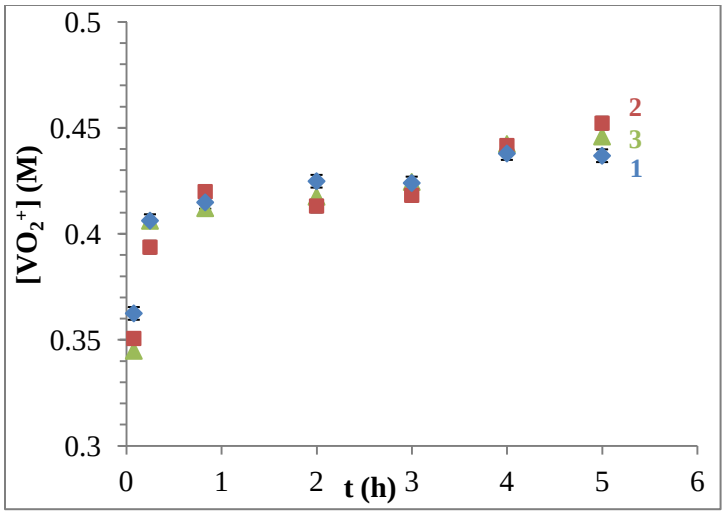

Fig.IV.10: Temporal evolutions of the dissolved VO_2^+ concentration (released by the dissolution of a V_2O_5 commercial powder) for various initial sizes of the solid particles of V_2O_5 obtained by sieving; $[H_2SO_4]$ = 3 M, stirring 500 rpm, sieved V_2O_5 powder, T = 40°C. (1) 80 < d_p < 120 µm; (2) 120 < d_p < 200 µm; (3) 200 < d_p < 315 µm.

Consequently, the effect of stirring on the dissolution was not studied.
Since the dissolution is not significantly affected by the particles size, the possibility of kinetic control by surface passivation was evaluated.

A simplified reaction scheme is proposed below for the vanadium pentoxide dissolution (Rx.IV.2):

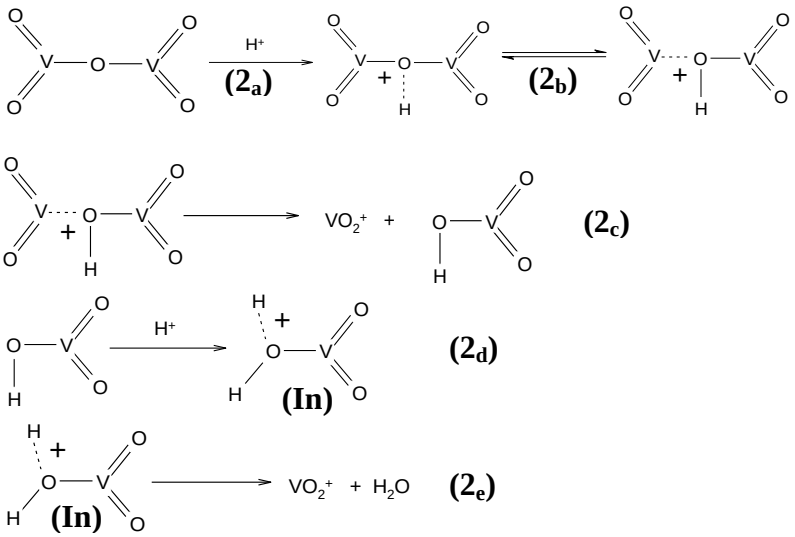

Hydrogen ion attacks the oxide and the product obtained from reaction (**2$_b$**) decomposes according to reaction (**2$_c$**); then by reaction with H^+, it forms an intermediate (In) which dehydrates to lead to VO_2^+.

However, another reaction pursue of the intermediate (**In**) could be its polymerization according to various reactions and in the last case, the external surface of each solid particle could be entirely covered by a passive layer that prevents the dissolution and could be the reason for which the observed saturation concentration of VO_2^+ remains low.

To clarify this point, the following dissolution experiment was carried out: a solid-liquid suspension of the commercial V_2O_5 sieved powder ($200 < d_p < 315$ µm) was introduced into a H_2SO_4 3 M solution at 25 °C and stirred during 5 h. The results are illustrated in Fig.IV.11: the $[VO_2^+]$ increases to reach the saturation concentration (~ 0.55 M after t ~ 1h) then remains constant. Then the suspension was filtered to remove the residual solid and a fresh sample of the powder was added into the filtrate. The dissolution experiment was pursued for 6 h, and the temporal evolution of the concentration of the vanadium is indicated into Fig.IV.11 (for t > 22 h until t = 28 h). The renewal of the solid does not change the dissolved amount of vanadium, implying that the equilibrium was reached and no further dissolution can be achieved. This test confirms that there is no passivating or inhibiting layer formed on the surface of the particles.

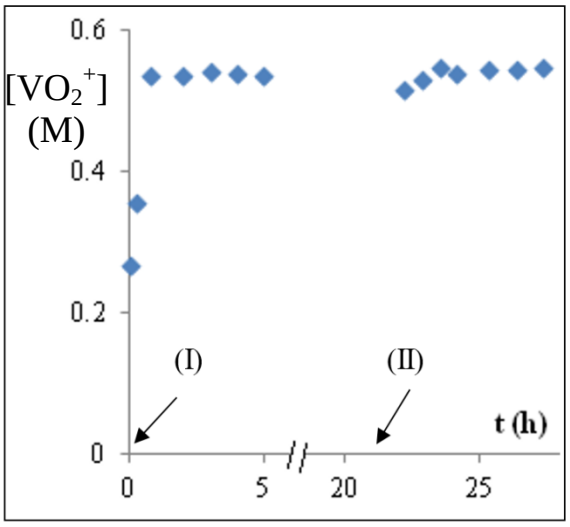

Fig.IV.11: Temporal evolution of the VO_2^+ concentration (released by the dissolution of a V_2O_5 commercial powder) for two different additions of solid samples of V_2O_5 into the liquid; 15 cm^3 of $[H_2SO_4]$ = 3M, stirring 500 rpm, T = 25 °C, sieved V_2O_5 powder ($200 < d_p < 315$ µm). (I) first introduction of 2.2 g of V_2O_5; (II) filtration and second introduction of 2.2 g of V_2O_5.

IV.3.4. Equilibrium data

The saturation concentration of VO_2^+, obtained for t > 5 h (extracted from Fig.IV.9), are reported in Fig.IV.12, simultaneously with the values from M. Skyllas–Kazacos et al. [2]. Note that the values extracted from the bibliography were multiplied by 2 in order to obtain the concentration of VO_2^+, instead of the solubility of V_2O_5 used in the cited reference. The saturation concentration of VO_2^+ decreases when the applied temperature increases, even if a shorter time is required to reach the equilibrium.

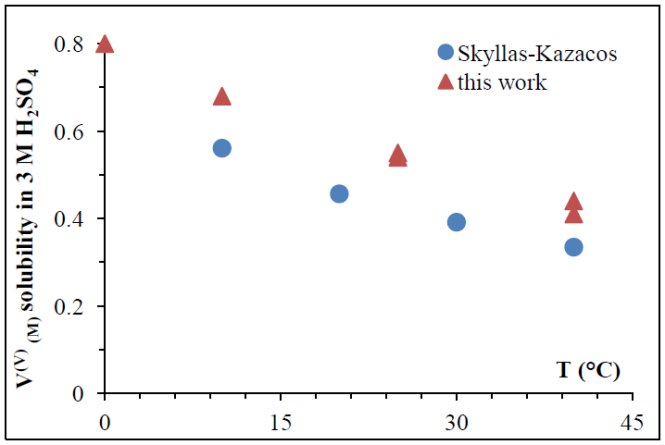

Fig.IV.12: Influence of temperature on the solubility of $V^{(V)}$. Triangles: this work; disks: M. Skyllas-Kazacos et al. [2].

The equilibrium constant of reaction (Rx.IV.2) can be written as a function of the activities of the species in solution:

$$K_{(5)} = \frac{\left(a_{VO_2^+}\right)^2 \times a_{H_2O}}{a_{V_2O_5\ solid} \times \left(a_{H^+}\right)^2} = \frac{a_{H_2O} \times \left(\gamma_{VO_2^+}\right)^2}{a_{V_2O_5\ solid} \times \left(\gamma_{H^+}\right)^2} \times \left(\frac{[VO_2^+]}{[H^+]^\circ - [VO_2^+]}\right)^2 \qquad \text{Eq.IV.11}$$

$$\text{where } \xi \text{ is assumed to be constant } \xi = \frac{a_{H_2O} \times \left(\gamma_{VO_2^+}\right)^2}{a_{V_2O_5\ solid} \times \left(\gamma_{H^+}\right)^2}$$

In the present case, the concentrations of the VO_2^+ at saturation are lower than the values obtained for VO^{2+} at saturation (Fig.IV.9: 0.4 to 0.7 M for stirring duration of 5 h). The effect of the concentration on the activity coefficient will also be examined in a future work via the Pitzer model.

For the time being, in order to get a preliminary rough estimation of the sensitivity of the vanadium pentoxide solubility against the temperature, the term $\frac{a_{H_2O} \times \left(\gamma_{VO_2^+}\right)^2}{a_{V_2O_5\ solid} \times \left(\gamma_{H^+}\right)^2}$ will be considered constant and named $\boldsymbol{\xi}$. Then a logarithmic analysis of the data at the equilibrium (Fig. 9) versus the reverse temperature was performed according to the following equation:

$$\ln\left(\frac{[VO_2^+]_{sat}}{[H^+]^\circ - [VO_2^+]_{sat}}\right) = 0.5 \times (constant - ln\xi) - \frac{k'}{2R} \times \frac{1}{T} \qquad \text{Eq.IV.12}$$

The linear regression analysis of the experimental results leads to the following equation $\ln\left(\frac{[VO_2^+]_{sat}}{[H^+]^\circ - [VO_2^+]_{sat}}\right) = -9.15 + \frac{2272}{T}$ with a correlation coefficient with the experimental results of R^2=0.9997, a satisfactory value taking into account the uncertainties on the dependence of the activity coefficient to the concentration.

The slope of the above equation ($+2272 = k'/(2R)$), enables to deduce k'= -37.8 kJ/mol, a negative value; it could be attributed, very approximately, to the changes in the enthalpy of the reaction between H^+ and V_2O_5 which appears to be an exothermic process. This is also confirmed by the bibliography and particularly the studies of F. Rahman et al. [5] which claims that the reaction (-Rx.IV.2) is an endothermic reaction. Note that, the obtained negative value is in agreement with the effect of temperature on the saturation concentration: the saturation concentration of VO_2^+ decreases when the temperature of the stirred suspension increases.
Besides comparison of k for the vanadyl sulfate (+16.3 kJ/mol) and k' for the vanadium pentoxide (-37.8kJ/mol) enables to conclude that the dissolution of both vanadium compounds follows different schemes: the process is endothermic for the dissolution of $VOSO_4$ and exothermic and more 'difficult' for the breaking of the oxide bonds (V-O bond have a more covalent character than bond VO-SO_4 bond).

IV.3.5. Kinetic model of the dissolution

The comparison of the dissolution of both $VOSO_4$ and V_2O_5 leads to the following conclusions:
- The time required to saturate the solution with VO_2^+ is in the order of "some hours" compared to a time in the order of some minutes for VO^{2+}, especially for 'low' temperature (0°C). Moreover, the saturation concentration of the VO_2^+ is, as function of T, much lower than the saturation concentration of VO^{2+};

- Taking into account the fact that 5 h were required to saturate the $V^{(V)}$ solution, it can be concluded that the mass transfer is not a limiting factor of the oxide dissolution. Besides, it was shown that the observed limitation in the V_2O_5 dissolution does not come from the physical properties of the powder, nor from an eventual secondary reaction taking place on the particles' surface and blocking the main dissolution (§ IV.3.3).

Therefore, the dissolution of the $V^{(V)}$ will be assumed to be limited by the chemistry of Rx.IV.2, assumed to be a slow equilibrium, of which the global rate can be expressed by the Eq.IV.13.

$$V_2O_{5\,(s)} + 2\ H^+ \underset{k_{(-2)}}{\overset{k_{(2)}}{\rightleftharpoons}} 2\ VO_2^+ + H_2O \qquad \text{Rx.IV.2}$$

$$r_{(2)} = +\frac{1}{2}\frac{d[VO_2^+]}{dt} = k_{(2)} \times \left(\frac{N_\sigma}{N_a}\right)^\alpha \times \left(\frac{moles\ of\ H^+}{V_{suspension}}\right)^\beta - k_{(-2)} \times \left(\frac{moles\ of\ VO_2^+}{V_{suspension}}\right)^\gamma \quad \text{Eq.IV.13}$$

(Refer to **appendix X13** for the detailed development of Eq.IV.13)

Thus, for particles 'i' having, at the time t: - S_i as surface
- $N_{\sigma i}$ sites on their surface, and
- releasing by dissolution $2(X)_{S_i} moles\ of\ VO_2^+$

the dissolution rate Eq.IV.13 can be expressed as following:

$$r_{(2)\,S_i} = +\frac{1}{2}\frac{d[VO_2^+]_{S_i}}{dt} = \frac{1}{2}\frac{d\,(2X)_{S_i}}{V_{suspension}\,dt} = \frac{d(X)_{S_i}}{V_{suspension}\,dt} = k_{(2)} \times (\frac{N_{\sigma i}}{N_a})^{\alpha} \times \frac{\left\{n°_H - 2\times(X)_{S_i}\right\}^{\beta}}{V_{suspension}^{\beta}} - k_{(-2)}\frac{\left\{2\times(X)_{S_i}\right\}^{\gamma}}{V_{suspension}^{\gamma}}$$

Eq.IV.14

The same equation will be written three times, because for the calculation, three particle surfaces *S_1, S_2 and S_3* are considered relatively to three particle diameters: 10, 60 and 1000 µm according to the Fig.IV.8-2.

Then the resolution of each equation will provide the released moles number $(2X)_{S_i}$of VO_2^+, and in order to determine the global released moles number of VO_2^+, it is necessary to sum the four individual moles numbers, i.e. $(2X)_{global} = (2X)_{S_1} + (2X)_{S_2} + (2X)_{S_3}$.

On the other hand, the expression of N_σ, considered to be the number of available V_2O_5 sites, as a function of the particle radius R_i and the vanadium initial concentration can be written as:

$$N_{\sigma i} = \frac{N_i}{\sigma°} \times \left(\frac{3\,(4\pi)^{0.5}\,M}{\rho}\right)^{2/3} \times \left(n°_V - X_{R_i}\right)^{2/3}$$

Substituting it in Eq.IV.14 and considering the reaction orders with respect to V_2O_5, H^+ and VO_2^+, to be equal to their stoichiometric coefficients, the expression of global rate of the reaction is:

$$r_{(2)\,S_i} = \frac{d(X)_{S_i}}{dt} = k_{(2)} \times \frac{N_i}{N_a \times \sigma°} \times \left(\frac{3\,(4\pi)^{0.5}\,M}{\rho}\right)^{2/3} \times \left(n°_V - X_{R_i}\right)^{2/3} \times \frac{\left\{n°_H - 2\times(X)_{S_i}\right\}^2}{V_{suspension}} - k_{(-2)}\frac{\left\{2\times(X)_{S_i}\right\}^2}{V_{suspension}}$$

Eq.IV.15

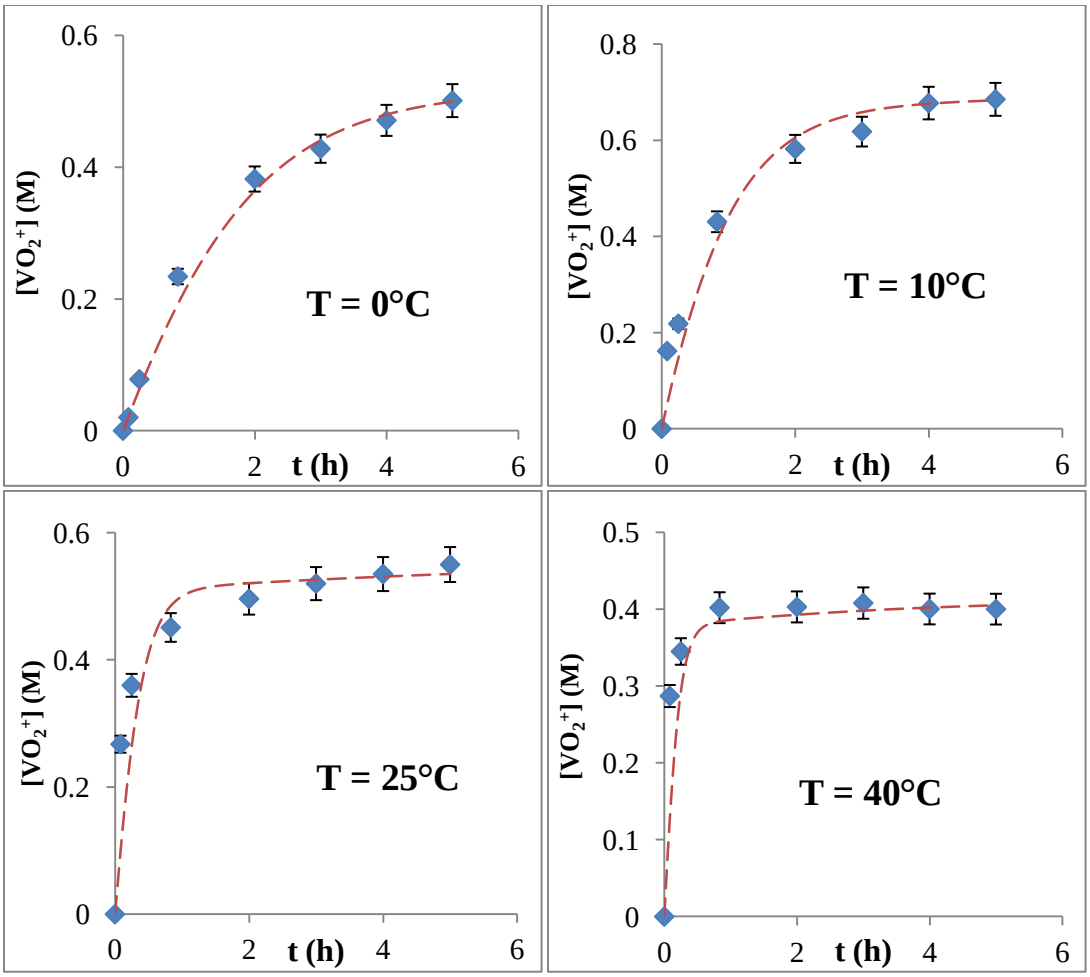

Fig.IV.13: Comparison between the experimental data (diamonds, imported from Fig.IV.9) and the model (dashed lines, calculated using Eq.IV.15) for the temporal evolution of the concentration of VO_2^+ released by the dissolution of a V_2O_5 commercial powder, at various temperatures.

Eq.IV.15, solved numerically using the Euler method, provides the variation of the quantity of VO_2^+ as a function of time. The only unknown parameters are $k_{(2)}$ and $k_{(-2)}$, the kinetic constants of the forward and backward reaction. They will be adjusted in order to determine the theoretical evolution of the VO_2^+ concentration which correctly correlates with the experimental one.

Fig.IV.13 shows the correlation between the calculated values of dissolved VO_2^+ (dashed lines) and the experimental data (diamonds). The values of the kinetic constants, enabling to get a satisfactory agreement between theory and experiment, are indicated in table IV.1.
The results show that the backward kinetic constant $k_{(-2)}$ is more sensitive to the temperature than the forward $k_{(2)}$. Besides, for all the examined temperatures, $k_{(-2)}$ is higher than the $k_{(2)}$. This means that the dissolution of the oxide is allowed only for 'relatively' low concentrations of VO_2^+, enabling to keep the term of the backward rate lower than this of the forward rate.

Note also that, because the order against the H^+ concentration (in the forward term of the rate) is equal to 2, the acidic media is beneficial to the dissolution of the oxide and this is also in agreement with the results of Rahman et al. [5].

Table IV.1: Iteratively estimated values of the kinetic constants $k_{(2)}$ and $k_{(-2)}$ for the studied temperatures, and their corresponding activation energies (estimations).

Temperature (°C)	$k_{(5)}$ ($mol^{-2}.s^{-1}.L.g$)	$k_{(-5)}$ ($mol^{-1}.s^{-1}.L$)
0	0.9×10^{-4}	2.3×10^{-4}
10	2.6×10^{-4}	3.4×10^{-4}
25	4.8×10^{-4}	13×10^{-4}
40	7×10^{-4}	41×10^{-4}
Activation energy (estimated by $k = Ae^{-Ea/RT}$)	$E_{a(5)}$ = 34.5 kJ/mol	$E_{a(-5)}$ = 52.9 kJ/mol

IV.4. Conclusion

Numerous works exist in the field of the vanadium battery and one important objective is to avoid the vanadium pentoxide precipitation, because its dissolution seems difficult. In addition, the published studies do not exhibit the determination of the physical limitations and phenomena to be overcomed, in order to act upstream during the functioning of the VRFB. The aim of the present chapter was the study of the dissolution mechanisms of the vanadyl sulfate $VOSO_4$ and vanadium pentoxide V_2O_5 in 3 M sulfuric acid, under various operative conditions, and also to bring knowledge on the understanding of the phenomena governing these dissolutions.
Several experimental data giving the temporal evolution of the dissolved vanadium concentrations versus various operating parameters were acquired and supplied. Moreover, kinetic laws describing both dissolution limitations phenomena were determined and explained. As expected these compounds exhibit different behaviors towards dissolution. The general results show that the dissolution of $VOSO_4.5H_2O$, an 'ionic salt', appears to be easier and more rapid, comparatively to that of the V_2O_5 oxide (which is covalently bonded).

Their initial dissolution rate increases with temperature, for both compounds $VOSO_4$ and V_2O_5, and the rough estimations of the activation energies at the beginning of the dissolution (18.8 kJ/mol for $VOSO_4$ and 73 kJ/mol for V_2O_5) clearly show that the temperature influence two different phenomena: the mass transport for the vanadyl sulfate, and the reaction with the proton for the vanadium pentoxide.

The saturation concentration of the VO^{2+} is reached after few minutes of stirring (< 10 min), while several hours (> 5 h) were required for the VO_2^+ released by the oxide V_2O_5 to reach saturation (and more than 1 day at 0 °C). In addition the solubility of the $V^{(IV)}$ salt is higher than

the solubility of the oxide (at least two times, even three for certain temperatures): VO^{2+}concentrations of 2 M can be achieved from the dissolution of $VOSO_4$ at T ≥ 30°C, while for the oxide dissolution the VO_2^+ saturation concentration reaches ~ 0.45 M at 40°C.

Moreover, conversely to the $V^{(IV)}$, in the case of vanadium pentoxide decreasing the temperature causes the saturation concentration of VO_2^+ to increase: from 0.42 to 0.78 M respectively at 40 and 0°C, and the whole dissolution process appears to be exothermic (k' = - 37.8 kJ/mol).

Concerning the kinetic models, the dissolution of $VOSO_4$ consists of the dissociation in the acid media, followed by its dispersion in the bulk. The whole process is limited by mass transport (more specifically diffusion and convection). The accumulation flux of VO^{2+} was expressed using Fick's Ist law and the Sherwood correlation and the simulated results enable to reproduce experimental measurements and to validate the mass transport limitation. For V_2O_5, the dissolution rate appears to be limited by a chemical reaction (acidic attack followed by the breaking bonds). A simple reaction scheme was proposed for the dissolution and its rate was expressed assuming the chemical reaction as an elementary reaction. The model agrees with the experimental data and the resulting kinetic constants show a backward reaction (-5) more sensitive to temperature and having a rate in certain conditions higher than the rate of the forward reaction (5).
Note that the obtained results were very sensitive to the sulfuric acid concentration which changes during the battery operation (increases during the charge and decreases during the discharge). The 3 M of sulfuric acid was chosen as a compromise between its positive effect on the dissolution of the vanadium pentoxide and its negative effect on the dissolution of vanadium sulfate.
To sum up, in the absence of chemical additives enabling to keep the $V^{(V)}$ under dissolved form and avoid precipitation of the vanadium pentoxide, it is required to operate in strong acidic conditions, with a "discharged battery" instead of a "battery completely charged". Moreover, a charged vanadium battery will exhibit a more stable behavior if stored in low (T < 20°C) temperature conditions, rather than in high temperature conditions (T > 40°C).

As for the behavior of the solid particles used in excess for the present work in the VRFB posolyte, it appears that the $VOSO_4$ would be expected to dissolve fast (on the scale of t < 5 min) when its concentration in solution drops to a value lower than the solubility, which is a positive input for the upcoming studies. As for the $V^{(V)}$, it would be preferable to maintain it under dissolved form given its low dissolution kinetics and solubility; however, this was discussed previously (chapters I and III) and it was found that concentrated solutions of VO_2^+ (up to 5 M) can remain stable in concentrated sulfuric acid (~ 7 M total sulfate) which would help overcome the dissolution problem of the oxide.

References:

[1] C. Choi, S. Kim, R. Kim, Y. Choi, S. Kim, H. Jung, J.H. Yang, H.T. Kim, "A review of vanadium electrolytes for vanadium redox flow batteries", Renewable and Sustainable Energy Reviews, 69, 2017, 263–274, doi: 10.1016/j.rser.2016.11.188.

[2] M. Skyllas-Kazacos, L. Cao, M. Kazacos, N. Kausar, A. Mousa, "Vanadium Electrolyte Studies for the Vanadium Redox Battery-A Review", 9(13), 2016 1521–1543, doi: 10.1002/cssc.201600102.

[3] L. Li, S. Kim, W. Wang, M. Vijayakumar, Z. Nie, B. Cheng, J. Zhang, G. Xia, J. Hu, G. Graff, J. Liu, Z.Yang, " A Stable Vanadium Redox Flow Battery with High Energy Density for Large Scale Energy Storage", Advanced Energy Materials, 1, 2011, 394-400, doi: 10.1002/aenm.201100008

[4] F. Rahman, "Stability and properties of supersaturated vanadium electrolytes for high energy density vanadium redox battery", PhD Thesis, University of New South Wales, Australia, 1998

[5] F. Rahman, M. Skyllas-Kazacos, "Vanadium redox battery: Positive half-cell electrolyte studies", J. Power Sources, 189(2), 2009, 1212-1219, doi: 10.1016/j.jpowsour.2008.12.113

[6] M. Vijayakumar, L. Li, G. Graff, J. Liu, H. Zhang, Z. Yang, J.Z. Hu, "Towards understanding the poor thermal stability of V5+ electrolyte solution in Vanadium Redox Flow Batteries", J. Power Sources, 196, 2011, 3669-3672, doi: 10.1016/j.jpowsour.2010.11.126

[7] N. Kausar, "Studies of V(IV) and V(V) species in vanadium cell electrolyte", University of New South Wales, Australia, 2002

[8] K. Post, R.G. Robins, "Thermodynamic diagrams for the vanadium-water system at 298.15K", Electrochimica Acta, 21(6), 1976, 401-405, doi: 10.1016/0013-4686(76)85115-8.

[9] C.F. Baes, R.S. Mesmer, "The hydrolysis of cations", Wiley, New York, 1976; ISBN: 0471039853.

[10] Q. Fu, W. Sun, "Mie theory for light scattering by a spherical particle in an absorbing medium", Appl. Opt., 40(9), 2001, 1354-1361, doi: 10.1364/AO.40.001354

[11] J. Selbin, "The chemistry of oxovanadium (IV)", Chem. Rev., 65(2), 1965, 153-175, **doi:** 10.1021/cr60234a001.

[12] F. Rahman, M. Skyllas-Kazacos, "Solubility of vanadyl sulfate in concentrated sulfuric acid solutions", J. Power Sources, 72(2), 1998, 105-110, doi: 10.1016/S0378-7753(97)02692-X.

[13] R.M. Wallace, "Determination of the Second Dissociation Constant of Sulfuric Acid by Donnan Membrane Equilibrium", J. Phys. Chem., 70, 1966, 3922–3927, doi: 10.1021/j100884a029

[14] E.L. Cussler, "Diffusion - Mass Transfer in Fluid Systems", Third Edition, Cambridge, 1984

[15] O.T. Fassulo, "Sulfuric acid; use and handling", University of Minnesota - New York: McGraw-Hill, 1965

[16] Z. Jiang, K. Klyukin, V. Alexandrov, "Structure, hydrolysis, and diffusion of aqueous vanadium ions from Car-Parrinello molecular dynamics", J. Chem. Phys., 145, 2016, 114303, doi: 10.1063/1.4962748

Chapter V – Influence of the presence of vanadium particles on the performance of a filter press reactor under charge/discharge cycling

Table of contents:

Introduction

This chapter presents the studies of the impact of the presence of solid particles (vanadium salts or additives) on the performances of an all vanadium redox flow battery (VRFB), which is chosen to operate in the presence of suspensions, in order to reach the objective of the thesis: to increase the energy density stored, from the existing one i.e. 40 Wh/kg to an energy to at least 5 folds higher. To that end, discharge–recharge cycles were undertaken in a filter press divided electrochemical reactor, constituting the core of the battery, and connected to two external storage reservoirs.
The experimental setup of the VRFB used in this work as well as the experimental conditions involved will be described in details below.
The $V^{(V)}/V^{(IV)}$ and the $V^{(III)}/V^{(II)}$ electrolytes (the posolyte and the negolyte respectively) involved were, in general, initially constituted by a vanadium solution at 1.7 mol/L, to which was added an excess of the corresponding powder to reach the required quantity (often given as an equivalent concentration of vanadium). Thus, the studied suspensions have equivalent concentrations of 2.5, 3.2 and 3.5 mol/L in vanadium, prepared initially in 2 mol/L of sulfuric acid. Besides, the effect, on the performances of the battery, of the presence of the solid vanadium and/or KB nanoparticles in the posolyte and/or in the negolyte will be also examined, in order to try to correlate the enhancement of the main parameters against the quantity of solid particles.

All the studies carried out in this present chapter expect to enable access to the characteristic parameters of the battery (cell potential, electrodes overpotentials, active species concentrations…) allowing calculating and evaluating conversions and energy efficiencies, to compare with existing systems.

V.1. Experimental set-up and general procedures

V.1.1. Lab scale filter press electrochemical divided reactor

A filter press **electrochemical divided reactor** composed of two compartments separated by a cationic selective membrane (Fig.V.1) constitutes the core of the studied VRFB. The working electrodes **(1)** (used also as current collectors) are massive graphite plates (50 x 40 x 15 mm) built-in inside **(2)** of the plastic plates **(3)**; the geometrical surface of the electrode is the visible surface of the graphite plate, i.e. 20 cm^2. The PEEK (PolyEtherEtherKetone) is used for the reactor's external support plates **(3)** (85 x 95 x 30 mm), thanks to its mechanical and chemical resistance to the acidic and oxidative properties of the electrolytes.
It should be noted that, a reactor made with PVC (PolyVinylChloride) was initially used; however it was attacked by the electrolytes and released plastic particles inside the solutions.

The electrical connection is insured through a copper rod **(4)** which is inserted by the side face of the PEEK plate and then screwed on the side face of each graphite plate. To avoid copper oxidation and solution contamination: i) the graphite plates are inserted into the corresponding location created by machining of the PEEK plates; ii) resin is added to fill all the possible remaining openings and corners (for both graphite and copper), thus expecting to suppress any liquid infiltration.

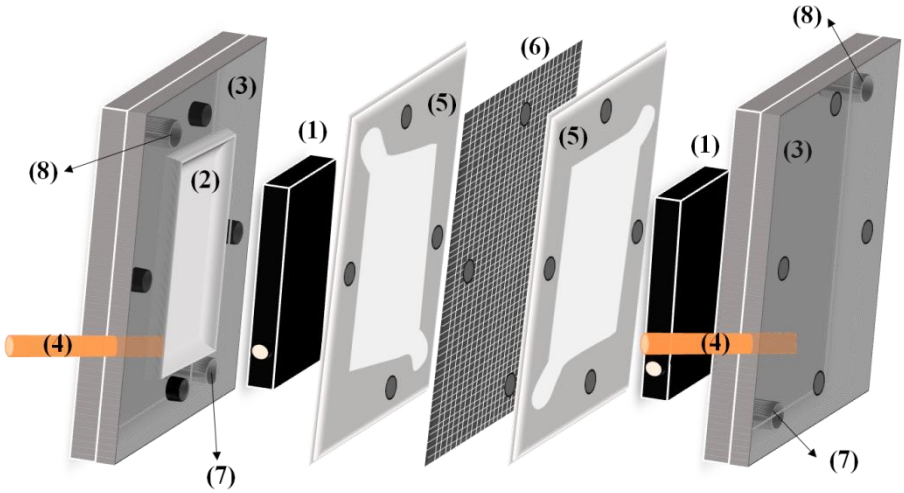

Fig.V.1: Dismantled filter press divided electrochemical reactor used for this work's vanadium redox flow battery: **(1)**/ graphite plates i.e. working electrodes; **(2)**/ parallelepiped cavity within the peek to place the graphite electrode; **(3)**/ PEEK plates constituting the body of the reactor; **(4)**/ Electrical connectors, i.e. copper rods crossing the peek plate and screwed on the side face of the graphite; **(5)**/ silicon gaskets defining the shape of the electrolytic compartment; **(6)**/ Nafion 117 cationic membrane; **(7)**/ inlet of the electrolytes; **(8)**/ outlet of the electrolytes. The black circles on the PEEK plates, joints and membrane correspond to the holes for the screws to assemble the system and avoid leakages.

Silicon gaskets were used to define the thickness (and consequently the shape and the volume) of the electrolytic compartment **(5)**. Their thickness can vary from 1 to 4 mm and the corresponding volume from 2 to 8 cm^3. Silicon appeared to be resistant to the acid media and did not deteriorate throughout all the experiments performed. The shape of the compartments was the one usually chosen for this kind of geometry to obtain a relatively uniform flow of the electrolyte and also to enable to operate with the highest surface of the graphite electrode.

The membrane used to separate the two compartments **(6)** is a Nafion 117 reinforced membrane known for its chemical, thermal and mechanical resistance. It allows the preferential passage of protons through interactions with sulfonic acid (SO_3H) terminal groups, grafted on the polymer. However, it allows also the migration of vanadium ions since it is a cationic membrane but at a lower rate given the large size of vanadium ions compared to protons and their lower diffusion coefficients (table V.1).

Table V.1: Diffusion coefficients through a Nafion membrane for the different species present in the electrolytes of the VRFB [1]

	D (m^2/s)
$V^{(II)}$	$3.125x10^{-12}$
$V^{(III)}$	$5.93x10^{-12}$
$V^{(IV)}$	$5x10^{-12}$
$V^{(V)}$	$1.7x10^{-12}$
H^+	$3.35x10^{-9}$
HSO_4^-	$4x10^{-11}$

The electrolyte flows from the bottom (inlet, **(7)**) to the top (outlet **(8)**) within the gasket and it is recycled back to the storage tanks, in which the electrolytes (solutions/suspensions) are continuously stirred (500 RPM) using the same cross-shaped stirrer (CSS) as the one used previously (chapter III); the reservoirs are thermoregulated at 25 °C. The internal diameter of the inlets/outlets is 8 mm, considered as sufficient to enable easy flow of the suspensions. Nitrogen bubbling enables to keep the negolyte under inert atmosphere, to avoid the re-oxidation of the formed $V^{(II)}$ before its electrochemical reduction during the discharge cycle. A peristaltic pump (Cole-Parmer, N° Réf. 87360) equipped with two channels (stainless steel rotors), enables the flow of the suspensions. The pipes are from Masterflex (*Fisher Scientific*) and are chosen to be resistant to the acidic media. The pump is regulated with an external control box and the flow rate is fixed at 40 L/h ($1.11x10^{-5}$ m^3/s) for all the electrolyses performed on the reactor; it was noticed that this flow rate allows obtaining a homogeneous flow of the electrolytes even in the presence of suspensions.

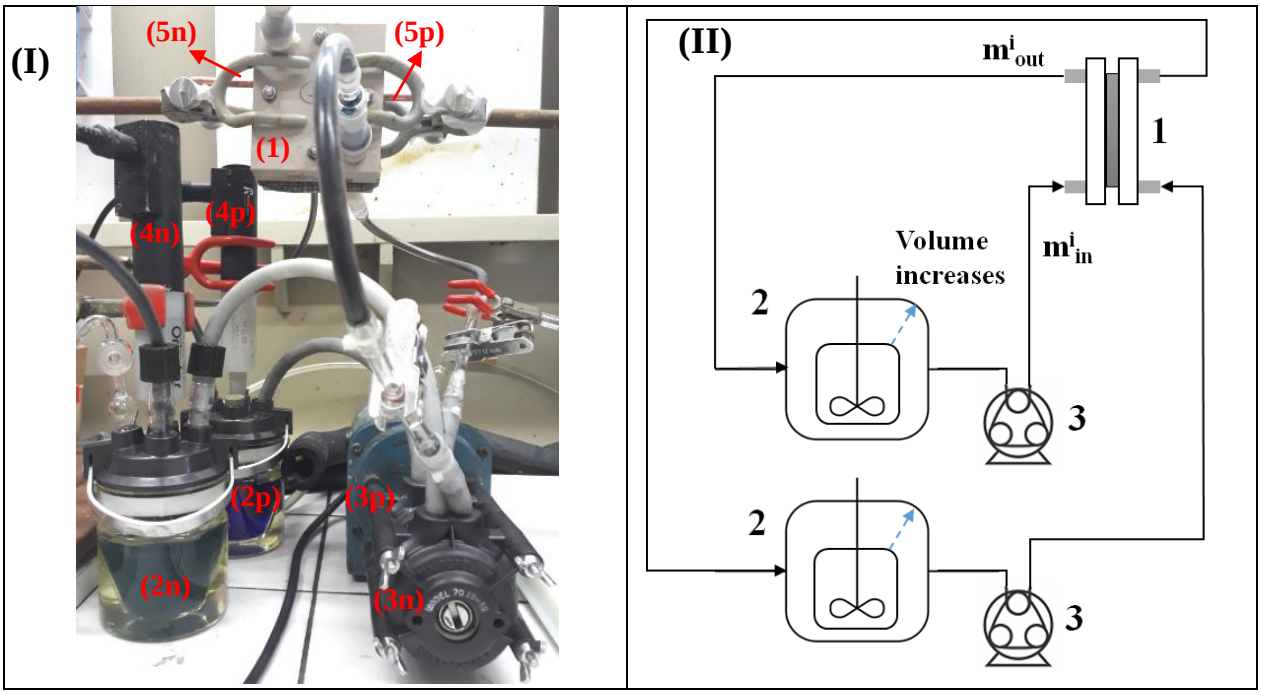

Fig.V.2: **(I)**: Picture of the experimental set-up assumed as a simple element of a vanadium redox flow battery: (1): the filter press reactor; p and n means posolyte and negolyte respectively; (2p) and (2n) storage tanks; (3p) and (3n) peristaltic double-headed pump; (4p) and (4n) bodies of a rotating electrode, used here as stirrers enabling the rotation of the cross shaped stirrers (CSS); (5p) and (5n) copper rods used as electrical connectors; **(II)**: Schematic representation of the experimental setup: (1)/ reactor; (2)/ well-mixed storage tanks; (3)/ peristaltic pumps; m^i_{in}: moles number of vanadium of oxidation state "i" at the **inlet of the reactor** (which corresponds to the outlet of the storage tank); m^i_{out}: moles number of vanadium of oxidation state "i" at the **outlet of the reactor** (which corresponds to the inlet of the storage tank)

V.1.2. Apparatus used

The electrolyses were performed under galvanostatic mode (applied constant current), using a potentiostat PGSTAT300 from *Metrohm*, monitored with the Nova 2.1 software (the reference and the counter electrodes wires were connected together); the potentiostat enables the monitoring of the cell voltage ΔV.
In addition, a 50 µm platinum wire, acting as a "pseudo-reference" or a "comparison electrode" was inserted at the entrance of each compartment. This Pt wire was connected on the outside of the reactor with a copper wire.

A *KeySight Benchvue* data logger was used, during the electrolyses, to continuously monitor the cell voltage ΔV (directly on the copper rods), as well as the potentials of the positive and the negative electrodes versus the Pt wire pseudo-reference; in fact, the latter measured values correspond to the overpotentials (or overvoltages) η of the electrodes. Indeed, in the absence of polarization, both the Pt wire and the graphite electrode act as electronic conductors, hence, their difference of potential can be considered almost zero. For example, for the positive graphite electrode:

$$E_{Graphite/SCE} - E_{Platinum/SCE} = E^{G}_{I=0} - E^{Pt}_{I=0} \approx 0$$

When a current is applied on the (positive) working electrode (the Pt wire is not polarized), the potentials measured, can be expressed as follows:

$$E_{Graphite/SCE} = E^{G}_{I=0} + \eta \quad \text{and} \quad E_{Platinum/SCE} = E^{Pt}_{I=0}$$

$$E_{Graphite/SCE} - E_{Platinum/SCE} = E^{G}_{I=0} + \eta - E^{Pt}_{I=0} = \eta + \boldsymbol{\varepsilon} \approx \eta \qquad \text{Eq.V.1}$$

$\boldsymbol{\varepsilon}$ is the residual potential difference between the Pt wire and the graphite plate; $\boldsymbol{\varepsilon}$ cannot be strictly zero because even though the Pt is not polarized, it is affected by the polarization of the WE.

It should be noted as well that an amperometer is inserted in series between the potentiostat and the counter electrode in order to have a continuous visual control of the applied current.

As for the follow-up of the species, the analytical methods described in chapter II are used here to quantify the four oxidation states of the vanadium during the electrolyses:

- $V^{(II)}$ and $V^{(V)}$ are titrated by potentiometry with a redox reaction with I_3^- and $Fe^{(II)}$ respectively;
- $V^{(III)}$ and $V^{(IV)}$ are analyzed by UV-Vis spectrophotometry at their characteristic wavelengths (400 and 760 nm respectively) after the corresponding dilutions in the 3 M sulfuric acid.

Some specific information to each experiment will be provided along the chapter when necessary.

V.1.3. Operating parameters and procedures

The aim of the experiments that will be presented in this chapter is to validate that it is possible to carry out discharge/recharge cycles of the battery using high load electrolytes in the form of suspensions possible to flow. To carry out the electrolyses, the galvanostatic mode was chosen; however, because of the eventual presence, formation or precipitation of the vanadium salts, the maximum current which is possible to achieve (i.e. the pseudo-limiting current for each electrode) will be impacted, depending on the quantity and nature of the added solid. Hence, each suspension and its corresponding electrolysis is a case of its own, and the knowledge of the maximum acceptable current by the battery, requires a complementary study performed on the reactor for each experiment.

Thus, the limiting current of the initial solution or suspension was estimated (when possible) by plotting the voltammetric curves at the steady state ($I = f(\eta)$) at the initial time. In spite of the various problems, it is possible to get a satisfactory estimation of the actual 'faradic current' corresponding to the reaction of the dissolved species on its corresponding electrode. As an example, a schematic presentation of the curves expected for a classical reversible system with no solid particles, was indicated in Fig.V.3, for recharge (**a** and **b**) and discharge (**c** and **d**).

To carry out the electrolyses, we chose to apply initially a current corresponding to the half (50 %) of the estimated initial limiting current (Fig.V.3, (**a** and **c**)). During the electrolyses the quantity of the electroactive species decreases, thus inducing the limiting current also to decrease, as well as the presence of a critical time for which the decreasing limiting current (for the considered limiting reagent) becomes equal to the applied current. If the electrolysis is pursued at the same applied current, then the faradic yield (y_f) will decrease and secondary reactions (such as the oxidation or reduction of the solvent) will occur.
Besides, at this critical time the potential of the electrode of the limiting reagent shifts to the solvent region, thus implying: i) a rapid increase of the cell voltage ΔV (Fig.V.3, **(b)**) for the recharge or ii) a rapid decrease of the cell voltage ΔV (Fig.V.3, **(d)**) for the discharge.
Note that, in this figure, it is assumed that i) there is not any ohmic drop, and ii) for a completely dissolved salt, the limiting current is proportional to the concentration of the dissociated metallic ions; thus, when the conversion of the latter reaches 50%, the limiting current is supposed to decrease by half as well (that is strictly wrong because the concentration of the sulfuric acid also changes, thus implying changes in viscosity and diffusion coefficients).

Note that the cycles of charge discharge were performed, starting with various compositions of the solution in each oxidation state of the vanadium. Indeed, it is difficult to perform electrolyses and to reach a complete conversion (0 to 100 %) of a certain reagent, because the time required is often relatively long (more than 8 h). Thus, it becomes also difficult to performs cycles in exactly the same conditions (breaks/overnight stopping of the electrolysis, changes in the temperature, possible precipitation, oxidation by O_2 of the $V^{(II)}$,…), so any comparison becomes difficult. A possible solution to perform electrolyses enabling to get comparative information is to reduce the examined interval of conversions, starting for example the electrolysis with an initial composition of 50 % of the oxidizer and 50 % of the reductant. In these conditions it is easy to perform comparable operations/cycles of charge discharge, in various conditions, keeping a work interval in the conversions of +/- 20 %.

Lastly, it should be noted that the surface condition of the two electrodes is not identical at the beginning the study. The graphite plate in contact with the posolyte has endured degradation due to a previous electrolysis which was carried out under a high applied current enabling the oxygen evolution. The partial pressure of the generated O_2, in addition to the strong oxidative character of the VO_2^+ could be responsible for the graphite electrode destruction. The polishing of the surface of the electrode was tried in order to get it back to its initial state but that was not possible. Comparatively, the surface of the electrode in contact with the negolyte is smooth with no appearance of any degradation.

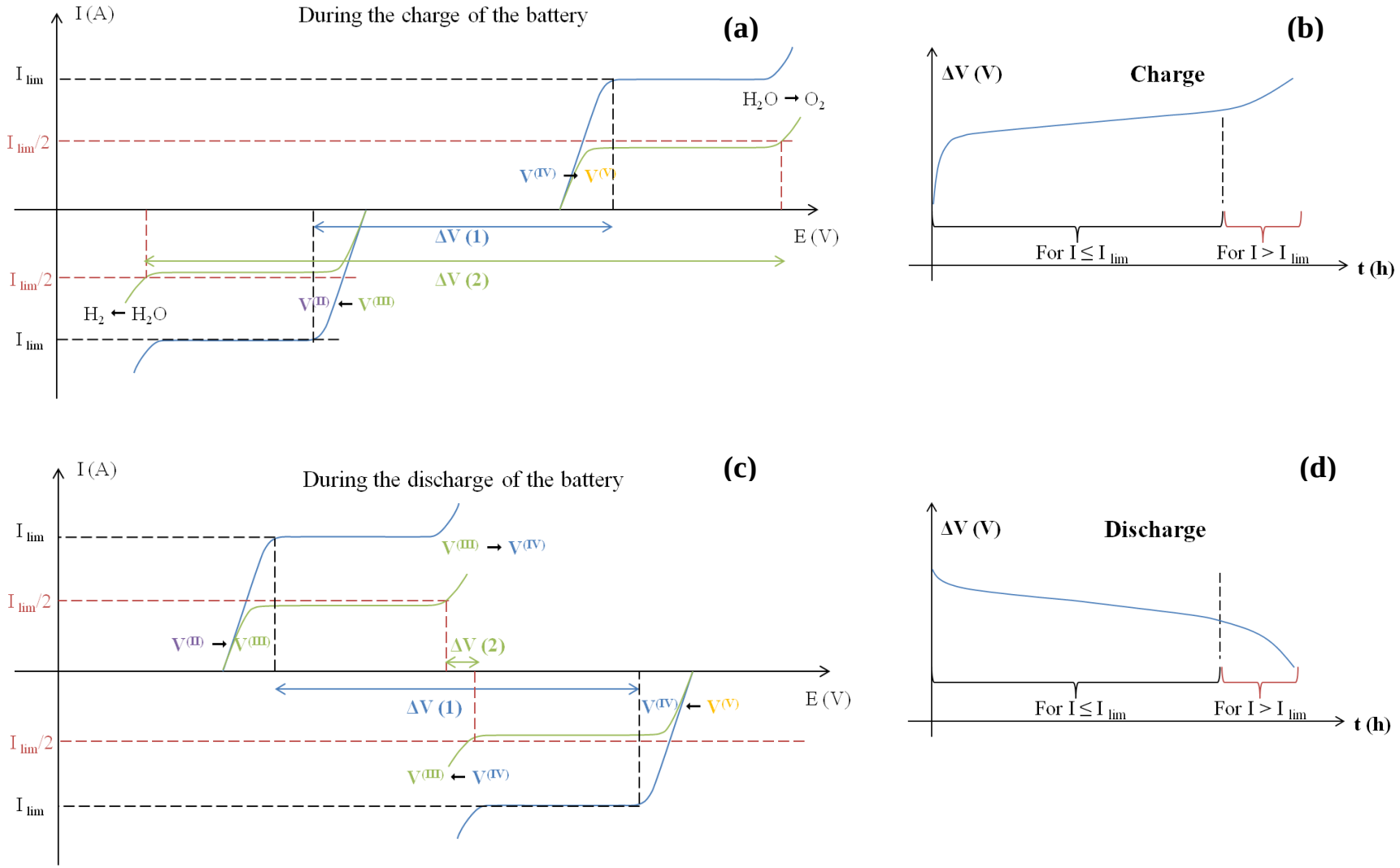

Fig.V.3: Schematic presentation of the theoretical I = f(E) curves obtained for a typical electrochemical system (assumed as reversible) during charge (**a**) and discharge (**c**) as a function of the applied and limiting current. On the right are presented the cell voltage temporal evolutions as a function of the same parameters, also during charge (**b**) and discharge (**d**)

V.2. Charge-discharge cycles in homogeneous media (vanadium near saturation)

In this section it is expected to perform the recharge/discharge cycles with a saturated solution of vanadium in order to get information (conversion, faradic/voltage and energetic yields) for comparison with the electrolyses involving suspensions (constituting the finality of the study).
The initial state of the reactor is chosen to be the 'fully discharged battery', i.e. the $VOSO_4$ commercially available in the posolyte and the $V_2(SO_4)_3$ for the negolyte; the latter is a powder prepared from the electro-reduction of $VOSO_4$ (refer to chapter II).

The temperature is fixed at 25 °C for all the electrolyses performed; at this temperature the saturation concentrations of the initial species, according to the bibliography, in 2 M sulfuric acid are: $[VO^{2+}]_{sat.} \approx 2.6$ M and $[V^{3+}]_{sat.} \approx 2.26$ M [2]. However, as it was indicated in chapter III (section of preparation of the $V^{(III)}$ solutions, § III.2.1.), the achieved concentration by direct dissolution of the $V_2(SO_4)_3$ powder could not be greater than 1.1 M. Discrepancies between the various values of the solubility could be due i) to the operating mode to determine these values (the measurements cited in the bibliography were performed by precipitation of a super-saturated solution) and ii) to the possibility to have in solution various metastable forms of the vanadium (i.e. for example various hydration states).
In any case, the concentration chosen as starting point of most electrolyses is equal to 1.7 $mol.L^{-1}$ for both the negolyte and the posolyte. While the posolyte is entirely homogeneous, the negolyte contains a mixture of dissolved V^{3+} at 1.1 M and the equivalent of 0.6 mol/L in solid form. The suspension appears to be fluid and the presence of solid particles does not seem to significantly affect the flowing within the reactor.
All the electrolyses will be performed under galvanostatic conditions; the applied current will be chosen as function of a hypothetical limiting current, of which an estimation will be made thanks to the plotted $I = f(\eta)$ curves.

The reactions taking place during the recharge of the battery, in their simplified form and already presented in the previous chapters, are:

$VO^{2+} + H_2O \rightarrow VO_2^{+} + 2\,H^{+} + e^{-}$ ($E° = 1.00$ V/ESH) Rx.V.1

$V^{3+} + e^{-} \rightarrow V^{2+}$ ($E° = -0.26$ V/ESH) Rx.V.2

The global reaction of the VRFB would then be:

$VO^{2+} + V^{3+} + H_2O \rightarrow VO_2^{+} + V^{2+} + 2\,H^{+}$ ($\Delta V_{I=0} = 1.26$ V/ESH) Rx.V.3

V.2.1. Preliminary charge-discharge cycle – electrolysis procedure description and optimization

This section describes a preliminary charge-discharge cycle and examines all the points encountered; typically the various preliminary operations to carry out the experiment are presented, then the magnitude of the selected operating parameters is commented. Besides the

various definitions of the parameters describing the performance of the battery are introduced and finally the identification of general problems in connection with the electrolysis is discussed. We have fixed a conversion of 50% to achieve for the $V^{(IV)}$ oxidation (recharge of the battery), and then to reverse the electrolysis in order to carry out the discharge.

V.2.1.1. Plot of the Current-overpotential (*I=f(η)*) curves for the initial system

In order to estimate the maximum admissible current and then to deduce the current to apply, the current overpotential curves were plotted for the considered initial system and presented in the Fig.V.4. Their interpretation reveals numerous properties of the system:

- As discussed above, the results confirm that both curves start at an overvoltage value close to 0 V, since in the absence of current (no polarization of the WE) both electrodes, 'graphite plate/platinum wire', are in contact with the same solution (for the posolyte and the negolyte);

- For the posolyte (Rx.V.1), the current increases exponentially and reaches 1 A (the maximum current delivered by the potentiostat). This means that the mass transfer limitation for the $V^{(IV)}$ oxidation occurs for currents higher than 1 A. A rough estimation of the limiting current can be made by an analogy of the *I = f(E)* curves plotted on an immobile solid graphite rod with a solution of $V^{(IV)}$ at 1.5 M (chapter III). The value of I_{lim} was found to be equal to ~ 0.15 A/cm^2 which is equivalent to 3 A for the graphite plate used in the present reactor (20 cm^2). Of course most of the operating parameters are different, but both results agree for a maximum current higher than 1A;

- The curve obtained with the negolyte exhibits a peak of low magnitude (0.05 A) in the over-potential range from -0.1 to -0.5 V; then appears an exponentially shaped signal for over-potentials lower than -0.5 V.
  The small peak could be attributed to the reduction of some oxygenated groups eventually present on the surface of the graphite. Despite the high overvoltage (> |-0.5| V) the exponential part could be attributed to the V^{3+} reduction, and the limited capacity of the potentiostat does not enable to reach any 'mass transfer limitation' (nor the corresponding limiting current). The high overpotential observed for the reduction of the V^{3+} is attributed to the presence of solid particles of $V_2(SO_4)_3$ (a quantity equivalent to 0.6 mol/L was present in solid form), probably adsorbed on the surface of the graphite and creating an additional resistance which causes the shift of the reduction to the more cathodic potentials. Note that this effect was also observed in chapter III, in the conventional three electrodes cell: we have demonstrated that the presence of $V^{(III)}$ solid particles leads to the disappearance of the reduction wave of V^{3+}.

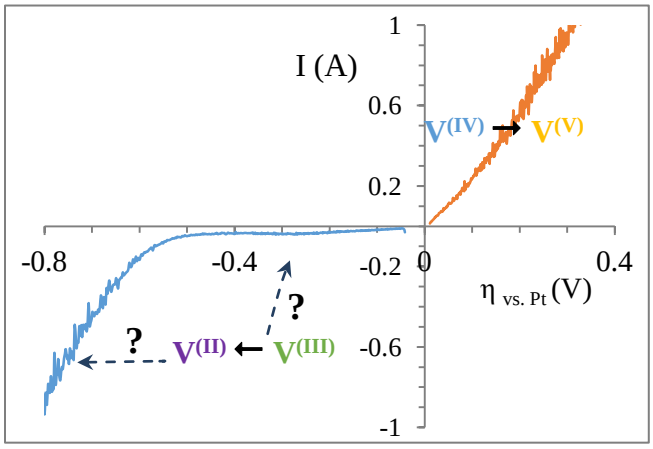

Fig.V.4: Evolution of the current as a function of the overpotential, measured between the corresponding electrode and the Pt wire used as pseudo-reference, for the posolyte and the negolyte at t = 0 (before the beginning of the electrolysis); $[VOSO_4]$ = 1.7 mol.L^{-1}; $V_2(SO_4)_3$: 1.1/2 M in dissolved form + 0.6/2 M in solid form. WE = solid graphite (S_g = 20 cm^2); RE = Pt wire; CE = solid graphite; flow rate of posolyte or negolyte = 40 L/h; r = 10 mV.s^{-1}; $T_{reservoirs}$ = 25 °C.

To sum up, this study clearly shows that the initial maximum current admissible by this type of battery is higher than 1 A; thus, it is decided to carry out the electrolyses by applying I = 0.6 A for a surface area of 20 cm².

Under constant current, the time t required to reach a conversion of 50% of the initial quantity of the vanadium introduced (*initial moles number in the posolyte = initial moles number in the negolyte = 0.119 mol*) is calculated from the theoretical amount of charge Q (Eq.V.2).

$$Q = n_e\text{-F} \times \text{moles converted} = I \times t \qquad \text{Eq.V.2}$$

Appling Eq.V.2 led to a theoretical electrolysis time of 2.66 h (160 min), enabling to reach an equimolar concentration (0.85 mol/L) for each one of the four oxidation states of the vanadium.

V.2.1.2. Performing the electrolysis: half cycle 'recharge'

The electrolysis (charge of the battery) was performed for that exact duration (2.7 h) under the chosen constant current (0.6 A). In Fig.V.5 the temporal evolutions of the overpotentials of both electrodes **(I)** and the cell voltage ΔV **(II)** are presented. Note that the shape of the curve *ΔV=f(t)* totally agrees with that predicted in the Fig.V.3-(b).

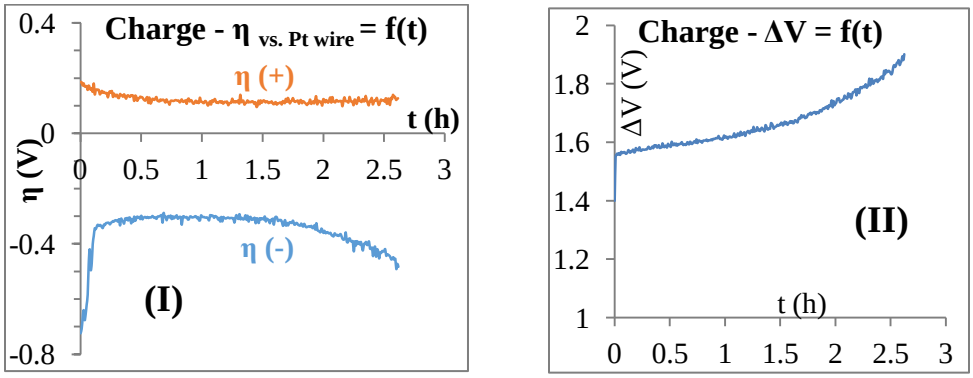

Fig.V.5: Temporal evolutions of the overpotentials of the positive and negative electrodes **(I)** and the cell voltage ΔV **(II)**, during the galvanostatic electrolysis performed using a filter press electrochemical reactor coupled with two storage tanks; $[VO^{2+}]_{t=0} = [V^{3+}]_{eq.,\ t=0}$ = 1.7 M; $I_{applied}$ = 0.6 A; flow rate for posolyte or negolyte = 40 L/h; $T_{reservoirs}$ = 25 °C.

The overvoltage at the positive electrode appears to be relatively low (< 0.15 V) and practically constant, meaning that the applied current of 0.6 A corresponds to an activation limitation at the positive electrode, even after 2.7 h of electrolysis. This confirms that there is not i) any irreversible phenomenon at the positive electrode and also that the remaining concentration of the dissolved VO^{2+} (0.85 mol/L) is enough to ensure a maximum admissible current higher than 0.6 A.

The overvoltage evolution at the negative electrode appears to be more complicated than that at the positive electrode. Starting with a magnitude of - 0.7 V (in agreement with that observed in the $I = f(\eta)$ curve of Fig.V.4), the overpotential rapidly "decreases to ~ |- 0.3| V", thus indicating an 'activation' of the electrode surface. Complete reduction of residual oxygenated groups could be a possible reason of this activation; the prior presence of these groups could have inhibited the reaction of the V^{3+} ions on the electrode by lowering the interactions and creating a repelling layer on the surface. Note that this phenomenon is systematically observed during the various electrolyses carried out. For higher electrolyses durations, the overvoltage remains practically constant until the last hour of the electrolyses where an "increase" was observed. Note that during the electrolysis, the concentration of the dissolved vanadium decreases (by reduction to V^{2+}); this implies dissolution of the residual $V_2(SO_4)_3$ solid salt and consequently a decrease of the overvoltage. It seems possible to consider that the increase of the overvoltage is caused by the lowering of the concentration of the V^{3+} in the bulk (and consequently by an applied current lower than the limiting current at this time) if the dissolution kinetics of the powder is slower than the electrochemical conversion.

The cell voltage depends on the overpotentials as well as on the three ohmic drops (posolyte, membrane and negolyte). The electrolysis causes the concentration of the $V^{(IV)}$ to decrease, but simultaneously the concentrations of $V^{(V)}$ and H^+ increase (in the posolyte). Even if the mixture remains homogeneous, its viscosity increases, and it is expected the same for the conductivity.
On the negolyte side, the electrolysis causes the solid fraction of the $V_2(SO_4)_3$ to decrease and simultaneously creates sulfates SO_4^{2-}, thus leading to a decrease of the conductivity. Here, the comparison of the cell voltage (Fig.V.5-(II)) and the overpotentials temporal evolutions (Fig.V.5-(I)), show that the overpotential of the negolyte seems to mainly affect the cell voltage.

To follow the electrolysis, and to access to its performances parameters (i.e. the various yields) it is necessary to determine the experimental conversion of the $V^{(IV)}$ (or $V^{(III)}$) defined by the Eq.V.3 and to compare that with the theoretical one (Eq.V.4).

Experimental conversion of the $V^{(IV)}$ (or $V^{(III)}$):

$$X_{exp.} = 100 \times \frac{Converted\ quantity}{Initial\ quantity} \qquad \text{Eq.V.3}$$

If the volume of the mixture remains constant:

$$X_{exp.} = 100 \times \frac{initial\ concentration\ C° - temporal\ concentration\ at\ t\ determined\ experimentaly\ C_t}{initial\ concentration\ C°} \quad \text{Eq.V.3'}$$

Theoretical conversion of the $V^{(IV)}$ (or $V^{(III)}$):

$$X_{th} = 100 \times \frac{\int \frac{y_{f\,(t)} \times I \times dt}{F \times Volume}}{C°} \Longrightarrow \text{Under galvanostatic mode and assuming the faradic yield } y_{f\,(t)} = 100\ \% \Longrightarrow X_{th} = 100 \times \frac{I \times electrolysis\ duration}{C° \times F \times Volume} \quad \text{Eq.V.4}$$

The theoretical conversion is the same for the $V^{(III)}$ or $V^{(IV)}$ since what is consumed from these two is formed in the other two oxidation states of the corresponding redox couple.

Potentiometric titrations of $V^{(II)}$ and $V^{(V)}$, (as indicated in chapter II) were carried out to determine their conversion during the electrolysis (Eq.V.3). To that end a volume of approximately 0.2 mL (of the posolyte or the negolyte) was withdrawn (using a syringe of 1 mL graduated per 0.01 mL) and diluted in 30 mL in ultra-pure water (deaerated for the $V^{(II)}$).

The results of the electrolysis are presented in Fig.V.6.

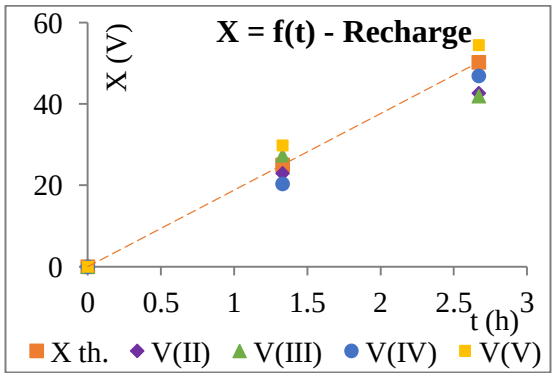

Fig.V.6: Temporal evolutions of the conversions of the vanadium species, during the galvanostatic electrolysis performed using a filter press electrochemical reactor coupled with two storage tanks; $[VO^{2+}]_{t=0} = [V^{3+}]_{eq.,\ t=0} = 1.7$ M; $I_{applied} = 0.6$ A; flow rate for posolyte or negolyte = 40 L/h; $T_{reservoirs} = 25$ °C. Orange cubes/dashed line: theoretical conversion. Experimental conversion: violet diamonds: $V^{(II)}$; green triangles: $V^{(III)}$; blue disks: $V^{(IV)}$; yellow squares: $V^{(V)}$.

A linear evolution was calculated for the theoretical conversion (because for this calculation, the faradaic yield is considered equal to 100%). The results of the analyses show a good agreement between these theoretical values and the experimental conversions for the four oxidation states of vanadium (see Fig.V.6: violet diamonds: $V^{(II)}$; green triangles: $V^{(III)}$; blue disks: $V^{(IV)}$; yellow squares: $V^{(V)}$). The discrepancies observed reach 5 % max. for the $V^{(IV)}/V^{(V)}$ redox system and 8 % max. for the $V^{(II)}/V^{(III)}$. This means that the faradaic yield reaches values from 92 to 95 %. Because some experimental conversions are higher than the corresponding theoretical values,

and also the reverse, we can conclude that the discrepancies are due to titration errors between the sampling and the dilutions. Nevertheless, the system appears to be functioning correctly for this first part of the experiment.

V.2.1.3. Plot of the $I = f(\eta)$ curves after the 50% recharge

As the amount of charge corresponding to a conversion of 50 % was achieved, the electrolysis was interrupted and the current – overvoltage ($I = f(\eta)$) curves were plotted for the four species (Fig.V.7). This action expects: i) to examine the state of the surface of the electrodes (for eventual precipitations) and ii) to determine the magnitude of the limiting current for the various oxidation states of vanadium. The obtained values would enable to fix the current to apply during the discharge of the battery.

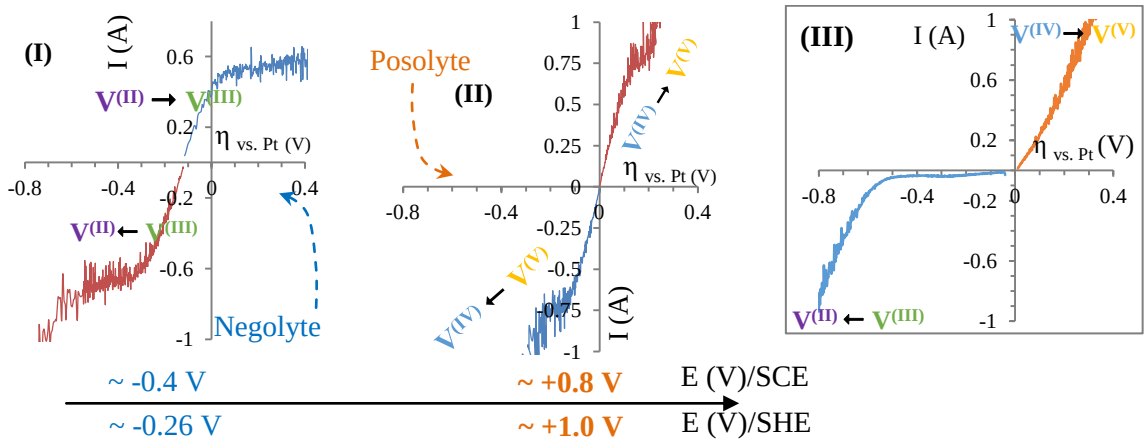

Fig.V.7: Current - overpotential curves plotted at the end of the recharge of the battery ($X_{theoretical}$ = 50 %) after supplying 50 % of the required amount of charge. **(I):** the negolyte; **(II):** the posolyte. **(III)** Imported from Fig.V.4 for comparison; WE = solid graphite (S_g = 20 cm^2); RE = Pt wires; CE = solid graphite; flow rate = 40 L/h; r = 10 $mV.s^{-1}$; $T_{reservoirs}$ = 25 °C.

Concerning the VO^{2+} oxidation to VO_2^+: the comparison of the anodic branch for graphs **(II)** and **(III)** enables to conclude the following:

- the required overvoltage to oxidize the $V^{(IV)}$ decreases, probably caused by a certain activation of the graphite electrode (corrosion caused by the electro-generated VO_2^+). It means that the electrode exhibits a higher electrocatalytic behavior against the $V^{(IV)}$;
- a limiting current is observed in the curve of $V^{(IV)}$ of graph (II), ~ 0.8 A for $\eta < 0.2$ V, (conversion of 50 %) while the curve at the beginning (Fig.V.4) is exponentially shaped. The obtained limiting current is still higher than the applied current for the battery recharge (0.6 A).

The same comparison was performed for the cathodic branch for graphs **(I)** and **(III)**, and the following conclusions can be made:

- a limiting current is observed on the curve of the $V^{(III)}$ of graph **(I)** (~ - 0.65 A for $|\eta|>$ 0.2 V) while the curve obtained at the beginning in **(III)** is exponentially shaped (after the residual low magnitude signal). The obtained limiting current is still slightly higher than the applied current for the battery recharge (|- 0.65| A > |- 0.6| A);
- as mentioned above, the required overpotential for the suppression of the low magnitude signal disappears and the curve $I = f(\eta)$ exhibits a 'more classical form'. The reduction of the $V^{(III)}$ appears as a practically reversible system (also implying a cleaner surface area of the electrode). This electrode activity enhancement during the charge, could be due 'also' to the dissolution of the $V_2(SO_4)_3$ solid particles possibly adsorbed on the electrode (the main reason remains the reduction of the oxygenated groups at the electrode).

On the other hand, a difference between the limiting currents for the negolyte (-0.75 A, cathodic branch in graph **(I)**) and the posolyte (0.8 A, anodic branch in graph **(II)**) can be noticed. Theoretically, starting at the same initial concentration and applying the same current should lead to the same conversion and subsequent current on both sides of the membrane if the diffusion coefficients are identical for all the species. Thus, we conclude that the diffusion coefficients are different, hence the difference observed between I_{lim} of $V^{(IV)}$ and $V^{(III)}$. In fact, for comparison, Yamamura et al. [3] determined the diffusion coefficients on a plastic formed carbon electrode (PFC) and it was found that $D_{V(IV)} = 3.9x10^{-10}$ m^2/s is greater than $D_{V(III)} = 2.4x10^{-10}$ m^2/s, which can confirm the higher limiting current observed for the $V^{(IV)}$ oxidation.

The third comparison concerns the curves for the V^{2+} oxidation to V^{3+} (anodic branch of graph **(I)**) and the VO_2^+ reduction to VO^{2+} (cathodic branch of graph **(II)**), i.e. the system operating as a battery in discharge: the limiting current observed the V^{2+} oxidation {graph **(I)**, ~ 0.54 A for η < 0.25 V} is lower than the limiting current observed the VO_2^+ reduction {graph **(II)**, ~ |- 0.75| A, for $|\eta|>$ 0.2 V}.
Knowing these limiting currents we decide to carry out the discharge half cycle in galvanostatic mode by applying the half of the lowest limiting current. Let us note that the potential scan rate applied is 10 $mV.s^{-1}$ to plot the $I = f(\eta)$ curves of the Fig.V.7.

V.2.1.4. Performing the electrolysis: half cycle 'discharge'

The lowest limiting current observed (Fig.V.7) is that of the oxidation of the V^{2+}, consequently we decide to apply the half for the half-cycle 'discharge of the battery'. Note that the current of – 0.27 A was applied at the positive electrode, to perform the spontaneous reaction V^{2+}/VO_2^+ under controlled rate. During this electrolysis the same parameters as previous were followed: the conversion, the limiting currents and the cell voltage. Even if the initial concentrations of the various species of vanadium are different from those of the previous part of the electrolysis, here, the idea is to carry out these preliminary operations, in order to i) determine unexpected problems, ii) to compare the evolution of the various voltages and the faradaic yield, and finally

iii) to get an idea about the magnitude of the various limiting currents of the four species of the vanadium.

The graphs **(I)** to **(IV)** of Fig.V.8 present the temporal evolutions of the cell voltage as well as the state of charge (SOC) of the battery, calculated from the analyzed $V^{(II)}$ and $V^{(V)}$.
Titrations of V^{2+} and VO_2^+ were performed following the procedure defined above and the conversions of the various species of vanadium were determined. The SOC is defined as the ratio between the concentration of $V^{(II)}$ or $V^{(V)}$ at time t and the total vanadium concentration (here 1.7 M) in solution.

Concerning the cell voltage Fig.V.8-(I), it remains practically stable (~1.2 V) during 1.5 h and then it rapidly decreases. This evolution could mean that at this time the limiting current of the less concentrated species becomes lower than the applied current; the corresponding overpotential increases until reaching the solvent region and consequently the useful cell voltage decreases. We decide to reduce the applied current to pursue the electrolysis; to that end we chose $I_{applied}$ = - 0.05 A after plotting the $I = f(\eta)$ curves before the beginning of the second part of the discharge (not shown here). This low value of the current naturally implies a long duration of electrolysis in order to convert back the vanadium species and to reach the initial state of the battery.

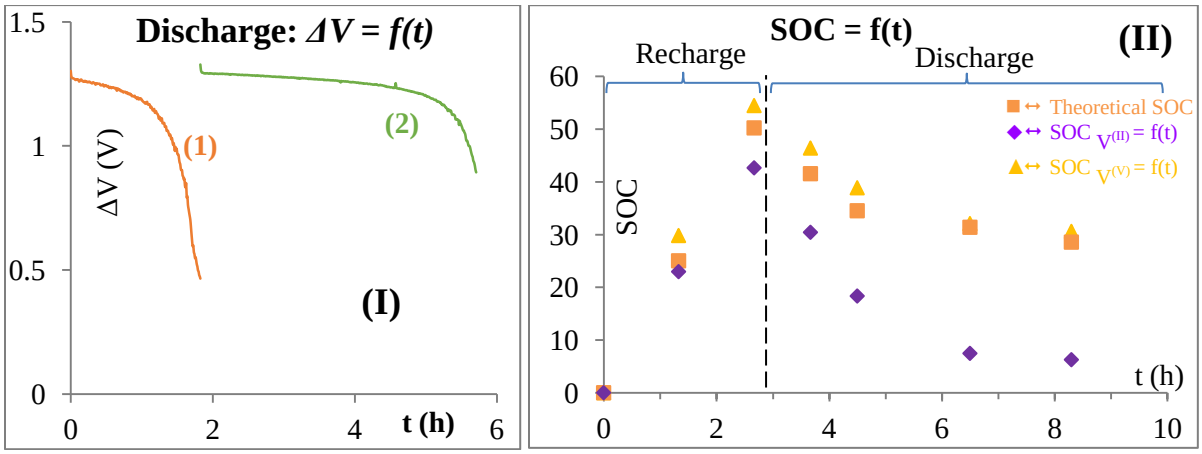

Fig.V.8: **(I)**: Evolution of the cell voltage with time during the discharge of the battery which was held in two parts: (1) at $I_{applied}$ = -0.27 A and (2) at $I_{applied}$ = -0.05 A; **(II)**: Comparison between the theoretical SOC (orange squares) and the experimental SOC calculated for the $V^{(V)}$ (yellow triangles) and $V^{(II)}$ (violet diamonds) during the discharge of the battery (t > 2.7 h) compared to the values calculated during the charge (t < 2.7 h).

The experimental SOC calculated from the $V^{(II)}$ concentration exhibits an important gap with the theoretical values; it is impossible to convert by electrochemistry more than the theoretical quantity. If the experimentally determined concentration is lower, it means that another oxidizer transforms the $V^{(II)}$ to $V^{(III)}$. Even if nitrogen was introduced into the storage tank and also in all glassware used during the titration, it seems obvious that oxygen was infiltrated into the $V^{(II)}$ solution and contributes to increase its conversion and lead to a 'lower SOC'.

As for the discrepancies observed in the case of $V^{(V)}$, in the first part of the discharge, at $I_{applied}$ = -0.27 A, the experimental SOC is slightly higher than the theory (Δ(SOC) ~ 4 %) they can be attributed to the titration (~ 6 % of error). The main reason which could explain the various experimental errors is the changes in the volume of both the posolyte or the negolyte, especially for long time electrolysis; the changes can be due to several reasons such as evaporation, transport to the opposite compartment of water (migration and osmosis), crossover of the vanadium or even chemical consumption of the water.

The $I = f(\eta)$ curves, plotted (not shown here) at the end of the discharge, exhibit:
- limiting currents for the $V^{(II)}$ oxidation equal to 0.07 A and for the $V^{(V)}$ reduction equal to -0.24 A. As explained before, to avoid the chemical oxidation of $V^{(II)}$ it is necessary to ensure a good protection of the negolyte against the oxygen and this means that our experimental setup needs improvement (tanks but also permeable pipes, connectors …);
- an exponential shape for the $V^{(IV)}$ oxidation, slightly more straightened than the one obtained at $t_{recharge} = 0$ (see Fig.V.4, orange curve);
- for the $V^{(III)}$ reduction a similar shape to that obtained at $t_{discharge} = 0$ (Fig.V.7-(I) see discussion in next sections)

Finally, a first parameter characteristic of the system is the ratio of the faradaic yields (for discharge/recharge), even if the initial concentrations of the vanadium salts and the achieved conversions are different. The results show that this ratio is close to 1 for the $V^{(III)}$, $V^{(IV)}$ and $V^{(V)}$ which means that the system is functional and that it is reversible at the chosen conditions.

A second important parameter characteristic of the system, which will allow comparing the efficiency of the battery (the classic homogeneous electrolytes against the suspensions aimed in this work), is the energetic yield calculated from charge-discharge cycles performed under similar conditions of current and time.
Here because of the various changes and unexpected problems, it is difficult to access to any significant value; that is why in the next part, electrolyses were performed in improved conditions, in order to minimize the effects of side phenomena.

V.2.2. Recharge-discharge cycling of the battery at $C_{vanadium}$ = 1.7 M

The previous preliminary electrolysis enabled to introduce the various operating parameters as well as to highlight practical problems; we propose now to perform real cycles of the battery along with the required quantifications and comparisons.
In order to perform cycles of charge-discharge with comparable parameters (applied current, conversions and duration), the electrolytes should preferably contain an equimolar mixture of both species of each redox couple in the corresponding compartment. Typically the posolyte

needs to contains $[VO^{2+}] = [VO_2^{+}] = 0.85$ M and the negolyte $[V^{3+}] = [V^{3+}] = 0.85$ M; both electrolytes contain sulfuric acid.
Therefore, the first step is to prepare the required solutions by electrolyzing solutions of VO^{2+} at 1.7 M and V^{3+} at 1.7 mol/L until reaching the required composition (50 % per oxidation state of vanadium), by using the experimental setup shown in Fig.V.2.

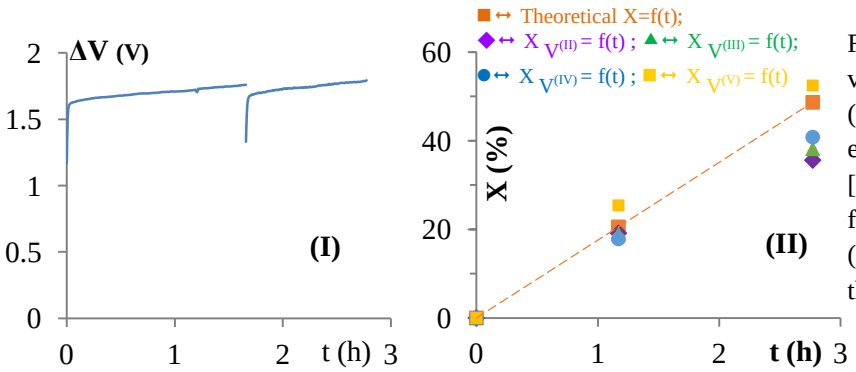

Fig.V.9: Temporal evolutions of the cell voltage (graph **(I)**) and the conversions (graph **(II)**) during the preparation of the electrolytes of the battery: $[VO^{2+}]_{t=0} = [V^{3+}]_{eq.,\ t=0} = 1.7$ M at $I_{applied} = 0.6$ A; flow rate = 40 L/h; Storage tanks stirred (500 RPM with the CSS) and thermoregulated (25 °C).

The electrolysis was performed in two steps due to a technical problem in the laboratory, but that did not affect the outcome of the operation which enabled to prepare the required initial composition: in the negative compartment 40 % for V^{2+} (i.e. 0.6 M in 75 cm^3) and 60 % for V^{3+}, while in the posolyte 50 % for $V^{(V)}$ (0.9 M in 75 cm^3) and 50 % for $V^{(IV)}$. Even with great care, oxygen penetrates in the circuit and consumes a part (10 %) of the $V^{(II)}$ formed.
The *I = f(η)* curves plotted at the end of the electrolysis (Fig.V.10), exhibit limiting currents for the four valences of the vanadium, but the magnitudes of these currents are different for each vanadium oxidation state.

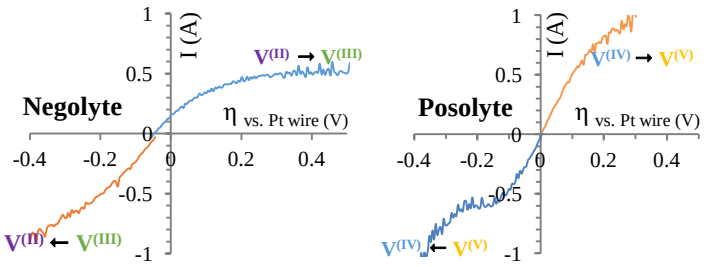

Fig.V.10: I = f(η) curves plotted at the end of the electrolysis performed to prepare the electrolytes of the battery: $[VO^{2+}]_{t=2.77\ h} = [VO_2^{+}]_{t=2.77\ h} \sim 0.85$ M; $[V^{2+}]_{t=2.77\ h} \sim 0.7$ M; $[V^{3+}]_{t=2.77\ h} \sim 1$ M**;** WE = solid graphite (S_g = 20 cm^2); RE = Pt wire; CE = solid graphite; flow rate = 40 L/h; r = 10 $mV.s^{-1}$; Storage tanks stirred (500 RPM of the CSS) and thermoregulated (25 °C).

After preparing the mixed valence electrolytes, the cycling of the battery can be performed. The chosen current for that was, first, fixed at ± 0.4 A for each operation, since it is lower than the limiting current of all the species involved (slightly lower of the I_{lim} of V^{2+}). The conversion rate aimed during the cycling is 10 % for each operation. The theoretical time for each half cycle was roughly estimated to be 50 min.

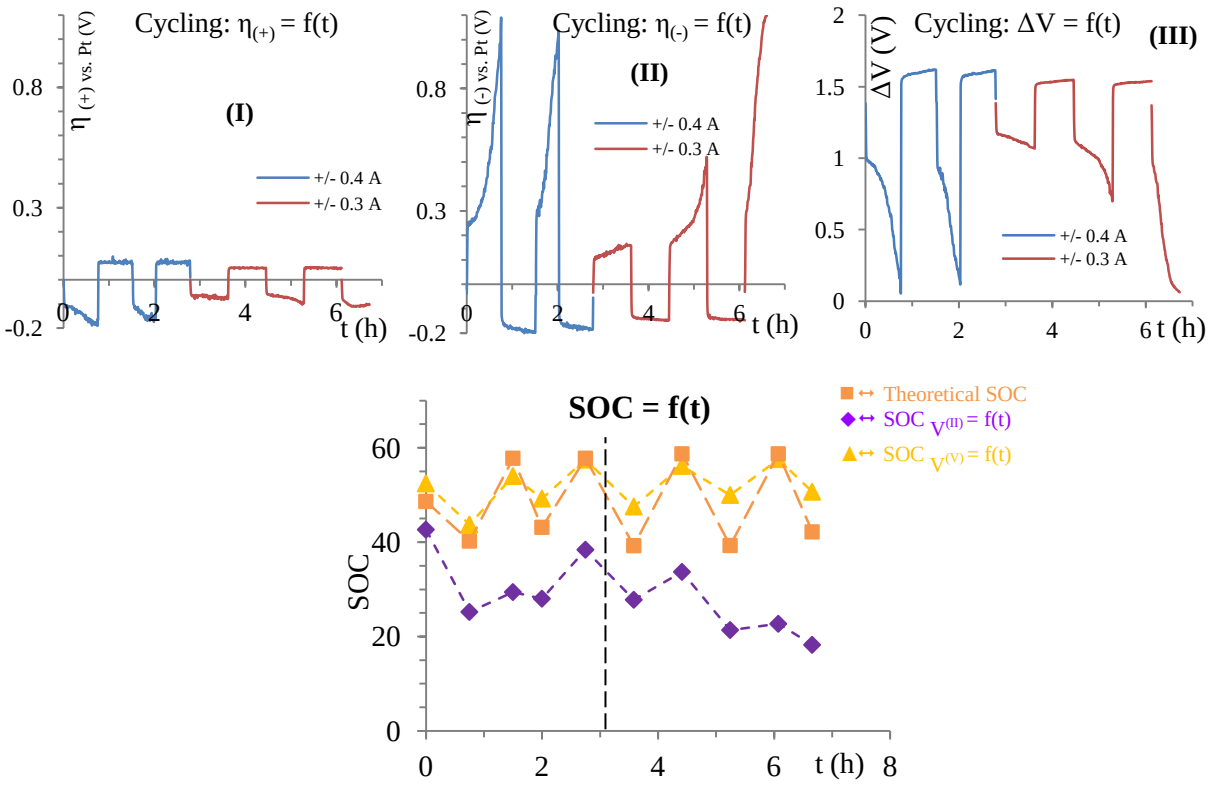

Fig.V.11: Results of the galvanostatic electrolyses (i.e. charge-discharge cycles of the battery) performed using a filter press electrochemical reactor coupled with two storage tanks. Electrolyses performed following two steps: 1st step - 2 complete cycles - $I_{applied}$= +/- 0.4 A - t ≤ 2.77h; 2d step - 2.5 complete cycles - $I_{applied}$ = +/- 0.3 A; 2.77 ≤ t(h) ≤ 6.7 h; The total vanadium concentration in each electrolyte is 1.7 M in 2 M initial sulfuric acid. Flow rate = 40 L/h; $T_{reservoirs}$ = 25°C.

Top: Temporal evolutions of the overpotentials of the positive **(I)** and negative electrodes **(II)** as well as of the cell voltage ΔV **(III)**. **Bottom:** Temporal evolutions of the SOC of VO_2^+ (yellow triangles) and V^{2+} (violet diamonds) determined experimentally and compared to the theoretical SOC (orange squares). The point at t = 0 corresponds to the SOC obtained at the end of the initial recharge (~ 50 % $SOC_{theoretical}$)

Five and a half cycles were performed and the various voltages temporal evolutions were presented in Fig.V.11 (graphs I to III). The corresponding concentrations of the four vanadium species were determined experimentally and indicated in the graphs (**IV** and **V**) of the same figure.

These results enable to extract various conclusions:

i) the duration of the cycles was dictated by the cell voltage (graph **(III)**); as it reaches values lower than + 0.5 V (for discharge) or 1.6 V for recharge, the half cycle was interrupted and the reverse operation was carried out. The curves show that the duration of the half cycle can vary from 30 to 50 minutes, thus implying variations in the obtained conversions and creation of a certain imbalance between the compositions of both compartments;

ii) the temporal evolution of the state of charge of the battery clearly indicates that:

- the SOC calculated from the posolyte changes (increases and decreases) with the same amplitude, and in the range of the theoretical value, thus meaning that the system behaves reversibly;
- the SOC calculated from the negolyte follows a certain dissymmetric evolution and is always lower than the theoretical value; being calculated from the concentration of V^{2+}, this means the transformation of this species is induced by a reaction different from the electrochemical transformation in the VRFB, and it was attributed earlier to the reaction with the oxygen infiltrated to the system;

iii) it appears that the rate of the change of the cell voltage (graph **(III)**) for the first 2 cycles during the recharge (ΔV oscillates between +1.54 and +1.6 V) is lower (i.e. ΔV is more stable) than the rate measured during the discharge (ΔV oscillates between 1 and 0 V for similar electrolyses durations). For the recharge, this appears to be a normal behavior because the applied current is less than the half of the limiting currents of both the $V^{(III)}$ and the $V^{(IV)}$ (Fig.V.10) and the time elapsed during the recharge is not sufficient to decrease their concentrations by more than 10%. Conversely, the rapid (few tens of min) and important (~1 V) variations of ΔV during the discharge, means that the applied current becomes rapidly higher than the limiting current of at least one system (Fig.V.10), probably the oxidation of the V^{2+}.

iv) reducing the applied current (0.4 to 0.3 A, cycles 3 to 5):

- slightly affects the cell voltage during the recharge; the latter remains practically constant, and even decreases;
- appears to stabilize 'a little bit' the cell voltage during the discharge, because the required time to reach the "applied current = limiting current" increases.

v) the positive electrode overpotential evolution confirms the above conclusions; it appears that the electrode behavior is stable; there is no permanent drift, and the magnitude of the changes of the overpotential remains 'low' ($\sim -0.15 < \eta_{(+)} < +0.1$ V). Moreover, as expected (and indicated above) decreasing the applied current causes the overpotential also to decrease;

vi) concerning the overpotential in the negative electrode, its evolution (which seems to partially dictate the evolution of the cell voltage) clearly shows that problems are due to the oxidation of the V^{2+} (i.e. during the discharge of the battery). Rapid increase of the overvoltage during the discharge confirms losses in V^{2+}, and consequently lowering of the limiting current, which becomes lower than the applied current. Note also that initially the magnitude of the applied current was very close to the limiting current (Fig.V.10). For electrolysis time higher than 2.7 h, lowering the applied current, seems to slightly stabilize the system (η is practically constant during the 3rd cycle and then slightly increases for the 4th cycle).

Note that during the cycles, $I = f(\eta)$ curves were plotted periodically (not shown here) in order to follow the overall system, i.e. to get an idea on the magnitudes of the limiting currents, and to compare their evolution with the corresponding concentrations. In general, the obtained curves are very similar in shape to those shown in Fig.V.10.

The dissymmetric amount of charge supplied (for recharge and also for discharge), also observed on the temporal evolutions of SOC (which show a bigger gap between the theory and the SOC of $V^{(II)}$ than between the SOC of $V^{(V)}$), seems to be the consequence of the high sensitivity of the V^{2+} against the oxygen (the V^{2+} is certainly consumed by the parasitic oxygen) and constitutes an important drawback of our experimental setup because it significantly reduces the performance of the battery.

The useful amount of charge for each operation/half cycle can be deduced from the monitoring of the concentrations (Fig.V.11-graphs **IV** and **V**); comparison of the latter with the theoretical amounts of charge (Q=I*t) enables to determine the faradic yield.

The energetic yield (energy recovered by the discharge to the energy supplied during the recharge) of these operations will be calculated and discussed further in this chapter (§ V.4) comparatively to the cycling of a battery involving suspensions instead of solutions.

In conclusion, this first charge-discharge operation (5.5 cycles) leads to the following conclusions:

- Under a total concentration of 1.7 M of vanadium salt in each compartment, the cycling of the battery with low conversions rates (~ 20%) appears as a reversible operation, no passivation/degradation nor any other parasitic phenomenon were evidenced at the electrodes;
- The fixed ‘low conversions’ do not enable any conclusion about the ‘heat’ or the water management in the battery. However for these conversions the faradaic yields remains ‘high’ (between 85 and 95 %) under a galvanostatic mode;
- The presence of the oxygen seems to be very problematic. Indeed, although bubbling of nitrogen was maintained into the bulk, oxygen permeates through the various elements (pipes, connectors) of the setup and re-oxidizes the V^{2+}, thus consuming charge, reducing the faradic yield and the battery performances.

V.2.3. Effect of the presence of carbon black nanoparticles on the battery current

V.2.3.1. Preparation of the electrolyte: recharge of the battery until a conversion of 50 %

The presence of Ketjen black (KB) nanoparticles has already been investigated (chapter III) in the three electrodes cell for the study of the electrochemical behavior of vanadium salts. It was found that the presence of small quantities of KB (0.17 % in weight of solution):

- enhances the oxidation current of $V^{(IV)}$ to $V^{(V)}$;
- the effect on the reduction current of $V^{(V)}$ to $V^{(IV)}$ and $V^{(III)}$ to $V^{(II)}$ was not examined for this amount of KB in solution but we suspect that it would have the same effect as that observed for the oxidation current of $V^{(IV)}$.

Therefore, the idea is to examine this effect in the case of preparative electrolyses, i.e. using the above described filter press electrochemical reactor (for the VRFB).
For this operation, 0.12 g of commercial KB were introduced in each electrolyte, i.e. into the posolyte (70 cm^3 of $[VO^{2+}]_{t=0}$ =1.7 M in 2 M H_2SO_4) and into the negolyte (70 cm^3 of $[V^{3+}]_{eq.,\ t=0}$ = 1.7 M in 2 M H_2SO_4). The resulting suspensions were left under stirring overnight in order to try to humidify and disperse the KB nanoparticles into the acidic electrolytes.

Before the beginning of the electrolysis, the $I = f(\eta)$ curves were plotted with these suspensions and the results (not shown here) were similar to what was observed in Fig.V.4 (i.e. without KB nanoparticles), except for the higher current magnitude but it is not really evidenced here because of the limited capacity of the potentiostat, I_{max} = 1 A.

Then the suspensions were submitted to electrolysis (recharge of the battery) expecting to achieve a conversion of 50%. The current chosen (0.6 A) is identical to the one applied above for a better comparison. During the electrolysis, it was observed that the carbon black was not totally "wetted" in the $V^{(III)}$ suspension (particles floating on the surface of the liquid), while the $V^{(IV)}$ suspension appears to be uniform (KB completely wetted). As previously discussed (chapters I and III), functional groups containing oxygen on the surface of the graphite enhance its electroactivity for the VO_2^+/VO^{2+} system [4-5]; moreover this phenomenon can be amplified by various thermochemical treatments [6]. Nevertheless, to our knowledge there is i) no effect produced by the KB on the current produced at the negative electrode, and ii) no effect on the humidification of the solution, probably because of the absence of interactions between the KB nanoparticles and the non-oxygenated species of the vanadium in solution, i.e. V^{3+} and V^{2+}.

In Fig.V.12 are presented some parameters monitored during the electrolysis. The graph **(II)** shows the cell voltage which remains practically constant during 4 h of electrolysis. Note that in the previous electrolysis carried out without KB (curve red in graph **(II)**) the cell voltage increases after ~2.7 h. The comparison of both graphs clearly demonstrates that the presence of KB causes the enhancement of the limiting current (both I_{lim} for VO^{2+} oxidation and V^{3+} reduction). Thus implies an increase of the time required to decrease the magnitudes of these limiting currents until the applied current.
The analysis of the overpotentials shows certain stability for both electrodes and confirms the above conclusions. The value of $\eta_{(-)}$ is stabilized around -0.17 V and increases slightly (from ~ |-0.15| to ~ |-0.26| V) during the 4 h electrolysis, while it doubles in the electrolysis without KB. The magnitude of $\eta_{(+)}$ is similar to the previous one (reversible system).

The presence of KB nanoparticles can affect the system in two ways:

- the first one is the decrease of the ionic conductivity of the solution because of the presence of solid particles; however this effect can be assumed as 'low' because of the low content of KB in the suspension (0.12 g for 70 cm^3, i.e. ~ 100 g);
- the second effect, appearing to be more significant, could be the electronic percolation (created by the KB aggregates) which contributes to increase the electronic transfer from the bulk to the electronic collector (WE), i.e. the electrode surface area. Note however, that this percolation needs to affect both the posolyte and the negolyte, but it is mentioned above that a fraction of the KB floats on the negolyte surface.

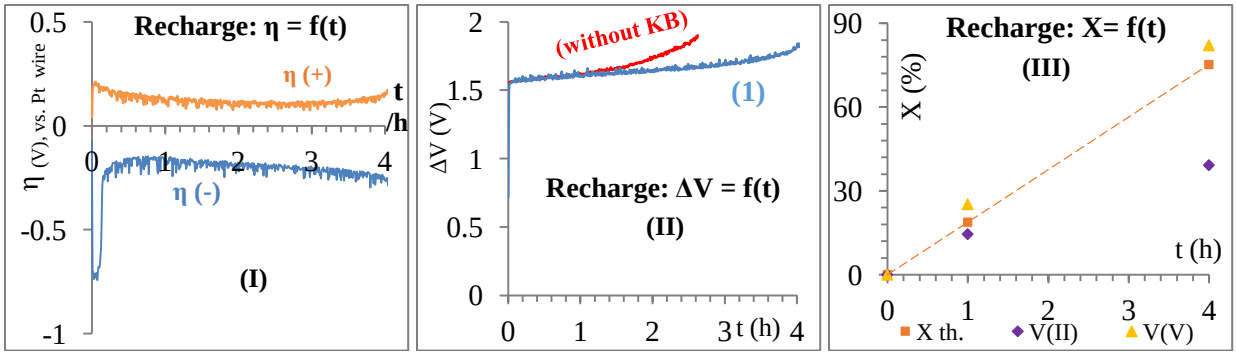

Fig.V.12: Results of the galvanostatic electrolysis (i.e. recharge of the VRFB) performed using a filter press electrochemical reactor coupled with two storage tanks; $I_{applied}$= 0.6 A; flow rate = 40 L/h; $T_{reservoirs}$ = 25°C.
Posolyte: 70 cm^3 of initial solution containing $[VO^{2+}]_{t=0}$ = 1.7 M and 0.12 g of KB nanoparticles in 2 M initial sulfuric acid; Negolyte: 70 cm^3 of initial solution containing $[V^{3+}]_{eq.,\ t=0}$ = 1.7 M and 0.12 g of KB nanoparticles in 2 M initial sulfuric acid;
The graphs provide the temporal evolutions: Graph **(I)**: overpotentials (of the positive and the negative electrodes); Graph **(II)**, blue curve (1): cell voltage ΔV; Graph **(III)**: theoretical (orange square - dashed line) and experimental (diamonds and triangles) ratios of the electrogenerated products (% of the initial concentration of the reagents converted to product) for VO_2^+ (from VO^{2+}) and V^{2+} (from V^{3+}). Graph **(II)**, red curve "without KB": imported from Fig.V.5-**(I)** for comparison.

The analysis of the (residual reagents) $V^{(IV)}$ and $V^{(III)}$, usually carried out by UV-Vis spectrometry, was not attempted because of the presence of KB nanoparticles, which disturbs the absorbance; besides the KB nanoparticles were difficult to remove by filtration.

The graph **(III)** of Fig.V.12 presents the temporal evolution of the theoretical (orange squares - dashed line) and the experimental (diamonds and triangles) ratio of the electrogenerated products (% of the initial concentration of the reagents converted to the product) for VO_2^+ (from VO^{2+}) and V^{2+} (from V^{3+}). The galvanostatic conditions under which the electrolysis is undertaken induces a linear variation of the theoretical conversion (which is the same for both products VO_2^+ and V^{2+}) with time. At $t_{electrolysis}$= 4 h, the value of the theoretical conversion of the VO^{2+} to VO_2^+ reaches 75 % (instead of the initially fixed 50 %). The observed increase is due to the enhancement of the current by the KB.

Besides two different behaviors are observed for the experimental conversion:

- concerning the temporal evolution of the ratio of the electrogenerated VO_2^+, it seems linear and slightly higher than the theoretical evolution of the conversion (at t = 4 h, $X_{th.}$~ 75 % < $X_{exp.}$~ 80 %). It is impossible to obtain more than the expected quantity; consequently, the difference (5 %) is attributed to the experimental errors (estimated to be ~ 6 %), and more specifically to the difficulty to have a good measurement of the electrolytes volume.
- the temporal evolution of the experimental conversion of the electrogenerated V^{2+}, is not linear and significantly lower than the theoretical values (at t = 4 h, $X_{th.}$ ~ 75 % < $X_{exp.}$ ~ 40 %). Moreover this conversion is slightly lower if compared to the one obtained during the electrolysis without KB nanoparticles (at t = 2.7 h, $X_{V^{3+} \text{ to } V^{2+}}$ ~ 42 %).

Two facts could explain this discrepancy:

i) the first one could be the consumption of the electrogenerated V^{2+} by chemical reaction with the oxygen which could be introduced into the negolyte: 1) in adsorbed form in the KB nanoparticles (the KB floats on the surface of the negolyte), or 2) from outside through the pipes and the connectors of the experimental setup;

ii) another possibility could be the existence of a secondary electrochemical reaction at the negative electrode (H^+ to H_2 for example) possibly caused by an eventual adsorption of the KB. This point will be discussed below with the *I = f(η)* curves.

Fig.V.13 presents the curves *I = f(η)* plotted after the end of the recharge (t = 4h). The obtained limiting currents agree with the above discussion concerning the obtained conversions of VO_2^+ ($|I_{lim}|_{V^{(V)}} > I_{lim\ V^{(IV)}}$) and of V^{2+} ($|I_{lim}|_{V^{(V)}} > I_{lim\ V^{(II)}}$).

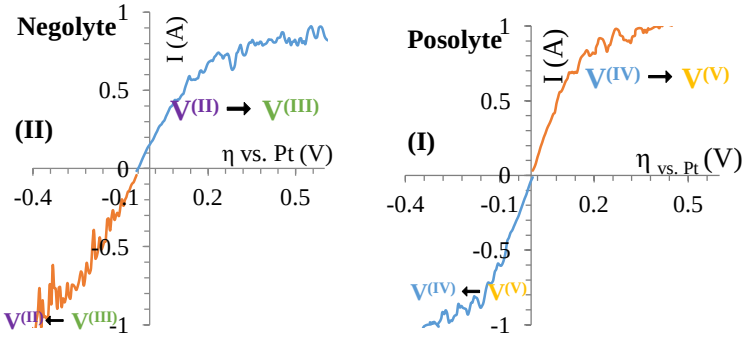

Fig.V.13: I = f(η) curves plotted at the end of the electrolysis (t = 4 h) performed with 0.12 g of KB in 70 cm^3 of electrolyte. $[VO^{2+}]_{t=0\ h}$ = $[V^{3+}]_{t=0}$ = 1.7 M. Estimated concentrations after 4 h of electrolysis: $[VO^{2+}]_{t=4\ h}$ ~ 0.3 M; $[VO_2^+]_{t=4\ h}$ ~ 1.4 M; $[V^{3+}]_{t=4\ h}$ ~ 1 M; $[V^{2+}]_{t=4\ h}$ ~ 0.67 M. WE = solid graphite (S_g = 20 cm^2); RE = Pt wire; CE = solid graphite; flow rate = 40 L/h; r = 10 $mV.s^{-1}$; Storage tanks stirred (500 RPM of the CSS) and thermoregulated (25 °C).

Note that the curve obtained for the reduction of V^{3+} shows a "rather fast system" exhibiting a limiting current (~ - 1 A) higher than the applied current during the electrolysis (0.6 A). This seems to exclude any negative effect of the KB on the graphite negative electrode, but rather privileges the effect of chemical reaction of V^{2+}/O_2.

Note also that the effect of the KB on the solid $V_2(SO_4)_3$ was not elucidated, however, it is obvious that the limiting current of the V^{3+} remains high, thus meaning that, at least, the KB

contributes to disperse and to dissolve the solid $V_2(SO_4)_3$ with no negative effect on the electrochemical reduction of V^{3+}.

Moreover assuming an ideal behavior of the posolyte for example, and taking into account a conversion of 75 %, we can propose a theoretical initial current for the oxidation of the $V^{(IV)}$: $I_{lim\ t=0} = I_{lim\ t=4h\ (1A\ at\ least)} \times (100\%\ of\ 1.7\ M)/(25\%\ of\ 1.7\ M) = 4$ A for 20 cm², i.e. 2 kA/m² which is very 'adequate' for an industrial application. Doing the same calculation for the recharge in the absence of KB (§ V.2.1.2) gives a theoretical initial current of 1.6 A for the oxidation of $V^{(IV)}$ to $V^{(V)}$, i.e. 0.8 kA/m^2, which means that the presence of KB nanoparticles increased the theoretical limiting current by 2.5 times.

To conclude in this section, even if the KB nanoparticles do not disperse completely into the negolyte, their effect on the positive electrode is beneficial because they enhance by 2.5 folds the maximum current that the positive electrode can deliver (until 2 kA/m²). Besides, it is expected that the values of the maximum current at the negative is also high (> 1 kA/m²), but lower than that of the positive because of the lower solubility of the vanadium (III) salt.

V.2.3.2. Performance of the battery during its discharge – Study of the improvement due to KB nanoparticles

The discharge of the battery in the presence of KB nanoparticles was performed in order to compare the results with the one obtained in the absence of KB (§ V.2.2), thus the operating parameters were kept the same; for example the $I_{applied}$ is - 0.27 A, a value lower than the limiting currents of $V^{(II)}$ and $V^{(V)}$ indicated by the $I = f(\eta)$ curves of Fig.V.13. The results obtained during the discharge are presented in Fig.V.14, graphs **(I)** and **(II)**.
The electrolysis was pursued until reaching the rapid decrease of the cell voltage (~ 2 h), which is ~ 50 min more than the one obtained for the electrolysis without KB. The presence of KB which causes the increase of the limiting currents is responsible for the longer electrolysis time, also implying a higher conversion during the discharge.

Once again the system appears (graph **(II)**, $\eta_{(-)}$) to be limited by the lower concentration of $V^{(II)}$.

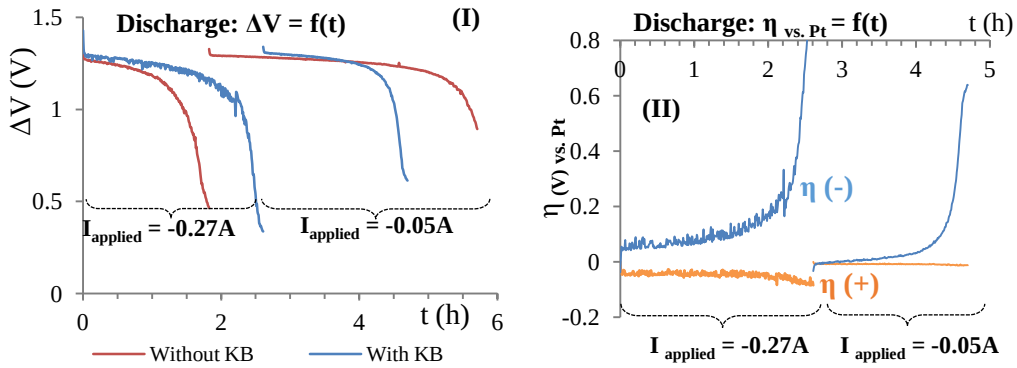

Fig.V.14: **(I)**: Evolution of the cell voltage with time during the discharge of the battery which was held in two parts: at $I_{applied}$ = -0.27 A and $I_{applied}$ = -0.05 A for the electrolytes containing KB particles, comparatively to the discharge in the absence of KB (red curves) held at the same currents (exported from Fig.V.8-(I)); **(II)**: evolution of the electrodes over-potentials with time, measured on both electrodes (positive (orange) and negative (blue)) with the Pt wire as a pseudo-reference and for the two applied currents; flow rate = 40 L/h; $T_{reservoirs}$ = 25 °C.

After 2.7 h the applied current was decreased to - 0.05 A and the electrolysis was pursued until the cell voltage abruptly decreases (and the over-potential increases). Compared to the results in section V.2.2, the duration of this second sequence is shorter since the first sequence of the discharge was performed for a longer time, which means that theoretically a higher conversion was achieved and the remaining species do not need a long time to be converted.
The magnitude of the over-potential of the positive electrode ($V^{(IV)}/V^{(V)}$) during the second sequence (t >2.7 h, I = -0.05 A) of this discharge, is practically zero, because i) the system is reversible and ii) the applied current is very low.
The *I = f(η)* curves, plotted at the end of the discharge, showed a limiting current of ~ 0.05 A for the $V^{(II)}$ and ~ - 0.4 A for the $V^{(V)}$ which constitutes an important gap between the two electrolytes.

At the end of the recharge, the faradaic yield of the $V^{(II)}$ is only 52 % compared to ~ 100 % for the $V^{(V)}$ (with an error of ~ 6 % for each analyzed concentration). At the end of the discharge, the experimental conversion of $V^{(II)}$ is higher than the theoretical value, as already seen previously in the absence of KB (Fig.V.8) and it was attributed to the spontaneous reaction of $V^{(II)}$ with oxygen instead of its electrochemical oxidation to $V^{(III)}$.

The presence of KB nanoparticles led, at constant electrolysis durations, to higher conversions than the electrolysis without KB, because of the enhancement of the surface of the electronic collector in the bulk.

The results obtained during these first experiments will constitute a base for the comparison with other electrolysis in different conditions. These electrolyses will be presented and discussed in the upcoming parts of the chapter and they include: the effect of the quantity of solid particles on

the charge-discharge of the battery, the effect of the presence of KB particles and the energy yield during cycling.

V.3. Effect of the presence of solid particles on the performance of an all-vanadium redox flow battery

In the following part of the chapter, the different experiments performed will be presented along with the corresponding experimental conditions and procedures and the obtained results. The comparison and analysis of these results will however be left for the next section (§ V.4.) where they will be assembled to be able to compare them correctly and conclude.

The first set of experiments will consist in studying the effect of the presence of vanadium solid particles on the behavior/performances of the battery (cell voltage, over-potentials and conversions), starting by the recharge to ~ 50 % of its capacity and then pursuing with the discharge back to its initial state; similar operations to those performed in sections V.2.1 and V.2.3 will be carried out (titrations, monitoring of parameters,…).

Then after analyzing and understanding the phenomena occurring in the presence of vanadium suspensions (with or without KB), the cycling of the battery will be undertaken, expecting to evaluate the energetic yield and to compare it to the same electrolyses carried out with vanadium solutions (without solids). The equivalent vanadium concentrations studied herein are 2.5 and 3.5 M of initial $V^{(III)}$ and $V^{(IV)}$ for the first part of the study and 3.2 M for the cycling without and with (0.17 %) of KB.

As a function of the availability of the vanadium powder, the solutions can be recycled (from previous solutions after adjustment), or prepared entirely from a new powder. The recycled solutions of the posolyte could contain residual quantities of $V^{(V)}$; the latter was quantified and taken into account. The recycled solutions of the negolyte contain solely $V^{(III)}$ because any eventual residual $V^{(II)}$ was rapidly oxidized by the oxygen. The suspensions were prepared by adding the required amount of powder into 70 cm^3 of a solution of 1.7 M of dissolved vanadium in 2 M initial sulfuric acid (partially dissolved in the case of $V^{(III)}$). The total volume of the resulting suspension is considered later for any calculation of the 'exact equivalent concentration' of species.

V.3.1. Study of a suspension containing an equivalent concentration of 2.5 M of vanadium

As performed previously, the electrolysis enabling to recharge the battery was started with a current of 0.6 A and the expected conversion to reach is 50 %. The overall duration of the electrolysis here is 5.5 h.

Fig.V.15 presents the monitoring of the cell voltage (graph **(I)**), and the overpotentials for the positive and for the negative electrodes (graph **(II)**) as well as the conversions (graph **(III)**).
The theoretical conversion reached is 58 % for both $VOSO_4$ and $V_2(SO_4)_3$. Their theoretical residual concentrations in the bulk are 1.27 M for VO^{2+} and ~ 1.7 M for V^{3+}. Note that here, as the electrolysis time increases, both VO^{2+} and V^{3+} are consumed, thus their respective salts dissolve and their concentration remains constant and equal to their solubility (assuming their dissolution kinetic is rapid).
Taking into account their solubility, at the end of the electrolysis the posolyte should not contain any solid; indeed, experimentally no solid particles were visible in the posolyte and all of the $VOSO_4.5H_2O$ powder was dissolved and the formed $V^{(V)}$ remained soluble.
Concerning the VO_2^+ its experimental conversion was calculated after deducting its initial residual amount present into the used solution; it was found at the end of the electrolysis that 59.7 % of $V^{(IV)}$ was converted to $V^{(V)}$.

Concerning the negolyte at the end of the electrolysis, theoretically, the concentrations of V^{3+} and V^{2+} must be equal to 1.45 and 1.05 M respectively (after a 58 % theoretical conversion). Besides their solubilities in the electrolysis conditions are 2.25 M for the V^{2+} and 1.1 M of V^{3+}, the limit of dissolution of $V_2(SO_4)_3$ observed in this work. Thus, there are supposedly no more solid particles in the negolyte. However, the experimental conversion shows that only 33% of V^{3+} was (experimentally) converted to V^{2+}, which means that there is still $V_2(SO_4)_3$ solid in the negolyte.

The curve in graph **(II)** shows that the cell voltage increases slowly from ~ 1.5 V to ~ 1.9 after 4.5 h of electrolysis, and then it increases more rapidly until reaching 2.1 V.
The analysis of the over-potential curves shows that:
- $\eta_{(+)}$ is practically constant and fluctuates between 110 and 140 mV;
- $\eta_{(-)}$ exhibits the same evolution as that indicated and commented on Fig.V.5;

The observed increases in both cell voltage and the overvoltage in the negative electrode could be explained by the fact that the concentration of V^{3+} dissolved in solution becomes lower than its solubility, and the saturation is not maintained due to a slow dissolution of the powder, thus, the corresponding limiting current becomes lower than the applied current.

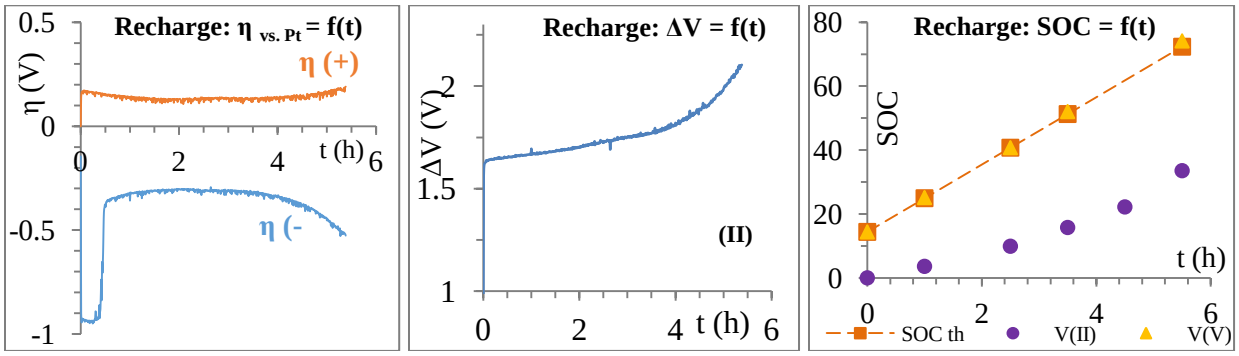

Fig.V.15: Results of the galvanostatic electrolysis (i.e. recharge of the VRFB) performed using a filter press electrochemical reactor coupled with two storage tanks. Total equivalent vanadium concentration at the beginning: 2.5 M for the posolyte and 2.5 M for the negolyte; $I_{applied}$= 0.6 A; flow rate = 40 L/h; $T_{reservoirs}$ = 25°C. The graphs provide the temporal evolutions: Graph **(I)**: overpotentials (of the positive (orange) and the negative (blue) electrodes); Graph **(II)**: cell voltage ΔV; Graph **(III)**: theoretical (orange squares - dashed line) and experimental (purple diamonds and yellow triangles) state of charge for V^{2+} (from V^{3+}) and VO_2^+ (from VO^{2+})

The analysis of Fig.V.15-(III) shows:

- the SOC of the posolyte does not start at 0 because as explained at the beginning the suspension was prepared by adding $VOSO_4$ powder into the solution retrieved from the1.7 M electrolysis, thus containing already some $V^{(V)}$ ($[VO_2^+]$ ~ 0.36 M);
- a good correlation (± 1.8 %) between the theoretical and the experimental SOC of the VO_2^+ in the posolyte. It should be noted that the concentration of $V^{(IV)}$ was determined during the recharge and that the total amount of vanadium in the posolyte ($V^{(IV)}$ + $V^{(V)}$) is constant at all times and equal to ~ 2.5 M;
- discrepancies between the theoretical and the experimental SOC of the $V^{(II)}$: the experimental values corresponds to more than the half of the theoretical ones. Various explanations can be proposed:
    - as explained before, the parasitic O_2 oxidize the V^{2+} produced by reduction of V^{3+};
    - the ratio SOC_{th}/SOC_{exp} decreases with time, which could mean that the V^{2+} is more easily attacked by oxygen when it is at low concentrations in solution; when $[V^{2+}]$ starts to increase it appears that the rate of spontaneous oxidation becomes lower but this needs to be verified in future studies.

The *I = f(η)* curves presented in Fig.V.16 were plotted after stopping the electrolysis; their analysis must provide information enabling to choose the corresponding current to apply in order to carry out the discharge. Note that, here, the idea is to choose a current magnitude enabling:

- to operate rapidly (the optimum time to carry out the experiments is ~ 8 h).
- to achieve the fixed conversion before reaching the potential range of the reaction of the solvent (i.e. to be selective for both recharge and discharge and to operate with high faradic yield);
- to avoid unexpected problems (heating implying uncontrolled evaporation, introduction of oxygen, destruction of the membrane…).

More systematic electrolyses must be performed later in order to enable rigorous comparisons.

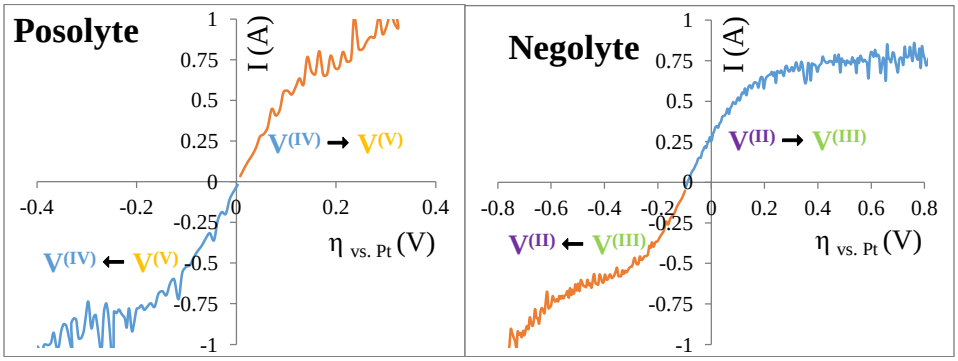

Fig.V.16: I = f(η) curves plotted at the end (t = 5.5 h) of the electrolysis described in Fig.V.19; Total initial vanadium concentration in each reservoir: equivalent to 2.5 M in 2 M initial sulfuric acid; Estimated concentrations of: $[VO^{2+}]_{t=5.5\ h}$ ~ 1.27 M; $[VO_2^{+}]_{t=5.5\ h}$ ~ 1.49 M; $[V^{2+}]_{t=5.5\ h}$ ~ 0.84 M; $[V^{3+}]_{t=5.5\ h}$ ~ 1.66 M; WE = solid graphite (S_g = 20 cm^2); RE = Pt wire; CE = solid graphite; flow rate = 40 L/h; r = 10 $mV.s^{-1}$; Storage tanks stirred (500 RPM of the CSS) and thermoregulated (25 °C); 85 cm^3 of electrolyte.

The V^{2+} limiting current (0.75 A) is higher than that of the V^{3+} (0.57 A at η = - 0.4 V). This means that either a conversion higher than 50 % was obtained for the negolyte as well, or the limiting current of the $V^{(III)}$ corresponds only to the dissolved fraction while the rest of the species are still in solid form, since at this point there was still vanadium (III) powder in the electrolyte. The first applied current for the discharge is fixed at – 0.37 A, corresponding to the half of the $V^{(II)}$ limiting current.

The temporal evolution of the cell voltage is indicated in Fig.V.17. The curve shows that the discharge has been carried out in three steps and under three different applied currents. In fact, as the cell voltage becomes lower than 0.5 V, the applied current was lowered and the electrolysis was pursued. The couples 'applied current/duration' were respectively: - 0.37A/1 h 25 minutes, - 0.25A/2 h 35 minutes, and - 0.07A/2 h 30 minutes.

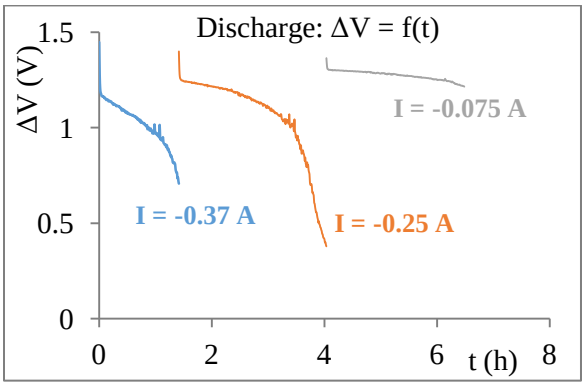

Fig.V.17: Temporal evolution of the cell voltage during the galvanostatic discharge of the battery, performed under three applied currents, respectively -0.37 A (blue), -0.25 A (orange) and -0.075 A (grey). Electrolytes: suspensions obtained during the battery recharge, at 50 % of conversion of the initial vanadium concentration (equivalent to 2.5 M); flow rate = 40 L/h/compartment; $T_{reservoirs}$ = 25 °C.

During the discharge, the *I = f(η)* curves for the oxidation of the V^{2+}, plotted at different stages, are presented in Fig.V.18-**(I)**. These curves exhibit a plateau indicating a mass transfer

limitation. Plotting the limiting current against the V^{2+} concentration (graph **(II)**) shows a linear evolution (Eq.V.5) and the obtained slope ($I_{lim}/[V^{2+}] = nFSk$) enables calculating the mass transfer coefficient $k = D/\delta$. Its value ($4.4 \times 10^{-6}\ m/s$) is relatively low, translating a relatively poor hydrodynamic performance into the electrolytic compartment (Note that here the idea is to have a uniform flow into the compartment and to avoid any case of clogging).

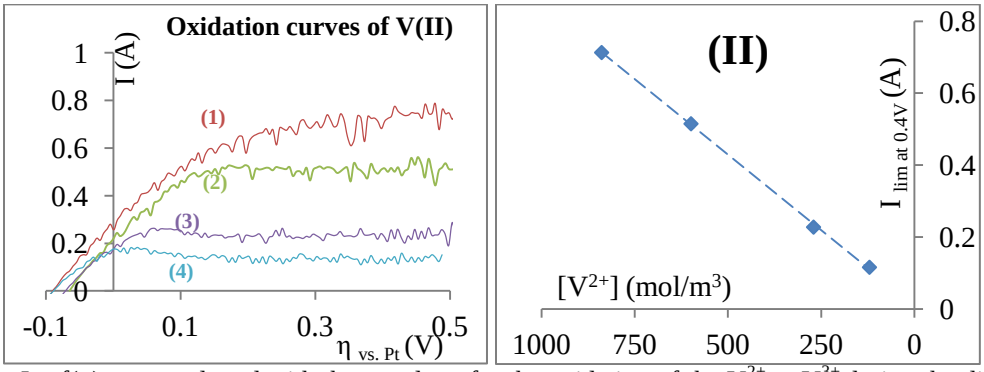

Fig.V.18: **(I)**: I = f(η) curves plotted with the negolyte, for the oxidation of the V^{2+} to V^{3+} during the different steps of the discharge: (1-red): before the start of the discharge; (2-green): at the end of the 1st step of the discharge at $I_{applied}$ = - 0.35 A; (3-violet): at the end of the 2nd step of the discharge at $I_{applied}$ = - 0.27 A; (4-blue): at the end of the 3rd step of the discharge at $I_{applied}$ = - 0.075 A. WE = solid graphite (S_g = 20 cm^2); RE = Pt wire; CE = solid graphite; flow rate = 40 L/h; r = 10 $mV.s^{-1}$; **(II)**: evolution of the current measured at η = 0.4 V as a function of the $V^{(II)}$ concentration.

$I_{lim,at\ 0.4\,V} = 8.5 \times 10^{-4}[V^{2+}]$ during the discharge of the VRFB Eq.V.5

According to T. Yamamura et al. [3], the diffusion coefficient of V^{2+} is equal to 2.4x10^{-10} m^2/s, measured on a graphite electrode, with $[V^{2+}]$ = 0.05 mol/dm^3 and $[H_2SO_4]$ = 1 mol/dm^3. Assuming this value is 'exact', an estimation of the thickness of the diffusion layer is 54.5 µm, which is between 1 and 5 folds higher than the value of δ obtained on a rotating disc electrode (~ 1-10 µm).

Lastly, the state of charge was estimated from the $V^{(II)}$ and $V^{(V)}$ concentrations to compare with the corresponding theoretical values. First, concerning the theoretical evolution, the linear shape observed during the recharge disappears during the discharge, simply because the discharge is undertaken under three different currents to remain lower than to the limiting current of the less concentrated species.

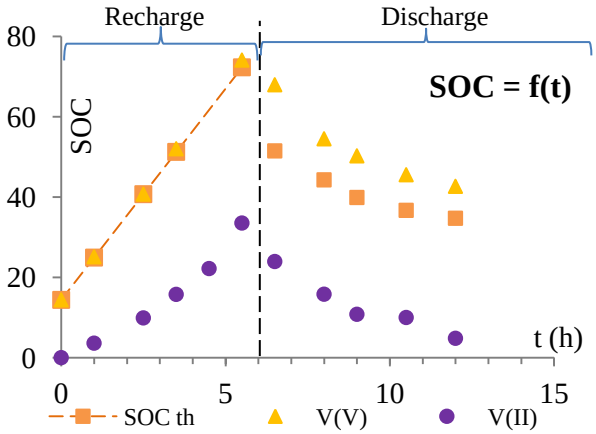

Fig.V.19: Comparison between the theoretical SOC (orange cubes) and the experimental SOC for $V^{(II)}$ (violet diamonds) and $V^{(V)}$ (yellow cubes) after the recharge to 50 % of initial vanadium suspensions at equivalent concentration of 2.5 M; flow rate = 40 L/h; $T_{reservoirs}$ = 25 °C; the recharge data is imported from Fig.V.15 for comparison.

The evolution of the SOC calculated from the negolyte during the discharge has the same behavior as the one observed during the charge (lower than the theoretical values). However, at this point this can be considered accurate since the value of conversion reached at the end of the recharge dictates the available amount of $V^{(II)}$ to perform the discharge. In addition, diffusion towards the posolyte can be a cause of loss of the $V^{(II)}$.
As for the $V^{(V)}$, a gap of ~ 10 % is observed and can be attributed to the uncontrollable changes of the electrolyte volume, due to the dissolution of the $VOSO_4$ powder during the recharge phase, plus the possible transport of water and/or vanadium from the negolyte. These changes can contribute, in addition to the experimental error, to the observed discrepancies.
The faradic yield estimated from the $V^{(V)}$ concentrations is near 75 % during the discharge.

V.3.2. Study of a highly loaded suspension (equivalent concentration of 3.5 M of vanadium)

The objective in this paragraph consists in preparing and electrolyzing a highly loaded suspension of vanadium containing an equivalent concentration of 3.5 M of each reagent ($VOSO_4$ and $V_2(SO_4)_3$. To that end the previously used suspensions, containing an equivalent concentration of 2.5 M of vanadium, were used to prepare the required suspension for the present experiment. Note that the $V^{(II)}$ remaining at the end of the previous discharge, has been oxidized by contact of the suspension with air, so the negolyte contains only $V^{(III)}$ in its two forms, dissolved and powder. As for the posolyte, the remaining $V^{(V)}$ concentration is titrated and is found to be equal to 1 M, which was taken into account when adding the excess $V^{(IV)}$ powder to reach a total vanadium equivalent concentration of 3.5 M.

The applied current was chosen to be the same as before, namely 0.6 A, and theoretically, at this current, 6.6 hours were required to convert 50 % of the species in each compartment (it should

be reminded that 50% is the conversion selected to start the comparative cycles of charge/discharge of the battery).

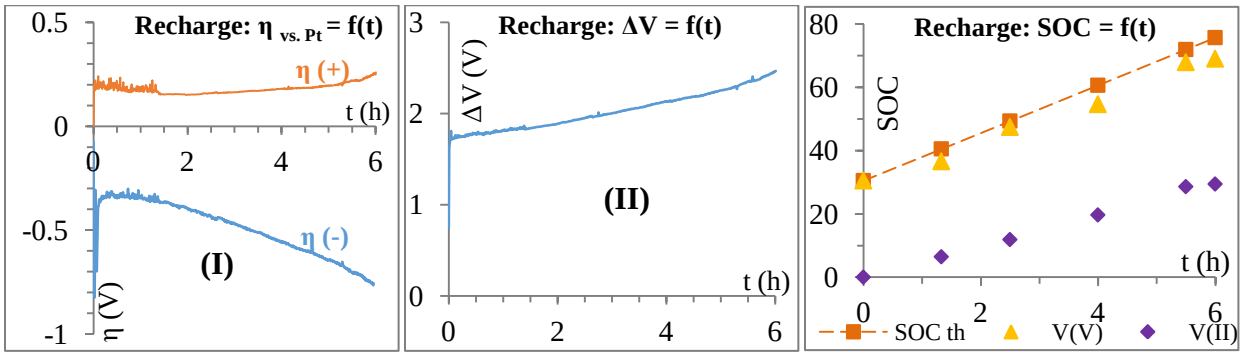

Fig.V.20: Results of the galvanostatic electrolysis (i.e. recharge of the VRFB) performed using a filter press electrochemical reactor coupled with two storage tanks. Total equivalent vanadium concentration at the beginning: 3.5 M for the posolyte and 3.5 M for the negolyte; $I_{applied}$= 0.6 A; flow rate = 40 L/h; $T_{storages\ tanks}$= 25°C. The graphs provide the temporal evolutions: Graph **(I)**: overpotentials (of the positive and the negative electrodes); Graph **(II)**: cell voltage ΔV; Graph **(III)**: theoretical (orange squares-dashed line) and experimental SOC calculated for the electrogenerated V^{2+} (from V^{3+}) (violet diamonds) and VO_2^+ (from VO^{2+}) (yellow triangles).

It should be noted that during the recharge (and later the discharge also) the negolyte appears as a viscous suspension while the posolyte was more fluid despite the presence of a small fraction of solid particles. Even with a strong stirring of the suspension, it is extremely difficult to take a simple aliquot of the suspensions which contains representative/reliable quantities of the liquid and of the solid. Hence, all the analyses indicated in the Fig.V.20-III cannot be taken into account. We performed these analyses simply to get an idea about the various concentrations. The SOC of the posolyte starts at 30 % because of the presence of 1 M VO_2^+ in the initial electrolyte and the behavior of $V^{(II)}$ has been explained in the previous electrolyses.

I = f(η) curves were plotted with the negolyte after the end of the recharge and presented in Fig.V.27. Then, the electrolyte mixtures were stored under stirring and nitrogen flow until the next day. Before to start the discharge, the same I = f(η) curves were plotted and presented in Fig.V.27 for comparison. The curves exhibit the same shape and similar magnitudes of the current for the reduction of V^{3+}. Concerning the oxidation of the V^{2+} some difference is evidenced in the limiting currents of the negolyte, and the plateau shifts to a peek; this could indicate a certain passivation of the electrode, probably due to a partial precipitation of the electrogenerated $V^{(II)}$. Another important point to mention is the anodic limiting (or peak) currents magnitudes for $V^{2+} \rightarrow V^{3+}$: they appear 'low/ ~ 0.68 A (for the curve 1b)' compared to the one observed (~ 0.75 A) for example with the negolyte, at a total vanadium equivalent concentration of 2.5 M (Fig.V.16). Strict comparison requires the knowledge of the exact conversion, operation difficult to achieve; however the higher fraction of the solid $V_2(SO_4)_3$ i.e. 3.5 against 2.5 equivalent mol/L could justify this decreases (by the increase of the apparent viscosity and the subsequent decrease of the diffusion coefficient).

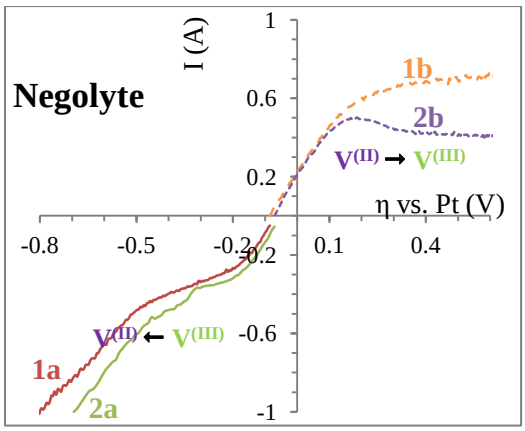

Fig.V.21: Comparison of the I = f(η) curves plotted with the negolyte 1) immediately after the interruption of the recharge electrolysis described in Fig.V.20 and 2) after 12 h of waiting under stirring and bubbling of nitrogen. WE = solid graphite (S_g = 20 cm^2); RE = Pt wire; CE = solid graphite; flow rate = 40 L/h; r = 10 $mV.s^{-1}$. $[VO^{2+}]_{t=6\ h}$ ~1.2 M; $[VO_2^{+}]_{t=6\ h}$ ~2.4 M; $[V^{3+}]_{t=6\ h}$ ~1.8 M; $[V^{2+}]_{t=6\ h}$ ~1 M.

Taking into account these results, we decide for the first discharge to apply a current of - 0.27 A (~ 50% of the limiting current of the $V^{(II)}$ (dissolved form)). The discharge was performed under three sequential steps of decreasing applied currents, respectively at - 0.27, - 0.075 and - 0.05 A, chosen in agreement with the evolution of the cell voltage. The evolution of the curves is similar to what was observed for previous electrolyses except that the electrolysis duration here is much higher compared for example with the one presented in Fig.V.17 performed with a higher current.

Note that a sudden drop of the cell voltage at t = 6.77 h is observed; in fact, the discharge was stopped overnight and continued the next day. It is obvious that the chemistry of the mixture, at least at the interface, has been changed; an eventual precipitation at the interface, or the establishment of an equilibrium between two different acid/base forms of the $V^{(III)}$ occurring during the night may be the cause of this behavior. The last fraction of the discharge enabling to achieve a total conversion of ~ 30 % of the $V^{(V)}$ was undertaken at -0.05 A.

The state of charge of the VRFB was estimated for the $V^{(II)}$ and $V^{(V)}$ during the discharge (Fig.V.22): the correlation between the theoretical and experimental values appear to be satisfactory (Δ(SOC) ≈ 5 %) in the case of the posolyte but completely incorrect in the case of $V^{(II)}$ which follows the tendency started during the recharge.

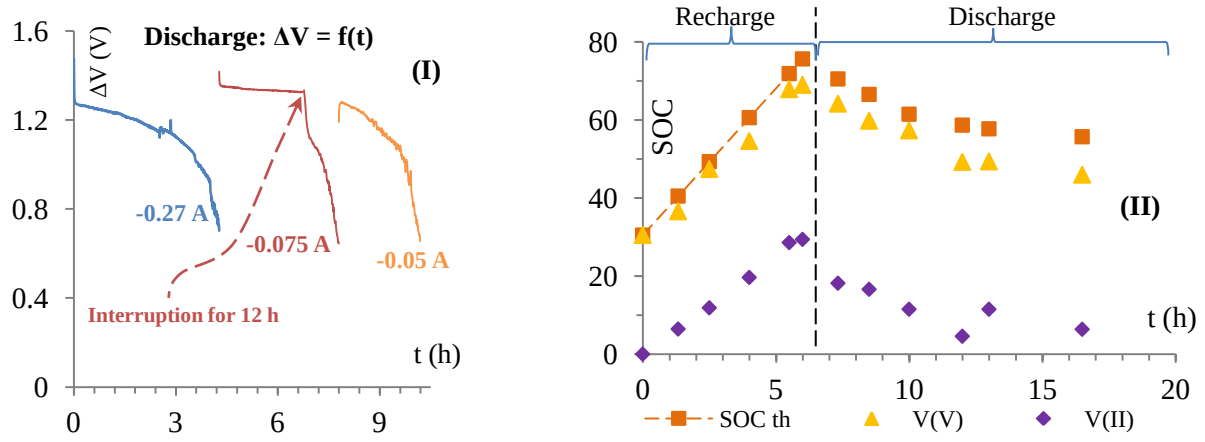

Fig.V.22: **(I)**: Temporal evolution of the cell voltage, during the discharge of the battery performed in three steps: at $I_{applied}$ = -0.27 A (blue), -0.075 A (red) and -0.05 A (orange); the electrolyte suspensions were obtained after a recharge by ~ 50 % of initial electrolytes containing the vanadium at a concentration equivalent to 3.5 M; flow rate = 40 L/h; $T_{reservoirs}$ = 25 °C; **(II)**: Comparison between the theoretical SOC (orange cubes) and the experimental SOC for $V^{(II)}$ (violet diamonds) and $V^{(V)}$ (yellow cubes) after the recharge to 50 % of initial vanadium suspensions at equivalent concentration of 3.5 M; flow rate = 40 L/h; $T_{reservoirs}$ = 25 °C; the recharge data is imported from Fig.V.20 for comparison.

The faradic yield, estimated from the $V^{(V)}$ concentrations, is near 100 % in the presence of an equivalent total vanadium concentration of 3.5 M, but this value is affected by the errors induced from the presence of solid particles and the modification of the suspensions volume and viscosity during the electrolysis, all contributing to the error of the experimental titration.

In conclusion, the study of the electrolysis of a suspension containing 3.5 M of equivalent vanadium concentrations appeared to have a setback corresponding to the analysis of the species during the charge and discharge. The presence of solid particles introduces an additional factor to be taken into account for the dilutions and measurements; yet, distinguishing between the two phases of the mixture is not possible or requires a multi-step experimental procedure that could have also its own setbacks.

The amount of added powder was not increased further than the equivalent of 3.5 M, since at this concentration the viscosity of the negolyte was already important through the electrolysis, and a bigger amount would cause additional circulation and clogging problems.

V.3.3. Cycling of the battery in the presence of solid particles: vanadium and KB

In this section the objective is to perform cycles of ‘recharge/discharge’ and to examine the performances of the battery (I, faradic and energy yield, unexpected problems) by monitoring and analysis of the evolutions of the various operating parameters. To that end, two different operations will be performed: ‘cycling in absence’ and ‘cycling in presence’ of the electronic conductive material, i.e. the KB nanoparticles. Moreover the idea is to operate with electrolytes

highly loaded in suspension containing vanadium powders. The above electrolysis was performed using an equivalent concentration of 3.5 M of vanadium; however, without any chemical additive, the obtained suspension of $V^{(III)}$ mainly was very viscous and relatively difficult to flow into the reactor and also to stir in the storage tank. Taking into account that KB will be introduced later, means that the resulting mixture will not be flowable (without any chemical additives).
Besides the highly loaded suspensions of the negolyte and the posolyte behave differently on the hydrodynamic point of view (see chapter II, § II.4). In fact, the various vanadium salts fix various numbers of water molecules [7]. That is why the initial load in vanadium is chosen to be 3.2 equivalent mol/L for the cycling.

For the cycling performed in the presence of KB, two initial solutions were prepared containing respectively 1.7 M of $V^{(IV)}$ and 1.7 M of $V^{(III)}$. Then 0.16 g of KB was added in each solution and the resulting suspensions were left under stirring overnight. Then the excess of vanadium powder enabling to reach the equivalent of 3.2 M was added, and the total volume of the obtained suspensions reaches 95 cm^3.

We decide to start the cycling having initially into the suspensions the four forms of the vanadium, i.e.:

- in the posolyte ~ 50% of $V^{(IV)}$ and 50 % of $V^{(V)}$;
- in the negolyte ~ 50% of $V^{(III)}$ and 50 % of $V^{(II)}$.

Besides we also decide to perform cycles achieving a conversion (in both the negolyte or in the posolyte) of 10 %/half-cycle, in order to enable feasible experiments in a reasonable time.

Thus the preliminary operations consisted in converting 50 % of the initial electrolytes through charging the battery at a constant current. This initial charging is not the targeted step of this study; hence, no particular attention was given to it. For the two experiments, in the presence and absence of KB nanoparticles, a current of 1 A was applied to the battery for 2 h after which the current was decreased to 0.6 A for 4 hours. The theoretical conversion achieved with these parameters is around 54 % which can be considered enough to start the studies of the cycling.

V.3.3.1. Equivalent vanadium concentration of 3.2 M

The experimental procedures applied for this electrolysis are the same as used before: plotting the $I = f(\eta)$ curves at t = 0, monitoring the cell voltage and overpotentials and analyzing the vanadium species to calculate the achieved conversion during the initial charge, then determine the corresponding current for the charge-discharge cycling of the prepared mixtures.

The initial step of preparation of the mixtures allowed obtained the following concentrations, considered as the t = 0 for the cycling: $[VO^{2+}]$ ~ 1.7±0.15 M, $[VO_2^{+}]$ ~ 1.75±0.05 M; $[V^{2+}]$ ~

1.48±0.05 M; $[V^{3+}]$ ~ 1.9±0.15 M, with an SOC of 54.7 %, according to the vanadium (V) concentration.

After analysis of the $I = f(\eta)$ curves, as well as some preliminary runs, the current magnitude to apply is ± 0.4 A for the cycling. The monitoring of the cycling was performed identically to the electrolyses before and the vanadium species were analyzed at the end of each half-cycle. A total of 4.5 cycles was undertaken in the battery, with t = 4 h the duration of a full cycle which was calculated as a function of the theoretical aimed conversion of 10 % per half-cycle.
The results, presented in Fig.V.23, show that reproducibility of the charge-discharge cycles is achieved after one complete cycle; the values of the cell voltage become constant in recharges and discharges for the cycles (2), (3) and (4). The analysis of the evolution of the overpotentials with time confirms the stabilization of the system after the first cycle.

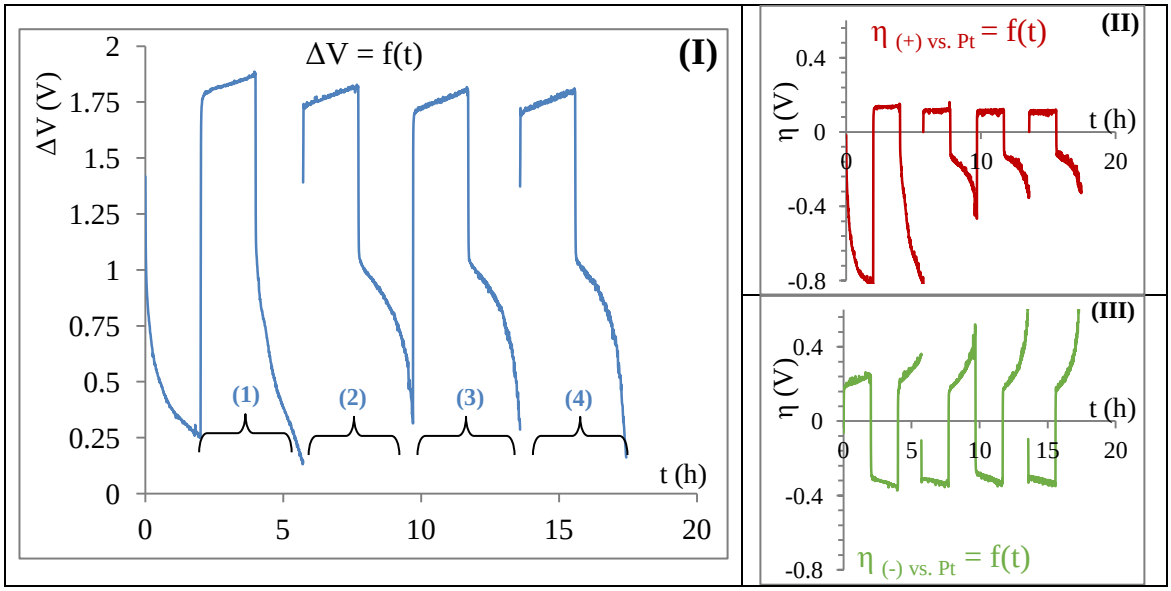

Fig.V.23: Evolution of the electrochemical parameters with time during charge-discharge cycles of the battery at an applied current of ± 0.4 A, for a mixture of $V^{(IV)}/V^{(V)}$ suspension in the posolyte ($[VO^{2+}]_{t=0,\ cycling}$ ~1.7±0.15 M, $[VO_2^{+}]_{t=0,\ cycling}$ ~1.65±0.05 M) and a mixture of $V^{(II)}/V^{(III)}$ ($[V^{2+}]_{t=0,\ cycling}$ ~1.4±0.05 M; $[V^{3+}]_{t=0,\ cycling}$ ~1.9±0.15 M) suspension in the negolyte; **(I)**: evolution of the cell voltage; **(II)**: evolution of the over-potential of the positive electrode; **(III)**: evolution of the over-potential of the negative electrode; the total vanadium concentration in each electrolyte is equivalent to 3.2 M in 2 M initial sulfuric acid; flow rate = 40 L/h; $T_{reservoirs}$ = 25°C.

The cell voltage values are presented in the table V.2. When the system is stabilized (cycles 2 to 4) the values of the cell voltage are between 1.70 and 1.81 V (beginning and end of each step) for the recharge and 1 to 0.8 V during the discharge.
Ideally, the evolution of ΔV during the discharge should resemble that of the charge; this could have been obtained with a lower imposed current which could be more suitable for the species

involved. The energetic yield obtained during cycling of an equivalent total vanadium concentration of 3.2 M was calculated and the results will be presented and discussed in section V.4.

Table.V.2: Evolution of the cell voltage values during the charge and the discharge; values measured at t ~ 2 min and t ~ 1 h of each half-cycle.

		$\Delta V_{t \sim 2\ min}$	$\Delta V_{t \sim 1\ h}$
Recharge	Cycle 2	1.73	1.83
	Cycle 3	1.70	1.82
	Cycle 4	1.72	1.81
Discharge	Cycle 2	1.05	0.85
	Cycle 3	1.04	0.84
	Cycle 4	1.05	0.81

The evolution of the state of charge of the battery estimated with the analyzed $V^{(V)}$ during cycling is presented in Fig.V.24 and compared to the theoretical SOC.

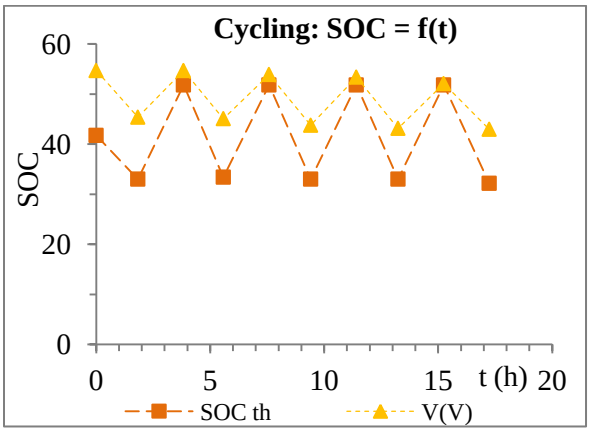

Fig.V.24: Temporal evolutions of the SOC of VO_2^+ (yellow triangles) determined experimentally and compared to the theoretical SOC (orange squares). The point at t = 0 corresponds to the SOC obtained at the end of the initial recharge (~ 40 % $SOC_{theoretical}$); total vanadium concentration equivalent to 3.2 M in the posolyte and the negolyte; V_{total} = 95 cm^3; $T_{reservoirs}$ = 25 °C.

The evolution of the experimental SOC follows the same trend as the one observed in the cycling performed for the 1.7 M vanadium concentration (Fig.V.11-(IV)). The values are in the range of the theoretical evolution: during recharge, the experimental value does not reach the desired theoretical value but for the discharge, a satisfactory correlation is witnessed.
The values calculated from the $V^{(II)}$ are not presented as they follow the same evolution as observed earlier (Fig.V.11-(IV), Fig.V.19, Fig.V.22).

The faradic yield calculated from the $V^{(V)}$ conversions during cycling is greater than 95 %, which is also the case of the cycling performed in the absence of solid particles (Fig.V.11), which

means that that the presence of vanadium powder in the VRFB does not have a negative impact on the yield of the system.
In addition, the cell voltage provided from the battery between the recharge and the discharge is around 1 V, compared to ~ 0.5 V in the case of the cycling at the electrolyte concentration of 1.7 M.

V.3.3.2. Equivalent vanadium concentration of 3.2 M in presence of KB

The effect of the presence of carbon nanoparticles has been already addressed in a vanadium saturated solution (in the absence of vanadium solid particles). In this part, the experimental procedure of cycling undertaken in the previous section will be repeated in the presence of KB (0.16 g in 95 cm^3 of electrolyte suspension).
The percent of KB introduced (0.17 %) is calculated without taking into account the real weight of the suspension, i.e. the 95 cm^3 are considered to weight 95 g which is certainly not the case.
The initial charge is performed under the same experimental conditions as the electrolysis without KB. The obtained concentrations for the titrated $V^{(II)}$ and $V^{(V)}$ are 1.36 and 1.69 M respectively with an SOC of ~ 53 % according to the $V^{(V)}$.
Then the cycling was started under the same applied current I = ± 0.4 A for the charge and discharge.

The evolution of the cell voltage (Fig.V.25) is similar to that obtained in the absence of KB; indeed, except for the first discharge (which enable to stabilize the system), the cell voltage for the following cycles are reproducible in terms of ΔV values and curve shape; it is not necessary to decrease the applied current. It can be also noticed that cycle (2) is wider than the others; the reason is that during the charge, it was unintentionally continued for fifty additional minutes, which led to adding these 50 min to the subsequent discharge in order to compensate the conversion. The magnitudes of the ΔV are reported in table V.2. When the system is stabilized (cycles 2 to 4) the values of the cell voltage are between 1.7 and 1.8 V (beginning and end of each step) for the recharge and 1.15 to 0.97 V during the discharge. The examination of the overpotentials shows that their evolutions are similar to that of ΔV.

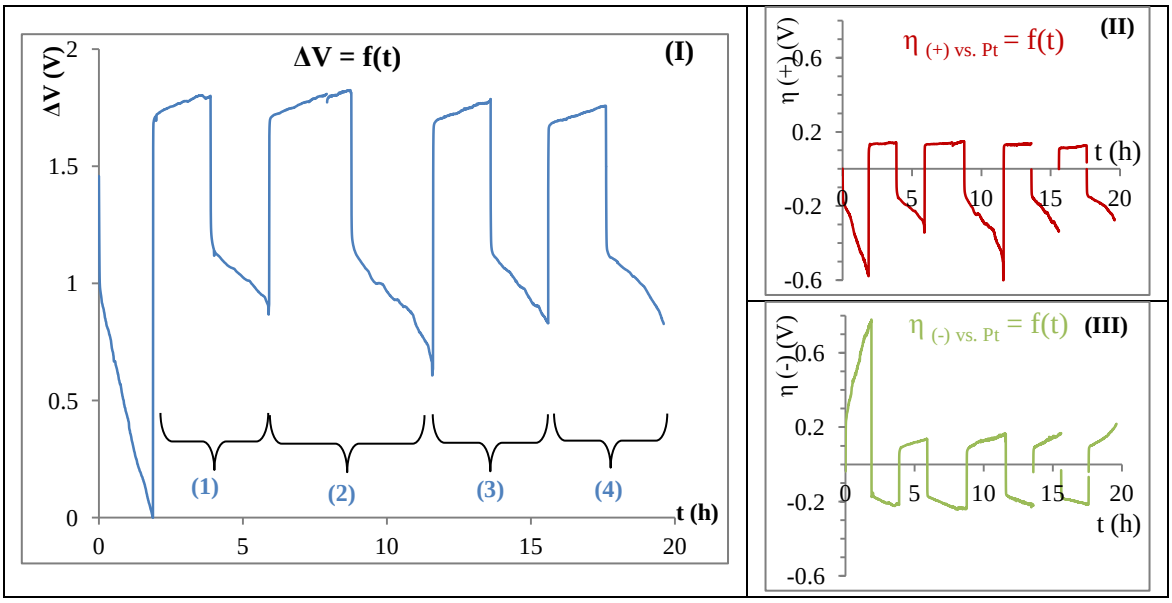

Fig.V.25: Evolution of the electrochemical parameters with time during charge-discharge cycles of the battery at an applied current of ± 0.4 A, for a mixture of $V^{(IV)}/V^{(V)}$ suspension in the posolyte ($[VO_2^+]_{t=0,\ cycling}$ ~1.69 M) and a mixture of $V^{(II)}/V^{(III)}$ suspension in the negolyte ($([V^{2+}]_{t=0,\ cycling}$ ~1.36 M); **(I)**: evolution of the cell voltage; **(II)**: evolution of the over-potential of the positive electrode; **(III)**: evolution of the over-potential of the negative electrode; the total vanadium concentration in each electrolyte is equivalent to 3.2 M in 2 M initial sulfuric acid containing 0.16 g of KB in 95 cm^3 of suspension; flow rate = 40 L/h; $T_{reservoirs}$ = 25°C.

Table.V.3: Evolution of the cell voltage values during the charge and the discharge; values measured at t ~ 2 min and t ~ 1h of each half-cycle

		$\Delta V_{t \sim 2\ min}$	$\Delta V_{t \sim 1\ h}$
Recharge	Cycle 1	1.7	1.8
	Cycle 2	1.72	1.77
	Cycle 3	1.66	1.79
	Cycle 4	1.66	1.74
Discharge	Cycle 1	1.15	1.04
	Cycle 2	1.1	0.97
	Cycle 3	1.13	1
	Cycle 4	1.1	0.98

The evolution of the state of charge of the battery estimated with the analyzed $V^{(V)}$ during cycling is presented in Fig.V.26 and compared to the theoretical SOC.

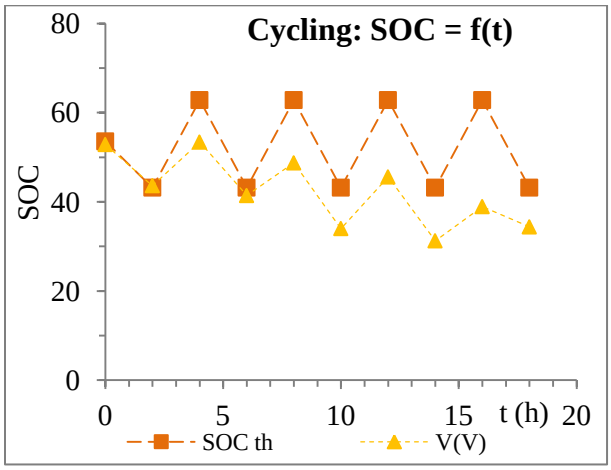

Fig.V.26: Temporal evolutions of the SOC of VO_2^+ (yellow triangles) determined experimentally and compared to the theoretical SOC (orange squares). The point at t = 0 corresponds to the SOC obtained at the end of the initial recharge (~ 40 % $SOC_{theoretical}$); total vanadium concentration equivalent to 3.2 M in the posolyte and the negolyte with 0.16 g of KB nanoparticles; V_{total} = 95 cm^3; $T_{reservoirs}$ = 25 °C.

The evolution of the experimental SOC estimated from the $V^{(V)}$ concentration appears to decline with time and deviate from the theoretical values and from the behavior observed earlier (1.7 M and 3.2 M without KB). This discrepancy can be attributed to the presence of KB solid particles in the electrolyte that would induce an additional error to the experimental analysis of the vanadium (sample withdraw, volume modification…). The faradic yield y_f is estimated to vary between 75 and 95 % throughout the cycling.

In conclusion, it appears that the presence of KB and solid vanadium particles together in the electrolyte mixtures were not harmful for the functioning of the battery (acceptable y_f). It was possible to charge the battery to around 50 % of its capacity and then perform 4 charge-discharge cycles under an applied current of 0.4 A for 20 cm^2 (200 A/m^2), in reproducible conditions and with a highly loaded suspension (equivalent concentration 3.2 mol/L).

V.4. Interpretation of the results and comparison between the electrolyses

After having presented the experimental results for different electrolyses, especially cycling, the comparison of the performances of the battery can be done through the calculation of the energetic yields recovered as a function of the composition of the electrolytes as well as the capacity (energy density) of the battery.

The study of the impact of the amount of vanadium solid particles on the charge-discharge of the VRFB was performed with equivalent concentrations of 1.7, 2.5 and 3.5 M of total vanadium in each reservoir prepared in an initial 2 M H_2SO_4 solution.
First it was necessary to charge the battery. This recharge, aiming to convert 50 % of the available quantity of vanadium, was undertaken with the same applied current (0.6 A) for the

three experiments in order to be able to compare the results. The three evolutions of the cell voltages are presented in Fig.V.27. As the equivalent concentration of the vanadium increases, the time for which ΔV is 'constant' is high.
The cell voltage increases because at least one of the limiting currents becomes lower than the applied current, thus a fraction of the applied current is spent for secondary reactions. The reason why the cell voltage remained constant longer is that the solid particles, added in excess of the solubility, dissolve and supply the suspension in active species thus helping to maintain a saturated electrolyte with a constant limiting current. When the dissolution is not fast enough to compensate the electronic conversion or the electrolyte does not contain any more solid particles, the limiting current starts to decrease which leads to the increase of the cell voltage.

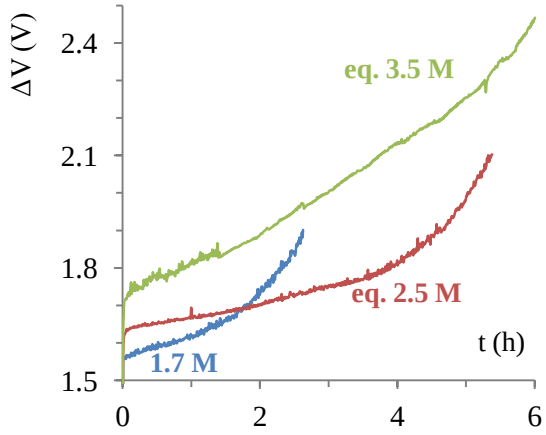

Fig.V.27: Comparison of the cell voltages temporal evolutions (ΔV = f(t)) of the VRFB obtained during its preliminary charge (to ~ 50 %), under an applied current of 0.6 A for three different concentrations of electrolyte solutions/suspensions, prepared in 2 M H_2SO_4: blue/ 1.7 M; red/ equivalent of 2.5 M; green/ equivalent of 3.5 M; flow rate = 40 L/h; $T_{reservoirs}$ = 25 °C.

Conversely to the other evolutions, a practically linear evolution was observed, from the beginning, for the curve corresponding to 3.5 M equivalent concentration. The fact that it contains more quantity (powder) of the vanadium than the previous one can help to explain this increase: indeed, the dissolution of the powder enables to increase the duration of the electrolysis and consequently the concentrations of both dissolved $V^{(V)}$ and $V^{(II)}$. This leads to an increase of the viscosity of the solution (or, more accurately, suspension at 50% of conversion) because the powder absorbed some of the existing water [7].

The comparison of the three overpotentials shows the same evolution with the vanadium concentrations as observed for the cell voltage which is normal since both values are interdependent. The temporal increase of the overpotentials values, with the increase of the amount of added powder is due to the increase of the viscosity and resistivity of the suspensions.

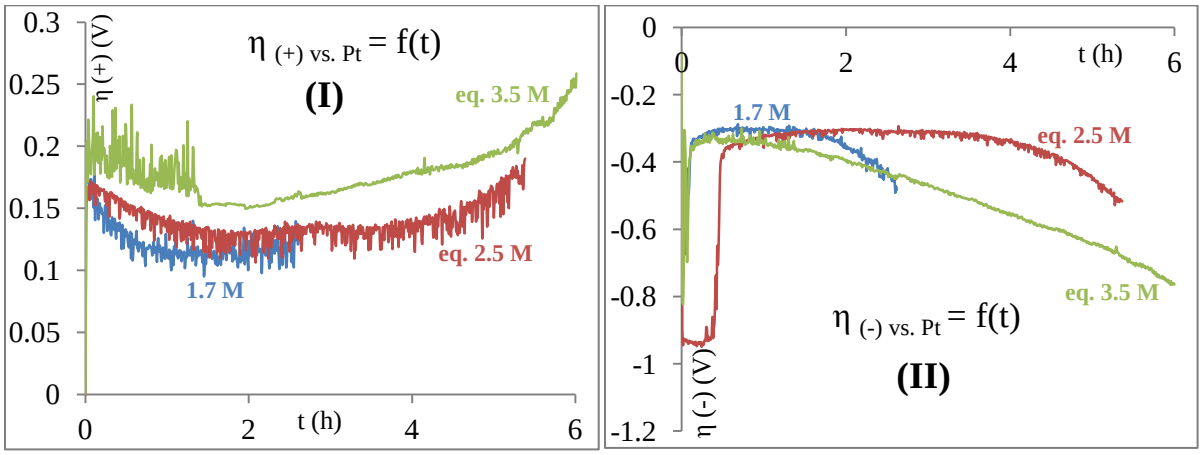

Fig.V.28: Comparison of the electrodes over-potentials of the VRFB measured between the graphite working electrode and the Pt wire in each compartment (**I**: posolyte; **II**: negolyte) during the initial charge at an applied current of 0.6 A for three different concentrations of electrolyte solutions/suspensions prepared in 2 M sulfuric acid: blue/1.7 M; red/equivalent of 2.5 M; green/equivalent of 3.5 M; flow rate = 40 L/h; $T_{reservoirs}$ = 25 °C.

Concerning the discharge undertaken for each electrolyte mixture, the comparison of the cell voltages is difficult because each discharge was done at an applied current suitable for the limiting electrolyte composition formed after the end of the initial charge.

The theoretical state of charge of the VRFB was calculated for all the experiments and compared to the experimental SOC, estimated thanks to the analysis performed for the concentrations $V^{(II)}$ and $V^{(V)}$ through potentiometric titration. It was found that the values calculated from the $V^{(V)}$ concentrations had a satisfactory correlation with the theory, with discrepancies (~ 5 %) attributed mostly to the experimental errors. However, all the analysis performed for the $V^{(II)}$ showed that the concentrations were always lower than the theory, implying a higher conversion which is impossible to obtain and this error was discussed in detail for each case.

As a conclusion for the effect of the amount of powder on one charge-discharge cycle in the battery, it appears that the presence of vanadium solid particles increases the ohmic drop of the system which impacts mostly the cell voltage. However, no negative impact was observed so far concerning the presence of these particles, i.e. neither the cell voltage was cancelled nor the electrodes passivated or inactivated because of the presence of solid. The impact of the viscosity modification during the cycling of the VRFB, by the dissolution of the powders, the generation of $V^{(II)}$ and $V^{(V)}$ and the production and consumption of acid at the posolyte, was not addressed and it would constitute an important aspect to address in future studies.

The cycling of the battery (i.e. 4 to 5 successive charge/discharge) was studied on three different electrolyte mixtures: near saturation concentration (1.7 M), equivalent concentration of 3.2 M and equivalent concentration of 3.2 M in the presence of KB particles. An initial charge was necessary to prepare the electrolytes for cycling by converting, at constant current, around 50 %

of the initial $V^{(III)}$ and $V^{(IV)}$ constituting the negolyte and the posolyte respectively. After that a current of ± 0.4 A was chosen for the cycling of the battery; this choice is a function of the lowest limiting current (V^{2+} or VO_2^+) obtained after the initial charge of the mixture. It was found that this choice of the applied current is crucial, especially for the lowest concentration during the discharge, where the cell potential would decrease rapidly before the end of the required time to reach the fixed conversion in the corresponding half cycle. Besides it was found that at constant equivalent vanadium concentration (3.2 M) the presence of KB was beneficial (increase of the limiting current/slight decrease of the cell voltage) and its impact was more pronounced during the discharge.

It should be noted that the curve corresponding to the cycling with KB (green curve) has been edited on its second cycle in order to visualize better the overlay with the cycling in the absence of KB. The values of ΔV are slightly lower when the electrolyte suspensions contain carbon nanoparticles: this could be attributed to the enhancement of the limiting current by the electronic percolation network created by the KB particles inside of the reactor (this enhancement causes the overvoltage to decrease, at constant applied current).
The energy yield EY of the VRFB needs to be calculated to really compare the effect of each parameter (for example the KB nanoparticles). EY corresponds to the ratio of the useful energy to the energy supplied, or in other words the quantity of energy recovered during the discharge to the energy spent for the recharge (Eq.V.6).

$$EY = \frac{E_{used}}{E_{supplied}} = \frac{E_{discharge}}{E_{charge}} = \frac{\int \Delta V \times I \times dt_{discharge}}{\int \Delta V \times I \times dt_{charge}} \qquad \text{Eq.V.6}$$

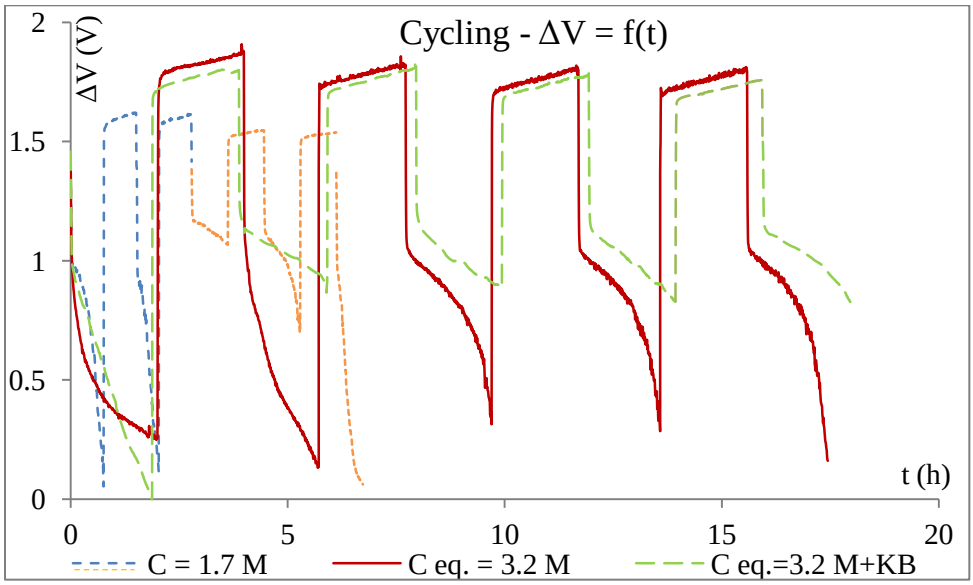

Fig.V.29: Comparison of the cell voltage of the VRFB obtained during cycling of the battery for three different concentrations of total vanadium prepared in 2 M sulfuric acid: blue (- - - -) and orange (-----)/ 1.7 M (§ V.2.2); red

(continuous line)/ equivalent of 3.2 M (§ V.3.3.1); green (long dashes)/ equivalent of 3.2 M + 0.16 g of KB in 95 cm^3 of electrolyte (§ V.3.3.2). Curves extracted from Fig.V.11, 23 and 25

Hence, by plotting $\Delta V_{(t)} \times I = f(t)$ at constant current and equivalent charge-discharge time for both steps, the integration of the surface under the curve gives the values of E_{used} and $E_{supplied}$.
For the lowest concentration of 1.7 M in total vanadium, since the applied current had to be decreased in order to be able to continue the cycling of the battery, the energy yield will be calculated for 1 cycle performed at ± 0.4 A and 1 cycle performed at ± 0.3 A. Also, the first discharge for all the concentrations will not be taken into account because it corresponds to the previous charge which was the preparation of the electrolyte mixtures; thus the four full cycles after that will serve for the calculations. The obtained results are presented in table V.4.

Table V.4: Comparison of the energy yield calculated for the cycles of the cycling performed for three electrolyte mixtures: $[V]_{total}$ = 1.7 M, $[V]_{total, eq.}$ = 3.2 M and $[V]_{total, eq.}$ = 3.2 M + KB

$[V]_{total, equivalent}$ (M)	t_{cycle} (h)	N° cycle	$I_{applied}$ (A)	EY (%)
1.7	1	1	0.4	38
	1h40	3	0.3	68.4
3.2	4 h/cycle	2	0.4	45.1
		3		44.5
		4		41.9
3.2 + KB	4 h/cycle	2	0.4	57.2
		3		58.2
		4		58.9

First, the comparison is performed between the cycles of each concentration to see if there is a loss in the efficiency during the cycling. For the 1.7 M vanadium concentration, it is clear that decreasing the applied current was beneficial to the efficiency of the battery and the energy yield increased by ~ 1.8 times. In addition the time of a full cycle at 0.3 A is longer which does not allow fully comparing the two values. Hence, it was tried to calculate the EY for an equivalent cycling time: the curve was edited and 20 minutes were taken off from the end of the charge and the end of the discharge and the EY was recalculated but that did not change the answer much and EY was found to be 70 %. In any case, to be able to compare the efficiency to the other concentrations, we have to use the value obtained at an applied current of 0.4 A, thus 38 %.

Secondly, for the cycling of the equivalent total concentration of 3.2 M, for cycles 2, 3 and 4, the energy yield decreases slightly with the number of cycles from 45 to 42 %; this decrease is not significant for the number of cycles performed. For the cycling in the presence of carbon black, the energy yield appears to increase slightly along the cycles from 57.2 to 58.9 %.

This could mean that the presence of the KB nanoparticles helps to stabilize the battery and maintain its efficiency through time. A higher number of cycles are required in order to confirm

that assumption in addition to a cycling at low vanadium concentration (1.7 M) in the presence of that same amount of KB.

Comparing the evolution of the energy efficiency with the total amount of vanadium present in the electrolyte mixture shows that, at a higher concentration, the energy yield is enhanced (7 % increase of EY) in addition to the increase of the energy density through the higher amount of vanadium in the electrolytes. On the other hand, the presence of 0.17 % in weight of KB particles in a 3.2 M equivalent of vanadium enhanced even more the energy yield of the VRFB and increased it by more than 10 %, at equivalent quantity of stored energy since the total vanadium concentration is the same.
Note that around 40 % of energy was lost between the recharge and the discharge. It is important to mention that in this study the idea was to increase the energy stored and as much as possible the power of the system. Consequently all the actions carried out concern this point: to get an operative battery containing highly loaded electrolytes. The optimization of the electrode surface was not included here; moreover several other operating parameters (water content, acid quantity, surfactant additives), need to be managed in order to reduces these important losses.

Remark: Another method allowing calculating EY is the comparison of the energy supplied during the recharge to the effective energy used for the conversion of the species, i.e. the quantity of vanadium transformed during the phase of charging the VRFB. In fact, the Gibbs free energy of the overall reaction (Rx.V.3) can be written as a function of the two half reactions (Rx.V.1 for $V^{(IV)}/V^{(V)}$ and Rx.V.2 for $V^{(II)}/V^{(III)}$) as:

$$\Delta_r G_3 = \Delta_r G_1 - \Delta_r G_2 \qquad \text{Eq.V.7}$$

For a reversible electrochemical reaction at constant temperature and pressure, the free enthalpy can be expressed as:

$$\Delta_r G = -nFE \qquad \text{Eq.V.8}$$

Where: $\Delta_r G$: Gibbs free energy change per mole of reaction (J/mol);
n: number of moles of electrons transferred in the reaction;

Replacing Eq.V.8 in Eq.V.7 leads to:

$$-n_3\, F\, E_3 = -n_1 F E_1 + -n_2 F E_2 \Rightarrow E_3 = E_1 - E_2 = \Delta V_{at\ I=0} \qquad \text{Eq.V.9}$$

Thus,
$$EY = \frac{\Delta V_{at\ I=0} \times n_{mol} \times F}{\int \Delta V_{at\ t} \times I \times dt_{charge}} \qquad \text{Eq.V.10}$$

Where: $\Delta V_{I=0}$: cell voltage in the absence of any current (V);
$\Delta V_{at\ t}$: cell voltage at any time through the charge (V);
n_{mol}: number of moles of vanadium converted during the charge (mol).

This approach can be used for the comparison of the EY as well, but it was clear from the conversions calculated through all the electrolysis that the vanadium quantities were not always

concordant especially between the negolyte and the posolyte. The experimental conversion was not reliable because of the problems of the volume of the mixture and also the withdrawn aliquots. Consequently, given the differences observed in the values of the calculated conversions and the comparison with the corresponding theoretical values, we decided that it would be better not to calculate the energy yield based on the analysis of vanadium concentrations and base the conclusion on the values obtained from the battery's voltage.

Another important parameter to compare is the amount of energy stored in the battery (𝔼) to be able to conclude on the researched effect of the use of suspensions as electrolytes. 𝔼 is defined as the ration of the energy stored during the charge (or recovered during the discharge) in Wh to the weight of the electrolyte mixture in kg (sulfuric acid + dissolved vanadium + excess powder). The results are presented in table V.5.

Table V.5: Average estimated energy density stored in the VRFB studied in this work

$[V]_{total,\ equivalent}$ (M)	1.7	3.2	3.2 + KB
$\mathbb{E}_{stored\ during\ recharge}$ (Wh/kg)	3	9.6	9.4
$\mathbb{E}_{recovered\ during\ discharge}$ (Wh/kg)	1.8	4.2	5.5

The analysis of the results shows that in the operating conditions of the present battery, the energy density is tripled when the vanadium equivalent concentration is increased by 1.88 folds. In fact, since the quantity of vanadium in the electrolyte tanks is higher, thanks to the presence of solid particles which dissolve during the functioning of the battery to supply the mixture with dissolved electroactive species, the amount of energy that could be stored would increase as well. Compared to the existing all-liquid vanadium batteries, the energy stored with the suspensions is ~ 4 times lower. However, we should keep in mind that the estimated values of 𝔼 are performed for cycles converting only 10 % of the total theoretical capacity of the battery (~ 8 Ah) per half-cycle at a current of 0.4 A and an electrode surface of 20 cm^2 (i = 0.02 A/cm^2).

It should be noted that the theoretical specific energy of the VRFB with the 3.2 M suspension is estimated to be ~ 86 kWh/m^3 of suspension compared to ~ 46 kWh/m^3 for the 1.7 M electrolyte, in a 2 M initial sulfuric acid concentration and at 25 °C.

In conclusion, it was found in this chapter so far, that the presence of solid particles in the electrolyte mixtures has a positive effect on the overall performance of the vanadium redox flow battery, whether these particles are vanadium powder or carbon black nanoparticles in small quantity (0.17 % in weight as proved in chapter III). The cycling of the battery was studied after

charging it to around 50 % of its capacity then performing 4 cycles at a constant current for three different electrolyte compositions, expecting a conversion of 10 % in each half cycle. It was found that in the presence of vanadium excess powder at an equivalent concentration of 3.2 M, the energy efficiency of the battery was increased by 7 % compared to the cycling at 1.7 M total vanadium and this increased to 10 % in the presence of vanadium and KB particles also compared to the cycling at 1.7 M total vanadium. On the other hand, the presence of solid brought i) an additional ohmic drop to the system reflected on the overall cell voltage and ii) a decrease in the diffusion coefficient, reflected on the limiting current and consequently on the individual over-potentials of the positive and the negative electrodes. The use of a Pt wire used as pseudoreference enabled to plot current – over-potential curves as required, and to determine the evolution of the limiting current throughout the electrolyses and to get an idea about the current to apply.
The presence of KB nanoparticles did not only benefit the energy yield of the battery but also impacts the amount of stored energy inside the battery as it was seen to triple comparatively to the 'all-liquid' reference of 1.7 M vanadium.

However, the quantity of added solid enabled to increase the equivalent concentration only by 1.75 times (3.5 M in 2 M initial sulfuric acid) compared to the existing VRFB (2 mol/L in 2 to 3 mol/L of sulfuric acid). The amount of powder was not increased further because the viscosity in the negolyte would constitute a problem due to the absorption of water by the excess powder of $V_2(SO_4)_3.xH_2O$. Surfactants effect as well as water management are two important points to consider in the future.

V.5. Establishment of theoretical mass balance models for an operating vanadium solid-liquid redox flow battery

The macroscopic mass balance equations were written for the various species of the battery, expecting to get a tool giving the theoretical evolution of their concentrations (and the conversion when possible), possibly for comparison with the experimentally determined concentrations, and also for examining the effect the various operating parameters (applied current, flow rate, temperature,...).
The VRFB used in this work is a filter press electrochemical divided reactor with two associated storage tanks. The reactor is a plug flow reactor i.e. the concentration of a species is uniform on a section of the reactor (orthogonal to the flow) but varies axially between its inlet and outlet.

In order to be able to set these equations and resolve them, a certain number of assumptions were introduced given the complexity of the system to which is added the presence of solid particles inducing dissolution – precipitation equilibriums. The macroscopic mass balances will be performed for the species into the reactor (assumed as pseudo stationary) and into the storage tanks which operates at the transient state. In fact i) as the volume of the reactor is lower than

that of the storage tank (6 cm^3 against 90 to 100 for the storage tank), and ii) as only galvanostatic electrolyses are performed, the system can be assumed (on the simple mass balance point of view) to be a single transient state stirred reactor.

In addition, the temperature is considered constant: the storage reservoirs are thermoregulated at 25 °C and we consider that the reactions inside the reactor are isothermal.

The species for which the mass balances will be written are 5 in total:

- four oxidation states of vanadium (VO_2^+, VO^{2+}, V^{3+} and V^{2+}) without taking into account the possible secondary forms present as well;
- protons H^+ (in fact H_3O^+, meaning the consumption of one water / H^+ !) generated by the dissociation of the sulfuric acid and from the reaction of the posolyte (Rx.V.1).

The other species present in the electrolytes, which are also an important component of the mixture, but for which the mass balance equations will not be written, are the following:

- water resulting/consumed from: i) the initial quantity introduced, ii) the dissolution and dissociation of the vanadium powders, iii) the reaction of the posolyte and iv) by the mass transport across the membrane;
- sulfates SO_4^{2-} only from the dissolution and dissociation of the vanadium powders. The second dissociation of the sulfuric acid:

  $HSO_4^- + H_2O \rightleftarrows H_3O^+ + SO_4^{2-}$ is low ($K_{HSO_4^-/SO_4^{2-}} = 0.013\ at\ 25°C$), concentrations in mol/kg [8], is not taken into account for the H^+ concentration nor for the sulfates;
- HSO_4^- is also present in the electrolytes but it will not be taken into account for the mass balance equations given the complexity of the possible reactions and different equilibriums involved.

Also, for each cited species there are several phenomena to take into account depending on the reaction and its placement (reactor or storage tank). These phenomena, occurring during the charge and resumed in table V.6, can be separated into: electrochemical reactions (oxidation and reduction), migration through the membrane, and physico-chemical reactions (precipitation and dissolution). During the discharge, the reverse phenomena occur for all of the species.

The simplified reactions taking place are reminded below:

$VO^{2+} + H_2O \leftrightarrows VO_2^+ + 2\ H^+ + e^-$ Rx.V.1

$V^{3+} + e^- \leftrightarrows V^{2+}$ Rx.V.2

In addition, the presence of solid particles implies important changes during their dissociation/precipitation:

$V_2(SO_4)_3.9H_2O \leftrightarrows 2\ V^{3+} + 3\ SO_4^{2-} + 9\ H_2O$ Rx.V.4

$$VOSO_4.5H_2O \leftrightarrows VO^{2+} + SO_4^{2-} + 5H_2O \qquad \text{Rx.V.5}$$
$$VSO_4.1.5H_2O \leftrightarrows V^{2+} + SO_4^{2-} + 1.5H_2O \qquad \text{Rx.V.6}$$

Table V.6: Phenomena taking place in the battery for the different species present in the electrolytes during the recharge of the battery.

Species	Phenomena in the reactor	Phenomena in the storage tanks
V^{2+}	- Produced by reduction of the dissolved V^{3+} (Rx.V.2)	- Accumulation of the produced species - Susceptible to precipitate when $[V^{2+}]_{solution} > s_{V^{2+}}$=2.75M at 25°C, $[H_2SO_4]$ = 2M [2]
V^{3+}	- Consumed for the reduction reaction to V^{2+}	- Dissolution of $V_2(SO_4)_3.9H_2O$ (Rx.V.4) The powder quantity decreases; $s_{V^{3+}}$=2.5M at 25°C, $[H_2SO_4]$ = 2M [2]
VO^{2+}	- Consumed for the oxidation reaction to VO_2^+ (Rx.V.1) - Susceptible to migrate to the negative compartment	- Dissolution of $VOSO_4.5H_2O$ (Rx.V.5) The powder quantity decreases; $s_{VO^{2+}}$=2.5M at 25°C, $[H_2SO_4]$ = 2M [2]
VO_2^+	- Produced by oxidation of the dissolved VO^{2+} - Susceptible to migrate to the negative compartment	- Accumulation of the produced species - No precipitation occurs during the electrolyses - $[VO_2^+]$ = 3 M in 5 M total sulfate stable for t > 1000 h at 20°C
H^+	- Produced by the oxidation reaction of $V^{(IV)}$ (Rx.V.1) - Susceptible to migrate to the negative compartment as H_3O^+	- Released by the first dissociation of the sulfuric acid - Susceptible to react with the sulfates produced by the dissociation of the vanadium salts
H_2O	- Consumed for the oxidation reaction to VO_2^+ - Susceptible to migrate to the negative compartment as H_3O^+ - Osmosis through the membrane	- Released by the dissolution and dissociation of $VOSO_4$ and $V_2(SO_4)_3$ (Rx.V.5 and Rx.V.4 respectively) - Consumed in case of V^{2+} precipitation (Rx.V.6)
SO_4^{2-}	- Electrochemically inert - Susceptible to migrate through the membrane (but will be neglected)	- Released by the dissolution and dissociation of $VOSO_4$ and $V_2(SO_4)_3$ (Rx.V.5 and Rx.V.4 respectively) - Consumed in the case of V^{2+} precipitation (Rx.V.6) - Reacts with H^+

It is noticed that in the case of the $V^{(V)}$ no precipitation reaction is added to the phenomenon taking place in the storage tanks: as a matter of fact, as described in the bibliography report of chapter I, the vanadium (V) can exist in a stable form at a concentration of up to 2 M during the functioning of the battery in a temperature range between 10 and 40 °C. In addition, in chapter III it was proved that it can be produced by electro-oxidation of $V^{(IV)}$ and can reach high concentrations (5 M, produced in the U-shaped cell) without precipitating. In the experiments

performed in the reactor (study of the effect of solid particles, cycling…) the total vanadium concentration never reached more than 3.5 M at 25 °C and even that was only converted to around 50 % so the maximum $V^{(V)}$ concentration reached at once is around 1.8 to 2 M, safe from precipitation.

All the precipitation and dissolution reactions will be assumed to occur in the storage tanks, because of the low volume of the electrochemical reactor compared to that of the storage tank.
As for the crossover of the species through the membrane, only migration is considered while diffusion and convection fluxes are assumed to be negligible. The convective flux in the Nafion membrane (which is 'dense') is negligible [9]. Concerning the diffusive flux, since it is directed by the concentration gradient of the vanadium species between the two compartments, it is believed that it remains 'low' and 'constant' between the recharge and the discharge of the battery and also similar for both compartments. Hence, it is decided not to incorporate it to the mass balance equations.

As for the migration through the membrane, during the recharge of the battery, the protons are transported from the positive electrode (oxidation of $V^{(IV)}$) to the negative electrode (reduction of $V^{(III)}$) to insure the circulation of the current inside the reactor (under ionic flow). They migrate in the form of H_3O^+ by passing through sulfate bonds inside the chain of the Nafion. Since it is a cationic membrane, all the positively charged ions present in the electrolyte are susceptible of migrating as well, which includes the four vanadium oxidation states. However, the migration of the vanadium ions across the membrane is much lower than that of the proton and depends on the transport number of each species (values of the diffusion coefficients given in tables V.7 and V.8). During the charge, VO_2^+ and VO^{2+} migrates with the proton and water towards the negative compartment and during the discharge, the V^{3+} and V^{2+} are the ones to migrate. The following side (electro)chemical reactions can occur in the positive electrode, during the discharge, under the condition that they are not directly reduced/oxidized on the electrode:

$$V^{2+} + 2\ VO_2^+ + 2\ H^+ \rightarrow 3\ VO^{2+} + H_2O \qquad \text{Rx.V.7}$$

$$V^{3+} + VO_2^+ \rightarrow 2\ VO^{2+} \qquad \text{Rx.V.8}$$

On the negative electrode and during the charge, the side reactions taking place are:

$$VO^{2+} + V^{2+} + 2\ H^+ \rightarrow 2\ V^{3+} + H_2O \qquad \text{Rx.V.9}$$

$$VO_2^+ + 2\ V^{2+} + 4\ H^+ \rightarrow 3\ V^{3+} + 2H_2O \qquad \text{Rx.V.10}$$

These reactions should be kept in mind but they will be taken into account for the calculations of the mass balances.

To summarize, the mass balance equations are constructed on the following assumptions:

1) All parts of the battery are considered isothermal (reactor and reservoirs);
2) The electrolyte flow is incompressible;

3) the solvent does not react during the electrolyses because the cell voltage and the amount of charge are controlled, thus hydrogen and oxygen are not produced;
4) Dissolution and precipitation reactions only occur in the storage tanks (thus expecting to avoid any passivation in the reactor).

The mass balance equations will be established as a function of the total mole quantity of the four species instead of the equivalent molar concentrations because of the existence of the solid fraction of the vanadium salts. This way it enables to overcome the necessity to distinguish between the dissolved and the solid part of the vanadium in the electrolyte which is not always evident.

The abbreviations used to designate the quantity of vanadium species, presented in Fig.V.2-(II), are reminded below:

$\mathbf{m^{i}_{in}}$: moles number of vanadium of oxidation state "i" at the **inlet of the reactor** (which corresponds to the outlet of the storage tank)
$\mathbf{m^{i}_{out}}$: moles number of vanadium of oxidation state "i" at the **outlet of the reactor** (which corresponds to the inlet of the storage tank)

V.5.1. Mass balance established during the recharge of the battery (galvanostatic mode)

The electrolyses were performed at a constant applied current, chosen as 50 % of the lowest experimentally measured limiting current: for example most often the oxidation of V^{2+} exhibits the lowest limiting current, thus it will used to determine the magnitude of the current to apply. As the concentration of the electroactive species remains constant (for example by dissolution of the solid particles present, i.e. $V^{(III)}$ in the negolyte and $V^{(IV)}$ in the posolyte), the limiting current also remains constant, and the total current applied is useful for the aimed reaction. The time for which the limiting current becomes equal to the applied current is called "critical time" (Fig.V.41). Therefore, if the applied current is not adjusted as function of the limiting current, a part of it does not serve for the main reaction of vanadium, but can be used for the solvent reaction for example.
The mass balance will be performed for the two cases: before $t_{critical}$ and after $t_{critical}$.

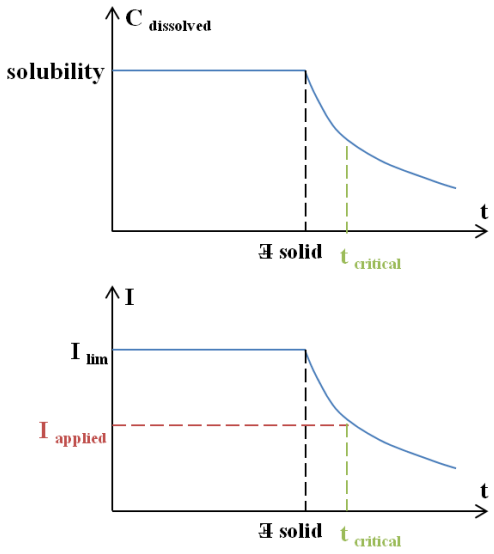

Fig.V.30: Schematic temporal evolutions of: i) the concentration of a species initially present under both dissolved and solid forms (top) and ii) the limiting current (bottom). The critical time is mentioned.

The mass balance equations will be applied to the electrolysis with an initial vanadium suspension with a concentration equivalent to 3500 mol/m^3 in 2 M sulfuric acid for each compartment. The solubility of $V^{(III)}$ (under the experience conditions) is 1100 mol/m^3. The concentration of the dissolved $V^{(IV)}$ will be assumed to be 1700 mol/m^3 (a value close to its solubility). The quantity required to reach 3.5 M will be added as solid powder.

- **For the negolyte**:

The 'complete' half electronic reaction of Rx.V.2, corresponding to the reduction of $V^{(III)}$, can be written as:

$$½\ V_2(SO_4)_3 + e^- \leftrightarrows VSO_4 + ½\ SO_4^{2-} \qquad \text{Rx.V.2'}$$

According to table V.6, for the V^{3+} in the reactor there is only the consumption by the electrochemical reaction of reduction to V^{2+}. The mass balance for $t \leq t_{critical}$ can be written as:

Input flux - outlet flux = reaction flux

$$\Longrightarrow \frac{m_{in}^{III}}{\tau_R} - \frac{m_{out}^{III}}{\tau_R} = \frac{I}{nF} \qquad \text{Eq.V.11}$$

Where: τ_R: residence time in the reactor (s) with $\tau_R = V_R/Q$;

V_R: volume of the electrochemical reactor (m^3);

Q: flow rate (m^3/s);

On the other hand, the $V^{(III)}$ in the storage tank undergoes dissolution to supply a constant concentration corresponding to the saturation. The mass balance in the storage tank, being expressed as a function of the variation of the moles number m with time, contains only the accumulation of the species:

Input flux - outlet flux = accumulation flux

$$\Longrightarrow \frac{m_{out}^{III}}{\tau_R} - \frac{m_{in}^{III}}{\tau_R} = +\frac{dm_{in}^{III}}{dt} = -\frac{I}{nF} \quad \Longrightarrow \quad m_{in,at\ t}^{III} = m_{in\ at\ t=0}^{III} - \frac{I}{nF}t \quad \text{for} \quad t < t_{critical} \quad \text{Eq.V.12}$$

When $|I_{applied}|$ becomes greater than $|I_{lim}|$, a part of the applied current is lost for secondary reactions and if it is not adjusted, then only the I_{lim} should be considered for the upcoming calculations, since the faradic current is no longer constant. Note also that, after the critical time, all the $V^{(III)}$ solid is dissolved and its concentration becomes lower than its solubility.

In this case, the mass balance for an elementary slice *dX* in the axial direction (0 ≤ length X of the electrode ≤ L), in the filter press electrochemical reactor (which behaves as a plug flow reactor), can be written as:

$$F_{in} - (F_{in} + dF) = F_{reaction}$$

and keeping the first term in the Taylor development leads to:

$$-Q\frac{dC}{dX} = -\frac{i\,\alpha}{nF} \qquad \text{Eq.V.13}$$

Where: Q: flow rate (m^3/s);

C: concentration of the dissolved active species (mol/m^3);

i: useful current density, i = nFkC (A/m^2);

a, L and S: are respectively the width, the length and the surface area of the electrode.

After integration between the inlet (X = 0) and the outlet (X = L = electrode length):

$$\Longrightarrow C_{out} = C_{in}e^{-\frac{k\,a\,L}{Q}}$$

Substituting the concentration C by the mol number ($c = \frac{m^{III}}{V_{reactor}}$) and keeping in mind that $V^{(III)}$ is entirely dissolved, leads to:

$$Q\frac{m_{out}^{III}}{V_{reactor}} = Q\frac{m_{in}^{III}}{V_{reactor}}e^{-\frac{kS}{Q}}$$

which can also be written as

$$\frac{m_{out}^{III}}{\tau_{ST}} = \frac{m_{in}^{III}}{\tau_{ST}}e^{-\frac{kS}{Q}} \qquad \text{Eq.V.14}$$

Where: τ_{ST}: residence time in the storage tank (s) with $\tau_{ST} = V_{suspension}/Q$;

The mass balance of $V^{(III)}$ in the storage tank for $t > t_{critical}$ remains unchanged (Eq.V.12): $\frac{m_{out}^{III}}{\tau_R} - \frac{m_{in}^{III}}{\tau_R} = +\frac{dm_{in}^{III}}{dt}$

The mol number (or concentration) of interest is the one in the storage tank (where there is the highest volume of electrolyte) i.e. m_{in}^{III}, thus by replacing the expression of m_{out}^{III} obtained in Eq.V.14 into the differential equation:

$\frac{m_{in}^{III}}{\tau_{ST}} e^{-\frac{kS}{Q}} - \frac{m_{in}^{III}}{\tau_{ST}} = + \frac{dm_{in}^{III}}{dt} \quad \Longrightarrow + \frac{dm_{in}^{III}}{m_{in}^{III}} = \frac{1}{\tau_{ST}} \left(e^{-\frac{kS}{Q}} - 1 \right) dt$; by integration between "t and t $_{critical}$" and "m_t^{III} and $m_{t_{critical}}^{III}$", it becomes:

$$m_t^{III} = m_{t_{critical}}^{III} e^{\frac{t - t_{critical}}{\tau_{ST}} \left(-1 + e^{-\frac{kS}{Q}} \right)} \qquad \text{Eq.V.15}$$

As for the $V^{(II)}$ evolution with time, it can be simply calculated by subtracting from the initial total vanadium moles number (into the negolyte), the quantity of $V^{(III)}$ remaining at time t:

$$m_t^{II} = m_{t=0}^{III} - m_t^{III} \qquad \text{Eq.V.16}$$

Assuming the volume of the suspension constant (and equal to the initial one), the limiting current of $V^{(III)}$ can be estimated at any time during the electrolysis to verify if indeed it is greater than the applied current and the time at which the last solid particle dissolves. The limiting current expression is given by:

$$I_{lim} = nFSk[V^{3+}]_{dissolved} \qquad \text{Eq.V.17}$$

The only missing parameter is k, the mass transfer coefficient, which can be fitted by using the *I = f(η)* curves plotted in the reactor (as performed in Fig.V.18 for $V^{(II)}$).
The value of k, used for the negolyte is 4.4×10^{-6} m/s, calculated from the electrolysis at a vanadium equivalent concentration of 2.5 mol/L (see section V.3.1)

- **For the posolyte**:

The developed form of the half electronic reaction of the oxidation of Rx.V.1 is written as:

$$VOSO_4 + 2.5\ H_2O \leftrightarrows 0.5\ (VO_2)_2SO_4 + e^- + 0.5\ HSO_4^- + 1.5\ H_3O^+ \qquad \text{Rx.V.1'}$$

The oxidation of $V^{(IV)}$ to $V^{(V)}$ in the reactor is also subjected to the transport of the species through the membrane towards the negative compartment. The species susceptible of crossing to the other side correspond to all the cations constituting the posolyte: VO^{2+}, VO_2^+ and H^+; the transfer of the anions (bisulfate and sulfate) across the cationic membrane will be neglected. As previously only the migration flux of the cations will be taken into account here.

The mass balance of $V^{(IV)}$ in the reactor during the recharge of the battery:

Input flux - outlet flux = reaction flux + migration flux

$$\Longrightarrow \frac{m_{in}^{IV}}{\tau_R} - \frac{m_{out}^{IV}}{\tau_R} = \frac{y_f\, I}{nF} + \frac{I \times t_{(V^{IV})}}{z\, F} \qquad \text{Eq.V.18}$$

Where: $t_{(V^{IV})}$: transport number relative to $V^{(IV)}$ (see below);

z = 2= valence of the VO^{2+};

n =1 e^-;
y_f = faradic yield, here assumed =100%.

The mass balance in the storage tank, expressed as a function of the variation of the moles number m with time, contains only the accumulation term: $\frac{m_{in}^{IV}}{\tau_R} - \frac{m_{out}^{IV}}{\tau_R} = -\frac{dm_{in}^{IV}}{dt}$ (since the dissolution affects the concentration and not the evolution of the mole quantity).

The transport number of $V^{(IV)}$ across the Nafion membrane is expressed as following:

$$t_{V^{(IV)}} = \frac{z_{V^{(IV)}}^2 F^2 [VO^{2+}]_s D_{V^{(IV)}}}{\sum_{\forall\, ion\ jp^{\mp}} \left([z_{jp^{\mp}}^2 \times F^2 \times [jp^{\mp}] \times D_{jp^{\mp}} \right)} \qquad \text{Eq.V.19}$$

And here for $V^{(IV)}$: $t_{V^{(IV)}} = \frac{z_{V^{(IV)}}^2 F^2 [VO^{2+}]_s D_{V^{(IV)}}}{[z_{H^+}^2 F^2 [H^+]_{total} D_{H^+} + z_{V^{(V)}}^2 F^2 [VO_2^+]_t D_{V^{(V)}} + z_{V^{(IV)}}^2 F^2 [VO^{2+}]_s D_{V^{(IV)}}]}$

The different parameters used for the calculation of the transport number are grouped in table V.7.

Table V.7: Parameters used for the resolution of Eq.V.19, applied to determine the transport number of $V^{(IV)}$

	z	D (m^2/s) [1]	$C_{at\ t\ =\ 0}$ (mol/m^3)	$C_{at\ t\ =\ t\ critical}$ (mol/m^3)
$V^{(IV)}$	2	$5x10^{-12}$	1700 = solubility	800
$V^{(V)}$	1	$1.7x10^{-12}$	0	2700
H^+	1	$3.35x10^{-9}$	2000	3500

The concentrations at $t_{critical}$ are calculated with the assumption that there are no more solid particles in solution and the limiting current is equal to the applied current. The concentration of H^+ is estimated by using Rx.V.1' for the amount of H^+ produced during the charge and the amount lost by migration through the membrane. The remaining concentration of $V^{(IV)}$ and the formed concentration of $V^{(V)}$ can be estimated through the equation of I_{lim}. All of the estimated values are later verified from the corresponding mass balance calculations and adjusted if needed to find the correct value of the transport number.
Also, the values of the diffusion coefficients correspond to the diffusion of the corresponding species in solution.

The HSO_4^- and SO_4^{2-} concentrations are not taken into account, as explained earlier. In fact, the equilibrium $HSO_4^- + H_2O \rightleftarrows H_3O^+ + SO_4^{2-}$ can affect the acidity of the suspension and thus potentially the different forms of $V^{(III)}$ and $V^{(V)}$ discussed in chapter III, which would then be complicated to consider for the mass balance equations,

The transport number is considered to have a linear evolution over time (the denominator of the Eq.V.19 will be assumed to remain constant, i.e. if a concentration increases the other decreases

with the same magnitude). The values at t = 0 before the start of the charge and at t = $t_{critical}$ are calculated and the average value is used as the corresponding transport number for the $V^{(IV)}$ for the first part of the study.

Then, the mass balance for the storage tank of the posolyte is combined with the Eq.V.18 equation and leads to:

$$-\frac{dm_{in}^{IV}}{dt} = \frac{y_f\, I}{nF} + \frac{I \times t_{(V^{IV})}}{z\, F}$$

And after integration from t = 0 to $t \leq t_{critical}$

$$m_{in\ at\ t}^{IV} = m_{in\ at\ t=0}^{IV} - \frac{I}{F}\left(1 + \frac{t_{(V^{IV})}}{2}\right)t \qquad \text{Eq.V.20}$$

This equation is thus used as long as I_{lim} is above the value of the constant applied current with a value of $t_{(V^{IV})}$ across the nafion membrane equal to 3.06×10^{-3}.

For the second part ($t \geq t_{critical}$), the same reasoning used for Eq.V.19 is applied here for the posolyte compartment at the electrode but with the addition of a term corresponding to the migration of $V^{(IV)}$ through the membrane:

$$-Q\frac{\partial C}{\partial X}dX = \frac{i_{lim}\,\alpha}{nF}dX + \frac{t_{(V^{IV})}\, i_{lim}\,\alpha}{z\, F}dX \Longrightarrow dC = -\frac{i_{lim}\,\alpha}{FQ}(1 + 0.5\, t_{(V^{IV})})dX$$

Assuming $i_{lim} = FkC$, and, $t_{(V^{IV})}$ equal to its average value (between the value obtained at t $_{critical}$ and the value calculated for the concentrations corresponding to the end of the charge), the integration between the inlet (X = 0) and the outlet (X = L = electrode length) leads to :

$$C_{out} = C_{in} e^{-\frac{k\,\alpha\,L}{Q}\left\{1+0.5\, t_{(V^{IV})}\right\}}$$

The evolution of the mole quantity of $V^{(IV)}$ is obtained by dividing with the total volume of the mixture:

$$m_{out}^{IV} = m_{in}^{IV} e^{-\frac{kS}{Q}\left\{1+0.5\, t_{(V^{IV})}\right\}} \qquad \text{Eq.V.21}$$

The concentrations of H^+, VO^{2+} and VO_2^+ at the end of the charge are 3925, 40 and 3460 mol/m^3 respectively and the obtained value of $t_{(V^{IV})}$ is 7.10^{-4}.

The mass balance on the reservoir is then written as: $\frac{m_{in}^{IV}}{\tau_{ST}} - \frac{m_{out}^{IV}}{\tau_{ST}} = -\frac{dm_{in}^{IV}}{dt}$

Combining this equation to the Eq.V.21 enables to suppress the term m_{out}^{IV} and leads to:

$$\frac{dm_{in}^{IV}}{m_{in}^{IV}} = \frac{1}{\tau_{ST}}\left(-1 + e^{-\frac{kS}{Q}\left\{1+0.5\, t_{(V^{IV})}\right\}}\right)dt \quad \text{and after integration for } t \geq t_{critical},$$

$$m_{in\ at\ t}^{IV} = m_{in\ at\ t_{critical}}^{IV} \times exp\left(\frac{t-t_{critical}}{\tau_R}\left(-1+e^{-\frac{kS}{Q}\left\{1+0.5\ t_{(V^{IV})}\right\}}\right)\right) \qquad \text{Eq.V.22}$$

The value of the mass transfer coefficient k is determined from the *I = f(η)* curves plotted during the functioning of the reactor. It was calculated for the $V^{(V)}$ curves for the different concentrations studied in the reactor and it was found to decrease slightly (from $3.63x10^{-6}$ m/s for 1.7 M in total vanadium to $3.1x10^{-6}$ m/s for the 3.5 M equivalent total vanadium concentration) when the equivalent vanadium concentration increases, i.e. when the amount of powder in the electrolytes increases.

This behavior appears to be normal because the presence of solid particles increases the apparent viscosity of the mixture in addition to decreasing the available space for diffusion. We were able to calculate the value of k with the $V^{(IV)}$ curve at the end of the 50 % charge of the 3.5 M electrolysis, and it was found to be equal to $3.37x10^{-6}$ m/s, which is the value that will be used for the mass balance calculations.

As for the mole number of $V^{(V)}$ evolution with time, it can be deduced by subtracting from the initial total vanadium moles number, the quantity of $V^{(IV)}$ remaining at time t, m^{IV}_t. In the case of $V^{(V)}$, its migration to the negolyte should be taken into account; however, its transport number $t_{(V^{(V)})}$, calculated following the same way as the one followed for the $V^{(IV)}$, is found to have an order of magnitude $10^{-4} < t_{(V^{(V)})} < 3x10^{-4}$ which makes the migration flux negligible and allows the use of Eq.V.29 for the calculations.

$$m_t^V = m_{t=0}^{IV} - m_t^{IV} \qquad \text{Eq.V.23}$$

Also, the limiting current of $V^{(IV)}$ can be calculated in the same way using the equation proposed in Eq.V.23, with $k = 3.37x10^{-6}$ m/s.

- **Mass balance of the H_3O^+ (or free protons) in the posolyte:**

Free protons are produced by the oxidation reaction of the $V^{(IV)}$ (during the charge of the battery); H^+ plays a major role in the ionic conductivity through its migration especially across the membrane. Hence, the mass balance during the galvanostatic electrolysis for $I < I_{lim}$ (i.e. before the critical time) can be expressed as following:

- in the reactor: Input flux - outlet flux = 1.5 × Reaction flux + migration flux to the negolyte

$$\frac{m_{in}^{H^+}}{\tau_R} - \frac{m_{out}^{H^+}}{\tau_R} = -\frac{y_f \times 1.5 \times I}{nF} + \frac{I \times t_{(H^+)}}{z_{H^+} F}$$

- in the storage tank: Input flux - outlet flux = accumulation flux

$$\Rightarrow \frac{m_{in}^{H^+}}{\tau_R} - \frac{m_{out}^{H^+}}{\tau_R} = - \frac{dm_{in}^{H^+}}{dt}$$

The transference number of H^+ has the same equation as the one used for $V^{(IV)}$ (Eq.V.19) except that the numerator is replaced by the corresponding H^+ values instead of those of the $V^{(IV)}$. For the calculation of $t_{H^+}$the values in table V.7 as used as well and it is found to be equal to 0.95, which can be considered a little high for the transport of H^+, but it can also confirm the theoretically good selectivity of the Nafion 117 membrane used in the reactor.

Combination of the above equations, and assuming $t_{(H^+)}$ constant, as well as the faradic yield quantitative, gives after integration:

$$m_{in\ at\ t}^{H^+} = m_{in\ at\ t=0}^{H^+} + \frac{I}{F}\left(1.5 - t_{(H^+)}\right) \times t \qquad \text{Eq.V.24}$$

After the applied current becomes equal to the limiting current of the electrolytes, the mass balance equations should be adapted accordingly. The corresponding equations written for H_3O^+ depend on the limiting current defined by the vanadium (IV), reacting on the electrode. In addition, during the charge, the exceeding current from $I_{applied}$ ($I > I_{lim}$) serves for the oxidation of the solvent and thus the production of H^+.

In the reactor: Input flux - outlet flux = 1.5 × Reaction $_{(\text{of the vanadium})}$ flux + migration flux to the negolyte + 1× Reaction $_{(\text{of the solvent})}$ flux

$$-Q\frac{\partial C}{\partial X}dX = -1.5\frac{i_{lim}\,\alpha}{nF}dX + \frac{t_{(H^+)}\,i_{lim}\,\alpha}{z\,F}dX + 1\frac{(I_{applied} - i_{lim})\,\alpha}{nF}dX \qquad \text{Eq.V.25}$$

However, i_{lim} is expressed as $i_{lim} = nFk[VO^{2+}]$, and the resolution of Eq.V.25 would require a double integration to be able to have mass balance of the H^+ after $t_{critical}$.

The curves obtained for the posolyte and the negolyte for the theoretical temporal evolution of the mole number for the four oxidation states constituting the electrolytes are presented in Fig.V.31.

It can be noticed that the critical time at the posolyte is reached first (t = 11 h compared to 12.3 h for the negolyte). This can be explained by the fact that the migration flux reduces more rapidly the $V^{(IV)}$ concentration than that of the $V^{(III)}$ which does not migrate during the recharge, in addition to a lower solubility of the $V^{(III)}$ which allows to maintain the limiting current, theoretically, constant for a longer time.
On the other hand, the comparison between the theoretical and experimental values shows a satisfactory agreement for $V^{(V)}$, $V^{(III)}$ and $V^{(II)}$ taking into account the analytical difficulties because of the presence of the solid powder.

For the $V^{(IV)}$ the observed discrepancies are significantly higher. As an example at 4 h the ratio $\frac{m_{exp}^{IV}}{m_{th}^{IV}}$ is $\frac{0.17}{0.24}$ which means an experimental value 30 % lower than the theoretical one, while simultaneously the agreement for $V^{(V)}$ seems perfect. In fact the error in the $V^{(V)}$ analysis seems lower because it is totally dissolved, while for $V^{(IV)}$ it is difficult to measure the mass of the remaining solid.

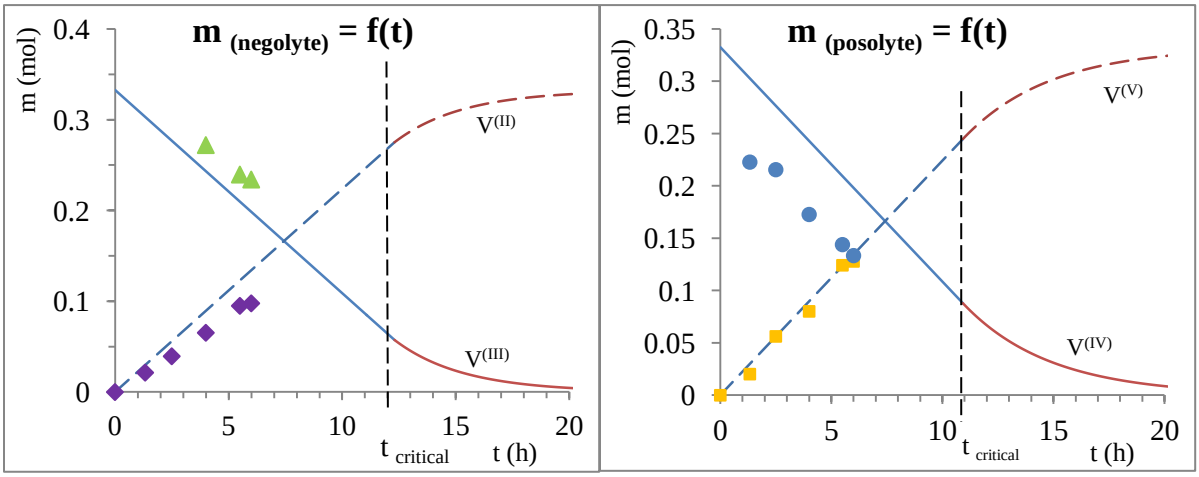

Fig.V.31: Comparison of the theoretical (lines) and experimental (dots) temporal evolutions of the mole quantity of the four oxidation states of vanadium in their respective electrolyte mixtures (left: negolyte, right: posolyte) during charge of the battery at a constant applied current of 0.6 A; Theoretical lines obtained from mass balance equations (plain lines: $V^{(III)}$ and $V^{(IV)}$; dashed lines: $V^{(II)}$ and $V^{(V)}$; blue: before $t_{critical}$; red: after $t_{critical}$) and experimental points (extracted from § V.3.2.) ($V^{(II)}$: violet diamonds; $V^{(III)}$: green triangles; $V^{(IV)}$: blue disks; $V^{(V)}$: yellow cubes) obtained for a total equivalent vanadium concentration of 3.5 mol/L in 2 M initial sulfuric acid.

As for the possible precipitation of $V^{(II)}$ due to a concentration exceeding the solubility ($s_{V(II)}$ = 2.75 mol/L at 25 °C in 2 mol/L H_2SO_4 [2]), it should have occurred as of t = 11.7 h (before $t_{critical}$) but it appears that the vanadium (II) has a latency time before starting to precipitate. In fact, according to Mousa et al. [10], a supersaturated solution of $V^{(II)}$ at a concentration of 2 M in 5.5 M total sulfate at 20 °C, needs 24.6 h under stirring to start precipitation (under these conditions the saturation concentration is around 1.83 M). Nevertheless, since the supersaturation in this study is higher if the charge is completed, and an additional circulation through the reactor is added to the simple stirring in the storage reservoir, it is possible that the precipitation of the $V^{(II)}$ could be observed earlier than predicted by the bibliography and this will be taken into account for this work for the mass balance during the discharge: the solubility of $V^{(II)}$ is fixed at 2.75 mol/L.

V.5.2. Theoretical mass balance established for the discharge of the battery (galvanostatic mode)

During the discharge, the same reasoning as the one used during the charge for $V^{(III)}$ and $V^{(IV)}$ mass balance equations can be followed here to write the mass balance for the $V^{(II)}$ and $V^{(V)}$ oxidation and reduction. Similarly the mass balance is divided between what happens in the reactor and what happens in the electrolytes storage tanks. The initial values at t = 0 of the discharge will be taken from the values corresponding to the end of the previous charge.

- **For the negolyte:**

The phenomena taking place during the discharge are the opposite of what is written in table V.6; for example, the V^{2+} undergoes oxidation to V^{3+} in the reactor, and both V^{2+} and V^{3+} are subjected to migration transport through the membrane to the posolyte. Here as well the only transport phenomenon taken into account is migration with the same expression for the transport number as the one used in Eq.V.25 by replacing the concentrations of $V^{(IV)}$ and $V^{(V)}$ by those of $V^{(II)}$ and $V^{(III)}$ respectively.

The values of the parameters used for the estimation of $t_{V^{(II)}}$ are given in table V.8; the saturation concentration of $V^{(II)}$ is fixed, as noted above, at 2.75 M and will be used as the concentration at the beginning of the discharge for the calculation of the transport number which was found to be equal to $1.4.10^{-3}$. The estimation of the concentrations used for the calculation of $t_{(V^{II})}$ follows the same logic that was used to find the concentrations in table V.7.

Table V.8: Parameters used for the calculation of the transport number of $V^{(II)}$ during the discharge

	z	D (m^2/s) [1]	$C_{at\ t = 0}$ (mol/m^3)	$C_{at\ t = t\ critical}$ (mol/m^3)
$V^{(II)}$	2	$3.125x10^{-12}$	2750 = solubility	700
$V^{(III)}$	3	$5.93x10^{-12}$	16	2800
H^+	1	$3.35x10^{-9}$	5325	2680

The mass-balance equations of $V^{(II)}$, $V^{(III)}$ and H_3O^+ during the discharge are grouped in table V.9. The H^+ does not participate to the oxidation reaction, thus it will only be considered in the reactor for the migration. The initial concentration at t = 0 is calculated from adding the amount of protons that existed at the beginning of the recharge and the ones that migrated from the posolyte during the recharge with $t_{H+} = 0.95$ (calculated during the recharge in the posolyte from Table V.7). Then the concentration will reduce with time due to the migration back to the posolyte to insure the ionic conductivity.
The migration of $V^{(III)}$ to the anode will be neglected (like that of the $V^{(V)}$) because the transport coefficient is estimated to be around 10^{-4}.

Table V.9: Mass balance equations for the negolyte species $V^{(II)}$, $V^{(III)}$ and H_3O^+ in the reactor and the storage tank during the discharge

	In the reactor	In the storage tank
$V^{(II)}$ before t $_{critical}$	$m_{in}^{II} - m_{out}^{II} = \tau_R \frac{I}{F}(1 + \frac{t_{(V^{II})}}{2})$	$m_{in\,at\,t}^{II} = m_{in\,at\,t=0}^{II} - \frac{I}{F}(1 + \frac{t_{(V^{II})}}{2})t$
$V^{(II)}$ after t $_{critical}$	$m_{out}^{II} = m_{in}^{II} e^{-\frac{kS}{Q}(1+\frac{t_{V(II)}}{2})}$	$m_{in\,at\,t}^{II} = m_{in\,at\,t_{critical}}^{II} e^{\frac{t-t_{critical}}{\tau_{ST}}(-1+e^{-\frac{kS}{Q}(1+\frac{t_{(V^{II})}}{2})})}$
$V^{(III)}$	$m_t^{III} = m_{from\,charge}^{III} + (m_{t=0}^{II} - m_t^{II})$	
H_3O^+ before t $_{critical}$	$m_{in}^{H^+} - m_{out}^{H^+} = \tau_R \frac{It_{(H^+)}}{F}$	$m_{in\,at\,t}^{H^+} = m_{in\,at\,t=0}^{H^+} - \frac{It_{(H^+)}}{F}t$

As for the mass balance of H_3O^+ after t $_{critical}$, even if it does not participate in the electrochemical reaction of the oxidation of $V^{(II)}$ to $V^{(III)}$, but similarly to what was explained for the posolyte, the exceeding current will serve for here for the reduction of the solvent, thus consuming the protons. A similar equation to Eq.V.31 should be written for integration, but the resolution of both equations will not be performed in the present work.

In addition, the mass balance equations in the negolyte do not take into account the instability to air of the vanadium (II) which plays an important role during the electrolysis especially for long periods where the oxygen is bound to enter eventually, and its effect was perceived during the different electrolysis performed in this work.

The applied current for the discharge is chosen to be equal to that of the recharge (I = 0.6 A) for the calculations of the mass balance equations, but in this case it will be difficult to confront the calculated values to the experimental ones obtained because, for that, three different currents were applied in order to be always under the limiting current and the discharge was applied to a 40 % charged battery not a fully charged one.

- **For the posolyte:**

The discharge of the battery induces the reduction of $V^{(V)}$ to $V^{(IV)}$, hence, the species of interest in this case will be the $V^{(V)}$ and its mass balance will be established. There is no migration flux to consider for the $V^{(V)}$ to the negolyte. Besides, the H_3O^+ migrates from the negolyte to the posolyte and it is partially consumed during the electrochemical reaction of the reduction of $V^{(V)}$. During the discharge, the limiting current of the reduction of $V^{(V)}$ starts to decrease from the beginning since there is no solid particles to maintain a constant concentration and thus a constant current. However, this evolution could be counterbalanced by the decrease of the solution viscosity and consequently the decrease of the thickness of the diffusion layer δ and then the increase of the limiting current; yet, due to the lack of experimental data concerning the

evolution of the viscosity during the cycling in the case of the suspensions studied herein, this effect will not be taken into account.
The mass balance equations for the species in the posolyte during the discharge are presented in Table V.10.

Table V.10: Mass balance equations for the posolyte species $V^{(V)}$, $V^{(IV)}$ and H_3O^+ in the reactor and the storage tank during the discharge

	In the reactor	In the storage tank
$V^{(V)}$ for $I_{lim} > I_{applied}$	$m_{in}^{V} - m_{out}^{V} = \tau_R \frac{I}{F}$	$m_{in\ at\ t}^{V} = m_{in\ at\ t=0}^{V} - \frac{I}{F} t$
$V^{(V)}$ for $I_{lim} < I_{applied}$	$m_{out}^{V} = m_{in}^{V} e^{-\frac{kS}{Q}}$	$m_{in\ at\ t}^{V} = m_{in\ at\ t_{critical}}^{V} e^{\frac{t - t_{critical}}{\tau_{ST}}\left(-1+e^{-\frac{kS}{Q}}\right)}$
$V^{(IV)}$	$m_{in\ at\ t}^{IV} = m_{from\ charge}^{IV} + (m_{in\ at\ t=0}^{V} - m_{in\ at\ t}^{V})$	
H_3O^+ for $I_{lim} > I_{applied}$	$m_{in}^{H^+} - m_{out}^{H^+} = \tau_R \frac{1.5\ I}{F}$	$m_{in\ at\ t}^{H^+} = m_{in\ at\ t=0}^{H^+} - \frac{1.5\ I}{F} t$

The concentrations at the beginning of the discharge are the ones obtained at the end of the recharge. Having established the mass balance equations for all the species, they can now be resolved.

The results show that the obtained curves for $V^{(II)}$ and $V^{(V)}$ are exactly the same ones of $V^{(III)}$ and $V^{(IV)}$ that were obtained during the recharge. It appears that the migration does not have a significant effect on the total moles transformed. The $V^{(II)}$ (and negligible $V^{(III)}$) migrating from the negolyte during discharge (and $V^{(IV)}/V^{(V)}$ migrating from the posolyte during the recharge) should also be taken into account in the total vanadium concentration in the posolyte, but it appears that from the first cycle, the value of the migration is low (< $5x10^{-3}$ mol/L) and this could be attributed to the low values of the transport number of the vanadium species (in the range of 10^{-3}-10^{-4}) thanks to the high demonstrated selectivity of the membrane witnessed by the high transport number of the protons (0.95-0.96)).
The effect of migration might be more pronounced after numerous charge-discharge cycles.

The main difference observed between the recharge and the discharge is the evolution of the limiting current which remains practically stable during the recharge until achieving ~ 50 % of the conversion, whereas during the discharge it starts its decrease directly in the posolyte and after only 3 hours in the negolyte. This of course depends on the composition of the electrolytes.

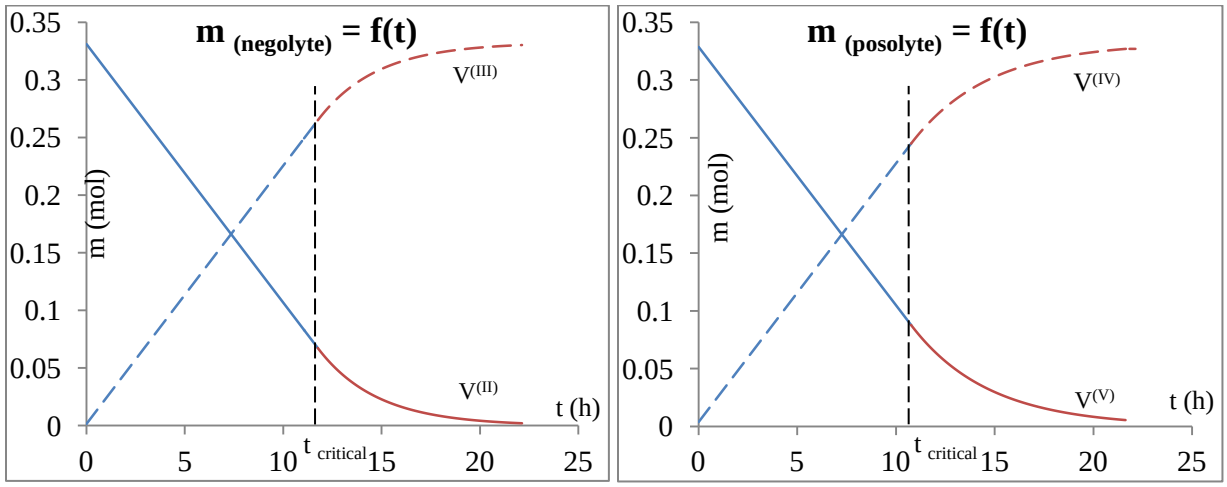

Fig.V.32: Comparison of the theoretical evolution with time of the mole quantity of the four oxidation states of vanadium in their respective electrolyte mixtures (left: negolyte, right: posolyte) during discharge of the battery at a constant applied current of 0.6 A after a complete charge; plain lines: $V^{(II)}$ and $V^{(V)}$; dashed lines: $V^{(III)}$ and $V^{(IV)}$; blue: before $t_{critical}$; red: after $t_{critical}$; total equivalent vanadium concentration is 3.5 mol/L.

The same equations can be applied continuously for full charge-discharge cycles to monitor the evolution of the vanadium concentrations and be able to see differences generated by the migration and possible side reactions.

On the other hand, the mass balance of the protons was not calculated but it appears that it has an important role in the different phenomena taking place in the battery (electrochemical reactions, migration, osmosis…). This applies as well on the total sulfate and water content in the electrolytes which constitute an important part in the dissolution and precipitation of the solid particles added in excess. Thus, the management of the acid concentration and water content of the electrolytes appears to be important for a good functioning of the battery (conductivity, viscosity, precipitation…).

The modeling of the VRFB has been addressed widely in the bibliography and they treat different aspects of the battery. In fact, each parameter and the related phenomena constitutes a study by itself; for example, Knehr et al. [11] studied the effect of the variation of the electrolyte viscosity on the transport through the membrane: they established a 2-dimensional, isothermal, transient model to simulate charge/discharge cycles with varying flow rates and electrolyte viscosities. They suggest that the viscosities of the posolyte and the negolyte deviate from each other during cycling and using an identical flow rate for the two compartments introduces a pressure gradient between the two half-cells. This causes the crossover to increase by convection. To overcome this problem they suggest using different flow rates for the two half-cells, reflecting the different viscosities.

You et al. [12] developed a model to predict the effects of applied current density, electrode thickness ratio and local mass transfer coefficient on the performance of the VRFB while Zhou et al. [13] studied the effect of the ion concentration on their mobility and they found that the model has limited ability in the prediction of battery behavior at high current densities if the dependency of the mobility on the ion concentration is not taken into account. On the other hand, Smith et al. [14] studied the effect of the electrolyte concentration, flow rate and a variety of carbon felt electrodes on the performances of the VRFB and they were able to determine the optimal parameters (a flow rate in the range of 1.5-2 mL/min for a vanadium concentration of 1.1 mol/L) by correlating the experimental results to their mathematical model.

In conclusion, the modeling of the battery using mass balance equations has not been addressed widely but the focus is generally towards the cell voltage, the OCP and the SOC calculated from the total capacity of the battery and depending on the applied current density. Also, numerous studies can be found concerning the modeling of the transport through the membrane to better understand the effect of the crossover [9, 15-17].

V.6. Conclusion

In this chapter, the effect, on the cycling of the VRFB, of the presence of solid particles in the electrolytes was investigated using a filter press divided reactor connected to two external storage tanks. The studied solid particles are vanadium salts ($VOSO_4$ and $V_2(SO_4)_3$) and the carbon nanoparticles, the aim being to increase the energy density of the VRFB. To that end the chosen method is to increase the mass quantity present in a certain volume of electrolyte, until the suspension becomes practically not flowable.
Galvanostatic electrolyses were performed using suspensions containing successively increased mass concentration of the vanadium under various conditions, expecting and trying to deduce the parameters enabling to determine the various yields and performances; the parameters monitored during the functioning of the battery are the cell voltage, the electrodes overpotentials (*$I=f(\eta)$ curves*) and the vanadium concentrations, which allowed the calculation of the state of charge, the conversions, the faradic yield and the energy efficiency during cycling.

Numerous problems were highlighted throughout this chapter and many discrepancies between the theoretical and the experimental (estimated) values of the conversion (or SOC) were evidenced, such as a 30 % gap in the case of $V^{(II)}$. That is why various results were only partially reliable.
The most important problem is the analysis of the concentration/moles number of the vanadium species, especially into the liquid/solid suspensions; indeed the presence of solid particles, and also the modification of the volumes of both the posolyte and the negolyte (by migration and osmosis during the electrolysis), induces the impossibility to sample any aliquot with a uniform

composition (because of the solid) and to be sure of both the volume of this aliquot as well as the overall volume of the suspension.
Other evidenced problems are: i) the parasitic reaction of $V^{(II)}$ with the oxygen, despite the continuous nitrogen bubbling and ii) the shift in the concentrations of the various vanadium species because of the flux transferred between compartments. At this stage we do not have the required data to quantify these phenomena.

Despite these problems, various values of some parameters were proposed and discussed; thus it was found that the faradic yield of the performed electrolyses is greater than 75 % for all the 'total vanadium concentrations' involved into the electrolytes (solution or suspension), i.e. 1.7 M (Liquid), 2.5 M (Liquid + Solid) and equivalent of 3.5 M (Liquid + Solid) in 2 M initial H_2SO_4, at 25 °C. This value, even depending of course on the applied current, appears to be relatively low: i) taking into account that the cell voltage was controlled and maintained out of the solvent potential range and ii) when compared to the faradic yields found in the bibliography, i.e. > 85% [18].

The energy yield was roughly estimated for cycling of the battery (at near saturation and in the presence of vanadium particles and/or KB) under an applied current density of 0.02 A/cm^2. It was found that EY increases from 38 % at near saturation to ~ 44 % for the equivalent vanadium concentration of 3.2 M and increases more to 58 % in the presence of 0.17 % of KB in the 3.2 M suspension. Thus, it appears that at the chosen current density, the presence of KB nanoparticles enhances the performance of the system (faradic yield 5 % and energetic yield 10 %). Even improved, these values appear significantly low when compared to the EY found in the bibliography, i.e. > 80 % [19]. As indicated above, difficulties on the taking of aliquots is the main reason of the important uncertainties on the experimental value.

On the other hand, the energy density, aimed in this work, appeared to triple in the presence of solid particles: the average energy stored during the charge increases from 3 to ~ 9.5 Wh/kg and from 1.8 to ~ 4.5 Wh/kg for the energy recovered during the discharge. These values are far from the 40 Wh/kg stated for the existing VRFB, but the comparison is valid between the electrolysis performed for our system and it proves that indeed the energy density is increased by ~ 3 folds in the presence of particles. It should be noted that the conversion rate achieved during the cycles for which the energy density was calculated is 10 %/half-cycle ($40 < SOC_{(\%)} < 50$).

Finally, a simplified model based on the macroscopic mass balances of the four vanadium species was established for the recharge and discharge of the battery, performed in galvanostatic mode and in the presence of Liquid-Solid suspensions. The balance was written on the basis of the mole number of each oxidation state of the vanadium, thus avoiding the problem of the determination of the volume of the electrolytes. Moreover, the molar quantities of the vanadium were determined for electrolyses durations both higher and lower than the critical time (where

applied current = limiting current). The theoretical temporal evolution of the concentrations of the various vanadium species were compared to the corresponding experimental one (the latter containing strong uncertainties). For the electrolysis performed with the highest total concentration of the vanadium (at t = 0 $[V]_{tot}$ = 3.5 M), satisfactory agreements were observed for the $V^{(II)}$, $V^{(III)}$ and $V^{(V)}$ while the values of the concentrations of $V^{(IV)}$ exhibited a 20 % difference, partially due to the analysis.

The choice to operate with loaded suspension causes important modifications to the system, such as i) increase of the viscosity, ii) presence of solid particles of the vanadium, iii) chemical equilibria involving at least two acid/basis forms (hydrates) of one oxidation state of vanadium (for example $V^{(III)}$ or $V^{(V)}$), which constitutes drawbacks lowering the performances of the system (EY and y_f); nevertheless, the stored energy increases at least 3 times.

Numerous parameters should be taken into account for future studies to improve the conversions, the faradic and energetic yields, such as the suspensions viscosities, the parasitic oxygen, the transport through the membrane and the acid concentration effect.

References:

[1] E. Agar, K.W. Knehr, D. Chen, M.A. Hickner, E.C. Kumba, "Species transport mechanisms governing capacity loss in vanadium flow batteries: Comparing Nafion® and sulfonated Radel membranes", Electrochimica Acta, 98, 2013, 66-74, doi: 10.1016/j.electacta.2013.03.030

[2] M. Skyllas-Kazacos, L. Cao, M. Kazacos, N. Kausar, A. Mousa, "Vanadium Electrolyte Studies for the Vanadium Redox Battery-A Review", ChemSusChem, 9, 2016, 1521-1543, 2016, doi: 10.1002/cssc.201600102

[3] T. Yamamura, N. Watanabe, T. Yano, Y. Shiokawa, "Electron-Transfer Kinetics of Np^{3+}/Np^{4+}, NpO_2^{+}/NpO_2^{2+}, V^{2+}/V^{3+}, and VO^{2+}/VO_2^{+} at Carbon Electrodes", J. Electrochem. Soc., 152 (4), 2005, A830, doi: 10.1149/1.1870794

[4] K.J. Kim, M.S. Park, Y.J. Kim, J.H. Kim, S.X. Dou, M. Skyllas-Kazacos, "A technology review of electrodes and reaction mechanisms in vanadium redox flow batteries", J. Mater. Chem. A, 3, 2015, 16913-16933, doi: 10.1039/C5TA02613J

[5] W.G. Zhang, J.G. Xi, Z.H. Li, H.P. Zhou, L.Liu, Z.H. Wu, X.P. Qiu, "Electrochemical activation of graphite felt electrode for VO^{2+}/VO_2^{+} redox couple application", Electrochim. Acta, 2013, 89, 429-435, doi: 10.1016/j.electacta.2012.11.072

[6] A. Hassan, T. Tzedakis, "Enhancement of the electrochemical activity of a commercial graphite felt for vanadium redox flow battery (VRFB), by chemical treatment with acidic solution of $K_2Cr_2O_7$", Journal of Energy Storage, 26, 2019, 100967, doi: 10.1016/j.est.2019.100967

[7] W. Moura De Carvalho Jr, L. Cassayre, D. Quaranta, F. Chauvet, R. El-Hage, T. Tzedakis, Beatrice B., "Stability of highly supersaturated vanadium electrolyte solution and characterization of precipitated phases for Vanadium Redox Flow Battery", J. Power Sources, 2020, under review

[8] R.M. Wallace, "Determination of the second dissociation constant in sulfuric acid by Donnan Membrane Equilibrium", J. Phys. Chem. 70 (12), 1966, 3922-3927, doi: 10.1021/j100884a029

[9] K. Oh, S. Won, H. Ju, "A comparative study of species migration and diffusion mechanisms in all-vanadium redox flow batteries", Electrochimica Acta, 181, 2015, 238-247, doi: 10.1016/j.electacta.2015.03.012

[10] A. Mousa, M. Skyllas-Kazacos, "Kinetics of V^{III} and V^{II} sulfate precipitation processes in negative half-cell electrolyte of the vanadium redox flow battery", ChemElectroChem, 4, 2017, 130-142, doi: 10.1002/celc.201600426

[11] K.W. Knehr, E.C. Kumbur, "Role of convection and related effects on species crossover and capacity loss in vanadium redox flow batteries", Electrochemistry Communications, 23, 2012, 76-79, doi: 10.1016/j.elecom.2012.07.008

[12] D. You, H. Zhang, J. Chen, "A simple model for the vanadium redox battery", Electrochimica Acta, 54 (27), 2009, 6827-6836, doi: 10.1016/j.electacta.2009.06.086

[13] X.L. Zhou, T.S. Zhao, L. An, Y.K. Zeng, X.H. Yan, "A vanadium redox flow battery model incorporating the effect of ion concentrations on ion mobility", Applied Energy, 158, 2015, 157-166, doi: 10.1016/j.apenergy.2015.08.028

[14] M.J. Watt-Smith, P. Ridley, R.G.A. Wills, A.A. Shah, F.C. Walsh, "The importance of key operational variables and electrolyte monitoring to the performance of an all vanadium redox flow battery", J. Chem. Technol. Biotechnol., 88 (1), 2013, 126-138, doi: 10.1002/jctb.3870
[15] S. Won, K. Oh, H. Ju, "Numerical analysis of vanadium crossover effects in all-vanadium redox flow batteries", Electrochimica Acta, 177, 2015, 310-320, doi: 10.1016/j.electacta.2015.01.166
[16] K.W. Knehr, Ertan Agar, C. R. Dennison, A. R. Kalidindi, E. C. Kumbur, "A Transient Vanadium Flow Battery Model Incorporating Vanadium Crossover andWater Transport through the Membrane", J. Electrochem. Soc., 159 (9), 2012, A1446-A1459, doi: 10.1149/2.017209jes
[17] M. Skyllas-Kazacos, L. Goh, "Modeling of vanadium ion diffusion across the ion exchange membrane in the vanadium redox battery", Journal of Membrane Science, 399-400, 2012, 43-48, doi: 10.1016/j.memsci.2012.01.024
[18] K. Lourenssen, J. Williams, F. Ahmadpour, R. Clemmer, S. Tasnim, "Vanadium redox flow batteries: A comprehensive review", Journal of Energy Storage, 25, 2019, 100844, doi: 10.1016/j.est.2019.100844
[19] Á. Cunha, J. Martins, N. Rodrigues, F.P. Brito, "Vanadium redox flow batteries: a technology review", Int. J. Energy Res., 39, 2015, 889-918, doi: 10.1002/er

General conclusion

This work was conducted as a part of a project concerning the conception, design and optimization of a vanadium redox flow battery (VRFB), aiming to increase its energy density, by decreasing the volume of the electrolytes and increasing the concentration of the active species. In fact, the main drawback of the VRFB is the limited solubility of the vanadium salts in sulfuric acid, which reaches a maximum of 2 M in 3 M H_2SO_4 and in a temperature range of 10 to 40 °C. To overcome this limitation, the present study focused on the increase of the stored energy by using vanadium suspensions, containing excess vanadium solid particles, instead of only dissolved species. In addition, the effect of the presence of carbon nanoparticles (KB), acting as electron conductor in the suspension, was also investigated thus expecting to benefit of the electronic percolation and to enhance the current admissible by the system (thus optimizing the power density of the battery).

Suitable analytical techniques were required for the quantification of the four oxidation states of the vanadium and this part was carried out first. Potentiometric titration was involved to quantify the $V^{(II)}$ and $V^{(V)}$ by redox reaction with I_2 and $Fe^{(II)}$ respectively, without the interference of their complementary oxidation states. Besides, the quantification of the $V^{(III)}$ and $V^{(IV)}$ was performed by UV-Vis spectroscopy; their respective extinction coefficients were determined: $\varepsilon_{V(III),\ 401\ nm}$ = 11.17 $L.mol^{-1}.cm^{-1}$ and $\varepsilon_{V(IV),\ 760\ nm}$ = 19.92 $L.mol^{-1}.cm^{-1}$ in 3 M sulfuric acid. Note that, for UV-Vis spectroscopy analysis, the sample needs to be clear without any solid particle, fact which limits seriously the technique here. However, using a 0.1 µm PTFE filter enables getting samples sufficiently clear to be analyzed precisely.
Experimental setups were conceived and manufactured to be used for the estimation of the effective/apparent viscosity of the various vanadium solutions and suspensions; the density of these mixtures was also measured. It was found that that the apparent viscosity of a 5 M vanadium (V) solution is about 30 times higher than that of a 2 M vanadium (IV) solution at 20 °C ($\mu_{apparent,\ V^{(IV)}}$ = 6x10^{-3} Pa.s << $\mu_{apparent,\ V^{(V)}}$ = 0.17 Pa.s). The variation of the viscosity of the $V^{(V)}$ with temperature was fitted by a second order polynomial law in the temperature range of 14 to 20 °C ($\mu_{apparent\,V^{(V)}} = 1.9 \times 10^{-3} T_{(K)} - 1.11 T_{(K)} + 163$). This same viscosity varies against the vanadium (IV) concentration following an exponential shaped function ($\mu_{apparent\,V^{(IV)}} = \alpha e^{0.75[VO^{2+}]}$, with $\alpha = f(T)$). As for the density of suspensions, it was found that, adding excess powder into a saturated solution leads to a linear increase of the total volume over the added mass ($V_{total\ of\ suspension\ (mL)} = 0.5 \times m_{added\ VOSO_4\ (g)} + V_{saturated\ solution\ (mL)}$). This correlation was used to determine the total volume of suspensions and thus to calculate the exact equivalent concentration of $VOSO_4$. This law will be also used to estimate the equivalent concentration of $V_2(SO_4)_3$ into the suspension.

The study of the electrochemical behavior of the various vanadium species (in suspension) was undertaken in a classic three electrodes cell; the study aims to determine the optimal composition

for a flowable suspension, exhibiting the highest limiting current. It was found that, in the absence of any surfactant, a suspension with a vanadium (IV) equivalent concentration ~ 5 M (1.5 M completely dissolved and 3.5 M in solid $VOSO_4$ form) behaves as a paste; consequently we have two possibilities: to decrease the mass concentration or to add surfactants enabling a better circulation in the reactor.

The graphite is the electrode material used; here it was investigated in two forms: solid and felt. Despite that the felt exhibits a greater active surface area (than the massive graphite) and thus generating higher currents ($S_{G\ felt}/S_{massive\ G} \approx 3.7$, determined from the limiting current), it was discarded because of the clogging problems observed in the presence of solid particles (vanadium and KB nanoparticles). Indeed, increasing the solid fraction of the suspension induces flow problems and causes a systematic decrease of the limiting current.

The electrochemical behavior of $V^{(IV)}/V^{(V)}$ system was studied on a graphite cylinder rotating electrode with an additional cross-shaped stirrer able to lift the particles and keep them in suspension. The presence of solid particles during the oxidation of $V^{(IV)}$ appeared to have a negative impact on the current. The current decrease was fitted as a second order polynomial function of the volume fraction of solid particles (f_s) : $I = 7.10^{-5} f_s^2 - 1.15.10^{-2} f_s + 1.08$.
However, the decrease of the current (mainly affecting the power density ($P_{(t)}=I_{(t)}\times\Delta V_{(t)}$) of the system) caused by the solid presence, does not constitute a major problem; in fact, here the aim is to increase the energy density, i.e. the mass concentration of the electroactive species. Besides, the presence of low (*~ 0.1 mass %*) quantities of KB nanoparticles in a vanadium suspension without surfactant, positively affects the current (~ 30 % of increase) for both posolyte and negolyte, and does not seem to strongly affect its viscosity nor its flowability.

Concentrated solutions of $V^{(V)}$ were obtained by electrochemical oxidation of suspensions of $VOSO_4$ (note that the electrolysis acidifies the posolyte). Studies of the electrochemical reduction of the $V^{(V)}$, in supersaturated solutions (no solid even for 5 M of $V^{(V)}$), show that the current decreases by half when the concentration of the solution increases twice (from 2.5 to 5 M). This fact was attributed in part to the important viscosity of the 5 M solution, impacting the diffusion coefficient of the active species, but also to the dimerization of the $V^{(V)}$ (probably $V_2O_3^{4+}$ dimer) at high acid concentrations leading to the formation of more than one species in solution which might not have the same reactivity.

An additional study of the posolyte was undertaken to get a better understanding of the dissolution mechanisms of the $VOSO_4$ and V_2O_5. That is an attempt: i) to explain the low solubility of the latter and ii) to establish simplified models enabling to simulate the temporal evolution of the corresponding concentrations and to correlate them with the experimental data. The general results showed that the dissolution of $VOSO_4.5H_2O$, an 'ionic salt', appears to be easier and faster than that of the V_2O_5 oxide. It was found that the dissolution of $VOSO_4$ consists

of the dissociation in the acid media, followed by its dispersion in the bulk. The whole process is limited by mass transport (more specifically diffusion and convection), while the dissolution rate of the oxide appears to be limited by a chemical reaction (acidic attack followed by the breaking bonds). A simple reaction scheme was proposed for the dissolution and its rate was expressed assuming the chemical reaction as an elementary reaction. In addition the solubility of the $V^{(IV)}$ salt was found to be higher than the solubility of the oxide (at least by two times, even three for certain temperatures): VO^{2+}concentrations of 2 M can be achieved from the dissolution of $VOSO_4$ at T ≥ 30°C, while for the oxide dissolution the VO_2^+ saturation concentration reaches ~ 0.45 M at 40°C. Note that bibliography shows several studies of the solubility of the vanadium in different conditions.

Moreover, conversely to the $V^{(IV)}$, in the case of vanadium pentoxide decreasing the temperature causes the solubility of VO_2^+ to increase: from 0.42 to 0.78 M respectively at 40 and 0°C, and the whole dissolution process appears to be exothermic ($k'_{dissolution}$ = - 37.8 kJ/mol).

The study of the negolyte was limited to the oxidation state $V^{(III)}$ in the three electrodes cell because of the difficulties encountered during the production and storage of $V^{(II)}$ (to protect it from oxidation by air). The study of the reduction curves of $V^{(III)}$ solutions at concentrations lower than 1 M showed two signals translating two acid-base species (V^{3+} and $V(OH)^{2+}$) which distribution seems to be strongly conditioned by the concentration of sulfuric acid. The Butler-Volmer analysis for both species at a total vanadium concentration of 0.25 M showed that the value of α is close for both of them (0.69 and 0.62) while the value of $k°$ increases from $0.69x10^{-3}$ to $1.03x10^{-3}$ m/s for the $V(OH)^{2+}$. These values of $k°$ are relatively high compared to what was found in the bibliography.
On the other hand, the I = f(E) curves of $V^{(III)}$ suspensions, performed on the solid graphite rod, did not show any characteristic wave or increase of the current between different fractions of added solid. It is certain that the reduction $V^{(III)}$ to $V^{(II)}$ occurs at the electrode (confirmed by the presence of a cathodic current greater than the residual current), but the solid seems to adsorb on the electrode and induce an additional overvoltage. The same behavior was observed in the filter-press reactor, where I = f(η) curves of $V^{(III)}$ suspensions were plotted at t = 0 before the start of the electrolysis; however, this tendency disappeared when the curves were plotted after performing some recharge of the battery and the reduction wave was restituted.

Finally, after gathering the required information and data, the effect of the presence of solid particles was examined during the cycling of the battery in a lab-scale filter press divided reactor and connected to two external storage tanks. It was found that the faradic yield was greater than 75 % for all the performed electrolyses, for vanadium concentrations of: 1.7 M, equivalent of 2.5 M (S+L) and equivalent of 3.5 M (S+L), in 2 M initial H_2SO_4, at 25 °C. The energy yield of the system was estimated during the cycling of the battery in two cases: i) at near saturation and ii) in the presence of vanadium particles and/or KB at a current density of 0.02 A/cm^2 and a flow

rate of 40 L/h: the EY (energy yield) increases from 38 % at near saturation to ~ 44 % for the equivalent vanadium concentration of 3.2 M and increases more to 58 % in the presence of 0.17 % of KB in the 3.2 M suspension.
On the other hand, the amount of energy density 'stored' increases in the presence of solid particles. Thus increasing the vanadium concentration from 1.7 to 3.2 M (with and without KB) causes: i) the average energy stored during the recharge of the battery to increase from 3 to ~ 9.5 Wh/kg, and ii) for the discharge the energy recovered increases from 1.8 to ~ 4.5 Wh/kg. These values were calculated for a conversion rate of 10 %/half-cycle and an SOC between 40 and 50 %.
Note that, the impact on the power density of the added viscosity and lower limiting current were not quantified.

Perspectives

The results obtained in the present work open vast research possibilities. In fact, several problems were highlighted during the functioning of the battery. Even if some of them were elucidated in this work, the mechanisms and the laws governing most of the others, require a strong investment before being controlled.

Among these issues, there is:

i) the reaction of the $V^{(II)}$ with parasitic oxygen; this requires to adapt all the elements of the experimental setup (especially pipes) with impermeable material. Moreover the kinetic law of the reaction needs to be determined;

ii) the effect, of the presence of solid powder of VSO_4, on the electrochemical behavior of the system $V^{(II)}/V^{(III)}$ has not been addressed in this thesis and it should be quantified in order to evidence any eventual limitation;

iii) the electrochemical behavior of the $V^{(III)}$ in the negolyte seems to strongly depend on the $V_2(SO_4)_3$ solid mass concentration, and requires clarification, in order to control its effect on the current;

iv) the chemistry of the four species of the vanadium requires a strong investment in order to prevent equilibria of dimerization or polymerization when operating with high concentrations (> 3.5 M in Solid + Dissolved vanadium);

v) the changes of the viscosity of the electrolytes during recharge and discharge, (by dissolution of the excess powder of one oxidation state and the formation of the powder of the other) needs to be highlighted; the eventual use of surfactants could be considered.

Moreover, other more classical problems, (partially treated as shown in the bibliography) needs to be examined and their eventual negative effect to be controlled; typical problems could be:

vi) the water management (osmosis, dissolution/precipitation), especially for high conversions of the electroactive species;

vii) the heat management of the battery;

viii) the crossover through the membrane.

The cycling of the battery should be performed for a higher number of cycles in order to examine its lifetime (erosion of membrane and electrode in the presence of solid particles and estimate better the energy efficiency).

Lastly, the design of a battery stack should be considered by extrapolation of the results obtained for the laboratory scale filter press reactor, and with that the modeling of the battery during charge-discharge cycles should be developed more by taking into account the secondary reactions, the sulfates, the protons and the water content.

Nomenclature

Abbreviations:

CAES	Compressed air energy storage
CE	Auxiliary or counter electrode
CSS	Cross-shaped stirrer
DMFC	Direct-methanol fuel cell
DOD	Depth of discharge
ESS	Energy storage systems
FW	Flywheels
GA	Gum arabic
GD	Graphite disc
GF	Graphite felt
GR	Solid graphite rod
ICP	Inductively coupled plasma
KB	Ketjen black
MPT	Micro-pump turbine
NASA	National Aeronautics and Space Administration
NMR	Nuclear magnetic resonance
OCP	Open circuit potential
OES	Optical emission spectrometry
PCM	Phase change materials
PEM	Polymer electrolyte membrane
PES	Polyether sulfone
PHES	Pumped hydro energy storage
PTFE	Polytetrafluoroethylene
RCE	Rotating cylinder electrode
RDE	Rotating disc electrode
RE	Reference electrode
RFB	Redox flow batteries
SCE	Saturated calomel electrode
SEM	Scanning electron microscope
SMES	Superconducting magnetic energy storage
SOC	State of charge
SSFC	Semi-solid flow cell
VRFB	Vanadium redox flow battery
WE	Working electrode

Latin letters:

A	Absorbance
$\boldsymbol{A}$	Arrhenius pre-exponential factor
$a_{VOSO_4\ solid}$	Activity of the solid compound
a	Constant (Leveque correlation)
C	Concentration of the active species (mol/L)
D	Diffusion coefficient (m^2/s)
$\Delta_R H$:	Reaction enthalpy (J/mol)
ΔU:	Internal energy (J/mol)
ΔV	Cell voltage (V)
d_p	Particle diameter at time t (µm)
d	Density
E	Potential (V)
$E°_{ox/red}$	Standard potentials of the redox couples (V)
$\mathbb{E}$	Energy density (Wh/kg)
E_a	Activation energy (J/mol)
EY	Energy yield (%)
$\boldsymbol{e}_{(t)}$	Thickness of the spherical crown film, function of the time (m)
F	Faraday constant 96500 $C.mol^{-1}$
f_s	Volume fraction of the solid particles
I	Current (A)
i	Useful current density, i = nFkC (A/m^2)
j	Number of iterations taken as 100
k	Kinetic constant following the Arrhenius law (unit function of the reaction order) and also: $k = D/\delta$ mass transfer coefficient (m/s)
k°	Intrinsic heterogeneous electronic transfer kinetic constant (or rate constant) (m/s)
M	Molarity ($mol.L^{-1}$)
MW	Molecular weight of the active species (kg/mol)
n	Number of the electrons exchanged during the reaction
n_{mol}	Moles number
Q	Flow rate (m^3/s)
Q	Faradic charge amount (C)
R	Ideal gas constant, R = 8.314 $J.mol^{-1}.K^{-1}$ =1.98 $cal.mol^{-1}.K^{-1}$ = 0.082 $L.atm.K^{-1}.mol^{-1}$
R°	Initial radius of the particle (m)
$R_{(t)}$	Radius of the particle at the dissolution time t (m)
Re	Reynolds number $= \frac{d_p \times \bar{u}}{\nu} = \bar{u} \times d_p \times \frac{\rho}{\mu}$
$\boldsymbol{r}°$	Initial reaction rate ($mol.L^{-1}.s^{-1}$)
r_{global}	Total rate of the reaction of the dissolution of V_2O_5 ($mol.L^{-1}s^{-1}$)
r	Scanning rate for voltammetry curves (mV/s)
S	Surface of the electrode (m^2)

Sc	Schmidt number =ν/D
Sh	Sherwood number ($Sh = \frac{k_{(t)} \times d_p}{D} = 2 + a \times Re^{1/2} \times Sc^{1/3}$ Leveque correlation)
s_i	solubility of species i (mol/L)
T	Temperature (°C)
t	Time (s)
t_i	Transport number relative to species i
$\bar{u}$:	Average rate of the liquid around the solid particle calculated from the stirring rate (m/s), assumed constant during the experiment time
X	Conversion (%)
y_f	Faradic yield (%)
z	Valence of an ion

Greek letters:

α, β	Anodic and cathodic electronic transfer coefficients
δ	Thickness of the diffusion layer
ε	Molar absorptivity or extinction coefficient ($L.mol^{-1}.cm^{-1}$)
η	Overpotential (or overvoltage) (V)
λ	Wavelength (nm)
μ	Dynamic viscosity (Pa.s)
ν	Kinematic viscosity (m^2/s) $= \mu/\rho$
ξ	Lowest moles number of the posolyte or the negolyte, contained in the battery
ρ	Specific gravity (kg/m^3)
τ_R	Residence time in the reactor (s) with $\tau_R = V_R/Q$
τ_{ST}	Residence time in the storage tank (s) with $\tau_{ST} = V_{suspension}/Q$
Φ	Diameter (m)
ω	Stirring rate (rpm)

Appendix X1: Electrochemical cell for the preparation of vanadium and basics of electrochemical analysis

1) U-shaped electrochemical cell

Electrochemical cells are devices capable of generating energy from chemical reactions and they exist in two types: galvanic (or voltaic) and electrolytic cells. A galvanic cell uses the energy released during a spontaneous redox reaction ($\Delta G < 0$) to generate electricity whereas an electrolytic cell consumes electrical energy from an external source to cause a non–spontaneous redox reaction to occur ($\Delta G > 0$).

The galvanic cell is composed of two beakers containing electrolyte solutions with their corresponding metallic electrodes and connected through a salt bridge, which is a U–shaped glass tube inserted in both solutions. This bridge is composed by ions that are not susceptible to interfere with the electroactive species in the beakers and its role is to maintain electrical neutrality within the internal circuit in both solutions by allowing ions to migrate between them. The difference with an electrolytic cell is that only a single compartment is employed in most applications, containing both electrodes and connected to an external circuit generating current, forcing electrons to flow and non-spontaneous reactions to occur.
In the case of this study, the undertaken reactions aim to prepare vanadium solutions at different oxidation states, and not all of the reactions are spontaneous; in addition, the process requires the presence of two separated redox couples, therefore, the electrochemical cell used for this work is a mix between both types of cells described above: it has the concept of the galvanic cell i.e. the separation in two compartments but the applicability of the electrolytic cell i.e. the necessity of an external power source.

2) Basics of electrochemical analysis in a three electrodes cell configuration

Usually, the working electrode in a three electrodes setup is a disk of small diameter fixed in the middle of an inert Teflon support which is mounted on a rotating electrode body that allows controlling the stirring of the solution at desired speeds.

$$\beta\ Red \rightarrow \alpha\ Ox + n\ e^- \qquad E° \text{ in V/ESH} \qquad \text{Rx.X1.1}$$

The current is measured between the WE and the CE, and the potential between the WE and the RE. The measured potential translates the thermodynamics of the studied redox couple and is described through the Nernst equation (Eq.X1.1). It links the activities of the studied species with the electrode potential “E” of the half reaction occurring on the electrode (for example Rx.X1.1), with the standard electrode potential, “E°” which is the value of the potential corresponding to

the characteristic potential of the redox couple, measured with a standard hydrogen electrode when the activities of all species are unity[2].

$$E = E° + \frac{RT}{nF} ln \frac{a_{ox}^{\alpha}}{a_{red}^{\beta}} \qquad \text{Eq.X1.1}$$

Where: E: measured potential of the redox couple (V);

E°: standard potential of the studied redox couple (V);

R: universal gas constant ($J.K^{-1}.mol^{-1}$);

T: temperature (K);

n: number of electrons transferred in the half-reaction;

F: Faraday's constant, ($C.mol^{-1}$);

a_{ox}: the chemical activity of the oxidized form of the active species;

a_{red}: the chemical activity of the reduced form of the active species;

α and β: the stoechiometric coefficients of the oxidizing and reducing forms respectively, according to the half-reaction taking place on the working electrode.

On the other hand, the current represents the kinetics of the reaction: it allows distinguishing the limiting phenomena involved which can be either the transport of the active species to the electrode, mainly diffusion, or the activation on the surface of the electrode which depends on the characteristics of each electrode and the affinity of the species with it. Each phenomenon is characterized by a domain on the I = f(E) curve (Fig.X1.1): the blue segment, called diffusion plateau, is where the transport of the species is the limiting parameter of the kinetics, while the red segment of the curve, shaped like an exponential, corresponds to a kinetic limitation by the activation/reaction at the electrode.

The current is described by the Butler-Volmer equation[3] [4]:

$$j = j_0 \times \left\{ \exp\left[\frac{\alpha_a zF}{RT}\eta\right] - \exp\left[-\frac{\alpha_c zF}{RT}\eta\right] \right\} \qquad \text{Eq.X1.2}$$

Where: j: electrode current density defined as $j = I/S$ ($A.m^{-2}$);

j_0: exchange current density, which is the current in the absence of electrolysis and at zero overpotential ($A.m^{-2}$);

α_a: anodic charge transfer coefficient;

α_c: cathodic charge transfer coefficient;

z: number of electrons involved in the electrode reaction;

[2] C.M.A. Brett, A.M.O. Brett, "Electrochemistry: Principles, Methods, and Applications", Oxford University Press, 1993

[3] A.J. Bard, L.R. Faulkner, "Electrochemical Methods: Fundamentals and Applications", John Wiley and sons, 2nd edition, 2001

[4] V.S. Bagotsky, "Fundamentals of electrochemistry", John Wiley and sons, 2nd edition, 2006

η: activation overpotential, defined as $\eta = E - E_{eq}$, where E is the electrode potential and E_{eq} the equilibrium potential.

The Butler-Volmer equation is usually simplified according to several assumptions made on the experimental conditions and the electrolyte, in order to be able to resolve it.

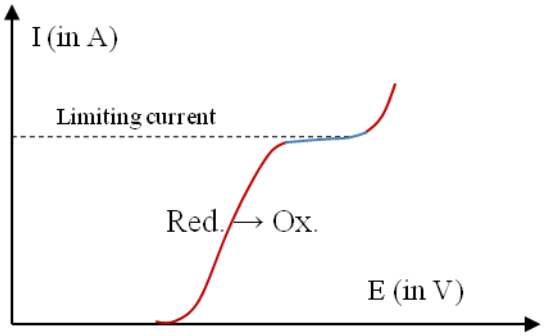

Fig.X1.1: Schematic representation of a classic current–potential curve, for the oxidation of an electroactive specie; the red segment corresponds to the limitation of the kinetics by the activation at the electrode and the blue segment is the diffusion plateau.

In addition, an important component of this setup is the working electrode; its characteristics (material, surface conditions such as roughness and porosity, geometrical surface…) impact the resulting current. As a matter of fact, two main types of processes can occur on the electrode: faradaic and non-faradaic. In the first case, the observed current is related to a chemical reaction on the electrode[5]: the electron transfer across the electrode-solution interface causes oxidation or reduction reactions to occur, according to Faraday's law which states that the amount of transformed species caused by the flow of current is proportional to the amount of electricity passed. However, sometimes processes such as adsorption and desorption occur at the surface of the electrode because of local changes at the electrode-solution interface with changing potential or solution composition. These processes are known as non-faradaic or capacitive and although the charge released from these phenomena does not cross the interface, they can still impact the resulting current because the external current can still flow.
Both faradaic and non-faradaic processes occur during the current–potential studies in a solution, but the faradaic processes are usually more of interest for the investigation of the reactions of the studied species. It corresponds mainly to how the analyzed system has evolved compared to its original state, meaning the quantity of substance that has been transformed. Faraday's law represents quantitatively the amount of electric charge, directly linked to the reaction rate and therefore the amount of transformed species[6]:

[5] J.Koryta, J.Dvorak, L.Kavan, "Principles of electrochemistry second edition", John Wiley and sons, 1993
[6] C. Lefrou, P. Fabry, J.C. Poignet, "Electrochemistry: The Basics, With Examples", Springer, 2012

$$Q = \int_{t}^{t+\Delta t} I_{(t)} dt = \frac{n_i n_e F}{\nu_i} \qquad \text{Eq.X1.3}$$

Where: Q: faradic charge amount exchanged during the time interval Δt (C);
I: current flowing through the interface (A);
Δt: time interval during which the current flows (s);
n_i: amount of substance of species *i* transformed during the time interval Δt (mol);
n_e: number of exchanged electrons for the reaction;
ν_i: stoechiometric number of species *i*;
F: Faraday constant ($C.mol^{-1}$).

The *I = f(E)* curves are performed via a potentiostat: its role is to force through the working electrode the required current in order to achieve the desired potential. As mentioned above, the current corresponds to the flow of electrons that are chemically required for the active electrochemical processes to happen at rates consistent with the potential[2].

Appendix X2: Potentiometric titration of $V^{(V)}$ by $Fe^{(II)}$ – Bibliographic approach

Potentiometric titration is one of the oldest methods used for quantifying chemical compounds based on the potential variation of an oxido-reduction reaction between two redox couples, and usually provides more reliable data than titrations using chemical indicators based on a color change or precipitation formation in the solution. The principle of this method involves the measurement of the potential difference between an indicator electrode and a reference electrode as a function of the poured volume of the titrant solution. A typical potentiometric cell is represented as:

$$\underbrace{\text{Reference electrode}}_{E_{ref}} \mid \overbrace{\text{analyte solution} \mid \text{indicator electrode}}^{E_{ind}}$$

The potential of the cell is: $E_{cell_{(i=0)}} = E_{ind} - E_{ref}$ Eq.X2.1

The reference electrode has a fixed potential at constant temperature and is independent of the composition of the analyte solution contrary to the indicator electrode which potential varies with variations in the concentration of the analyte. A combined glass electrode is used instead of two separate electrodes; it consists of a glass indicator electrode and a saturated calomel reference electrode combined together as one and immersed in the solution with an unknown pH. The potential being proportional to the pH, this electrode can be used for potentiometric titrations.

The oxido-reduction reaction takes place between two couples with zero current potentials $E_{i=0\ (V)/SHE}$ separated by at least 300 mV, in order to favor a spontaneous and total reaction. According to the gamma rule, the oxidizing agent from the couple with the higher $E_{i=0}$ reacts with the reducing agent of the couple with the lower $E_{i=0}$:

$$\begin{aligned} &\underline{\text{Reduction}} && Ox_1 + ne^- \rightarrow Red_1 \\ &\underline{\text{Oxidation}} && Red_2 \rightarrow Ox_2 + ne^- \\ &\underline{\text{Total}} && Ox_1 + Red_2 \rightarrow Ox_2 + Red_1 \end{aligned} \qquad \text{Rx.X2.1}$$

with $E_{i=0}\ (Ox_1/Red_1) > E_{i=0}\ (Ox_2/Red_2)$.

The end point or equivalence point is reached when a sudden drop/increase in potential is noted on the curve. This potential variation translates the equivalence between the molar quantity of the titrant and the titrated analyte, and the volume poured to reach this point is used to determine the concentration of the solution, using the stoechiometry of the oxido-reduction reaction taking place (Rx.X2.1):

$$n_1 = n_2 \Longrightarrow C_1V_1 = C_2V_2 \qquad \text{Eq.X2.2}$$

The only unknown value would be the concentration of the analyte.

Vanadium is a metal that can be found in many applications and its specific titration is essential given that it exists in metal alloys with chrome, manganese or tungsten, at relatively low concentrations. A number of methods were put in place such as the titration of the vanadate by ferrous sulfate and the vanadyl salt with permanganate in steel[7] or titration of a mixed solution of chrome and vanadium[8] and many others. However, aside from being a little old, most of these techniques either use additives to complex the vanadium for a better titration or include a number of tedious steps before and during the analysis to reach the endpoint.

In addition, the bibliography mostly concentrates on the titration of vanadium as $V^{(IV)}$ and $V^{(V)}$ with minimal to nonexistent techniques for $V^{(II)}$ and $V^{(III)}$ titration. Therefore, it was essential for the purpose of our work to put in place these methods.

Since $V^{(V)}$ cannot be analyzed by UV–Vis spectroscopy, it is essential to put in place a different method for its quantification. Using potentiometric titration for that purpose leads to search for a redox couple suitable for the reduction of VO_2^+ without interference from a prospective presence of VO^{2+} ions in the solution.
Quintar et al.[9] developed a method that allows the determination of $V^{(V)}$ in several ferrous and non-ferrous alloys, within a concentration interval of 5×10^{-5} to 2×10^{-3} M, by direct titration with EDTA on a chemically modified graphite electrode. The vanadium (V) solution was prepared by dissolution of NH_4VO_3 in ultra pure water and the pH was modified as required by adding phosphate or acetic acid at pH 6. However, it is necessary to include a separation step such as liquid–liquid extraction in order to separate the vanadium (V) from the other metallic elements composing the alloy to avoid interferences.

On the other hand, the titration of $V^{(V)}$ by ferrous sulfate solutions goes back to the 1940s and 1960s, where the $V^{(V)}$ was obtained by oxidizing solutions containing $V^{(IV)}$ using permanganate [6] [7]. However, this method was very delicate for several reasons mainly the reaction of vanadyl ions VO^{2+} with permanganate and the subsequent experimental steps leading to the elimination of the exceeding permanganate. The evolution of this method in the 1960s by Le Flem[10] induced the reduction of $V^{(V)}$ to $V^{(IV)}$ by reaction with an excess of $Fe^{(II)}$ ions (Rx.X2.2) which are then

[7] G. Roland, "Note concernant le dosage potentiométrique du vanadium dans les aciers", Anal. Chim. Acta, 28, 1963, 93-96, doi : 10.1016/S0003-2670(00)87201-3
[8] L. Ducret, "Dosage rapide du chrome et du vanadium", Anal. Chim. Acta, 1, 1947, 135-139, doi: 10.1016/S0003-2670(00)89728-7
[9] S.E. Quintar, J.P. Santagata, V.A. Cotinez, "Determination of vanadium (V) by direct automatic potentiometric titration with EDTA using a chemically modified electrode as a potentiometric sensor", Talanta 67 (2005) 843–847
[10] G. Le Flem, "Le système V_2O_5-ThO_2", Matériaux, Faculté des Sciences de l'Université de Bordeaux, 1964

titrated with a solution of potassium dichromate (Rx.X2.3). The solution of $V^{(V)}$ is prepared in a 3 N H_2SO_4 solution by dissolution of V_2O_5 and a diphenyl-amine barium sulfonate color indicator is added. The reactions, as given by Le Flem, are:

$$V^{5+} + Fe^{2+} \rightarrow V^{4+} + Fe^{3+} \qquad \text{Rx.X2.2}$$

$$6\ Fe^{2+} + Cr_2O_7^{2-} + 14\ H^+ \rightarrow 6\ Fe^{3+} + 2\ Cr^{3+} + 7H_2O \qquad \text{Rx.X2.3}$$

Other studies found that the direct titration of $V^{(V)}$ by $Fe^{(II)}$ without further analysis of the excess of $Fe^{(II)}$ was sufficient[11]. Titrations were performed on aliquots diluted in a 6 M H_2SO_4 solution and the titrant was a 0.1 M Fe^{2+} solution.

Also, the effect of the presence of ligands on the reaction of $Fe^{(II)}$ with $V^{(V)}$ was studied[12] and it was found that a large number of metallic ions, such as lithium, sodium and aluminum do not interfere with this reaction. Furthermore, the use of EDTA (ethylenediaminetetraacetic acid) as ligand buffer with zinc (II) in excess has been found to be very effective in the titration of vanadium (V) with iron (II) for improving the end-point detection.

[11] C. Madic, G.M. Begun, R.L. Hahn, J.P. Launay, W.E. Thiessen, "Dimerization of Aquadioxovanadium (V) Ion in Concentrated Perchloric and Sulfuric Acid Media", Inorg. Chem., 1984, 23, 469-476, doi: 10.1021/ic00172a019

[12] K. Umetsu, H. Itabashi, K. Satoh, T. Kawashima, "Effect of Ligands on the Redox Reaction of Metal Ions and the of a Ligand Buffer for Improving the End-Point Detection in the Potentiometric Titration of Vanadium (V) with Iron (II)", Analytical Sciences, 7, 1991, 115-118, doi: 10.2116/analsci.7.115

Appendix X3: Potentiometric titration of $V^{(III)}$ with $K_2Cr_2O_7$

The titration of vanadium (III) with potassium dichromate in phosphoric acid medium either by potentiometric titration or with a visual end-point has been studied[13] according to the following reactions:

$6 \times [\ V^{3+} + H_2O \rightarrow VO^{2+} + 2\ H^+ + e^-$ $\quad E° = 0.34$ V/SHE $\quad$ Rx.X3.1

$Cr_2O_7^{2-} + 14\ H^+ + 6\ e^- \rightarrow 2\ Cr^{3+} + 7\ H_2O$ $\quad E° = 1.33$ V/SHE $\quad$ Rx.X3.2

The global reaction will be:

$Cr_2O_7^{2-} + 2\ H^+ + 6\ V^{3+} \rightarrow 2\ Cr^{3+} + 6\ VO^{2+} + H_2O$ $\quad$ Rx.X3.3

It was found[12] that the titration with a diluted solution (0.05 N) of potassium dichromate $K_2Cr_2O_7$, leads to a curve with one potential jump, corresponding to the oxidation of $V^{(III)}$ to $V^{(IV)}$, while in more concentrated solutions (0.2 N) two consecutive potential jumps are obtained corresponding the oxidation of $V^{(III)}$ to $V^{(IV)}$ then to $V^{(V)}$. The method is not suitable for the analysis of $V^{(III)}$ in the VRFB because of the interference of the $V^{(II)}$ susceptible to be present simultaneously into the negolyte of the battery. However, the titration of $V^{(III)}$ by $K_2Cr_2O_7$ was tried anyway to test its validity in the experimental conditions of the negolyte prior to a battery charge cycle. To that end, a solution of 0.45 M of $V^{(III)}$ was prepared by dissolution of $V_2(SO_4)_3.9H_2O$ in 3 M H_2SO_4, to be titrated by a $5x10^{-3}$ M solution of $K_2Cr_2O_7$ (from UCB, 97 % purity) in 2 M H_2SO_4. The assumed reaction would be taking place between the two redox couples VO^{2+}/V^{3+} and $Cr_2O_7^{2-}/Cr^{3+}$ as presented in Rx.X3.3.

Theoretically, given that the two couples are separated by a potential difference of 0.99 V, the reaction is supposed to take place and succeed, allowing a quantification of $V^{(III)}$. However, that was not the case, a potential drop was not observed and the titration was not reproducible. Furthermore, a visual end-point could not be detected given that the solution of Cr^{3+} formed is green, like the V^{3+} solution, and the formation of a blue VO^{2+} solution cannot be seen.

Therefore, this method is not suitable for the potentiometric titration of $V^{(III)}$ in the negolyte of the VRFB.

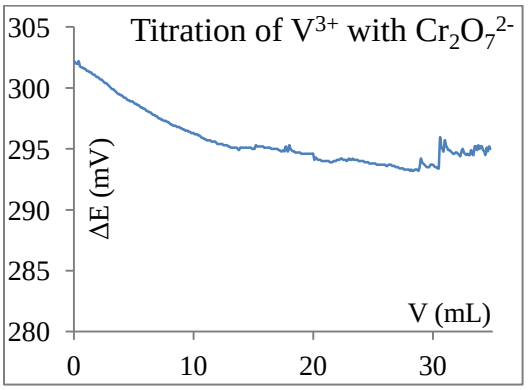

Fig.X3.1: Evolution of the potential ΔE of a V^{3+} solution as a function of the added volume of $Cr_2O_7^{2-}$ at $5x10^{-3}$ M; titration achieved using a combined "platinum indicator electrode and a silver/silver chloride reference electrode"

[13] G.G. Rao, P.K. Rao, "A new oxidimetric reagent: potassium dichromate in a strong phosphoric acid medium-VI: Potentiometric titration of vanadium (III) alone and in mixture with vanadium (IV)", Talanta, 13 (9), 1966, 1335-1340, doi: 10.1016/0039-9140(66)80223-0

Appendix X4: Potentiometric titration of $V^{(III)}$ with $Fe_2(SO_4)_3$

The studied redox couple is VO^{2+}/V^{3+} (E° = 0.34 V/SHE) because the standard potential of the V^{3+}/V^{2+} redox couple (– 0.26 V/SHE) is very low and finding a reducing agent with a lower potential, easy to put in solution and capable of reducing the $V^{(III)}$ is nearly impossible. The titration methods tested to find a suitable titrant for V^{3+} is with the redox couple Fe^{3+}/Fe^{2+} (E° = 0.77 V). The difference between the standard potential of the couples is 0.43 V, greater than the difference observed for the titration of $V^{(V)}$ by $Fe^{(II)}$ (0.23 V/SHE), so the reaction should be successful. A solution of 0.1 M of Fe^{3+} was prepared by dissolution of the ferric sulfate $Fe_2(SO_4)_3.xH_2O$ (from Sigma Aldrich, 97 %) in ultra pure water, acidified with H_2SO_4 5 M. The hydration of the sulfate was determined by ICP analysis and was found to be equal to 7: $Fe_2(SO_4)_3.7H_2O$. The solution of V^{3+} was prepared by dissolution of $V_2(SO_4)_3.9H_2O$ in 5 M H_2SO_4. The reactions taking place during the titration are the following:

$$V^{3+} + H_2O \rightarrow VO^{2+} + 2\,H^+ + e^- \qquad E° = 0.34\ V/SHE \qquad Rx.X4.1$$

$$Fe^{3+} + e^- \rightarrow Fe^{2+} \qquad E° = 0.77\ V/SHE \qquad Rx.X4.2$$

The global reaction will be:

$$Fe^{3+} + H_2O + V^{3+} \rightarrow Fe^{2+} + VO^{2+} + 2\,H^+ \qquad Rx.X4.3$$

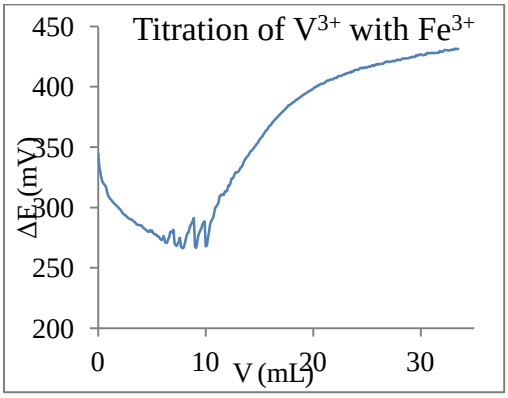

Fig.X4.1: Evolution of the potential ΔE of a V^{3+} solution as a function of the added volume of Fe^{3+} solution at 0.1 M; titration achieved using a combined "platinum indicator electrode and a silver/silver chloride reference electrode"

From the resulting curve of the titration, given in Fig.X4.1, it can be seen that there is no clear potential drop marking the end point of the titration, whereas a visual color shifting from green ($V^{(III)}$) to blue ($V^{(IV)}$) is observed in the solution. The theoretical equivalence point calculated through Rx.X4.3 by using the initial concentrations used, should have been after adding 18 to 20 mL of Fe^{3+} in the stirred V^{3+} solution. However, despite adding a bigger volume, the equivalence point was not observed on the curve. In addition, it can be seen that for $V_{added} < 10$ mL, the curve exhibits the presence of numerous fluctuations of the potential which are not generally observed in a potentiometric titration curve and can be interpreted as secondary reactions taking place in the solution or unstable complexes forming between the various species present in solution but it should be noted that no precipitation was observed during the titration. These fluctuations were observed on all the curves performed to study the reproducibility of the method. In light of the above results, the titration of $V^{(III)}$ with $Fe^{(III)}$ does not seem to be adequate for its quantification.

Appendix X5: Potentiometric titration of $V^{(III)}$ with $KMnO_4$

This method uses the permanganate MnO_4^-/Mn^{2+} ($KMnO_4$ 99 %, from Alfa Aesar) in ultra-pure water and acidified with 3 M sulfuric acid. In this case, the analyte solution of V^{3+} was prepared by dissolution of vanadium trioxide (V_2O_3 99.7 % from Alfa Aesar), in 3 M sulfuric acid. The reactions taking place are the following:

$$5 \text{ x } [\ V^{3+} + H_2O \rightarrow VO^{2+} + 2\ H^+ + e^- \qquad E° = 0.34 \text{ V/SHE} \qquad \text{Rx.X5.1}$$

$$MnO_4^- + 8\ H^+ + 5\ e^- \rightarrow Mn^{2+} + 4\ H_2O \qquad E° = 1.51 \text{ V/SHE} \qquad \text{Rx.X5.2}$$

The global reaction will be:

$$MnO_4^- + H_2O + 5\ V^{3+} \rightarrow Mn^{2+} + 5\ VO^{2+} + 2\ H^+ \qquad \text{Rx.X5.3}$$

However, this is not the only reaction susceptible to take place; since the standard potential of the VO_2^+/VO^{2+} ($E° = 1.00$ V/SHE) is lower than that of MnO_4^-/Mn^{2+}, the formed VO^{2+} is susceptible to react with the excess MnO_4^-:

$$MnO_4^- + H_2O + 5\ VO^{2+} \rightarrow Mn^{2+} + 5\ VO_2^+ + 2\ H^+ \qquad \text{Rx.X5.6}$$

The combination of reactions (5) and (6) gives the total reaction that would take place during the titration:

$$2\ MnO_4^- + 2\ H_2O + 5\ V^{3+} \rightarrow 2\ Mn^{2+} + 5\ VO_2^+ + 4\ H^+ \qquad \text{Rx.X5.7}$$

Depending on the number of potential drops on the titration curve, the V^{3+} concentration could be calculated: if the reaction takes place in only one step, directly from $V^{(III)}$ to $V^{(V)}$, only one equilibrium point will be found and Rx.X5.7 should be used for the calculations. However, if the two reactions undergo separately, then the curve would have two potential drops and Rx.X5.6 is used to quantify $V^{(III)}$ from the first one. The result presented in Fig.X5.1 shows two potential jumps and therefore a separate reaction for each redox couple. The small peak at the beginning of the curve corresponds to the autocatalytic reduction of MnO_4^- by Mn^{2+}.

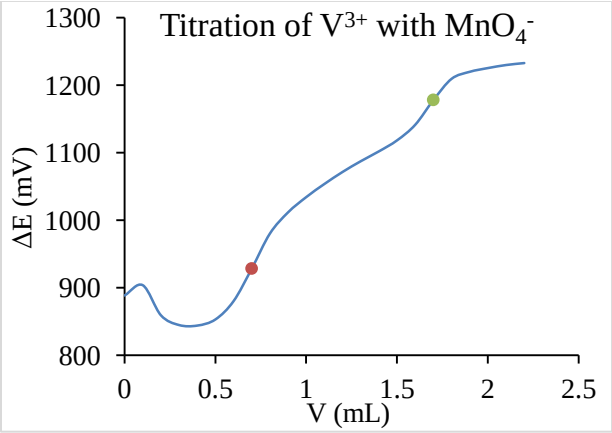

Fig.X5.1: Evolution of the potential ΔE of a V^{3+} solution as a function of the added volume of MnO_4^- solution at 0.1 M; titration achieved using a combined "platinum indicator electrode and a silver/silver chloride reference electrode"

During the titration, the color of the solution changed five times. Initially, the solution was black and opaque with non-dissolved V_2O_3 powder, which was used in excess due to the low solubility of the oxide in sulfuric acid. After the first few drops of permanganate into the stirred solution and before the first equivalence, the color becomes light green and the solution is clear with some remaining solid particles of powder. At the first equivalence, the color turns to light blue, typical of a $V^{(IV)}$ solution, before it changes to light yellow for the second equivalence, representing a $V^{(V)}$ solution. After that final point, the solution turns to violet-red, marking the end of the titration and an excess of MnO_4^-.
The excess powder of V_2O_3 seems to have disappeared after the first color change from opaque black to light transparent green, which means that the dissolution was favored during the titration. However, despite obtaining two separate end points, the calculation of the vanadium (III) concentration does not give the initial concentration of vanadium used for the titration, with a difference of 97 % between the theoretical value ($5x10^{-2}$ mol/L) and the one calculated via the titration ($1.42x10^{-3}$ mol/L).

In fact, when the titration was finished and the solution was left without agitation, its color turned to brown and a precipitate was formed. This may imply that the excess MnO_4^- and the formed Mn^{2+} reacted together in the presence of air to form the brown precipitate of MnO_2.
In order to make sure that it was not the vanadium being re-precipitated after dissolution, another experiment was undertaken and the titration was stopped at the second equivalence, i.e. without adding an excess of MnO_4^- in the titrated solution. The solution was clear with no remaining solid particles and it had a light yellow color, which is relative to $V^{(V)}$. This implies that $V^{(III)}$ was dissolved and oxidized to $V^{(V)}$. After leaving the solution in contact with air, no precipitate appeared and the solution remained clear for a few hours. Therefore, it was the presence of an excess of MnO_4^- that lead to the precipitation of MnO_2 after the end of the titration.
Nevertheless, this method does not allow to calculate the exact concentration of $V^{(III)}$ and this could be due to the formation of secondary species of manganese or vanadium during the titration, given that both elements exist in several oxidation states and their E–pH diagrams show a wide variety of species. Therefore, the titration of V^{3+} with MnO_4^- is not suitable for the quantitative titration of $V^{(III)}$ used in the VRFB.

Appendix X6: Potentiometric titration of $V^{(III)}$ with I_2

A solution of iodine (I_3^-) was used to try to titrate the V^{3+} by oxidizing it to VO^{2+}. The system (I_3^-/I^-) has a standard potential only 200 mV higher than that of VO^{2+}/V^{3+} making the affinity of the reaction between I_2 and V^{3+} lower, but the method was tried anyway. The preparation of the iodine solution required the use of potassium iodide (Aldrich Chemicals, 99+ %) in order to dissolve the iodine (Fisher Scientific, 99 %) in ultra-pure water. The solution is acidified with sulfuric acid used in the preparation of the vanadium solution, which was prepared with the same method used for the previous MnO_4^- titration. The reactions susceptible to take place during the titration are:

$$2 \times [\ V^{3+} + H_2O \rightarrow VO^{2+} + 2\ H^+ + e^- \qquad E° = 0.34\ V/SHE \qquad \text{Rx.X6.1}$$

$$I_2 + 2\ e^- \rightarrow 2\ I^- \qquad E° = 0.54\ V/SHE \qquad \text{Rx.X6.2}$$

The global reaction will be:

$$I_2 + 2\ V^{3+} + 2\ H_2O \rightarrow 2\ I^- + 2\ VO^{2+} + 4\ H^+ \qquad \text{Rx.X6.3}$$

Unlike the reaction with permanganate, where the formed vanadium (IV) would also react with MnO_4^-, the reaction between VO^{2+} and I_2 cannot take place, given that it does not follow the gamma rule.

In this experiment, the color of the solution did not change at all during the titration: it remained an opaque black solution with V_2O_3 powder in suspension. This indicates that no reaction occurred between V^{3+} and I_2. This can be confirmed by the potentiometric curve (Fig.X6.1) that shows no considerable variation in the potential and no equivalence point. Therefore, Rx.X6.3 does not take place as predicted, possibly due to the proximity of the standard potential values of the two redox couples involved.

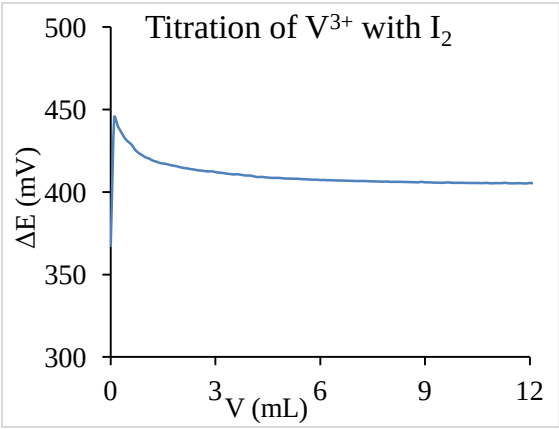

Fig.X6.1: Evolution of the potential ΔE of a V^{3+} solution as a function of the added volume of I_2 solution at 0.1 M; titration achieved using a combined "platinum indicator electrode and a silver/silver chloride reference electrode"

We can conclude that the VO^{2+}/V^{3+} redox couple cannot be considered as a stable and defined couple for a potentiometric titration given that the reactions between V^{3+} and four chosen

elements ($Cr^{(VII)}$, $Fe^{(III)}$, $Mn^{(V)}$ and $I^{(0)}$) did not give a quantitative response for the titration that was supposed to allow the calculation of the $V^{(III)}$ concentration. Besides, in case those reactions were successful, a complementary analysis should have been carried out in order to study the influence of the presence of $V^{(II)}$ in the analyte solution, since it will be a constituent of the negolyte. Given that the V^{3+}/V^{2+} couple has an $E° = – 0.26$ V/SHE, $V^{(II)}$ will be susceptible of reacting with all of the four suggested titrant solutions.

Appendix X7: Basics of ICP and NMR

1) Inductively Coupled Plasma

It is based on ionizing a sample of solution by contact with a stable plasma which is an electronically neutral ionized gas with a temperature range between 6000 and 10000 K [35]; an inert gas, often argon, is used to form the plasma. Two main detection techniques of quantification are usually used along with the ICP: mass spectrometry (ICP–MS) or optical emission spectrometry (ICP–OES) and the difference between them orient greatly the application of the technique.
For instance, ICP–OES quantification is based on measuring the released energy from excited atoms and ions at a wavelength characteristics of the analyzed element whereas ICP–MS measures an atom's mass and its lower detection limit can extend to parts per trillion (ppt), while the lower limit for ICP–OES is parts per billion (ppb).

In the ICP–OES, used in this work, the analyte sample is transported into the instrument as a stream of liquid sample. Inside the instrument, the liquid is converted into an aerosol through a process called nebulisation. The sample aerosol is then transported to the plasma where it is desolvated, vaporized, atomized, and excited and/or ionized by the plasma[14]. Then, the ionized particles of the analyte are sent to the detector: the excited atoms and ions emit a radiation with a characteristic wavelength for each element. The intensity of the radiation, proportional to the concentration of the element in solution, is detected and turned into electronic signals that are converted into interpretable data.

This technique has been used largely for the determination of vanadium in environmental, industrial, and biological samples. In order for the method to work, it was combined with other separation techniques prior to injection in the ICP to separate mainly $V^{(IV)}$ and $V^{(V)}$ that are usually found together in water and soil samples. These techniques include liquid–liquid extraction, anion exchange chromatography by formation of selective complexes with EDTA[15] or cation exchange columns based on acid modification of the species. These techniques seem to give promising results in the studied fields, but their application in the case of the VRB would be

[14] S. Ghosh, V.L. Prasanna, B. Sowjanya, P. Srivani, M. Alagaraja, D. Benji, "Inductively coupled plasma - Optical emission spectroscopy: A review", Asian J. Pharm. Ana., 3 (1), 2013, 24-33

[15] a) P.P. Coetzee, J.L. Fischer, M. Hu, "The separation and simultaneous determination of V(IV) and V(V) species complexed with EDTA by IC-ICP-OES", Water SA, 28 (1), 2002, 37-44, doi: 10.4314/wsa.v28i1.4865
b) N. Kilibarda, S.E. Afton, J.M. Harrington, F. Yan, K.E. Levine, "Rapid speciation and determination of vanadium compounds using ion-pair reversed-phase ultra-high-performance liquid chromatography inductively coupled plasma-sector field mass spectrometry", J. Chromatogr. A, 1304, 2013, 121– 126, doi: 10.1016/j.chroma.2013.06.074
c) F. Aureli, S. Ciardullo, M. Pagano, A. Raggi, F. Cubadda, "Speciation of vanadium (IV) and (V) in mineral water by anion exchange liquid chromatography-inductively coupled plasma mass spectrometry after EDTA complexation", J. Anal. At. Spectrom., 23, 2008, 1009-1016, doi: 10.1039/b805234b

more complicated given that the matrix would need further studies to find the adequate separation column and suitable complexing agents for each of the two redox couples of vanadium involved in the electrolyte solutions.

The analyzed solutions should be diluted before analysis so as not to saturate the detector and be able to calibrate it in a known concentration range for accurate results. All the analyzed vanadium solutions were diluted to 100 ppm or less (part per million, equivalent to $mg.L^{-1}$) as a concentration of vanadium element in sulfuric acid which is used for the calibration as well in order to eliminate the matrix effect. To perform such a dilution from concentrated vanadium electrolyte solutions, it is necessary to go through an intermediate less diluted solution to minimize mass and/or volume sampling errors, especially that the high concentrations in vanadium generates higher densities and viscosities that should be taken into account.

2) Nuclear Magnetic Resonance

Nuclear magnetic resonance spectroscopy, known as NMR, is an analytical technique used for the determination of molecule structures but also for determining the content and purity of a sample by comparing its spectrum against spectral libraries and basic structures spectrums. The principle of the method is based on atomic nuclei that possess a non-zero nuclear spin in the presence of a magnetic field with transitions that occur in the radio–frequency region of the spectrum[16]. In order to consider that the isotope of a chemical element has an intrinsic nuclear magnetic moment or in other words a non–zero nuclear spin, it should contain an odd number of neutrons and/or protons. The most commonly used nucleus in NMR is ^{1}H. All atomic species with an even number of nucleons have a total spin of zero and therefore cannot be analyzed by NMR spectroscopy. However, using their isotopes is usually an alternative employed in the studies and the best examples would be ^{13}C and ^{17}O, the isotopes of carbon and oxygen respectively.

When an external magnetic field is applied to the studied sample, an energy transfer occurs between the base energy to a higher energy level (generally a single energy gap). The energy transfer takes place at a wavelength corresponding to the characteristic radio frequencies of the isotope and when the spin returns to its base level, energy is emitted at that same frequency. A Fourrier transform is applied to the obtained signal in order to yield an NMR spectrum for the nucleus concerned[17]. On the other hand, instead of using radio–frequencies to represent the signal of each isotope, it was decided to use the “chemical shift”, expressed in ppm and independent from the magnetic field applied.

[16] R.K. Harris, “Nuclear magnetic resonance spectroscopy”, book, Englang, Longman scientific and technical, 1986
[17] F.A. Bovey, P.A. Mirau, H.S. Gutowsky, “Nuclear Magnetic Resonance Spectroscopy”, Elsevier, 1988

The NMR samples are analyzed in a thin-walled glass tube and are usually prepared in deuterated solvents, such as deuterochloroform $CDCl_3$, where more than 99 % of the protons are replaced with deuterium ^2H or ^2D, the isotope of hydrogen, in order to avoid detecting the signals from hydrogen atoms of the solvent in which the studied molecule is prepared.

Appendix X8: Effect of the presence of vanadium solid particles studied on a GF used as electrode

The geometrical surface of the felt used for this study is 1 cm^2, and a new electrode was activated and used for each suspension. The results are compared to the concentrated 1.5 mol/L VO^{2+} solution and it appears that they all have the same linear shape (Fig.X8.1); the oxidation plateau does not appear even if the electrodes' surface is decreased to 0.5 cm^2 (results not shown here). The analysis of the curves shows that the current decreases when the amount of powder in the suspension increases: this can be due to the fact that the active surface decreases due to the clogging of the elctrode by the inert $VOSO_4$ particles. The more the quantity of powder increases in solution, the more the surface is masked and it becomes more difficult to renew the active species in the diffusion layer.

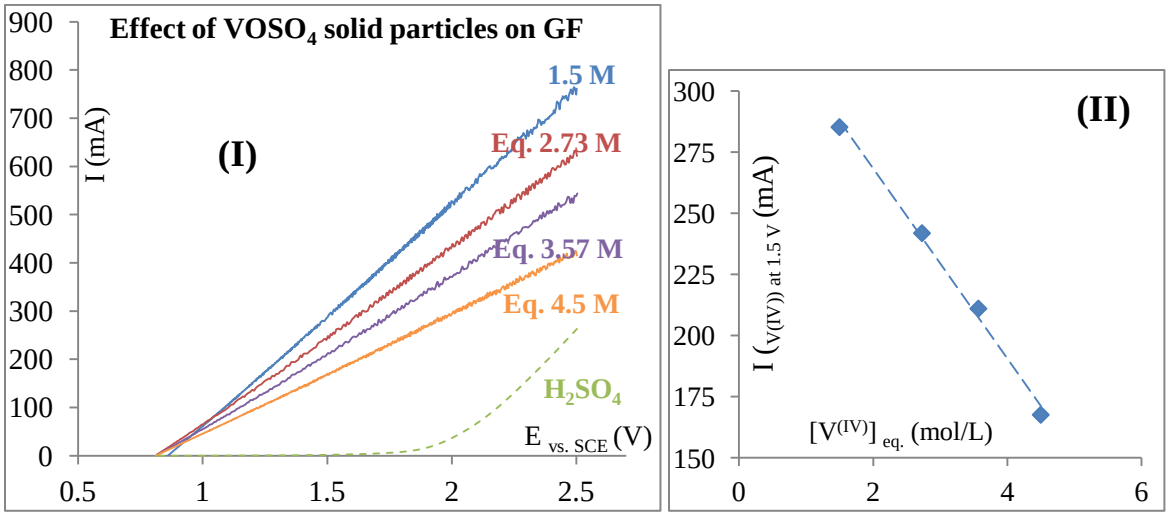

Fig.X8.1: **(I)**: Comparison of the I = f(E) curves performed on a GF electrode (S_g = 1 cm^2), immersed in a H_2SO_4 solution containing $V^{(IV)}$ at the following equivalent concentrations: 1.5 (blue), 2.73 (red), 3.57 (violet) and 4.5 mol/L (orange); RE = SCE, CE = Pt plate, ω ≈ 500 rpm (magnetic stirrer), r = 5 $mV.s^{-1}$;
(II): Linear evolution of the current as a function of the vanadium (IV) equivalent concentration in the studied suspensions; the values of I were taken at E = 1.5 V after subtracting the H_2SO_4 residual current.

However, these results are not negative since the current is not cancelled, but is rather decreased from ~ 290 mA to ~ 168 mA when the equivalent concentration increases from 1.5 to 4.5 M.

Effect of the stirring:

The obtained curves on the GF show no influence of the stirring on the oxidation current. For this electrode, an important ohmic drop is due to the electronic connection of the felt; this causes the shape of the curves to be practically straight overlying lines and does not allow observing the effect of any other parameter. Besides, the suspension contains an important quantity of particles which will accumulate inside the felt and consequently they will not be affected by the stirring.

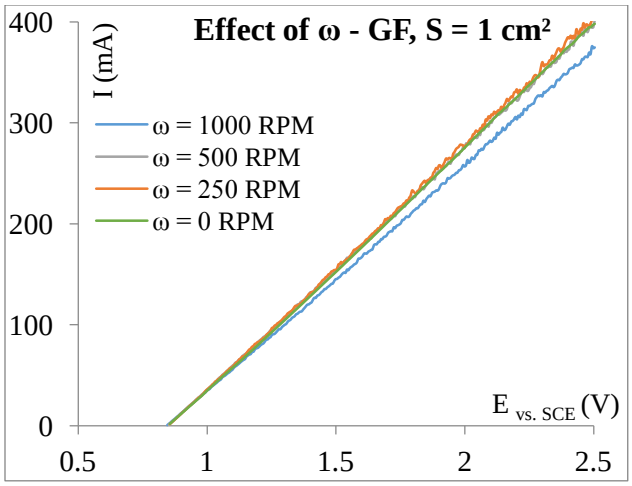

Fig.X8.2: Comparison of the I = f(E) curves performed on a GF electrode (S_g = 1 cm^2), immersed in a H_2SO_4 solution containing $V^{(IV)}$ at 4.5 M equivalent concentration at different stirring rates: 1000 RPM (blue), 500 RPM (grey), 250 RPM (orange) and 0 RPM (green); RE = SCE, CE = Pt plate, r = 5 $mV.s^{-1}$.

Effect of the addition of 1 % KB:

The same electrode used for the study of the effect of stirring was used and therefore, being already clogged by the vanadium particles, it showed no effect in the presence of KB. Using a new activated electrode would have the same response given that it would be clogged from the moment it is immersed in solution, so another approach was taken. An additional step of activation was undertaken to a new electrode: after performing the usual cyclic voltammetry, three linear voltammetry curves, in oxidation, were done in a 3 M sulfuric acid solution containing 1 % of KB, to try to activate even more the internal fibers of the felt and also fill the gaps of the felt with carbon particles susceptible of helping the current transfers, instead of vanadium inert solid grains. After that, the electrode was immersed in the vanadium-KB suspension and the obtained curves are presented in Fig.X8.3, along with the ones from the trial on the first electrode.

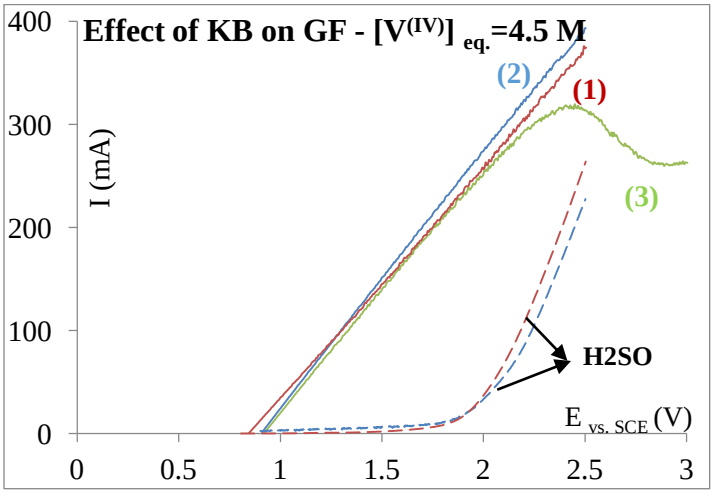

Fig.X8.3: Effect of the presence of 1 % in weight of KB on the I = f(E) curves performed on a graphite felt electrode (S_g = 1 cm^2) immersed in a solution of H_2SO_4 3 M containing $V^{(IV)}$ at an equivalent concentration of 4.5 M; (1/red): suspension without KB, curve extracted from Fig.X8.1-(I); (2/blue): suspension containing 1 % in weight KB, curve performed on the 'old electrode'; (3/green): suspension containing 1 % in weight KB, curve performed on the 'newly treated electrode'; RE = SCE, CE = Pt plate, r = 5 $mV.s^{-1}$.

The treated electrode (curve N°3) has a clearly different shape than the other two: it shows an oxidation peak, until now absent from the curves performed on the GF for the vanadium suspensions. This peak corresponds to a decrease of the current at the interface of the electrode, which is the same phenomenon observed on the GR in the absence of stirring (Fig.III.18 – GR – curve N°1). The proposed explanation applies in this case as well: the surface saturation no longer exists for lack of supply of species due to the clogging of the felt, but this time by the KB particles and hence, the current decreases.

Comparing now curves (1) and (3), the effect of KB on the current is not very pronounced for potentials lower than 2 V and even a slight decrease is observed if we compare it with curve (2). This can be due to: i) the vanadium particles getting between the KB grains, as described before, and thus the active surface is not increased by electronic percolation in the presence of KB or ii) the fact that the GF fibers are filled with KB prevent the contact between the dissolved VO^{2+} ions and the graphite felt and hence, the current decreases.

Appendix X9: Expression of I_{lim} as a function of the stirring rate ω

The limiting current (A1) measured on a *I = f(E)* curve is proportional to the mass transfer coefficient k.

$$I_{lim}=n\,F\,S\,k\,C_{V^{(IV)}} \qquad \text{(A1)}$$

k can be expressed as a power law (A2) of the angular velocity ($\omega=2\times\pi$ *in rad.s*$^{-1}$) of the stirrer using the Leveque correlation (A3):

$$k = a' + b' \times \omega^{\gamma} \qquad \text{(A2)}$$

$$Sh = a + b \times Re^{\gamma} \times Sc^{\kappa} \qquad \text{(A3)}$$

Indeed, substituting the Sherwood, Reynolds and Schmidt numbers (see definitions in nomenclature), the correlation becomes:

$$\frac{k\,d_e}{D} = a + b \times \left(\frac{\upsilon\rho d_e}{\mu}\right)^{\gamma} \times \left(\frac{\mu}{\rho\times D}\right)^{\kappa} \qquad \text{(A4)}$$

Assuming that the velocity υ in the Reynolds number is the angular velocity of the stirring device (RCE or CSS), then the equation can be written as:

$$k = \frac{a\times D}{d_e} + \left(b \times D^{1-\kappa} \times d_e^{\gamma-1} \times \rho^{\gamma-\kappa} \times \mu^{\kappa-\gamma}\right) \times \omega^{\gamma} \Rightarrow k = a' + b' \times \omega^{\gamma}$$

This relation shows the dependence of the mass transfer coefficient to the angular velocity of the stirrer, and consequently that of the limiting current:

$$I_{lim} = n\,F\,C_{V^{(IV)}}\,S\,(a' + b' \times \omega^{\gamma}) \Rightarrow I_{lim} = a'' \times S + b'' S \times \omega^{\gamma} \qquad \text{(A5)}$$

Appendix X10: Study of $V^{(V)}$ solutions at 2.5 and 5 M on a GF electrode

The graphite felt electrode used for plotting the I = f(E) curves was activated by cyclic voltammetry in sulfuric acid.The obtained results (Fig.X10.1) show a linear evolution of the current, as observed for the suspensions of $V^{(IV)}$ earlier, instead of the classic linear voltammetry curve and there was no significant difference between the two solutions.

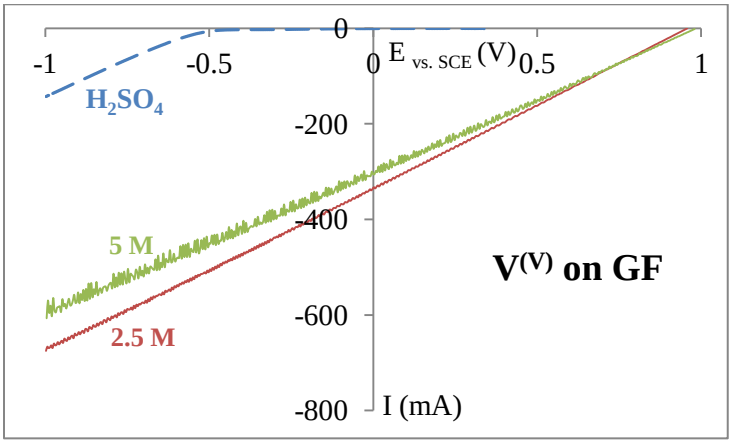

Fig.X10.1: Comparison of I = f(E) curves performed on a graphite felt electrode (S_g = 1 cm^2), immersed in 20 mL of two $V^{(V)}$ deaerated solutions: green/ $[V^{(V)}]$ = 5 M, obtained from electrolysis; red/ $[V^{(V)}]$ = 2.5 M obtained from the dilution of the latter in 3 M H_2SO_4 (blue curve); RE = SCE, CE = Pt plate, ω ≈ 500 RPM (magnetic bar), r = 5 $mV.s^{-1}$.

Obtaining approximately the same current for different concentrations is not normal, especially since even in the presence of solid particles in the case of $V^{(IV)}$ a decrease of the current was observed with the increasing fraction of solid. Therefore, we suggest that in this case, a significant ohmic drop generating from the electrode leads to these results. Hence, a modification of the electrodes' configuration is suggested: until now, the graphite felt electrode was a 1 cm wide band of 10 cm where the active 1 cm^2 geometrical surface was delimited by resin based glue. It is thought that the 9 remaining centimeters of the electrode until the electronic contact are the reason for the ohmic drop, so the new configuration is to attach only the active surface to a copper wire and isolate it with the same glue to prevent any infiltration of copper inside the solution or on the active surface of the electrode. The electrode is then activated through the same process as earlier before performing the electrochemical analysis.

The obtained curves have the same shape of the first ones but a difference in the current is now clear between the two solutions: the current increases by 1.7 folds when the concentration is diluted by half ($I_{2.5\ M\ at\ 0.5\ V}$ = - 268 mA > $I_{5\ M\ at\ 0.5\ V}$ = - 160 mA). The current has always been seen to increase with the active species concentration, so the results obtained herein do not agree with the theory. Given that the graphite felt have already shown several differences in behavior compared to graphite and was not chosen for the functioning of the battery, the interpretation of the results will be done for the curves performed on the graphite rod to see if we obtain also a decrease of the current.

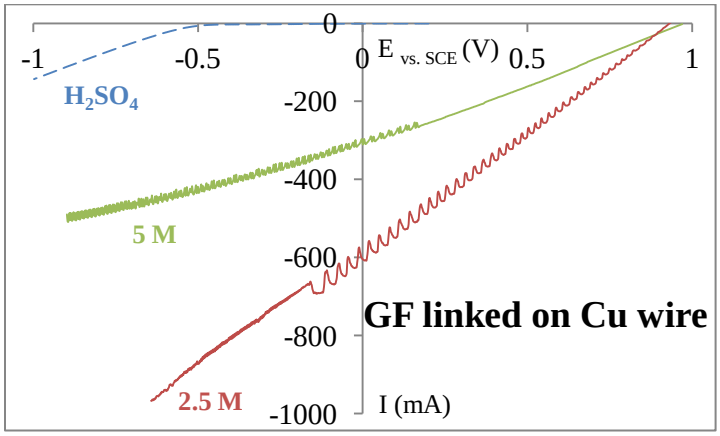

Fig.X10.2: Comparison of I = f(E) curves performed on a graphite felt electrode (S_g = 1 cm^2) linked to a copper wire and immersed in 20 mL of two $V^{(V)}$ deaerated solutions: green/ $[V^{(V)}]$ = 5 M, obtained from electrolysis; red/ $[V^{(V)}]$ = 2.5 M obtained from the dilution of the latter in 3 M H_2SO_4 (blue curve); RE = SCE, CE = Pt plate, ω ≈ 500 RPM (magnetic stirrer), r = 5 $mV.s^{-1}$.

Appendix X11: Effect of the $V^{(III)}$ concentration and the presence of solid particles on the reduction current to $V^{(II)}$ studied on a graphite felt

The activation process of the felt is the same as the one used for the study of the posolyte couple: 10 cycles in sulfuric acid between 2.5 and – 1 V at 50 mV/s.
The same solutions/suspensions used for the study of the $V^{(III)}$ reduction on the graphite rod are studied again in the same three electrodes setup with the only difference being the working electrode, except the 2.35 M suspension which was difficult to stir due to the formation of a paste-like mixture with the last added fraction of solid. The results will be presented in two separated graphs for the solutions and the suspensions because if all the curves are put in the same graph their interpretation will be difficult.

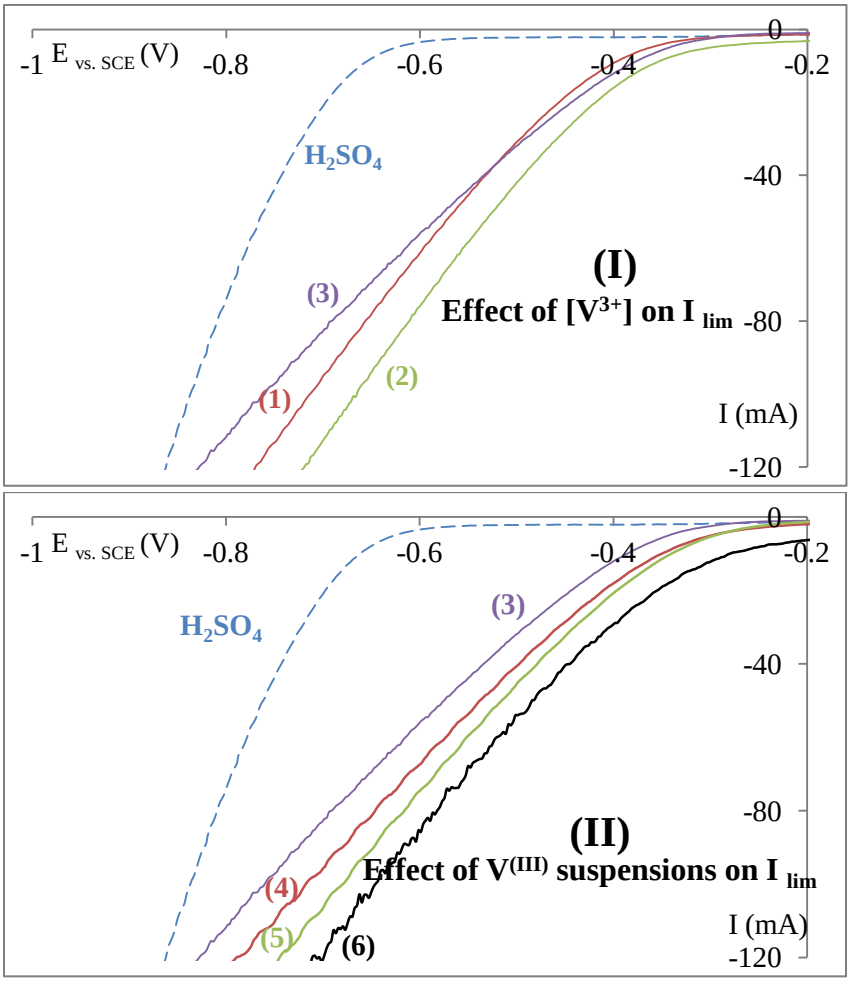

Fig.X11.1: **(I)**: Comparison of the I = f(E) curves performed on a graphite felt electrode (S_g = 1 cm^2) immersed in initial 25 mL of a 2 M H_2SO_4 solution (blue curve) containing V^{3+} at: (1): 0.25 M; (2): 0.5 M; (3): 1 M and **(II)**: (same 3) for comparison; (4) eq. of 1.4 M; (5) eq. of 1.8 M; (6) eq. of 2.1 M; RE: SCE, CE: Pt plate; ω ≈ 500 rpm (magnetic bar); r = 5 mV/s.

The current potential curves performed on the graphite felt exhibit all the same shape: increasing current without the appearance of the reduction wave. This behavior recalls what was observed for high concentrations and suspensions of $V^{(IV)}$ studied on the felt. However here, it starts even for the smallest concentration of 0.25 M. It can be also noticed that the curves shift towards more anodic potentials when the concentration of vanadium in solution/suspension increases.
The absence of the reduction wave can be attributed to a low affinity of the vanadium (III) to the graphite felt which would need a more elaborated activation than the one performed, to create more functional groups on the surface allowing increasing the electro-affinity with the active species and enhancing the reversibility of the system.
Nevertheless, at a fixed potential of – 0.4 V for example, it can be noticed that the current increases as a function of the vanadium quantity analyzed even without the presence of a characteristic reduction wave or diffusion plateau ($I_{1\ M,\ E = -0.4V} = -12\ V < I_{eq.\ 2.1\ M,\ E = -0.4V} = -29$ V). In addition, comparing the two suspensions at 2.1 M on the GR and the GF since they have the same shape, it appears that on the GF the current at – 0.4 V (I = - 29 mA) is greater, or more precisely the double of, the current obtained on the GR at that same potential (I = - 16 mA).
Hence, even without an important affinity of the system to the electrode material, the difference between the graphite felt and the solid rod is still present in terms of real active surface area which influences the resulting current.

Appendix X12: Development of the $V^{(IV)}$ dissolution kinetic law equation

The combination of Eq.IV.6, Eq.IV.7 and Eq.IV.8 enables to obtain the expression of $\frac{dR}{dt}$ (Eq.IV.9) also noted r expressing the variation of the particles radius over time and representing the dissolution rate of the $VOSO_4.5H_2O$. To reach this expression, the following calculation steps were followed:

➔ $Sh = \frac{k_{(t)} \times d_e}{D} = 2 + a \times Re^{\frac{1}{2}} \times Sc^{\frac{1}{3}} \rightarrow k_{(t)} = \frac{D}{2R}(2 + a \times Re^{\frac{1}{2}} \times Sc^{\frac{1}{3}})$

➔ $(\frac{dm}{dt})_{R \to \infty} = +S \times k_{(t)} \times (C_{sat} - C_{bulk})$

➔ $$\frac{d\left(\frac{4}{3}\pi \times \frac{\rho \times N}{M} \times (R^{\circ 3} - R^3)\right)}{dt} = 4\pi R^2 \times \left(\frac{D}{2R}\left(2 + a \times Re^{\frac{1}{2}} \times Sc^{\frac{1}{3}}\right)\right) \times (C_{sat} - \frac{4}{3}\pi \times \frac{\rho \times N}{M \times V_l} \times \left(R^{\circ 3} - R^3\right))$$

Developing the above equation leads to:

➔ $$\frac{-R \times dR}{dt} = \frac{MDC_{sat}}{\rho} - \frac{4}{3}\pi \frac{ND}{\rho V_l}(R^{\circ 3} - R^3) + \frac{aMC_{sat}}{2\rho}(2\bar{u})^{\frac{1}{2}} D^{\frac{2}{3}} \nu^{\left(-\frac{1}{6}\right)} R^{\frac{1}{2}} - \frac{4}{6}\pi \frac{aN}{V_l}(2\bar{u})^{\frac{1}{2}} D^{\frac{2}{3}} \nu^{\left(-\frac{1}{6}\right)} (R^{\circ 3} - R^3) R^{\frac{1}{2}}$$

➔ $r \Rightarrow \frac{dR}{dt} = \frac{A_1 - A_2\left(R^{\circ 3} - R^3\right) + A_3\sqrt{R} - A_4(R^{\circ 3} - R^3)\sqrt{R}}{-R}$ Eq. (9)

A_1	A_2	A_3	A_4
$\frac{M \times D \times C^{sat}}{\rho}$	$\frac{4}{3}\pi \frac{D \times N}{V_l}$	$\frac{aMC_{sat}}{2\rho}(2\bar{u})^{\frac{1}{2}} D^{\frac{2}{3}} \nu^{(-\frac{1}{6})}$	$\frac{4}{6}\pi \frac{aN}{V_l}(2\bar{u})^{\frac{1}{2}} D^{\frac{2}{3}} \nu^{\left(-\frac{1}{6}\right)}$

Appendix X13: Development of the $V^{(V)}$ dissolution kinetic law equation

$$r_{(5)} = +\frac{1}{2}\frac{d[VO_2^+]}{dt} = k_{(5)} \times (\frac{N_\sigma}{N_a})^{\alpha} \times \left(\frac{moles\ of\ H^+}{V_{suspension}}\right)^{\beta} - k_{(-5)} \times \left(\frac{moles\ of\ VO_2^+}{V_{suspension}}\right)^{\gamma} \quad \text{Eq.IV.13}$$

The following nomenclature will be used to treat this equation and to determine the theoretical concentration of VO_2^+:

- for the considered weight of the V_2O_5 particles having as initial diameter: 10, 60 and 1000 µm (from Fig.IV.8), it will be noted:
  - S_1°, S_2°, and S_3°: their average initial surface
  - S_1, S_2 and S_3: their average surface at the time t.
  - R_1°, R_2° and R_3° : their average initial radii:
  - R_1, R_2 and R_3: their average radii at the time t.
- also:
  - N_1, N_2 *and* N_3: are the number of particles having as initial diameter: 10, 60 and 1000 µm
  - $N_{\sigma1}$, $N_{\sigma2}$ *and* $N_{\sigma3}$: are the number of sites (i.e. the number of the V_2O_5 molecules) accessible to the proton H^+, at time t for the particles having as initial diameter: 10, 60 and 1000 µm
  - σ°: is the surface occupied by one molecule of V_2O_5
  - N_a: Avogadro number
- the exponents α, β and γ are the reaction orders, respectively for: a site constituted by V_2O_5, H^+ and VO_2^+;
- $k_{(5)}$ and $k_{(-5)}$ the forward and backward kinetic constants respectively.
- N_σ = the number of sites accessible to H^+, at time t =

$$= N_{\sigma1} + N_{\sigma2} + N_{\sigma3} = \frac{surface\ of\ the\ particles \text{ at the time t}}{\text{surface occupied by one molecule}} = \frac{\Sigma(N_j \times S_j)}{\sigma^\circ}$$

- in addition: "n_V°", and "n_H°" represents respectively the initial moles number of V_2O_5 and H^+,
  "X" the moles number of V_2O_5 dissolved at time t, by consumption of 2X moles of
  H^+, and releasing 2X moles of VO_2^+;

$$\boldsymbol{r_{(5)\,S_i} = +\frac{1}{2}\frac{d[VO_2^+]_{S_i}}{dt} = \frac{1}{2}\frac{d\,(2X)_{S_i}}{V_{suspension}\,dt} = \frac{d(X)_{S_i}}{V_{suspension}\,dt} = k_{(5)} \times (\frac{N_{\sigma i}}{N_a})^{\alpha} \times \frac{\left\{n^\circ_H - 2\times(X)_{S_i}\right\}^{\beta}}{V^{\beta}_{suspension}} - k_{(-5)}\frac{\left\{2\times(X)_{S_i}\right\}^{\gamma}}{V^{\gamma}_{suspension}}}$$

Eq.IV.14

Moreover, the following changes are required in order to transform Eq.IV.14 into a resolvable form:

$$N_{\sigma i} = \frac{S_i}{\sigma^\circ} = \frac{4\pi \times N_i}{\sigma^\circ} R_i^2 \qquad \textbf{(A)}$$

Besides the mass of the V_2O_5 introduced into the suspension is: $m_{V_2O_5} = m_{R_1} + m_{R_2} + m_{R_3}$

The mass of V_2O_5 particles having R_i as diameter can be expressed by the two following equations:

$m_{R_i} = Molecular\ weight$ of $\boldsymbol{V_2O_5} \times mol\ number\ of$ particles having $\boldsymbol{R_i} = M \times \boldsymbol{n_{V\,R_i}}$

and $m_{R_i} = \rho\, V_{solide\,R_i} = \rho\ \frac{4\pi R_i^3}{3}$

Combining both equations leads to: $M \times \boldsymbol{n_{V\,R_i}} = \rho\ \frac{4\pi R_i^3}{3} \Rightarrow \boldsymbol{R_i} = \left\{ \frac{3\ M\ n_{V\,R_i}}{4\,\pi\rho} \right\}^{1/3}$ **(B)**

Substituting **(B)** into **(A)** gives the number of sites having, at time t, R_i as initial diameter:

$N_{\sigma i} = \frac{4\pi \times N_i}{\sigma^\circ} \left(\left\{ \frac{3\ M\ n_{V\,R_i}}{4\,\pi\rho} \right\}^{1/3} \right)^2 \Rightarrow N_{\sigma i} = \frac{N_i}{\sigma^\circ} \times \left(\frac{3\,(4\pi)^{0.5}\ M\ n_{V\,R_i}}{\rho} \right)^{2/3}$

And substituting $n_{V\,R_i}$ $by\ \left(n^\circ_V - X_{R_i}\right)\ gives$: $\Rightarrow$

$$N_{\sigma i} = \frac{N_i}{\sigma^\circ} \times \left(\frac{3\,(4\pi)^{0.5}\,M}{\rho} \right)^{2/3} \times \left(n^\circ_V - X_{R_i}\right)^{2/3} \qquad \textbf{(C)}$$

Substituting **(C)** into the expression of the rate (Eq. (14)) leads to:

$$\boldsymbol{r_{(5)\,S_i}} = \frac{d(X)_{S_i}}{V_{suspension}\,dt} = \boldsymbol{k_{(5)}} \times \left(\frac{N_i}{N_a \times \sigma^\circ} \times \left(\frac{3\,(4\pi)^{0.5}\,M}{\rho} \right)^{2/3} \times \left(n^\circ_V - X_{R_i}\right)^{2/3} \right)^{\alpha} \times \frac{\left\{n^\circ_H - 2(X)_{S_i}\right\}^{\beta}}{V_{suspension}^{\beta}} - \boldsymbol{k_{(-5)}} \frac{\left\{2(X)_{S_i}\right\}^{\gamma}}{V_{suspension}^{\gamma}}$$

$$\boldsymbol{r_{(5)\,S_i}} = \frac{d(X)_{S_i}}{dt} = \mathrm{k}_{(5)} \left(\frac{N_i}{N_a \times \sigma^\circ} \times \left(\frac{3\,(4\pi)^{0.5}\,M}{\rho} \right)^{2/3} \right)^{\alpha} \times \left(\left(n^\circ_V - X_{R_i}\right)^{2/3} \right)^{\alpha} \frac{\left\{n^\circ_H - 2 \times (X)_{S_i}\right\}^{\beta}}{V_{suspension}^{\beta-1}} - \boldsymbol{k_{(-5)}} \frac{\left\{2 \times (X)_{S_i}\right\}^{\gamma}}{V_{suspension}^{\gamma-1}}$$ **(D)**

To solve this equation, the reaction orders are required and they will be assumed to be equal to the stoichiometric coefficients of each reactant, i.e. $\alpha = 1$ and $\beta = \gamma = 2$.

$$\boldsymbol{r_{(5)\,S_i}} = \frac{d(X)_{S_i}}{dt} = \mathbf{k}_{(5)} \times \frac{N_i}{N_a \times \sigma^\circ} \times \left(\frac{3\,(4\pi)^{0.5}\,M}{\rho} \right)^{2/3} \times \left(n^\circ_V - X_{R_i}\right)^{2/3} \times \frac{\left\{n^\circ_H - 2 \times (X)_{S_i}\right\}^{2}}{V_{suspension}} - \boldsymbol{k_{(-5)}} \frac{\left\{2 \times (X)_{S_i}\right\}^{2}}{V_{suspension}}$$ Eq.IV.15

Note that three equations must solved for the three particle sizes chosen, each one providing the mole number of VO_2^+ produced by the dissolution of the corresponding family of these particles as indicated in the following table.

Dissolution rate relative to the particles having, at time t, an average Radii Ri (i going from 1 to 3, as defined above)	$\boldsymbol{r_{(5)\,S_1}}$	$\boldsymbol{r_{(5)\,S_2}}$	$\boldsymbol{r_{(5)\,S_3}}$
the number of the particles having, at time t, an average Radii Ri	N_1	N_2	N_3
The mole number of VO_2^+ produced by the dissolution of the particles having, at time t, an average Radii Ri	$2X_{R_1}$	$2X_{R_2}$	$2X_{R_3}$
Total mole number of VO_2^+ produced by the dissolution of all the particles at the time t	$2X = 2X_{R_1} + 2X_{R_2} + 2X_{R_3}$		

Résumé :
Le présent projet concerne la conception et l'optimisation des batteries à circulation (RFB). Ces dernières sont des dispositifs permettant la conversion électrochimique de l'énergie électrique et son stockage sous forme chimique ; le processus inverse vise à récupérer l'énergie stockée sous forme d'électricité, selon la demande. Les RFB sont bien adaptées pour répondre au caractère intermittent des ressources des énergies renouvelables.
La batterie étudiée est la RFB tout vanadium (VRFB), qui a été développée dans les années 80 et dont l'avantage principal par rapport aux autres batteries à circulation (le Fe-Cr par exemple), est l'absence de contamination irréversible des deux électrolytes, ceci du faite que toutes les solutions sont des sels de vanadium. Cependant, la densité énergétique de ce système ne dépasse pas 40 $Wh.kg^{-1}$ (contre ~ 150 $Wh.kg^{-1}$ dans le cas des batteries stationnaires Li-ion) à cause de la faible solubilité des sels de vanadium (< 2 $mol.L^{-1}$) dans l'acide sulfurique utilisé comme électrolyte support.
Un objectif de la thèse est d'optimiser la formulation des mélanges d'électrolyte afin d'augmenter la densité énergétique de la batterie. Ceci consiste à i) mettre en place des méthodes électrochimiques pour la préparation, l'analyse et la caractérisation des électrolytes (posolyte $V^{(IV)}/V^{(V)}$ et négolyte $V^{(II)}/V^{(III)}$) pour trouver leur composition optimale et ii) à comprendre les phénomènes physico-chimiques ayant lieu durant les cycles de charge-décharge de la batterie et déterminer les lois régissant ces processus et ainsi surmonter toute limitation éventuelle.
L'étude a été menée dans une cellule classique à trois électrodes, permettant de travailler aisément avec un système électrochimique à la fois (en demi-batterie). Les résultats montrent que la présence de particules affecte négativement le courant de la batterie même si le solide permet d'augmenter la capacité de stockage. D'autre part, la présence d'un additif carboné dans le posolyte paraît avoir un effet bénéfique sur le courant grâce à l'extension du collecteur électronique dans le volume via la formation d'agrégats (percolation électronique dans la suspension).
Des mesures de conductivité, masse volumique, viscosité, débit ainsi que des méthodes de caractérisation de poudre (MEB, diffraction laser) ont été réalisés et apporté les données nécessaires. Un second objectif de la thèse est la conception et l'élaboration d'une VRFB, à l'échelle laboratoire, ayant une densité énergétique supérieure à 100 $Wh.kg^{-1}$, ainsi que l'optimisation tant que de possible la puissance du réacteur. Des bilans massique et énergétique sont réalisés pour les opérations de charge-décharge sous différentes conditions, afin d'établir les corrélations 'réponse du système (courant, tension et réversibilité) en fonction des divers paramètres opératoires'. Les conversions ainsi que les rendements faradiques et énergétiques sont évalués et optimisés.

Abstract:
This research focuses on the redox flow batteries (RFBs) conception and optimization. RFBs are devices performing the electrochemical conversion of electric energy to chemical energy (to store); the reverse process allows recovering the stored energy in the form of electricity according to demand. RFBs are well adapted to energy storage from intermittent renewable energy sources.
The battery studied is the all-vanadium RFB (VRFB) which was introduced in the 1980's. Owing to the nature of the electrolytes used in the VRFB, the effect of the irreversible cross-contamination, usually encountered in other RFBs such as the Fe-Cr system, is thus overcome. However, the energy density of this system remains lower than 40 $Wh.kg^{-1}$ (compared to ~ 150 $Wh.kg^{-1}$ for Li-ion stationary batteries) because of the low solubility (< 2 $mol.L^{-1}$) of the vanadium salts in sulfuric acid, used as supporting electrolyte.
An objective of this thesis is to optimize the formulation of the electrolytes in order to increase the stored energy density. This consists of: i) preparing, analyzing and characterizing the electrolytes (posolyte $V^{(IV)}/V^{(V)}$ and negolyte $V^{(II)}/V^{(III)}$), thus expecting to find their optimal composition and ii) understanding the physico-chemical phenomena occurring during the charge-discharge cycling and thus determining the laws governing these processes to overcome any eventual limitation.
These aspects were studied using a classical three electrodes cell, enabling to operate with one electrochemical system at a time (the half of the battery). The presence of particles seems to negatively affect the current of the battery even if it enables to increase the stored energy density. On the another hand, the presence of carbon nanoparticles in the posolyte appears to have a beneficial effect on the current due to the increase of the electrode surface area by the formation of aggregates (electronic percolation in the suspension).
This part also includes various physical measurements, such as conductivity, density, viscosity and flow rate, as well as powder characterization techniques (SEM, laser diffraction). Another objective is to conceive and elaborate a VRFB (at the laboratory scale) providing an energy density higher than 100 $Wh.kg^{-1}$, and optimizing as much as possible the power density of the reactor. Mass and charge balances are performed for charge/discharge cycles, to establish correlations that link the response of the system (current, voltage, energy and reversibility) to the (influencing) operating parameters. Conversions, faradic and energy yields were evaluated and optimized.